

UNIVERSIDADE FEDERAL DE SÃO CARLOS
CENTRO DE CIÊNCIAS EXATAS E DE TECNOLOGIA
DEPARTAMENTO DE QUÍMICA
PROGRAMA DE PÓS-GRADUAÇÃO EM QUÍMICA

**“Tris(trimethylsilyl)silane and Visible-Light
Irradiation: A New Metal- and Additive-Free
Photochemical Process for the Synthesis of
Indoles and Oxindoles”**

Gustavo Piva da Silva*

Dissertação apresentada como parte
dos requisitos para obtenção do título
de MESTRE EM QUÍMICA, área de
concentração: QUÍMICA ORGÂNICA.

Orientador: Prof. Dr. Márcio Weber Paixão

*** bolsista CNPq**

**São Carlos - SP
2016**

Ficha catalográfica elaborada pelo DePT da Biblioteca Comunitária UFSCar
Processamento Técnico
com os dados fornecidos pelo(a) autor(a)

S586t Silva, Gustavo Piva da
Tris(trimethylsilyl)silane and visible-light
irradiation : a new metal- and additive-free
photochemical process for the synthesis of indoles
and oxindoles / Gustavo Piva da Silva. -- São Carlos
: UFSCar, 2016.
166 p.

Dissertação (Mestrado) -- Universidade Federal de
São Carlos, 2016.

1. Indole. 2. Oxindole. 3. Photochemistry. I. Título.



UNIVERSIDADE FEDERAL DE SÃO CARLOS

Centro de Ciências Exatas e de Tecnologia
Programa de Pós-Graduação em Química

Folha de Aprovação

Assinaturas dos membros da comissão examinadora que avaliou e aprovou a Defesa de Dissertação de Mestrado do candidato Gustavo Piva da Silva, realizada em 29/07/2016:

Prof. Dr. Márcio Weber Paixão
UFSCar

Prof. Dr. Antonio Carlos Bender Burtoloso
IQSC/USP

Prof. Dr. Marco Antonio Barbosa Ferreira
UFSCar

**I dedicate this work to my parents, brother, sister,
my entire family, and my girlfriend,
for all of the support they have provided me.**

“The measure of intelligence is the ability to change”

Albert Einstein

Acknowledgements

I would like to thank my parents, Angela and Nelson, and my brothers Mariana and Vitor, for being my biggest motivation and example for always being by my side, and be the basis of everything I am. And also thank all my family for all the support. My girlfriend/fiancée Fernanda for all understanding, patience, encouragement, and especially the companionship at all times, and also her family that was always by my side.

Professor Márcio for all the guidance and tireless willingness to teach and discuss Chemistry and every incentive to scientific and personal growth. Professors Arlene and Ricardo for their cooperation and assistance in day-to-day laboratory and during the development of the work. Professor Rebecca Davis (University of Manitoba) and her group, for the opportunity to work, study, and unique learning experience.

Friends Akbar Ali, and Rodrigo Cesar (Jacaré), who were fundamental in developing the project and the immense contributions to the work obtain adequate quality. Also, thank you for all the professional discussion and moments of fun. To all friends of the laboratory that were present throughout this trajectory, contributing to discussions, helps, and of course for many moments of fun. Friends of the República Ponto V, and Valinhos-SP for providing the best moments of fun and partnership.

To all the professors and staff of DQ (UFSCar – SP - Brazil) and University of Manitoba (Canada) that somehow contributed to this work.

The all from whom I learned and contributed to my training.

CNPq for the scholarship granted, CAPES and FAPESP for financial support.

List of Abbreviations

Bu ₃ N	Tributylamine
CT	Charge transfer
DCM	Dichloromethane
DDQ	2,3-Dichloro-5,6-dicyano-1,4-benzoquinone
DMF	Dimethylformamide
DMSO	Dimethylsulfoxide
E	Energy
EDA	Electron donor-acceptor
ESA	Excited state absorption
EtOAc	Ethyl acetate
FDA	Food and drug administration
GC-MS	Gas chromatography – mass spectrometry
HOMO	Highest occupied molecular orbital
IC	Internal conversion
ISC	Intersystem crossing
LUMO	Lowest unoccupied molecular orbital
MeCN	Acetonitrile
MEOD	Deuterated methanol
PC	Photocatalyst
S	Spin multiplicity
THF	Tetrahydrofuran
TTMSS	Tris(trimethylsilyl)silane
UV	Ultraviolet-Visible
<i>h</i>	Planck's constant
ν	Frequency
λ	Wavelength
Φ	Quantum yield

List of Tables

TABLE 1: Optimization studies: Effect of the TTMSS loading.	57
TABLE 2: Optimization studies: Solvent screening.	58
TABLE 3: Optimization studies: Additional proton source.	59
TABLE 4: Optimization studies: Effect of the structure – <i>N</i> -protecting group.	60
TABLE 5: Kinetics studies: Area x Concentration of <i>N</i> -tosyl-propargyl aniline.	69
TABLE 6: Kinetics studies: Area x Concentration of TTMSS.	70
TABLE 7: Optimization studies – Synthesis of oxindole	76

List of Figures

FIGURE 1: HOMO-LUMO diagram.	29
FIGURE 2: Energy level diagram and summary of photochemical processes (Jablonski diagram: IC – internal conversion, ESA – excited state absorption, ISC – intersystem crossing).....	31
FIGURE 3: Absorption spectra of the separated reagents of the model reaction, and the reaction mixture.....	65
FIGURE 4: Successive intervals of irradiation and dark periods for the model reaction.	66
FIGURE 5: ¹ H NMR spectra of deuterated labelled compound.....	67
FIGURE 6: Calibration curve of N-tosyl-propargyl aniline.	69
FIGURE 7: Calibration curve of TTMSS.....	70
FIGURE 8: First order applied to N-tosyl-propargyl aniline.....	71
FIGURE 9: First order applied to TTMSS.....	71
FIGURE 10: Second order applied to N-tosyl-propargyl aniline.	72
FIGURE 11: Second order applied to TTMSS.....	72
FIGURE 12: Second order overall – first order with respect to each reagent.....	73
FIGURE 13: ¹ H NMR spectrum of 46a precursor, 400 MHz, CDCl ₃	109
FIGURE 14: ¹³ C NMR spectrum of 46a precursor, 100 MHz, CDCl ₃	109
FIGURE 15: ¹ H NMR spectrum of 46b precursor, 400 MHz, CDCl ₃	110
FIGURE 16: ¹³ C NMR spectrum of 46b precursor, 100 MHz, CDCl ₃	110
FIGURE 17: ¹ H NMR spectrum of 46c precursor, 400 MHz, CDCl ₃	111
FIGURE 18: ¹³ C NMR spectrum of 46c precursor, 100 MHz, CDCl ₃	111
FIGURE 19: ¹ H NMR spectrum of 46f precursor, 400 MHz, CDCl ₃	112
FIGURE 20: ¹³ C NMR spectrum of 46f precursor, 100 MHz, CDCl ₃	112
FIGURE 21: ¹ H NMR spectrum of 46h precursor, 400 MHz, CDCl ₃	113
FIGURE 22: ¹³ C NMR spectrum of 46h precursor, 100 MHz, CDCl ₃	113
FIGURE 23: ¹ H NMR spectrum of 46j precursor, 400 MHz, CDCl ₃	114
FIGURE 24: ¹ H NMR spectrum of 46k precursor, 400 MHz, CDCl ₃	114
FIGURE 25: ¹³ C NMR spectrum of 46k precursor, 100 MHz, CDCl ₃	115
FIGURE 26: ¹ H NMR spectrum of 46l precursor, 400 MHz, CDCl ₃	115
FIGURE 27: ¹³ C NMR spectrum of 46l precursor, 100 MHz, CDCl ₃	116
FIGURE 28: ¹ H NMR spectrum of 46m precursor, 400 MHz, CDCl ₃	116

FIGURE 29: ^1H NMR spectrum of 46o precursor, 400 MHz, CDCl_3	117
FIGURE 30: ^{13}C NMR spectrum of 46o precursor, 100 MHz, CDCl_3	117
FIGURE 31: ^1H NMR spectrum of 46a, 400 MHz, CDCl_3	118
FIGURE 32: ^{13}C NMR spectrum of 46a, 100 MHz, CDCl_3	118
FIGURE 33: ^1H NMR spectrum of 46b, 400 MHz, CDCl_3	119
FIGURE 34: ^{13}C NMR spectrum of 46b, 100 MHz, CDCl_3	119
FIGURE 35: ^1H NMR spectrum of 46c, 400 MHz, CDCl_3	120
FIGURE 36: ^{13}C NMR spectrum of 46c, 100 MHz, CDCl_3	120
FIGURE 37: ^1H NMR spectrum of 46d, 400 MHz, CDCl_3	121
FIGURE 38: ^1H NMR spectrum of 46e, 400 MHz, CDCl_3	121
FIGURE 39: ^{13}C NMR spectrum of 46e, 100 MHz, CDCl_3	122
FIGURE 40: ^1H NMR spectrum of 46f, 400 MHz, CDCl_3	122
FIGURE 41: ^{13}C NMR spectrum of 46f, 100 MHz, CDCl_3	123
FIGURE 42: ^1H NMR spectrum of 46g, 400 MHz, CDCl_3	123
FIGURE 43: ^1H NMR spectrum of 46h, 400 MHz, CDCl_3	124
FIGURE 44: ^{13}C NMR spectrum of 46h, 100 MHz, CDCl_3	124
FIGURE 45: ^1H NMR spectrum of 46k, 400 MHz, CDCl_3	125
FIGURE 46: ^{13}C NMR spectrum of 46k, 100 MHz, CDCl_3	125
FIGURE 47: ^1H NMR spectrum of 46l, 400 MHz, CDCl_3	126
FIGURE 48: ^{13}C NMR spectrum of 46l, 100 MHz, CDCl_3	126
FIGURE 49: ^1H NMR spectrum of 46m, 400 MHz, CDCl_3	127
FIGURE 50: ^1H NMR spectrum of 46n, 400 MHz, CDCl_3	127
FIGURE 51: ^{13}C NMR spectrum of 46n, 100 MHz, CDCl_3	128
FIGURE 52: ^1H NMR spectrum of 46o, 400 MHz, CDCl_3	128
FIGURE 53: ^{13}C NMR spectrum of 46o, 100 MHz, CDCl_3	129
FIGURE 54: ^1H NMR spectrum of 48c precursor, 400 MHz, CDCl_3	129
FIGURE 55: ^{13}C NMR spectrum of 48c precursor, 100 MHz, CDCl_3	130
FIGURE 56: ^1H NMR spectrum of 48e precursor, 400 MHz, CDCl_3	130
FIGURE 57: ^{13}C NMR spectrum of 48e precursor, 100 MHz, CDCl_3	131
FIGURE 58: ^1H NMR spectrum of 48f precursor, 400 MHz, CDCl_3	131
FIGURE 59: ^{13}C NMR spectrum of 48f precursor, 100 MHz, CDCl_3	132
FIGURE 60: ^1H NMR spectrum of 48g precursor, 400 MHz, CDCl_3	132
FIGURE 61: ^{13}C NMR spectrum of 48g precursor, 100 MHz, CDCl_3	133
FIGURE 62: ^1H NMR spectrum of 48h precursor, 400 MHz, CDCl_3	133

FIGURE 63: ^1H NMR spectrum of 48i precursor, 400 MHz, CDCl_3 .	134
FIGURE 64: ^{13}C NMR spectrum of 48i precursor, 100 MHz, CDCl_3 .	134
FIGURE 65: ^1H NMR spectrum of 48a, 400 MHz, CDCl_3 .	135
FIGURE 66: ^1H NMR spectrum of 48b, 400 MHz, CDCl_3 .	135
FIGURE 67: ^{13}C NMR spectrum of 48b, 100 MHz, CDCl_3 .	136
FIGURE 68: ^1H NMR spectrum of 48c, 400 MHz, CDCl_3 .	136
FIGURE 69: ^{13}C NMR spectrum of 48c, 100 MHz, CDCl_3 .	137
FIGURE 70: ^1H NMR spectrum of 48d, 400 MHz, CDCl_3 .	137
FIGURE 71: ^{13}C NMR spectrum of 48d, 100 MHz, CDCl_3 .	138
FIGURE 72: ^1H NMR spectrum of 48e, 400 MHz, CDCl_3 .	138
FIGURE 73: ^{13}C NMR spectrum of 48e, 100 MHz, CDCl_3 .	139
FIGURE 74: ^1H NMR spectrum of 48f, 400 MHz, CDCl_3 .	139
FIGURE 75: ^{13}C NMR spectrum of 48f, 100 MHz, CDCl_3 .	140
FIGURE 76: ^1H NMR spectrum of 48g, 400 MHz, CDCl_3 .	140
FIGURE 77: ^1H NMR spectrum of 48h, 400 MHz, CDCl_3 .	141
FIGURE 78: ^{13}C NMR spectrum of 48h, 100 MHz, CDCl_3 .	141
FIGURE 79: ^1H NMR spectrum of 48i, 400 MHz, CDCl_3 .	142
FIGURE 80: ^{13}C NMR spectrum of 48i, 100 MHz, CDCl_3 .	142
FIGURE 81: ^1H NMR spectrum of 47a, 400 MHz, CDCl_3 .	143
FIGURE 82: ^{13}C NMR spectrum of 47a, 100 MHz, CDCl_3 .	143
FIGURE 83: ^1H NMR spectrum of 47b, 400 MHz, CDCl_3 .	144
FIGURE 84: ^{13}C NMR spectrum of 47b, 100 MHz, CDCl_3 .	144
FIGURE 85: ^1H NMR spectrum of 47c, 400 MHz, CDCl_3 .	145
FIGURE 86: ^{13}C NMR spectrum of 47c, 100 MHz, CDCl_3 .	145
FIGURE 87: ^1H NMR spectrum of 47d, 400 MHz, CDCl_3 .	146
FIGURE 88: ^{13}C NMR spectrum of 47d, 100 MHz, CDCl_3 .	146
FIGURE 89: ^1H NMR spectrum of 47e, 400 MHz, CDCl_3 .	147
FIGURE 90: ^{13}C NMR spectrum of 47e, 100 MHz, CDCl_3 .	147
FIGURE 91: ^1H NMR spectrum of 47f, 400 MHz, CDCl_3 .	148
FIGURE 92: ^{13}C NMR spectrum of 47f, 100 MHz, CDCl_3 .	148
FIGURE 93: ^1H NMR spectrum of 47g, 400 MHz, CDCl_3 .	149
FIGURE 94: ^{13}C NMR spectrum of 47g, 100 MHz, CDCl_3 .	149
FIGURE 95: ^1H NMR spectrum of 47h, 400 MHz, CDCl_3 .	150
FIGURE 96: ^{13}C NMR spectrum of 47h, 100 MHz, CDCl_3 .	150

FIGURE 97: ^1H NMR spectrum of 47i, 400 MHz, CDCl_3	151
FIGURE 98: ^{13}C NMR spectrum of 47i, 100 MHz, CDCl_3	151
FIGURE 99: ^1H NMR spectrum of 47j, 400 MHz, CDCl_3	152
FIGURE 100: ^{13}C NMR spectrum of 47j, 100 MHz, CDCl_3	152
FIGURE 101: ^1H NMR spectrum of 47k, 400 MHz, CDCl_3	153
FIGURE 102: ^{13}C NMR spectrum of 47k, 100 MHz, CDCl_3	153
FIGURE 103: ^1H NMR spectrum of 47l, 400 MHz, CDCl_3	154
FIGURE 104: ^{13}C NMR spectrum of 47l, 100 MHz, CDCl_3	154
FIGURE 105: ^1H NMR spectrum of 47m, 400 MHz, CDCl_3	155
FIGURE 106: ^{13}C NMR spectrum of 47m, 100 MHz, CDCl_3	155
FIGURE 107: ^1H NMR spectrum of 47n, 400 MHz, CDCl_3	156
FIGURE 108: ^{13}C NMR spectrum of 47n, 100 MHz, CDCl_3	156
FIGURE 109: ^1H NMR spectrum of 47o, 400 MHz, CDCl_3	157
FIGURE 110: ^{13}C NMR spectrum of 47o, 100 MHz, CDCl_3	157
FIGURE 111: ^1H NMR spectrum of 49a, 400 MHz, CDCl_3	158
FIGURE 112: ^{13}C NMR spectrum of 49a, 100 MHz, CDCl_3	158
FIGURE 113: ^1H NMR spectrum of 49b, 400 MHz, CDCl_3	159
FIGURE 114: ^{13}C NMR spectrum of 49b, 100 MHz, CDCl_3	159
FIGURE 115: ^1H NMR spectrum of 49c, 400 MHz, CDCl_3	160
FIGURE 116: ^{13}C NMR spectrum of 49c, 100 MHz, CDCl_3	160
FIGURE 117: ^1H NMR spectrum of 49d, 400 MHz, CDCl_3	161
FIGURE 118: ^{13}C NMR spectrum of 49d, 100 MHz, CDCl_3	161
FIGURE 119: ^1H NMR spectrum of 49e, 400 MHz, CDCl_3	162
FIGURE 120: ^{13}C NMR spectrum of 49e, 100 MHz, CDCl_3	162
FIGURE 121: ^1H NMR spectrum of 49f, 400 MHz, CDCl_3	163
FIGURE 122: ^{13}C NMR spectrum of 49f, 100 MHz, CDCl_3	163
FIGURE 123: ^1H NMR spectrum 49g, 400 MHz, CDCl_3	164
FIGURE 124: ^{13}C NMR spectrum of 49g, 100 MHz, CDCl_3	164
FIGURE 125: ^1H NMR spectrum of 49h, 400 MHz, CDCl_3	165
FIGURE 126: ^{13}C NMR spectrum of 49h, 100 MHz, CDCl_3	165
FIGURE 127: ^1H NMR spectrum of 49i, 400 MHz, CDCl_3	166
FIGURE 128: ^{13}C NMR spectrum of 49i, 100 MHz, CDCl_3	166

List of Schemes

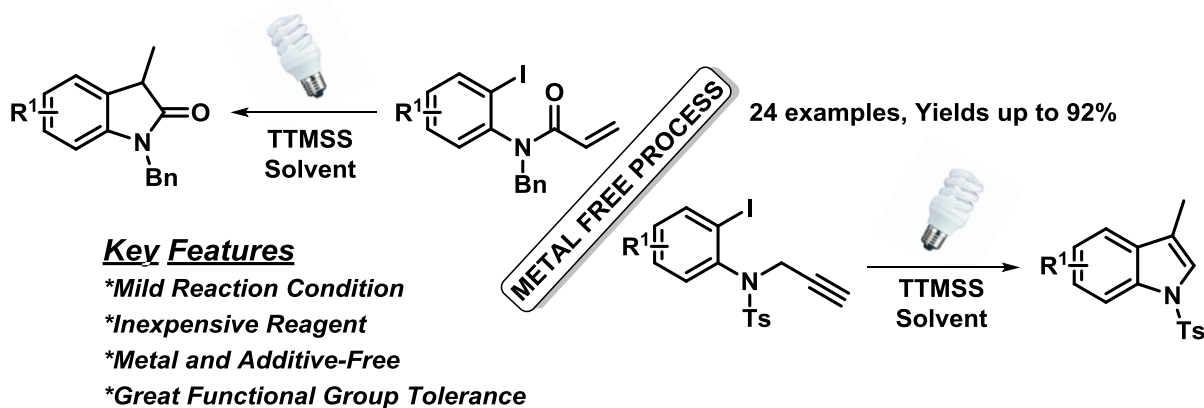
SCHEME 1: Metal-free process for the synthesis of indoles and oxindoles.	xix
SCHEME 2: Metodologia para a síntese de indóis e oxindóis livre de metais.	xxi
SCHEME 3: Santonin: Photochemical modifications.....	26
SCHEME 4: Cyclization reaction mediated by sunlight.	27
SCHEME 5: [2+2] Photocycloaddition reaction.	28
SCHEME 6: Photochemical route to access cyclopropane systems.	33
SCHEME 7: Photochemical alkylation of indoles driven by an EDA complex.	34
SCHEME 8: General representations for a photoinduced electron transfer mediated (A) a Photocatalyst and (B) Electron donor-acceptor (EDA complex).	35
SCHEME 9: Alkylation of indoles driven by an EDA complex.	36
SCHEME 10: Radical-nucleophilic substitution reactions mediated by EDA complexes.	37
SCHEME 11: α -trifluoromethylation of enolsilanes mediated by visible light.	38
SCHEME 12: Visible light-mediated direct arylation of heteroarenes using diaryliodonium salts in the absence of a photocatalyst.	38
SCHEME 13: Visible light mediated transformations with polyhalomethanes providing α -CH activation of tetrahydroisoquinoline.....	39
SCHEME 14: Pharmaceutical active compounds containing the indole scaffold.....	41
SCHEME 15: First catalytic asymmetric Fischer indolization.	42
SCHEME 16: Synthesis of functionalized indoles via palladium-catalyzed aerobic oxidative cycloisomerization.....	43
SCHEME 17: Proposed mechanism for the photocatalytic <i>N</i> -arylindoles synthesis..	44
SCHEME 18: Reduction of aryl iodide and intramolecular reductive cyclization.	45
SCHEME 19: Pharmaceutically active oxindoles.	46
SCHEME 20: Palladium-catalyzed oxindole synthesis and possible mechanistic pathways.	47
SCHEME 21: Metal-free synthesis of 2-oxindoles via $\text{PhI}(\text{OAc})_2$ -mediated oxidative C–C bond formation.	48
SCHEME 22: Visible light induced radical cyclization of <i>o</i> -iodophenylacrylamides. ...	49
SCHEME 23: Oxindole synthesis. (A) Synthesis of 3,3-disubstituted oxindoles by visible-light-mediated radical reaction of aryl diazonium salts with	

N-arylacrylamides. (B) Direct synthesis of sulfonated oxindoles from <i>N</i> -arylacrylamides and arylsulfinic acids using visible light by means of a cascade C-S/C-C formation process.	51
SCHEME 24: Project goal	53
SCHEME 25: Tris(trimethylsilyl)silane as a radical promoter.	56
SCHEME 26: Substrate scope for the visible-light-mediated indole synthesis.	61
SCHEME 27: Formal synthesis of Dolasetron.....	63
SCHEME 28: Controlled experiments.	63
SCHEME 29: Proposed mechanism for the visible-light-mediated indole synthesis.	74
SCHEME 30: Simplified retrosynthetic analysis.	75
SCHEME 31: Substrate scope for the visible-light-mediated oxindole synthesis.	77
SCHEME 32: Scope limitation of the methodology.	77
SCHEME 33: Synthesis of <i>N</i> -tosyl-protected aniline.	90
SCHEME 34: Synthesis of <i>N</i> -tosyl-propargyl aniline.	93
SCHEME 35: Synthesis of <i>N</i> -acrylamides.....	96
SCHEME 36: Synthesis of <i>N</i> -benzyl-acrylamides.	98

Abstract

TRIS(TRIMETHYLSILYL)SILANE AND VISIBLE-LIGHT IRRADIATION: A NEW METAL- AND ADDITIVE-FREE PHOTOCHEMICAL PROCESS FOR THE SYNTHESIS OF INDOLES AND OXINDOLES

A combined tris(trimethylsilyl)silane and visible-light-promoted intramolecular reductive cyclization protocol for the synthesis of indoles and oxindoles has been developed (Scheme 1).¹ This straightforward and efficient protocol shows a broad functional-group tolerance and enables rapid and practical synthesis of functionalized nitrogen-based heterocycles in high/moderate yields under additive and metal-free, mild photochemical conditions. Besides the synthetic developments, the reaction mechanism was also investigated by a set of controlled experiments and UV-visible analyses, as well as kinetic study.² From these studies, we have concluded that the reaction pathway for this strategy occurs through an Electron Donor-Acceptor (EDA) complex.³



SCHEME 1: Metal-free process for the synthesis of indoles and oxindoles.

¹ NGUYEN, J. D.; D'AMATO, E. M.; NARAYANAM, J. M. R.; STEPHENSON, C. R. J. "Engaging unactivated alkyl, alkenyl and aryl iodides in visible-light-mediated free radical reactions". *Nat. Chem.*, **4**: 854, 2012.

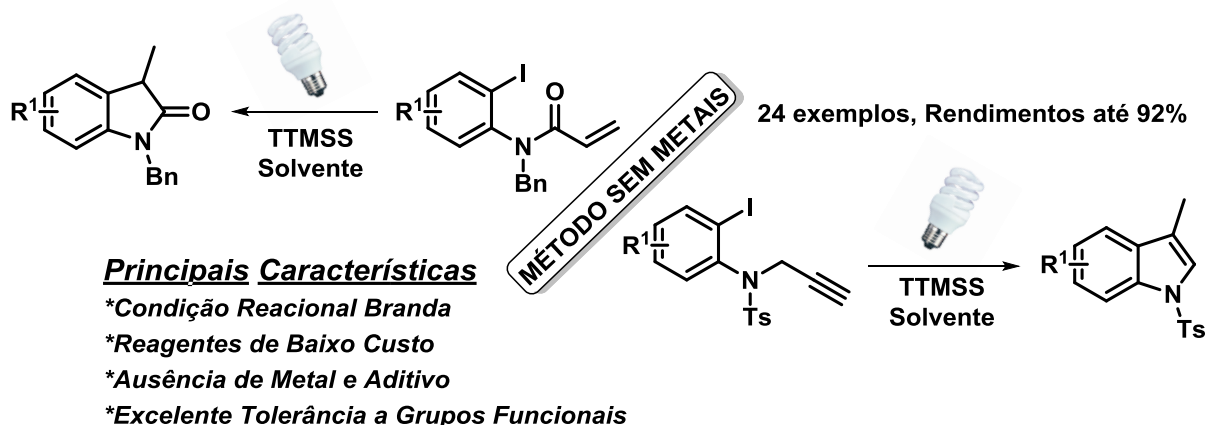
² SILVA, G. P.; ALI, A.; SILVA, R. C.; JIANG, H.; PAIXÃO, M. W. "Tris(trimethylsilyl)silane and visible-light irradiation: a new metal- and additive-free photochemical process for the synthesis of indoles and oxindoles". *Chem. Commun.*, **51**: 15110, 2015.

³ LIMA, C. G. S.; LIMA, T. D. M.; DUARTE, M.; JURBERG, I. D.; PAIXÃO, M. W. "Organic Synthesis Enabled by Light-Irradiation of EDA Complexes: Theoretical Background and Synthetic Applications". *ACS Catal.*, **6**: 1389, 2016.

Resumo

LUZ VISÍVEL E TRIS(TRIMETILSILIL)SILANO: UM NOVO PROCESSO FOTOQUÍMICO SEM ADIÇÃO DE METAL E ADITIVO PARA A SÍNTESE DE INDÓIS E OXINDÓIS

Uma nova metodologia para síntese de indóis e oxindóis foi desenvolvida através de um processo de ciclização redutiva intramolecular utilizando uma combinação da luz visível e tris(trimetilsilil)silano (Scheme 2).¹ Este protocolo sintético mostrou-se eficiente e abrangente a diversos substratos funcionalizados, permitindo assim uma rápida e prática síntese de compostos nitrogenados heterocíclicos com altos/moderados rendimentos diante de uma condição fotoquímica livre de metais, bem como aditivos. Além do desenvolvimento sintético, o mecanismo da reação também foi investigado por uma série de experimentos controlados e estudos espectroscópicos, bem como estudos cinéticos.² A partir destes estudos, concluímos que o caminho reacional para esta estratégia ocorre através de um complexo doador-aceptor (EDA).³



SCHEME 2: Metodologia para a síntese de indóis e oxindóis livre de metais.

Summary

Acknowledgements	xii
List of Abbreviations	ix
List of Tables	xi
List of Figures	xiii
List of Schemes	xvii
Abstract	xix
Resumo	xxi
Summary	xxiii
1 Introduction	25
1.1 Organic Photochemistry	25
1.2 Excited States.....	27
1.3 Electron Donor-Acceptor Complex	34
1.4 Indole and Oxindole Synthesis	40
2 Project Goals	53
3 Results and Discussion	55
3.1 Optimization Studies.....	55
3.2 Scope Evaluation.....	60
3.3 Mechanistic Insights	63
3.4 Kinetic Studies.....	66
3.5 Oxindole Synthesis.....	75
4 Conclusion	79
5 References	81
6 Experimental Section	89
6.1 General Experimental Information	89
6.2 General Experimental Procedures.....	90
6.2.1 Preparation of the starting materials	90
6.2.1.1 Preparation of the <i>N</i> -tosyl-protected aniline.....	90
6.2.1.2 Preparation of the <i>N</i> -tosyl-propargyl aniline (Compounds 46a-o) ¹	93

6.2.1.3 Preparation of the <i>N</i> -acrylamides	96
6.2.1.4 Preparation of the <i>N</i> -benzyl-acrylamides (Compounds 48a-i)	98
6.2.1.5 General procedure for the photochemical intramolecular cyclization reaction 100	
6.2.1.5.1 Indole Synthesis	100
6.2.1.5.2 Oxindole Synthesis.....	105
7 Appendix	109

1 Introduction

1.1 Organic Photochemistry

Chemical transformations can be accomplished using various sources of energy, namely thermal, microwave, ultrasonic, electrochemical and light, among others. The energy source plays an important role in the development of any new chemical process, and more specifically, in the achievement targeted molecules in a more efficient and selective way. In the last few years, a higher specificity has been required from the energy source in terms of breaking and forming chemical bonds. In this context, light has become a key energy source among the several existing ones, as it fulfills most of the requirements for modern chemical transformations.⁴

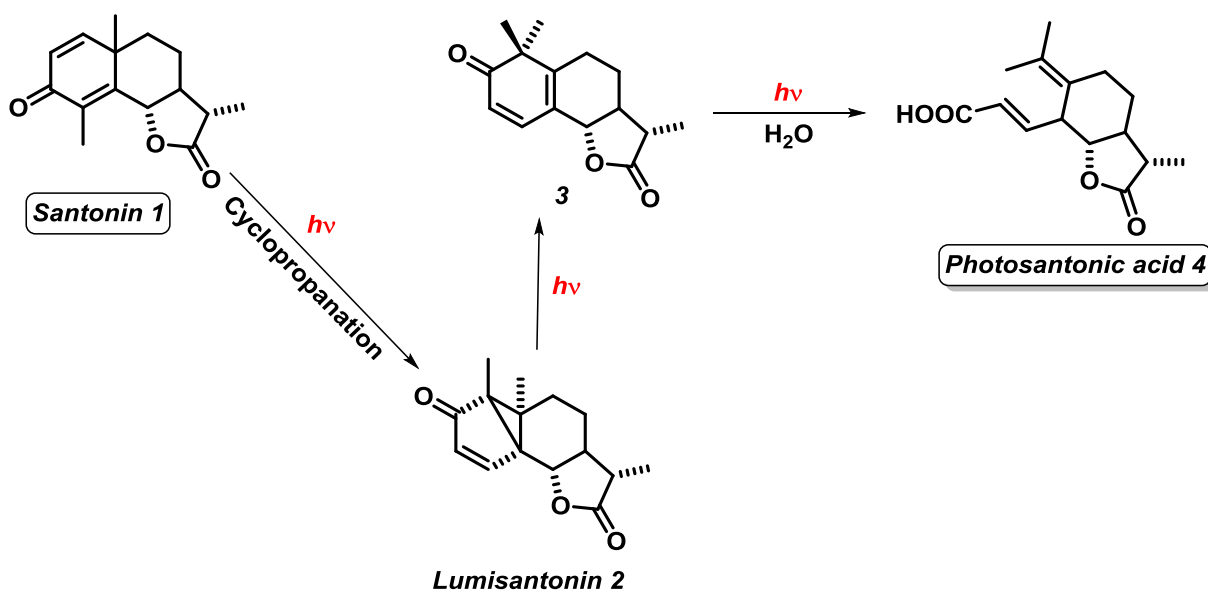
Light has long been used as an energy source in chemical process, but only in the 1960s it has found applications in the promotion of organic transformations, and as a result, many useful and fascinating reactions were uncovered. As a consequence, photochemistry is currently an important synthetic tool that enables the synthesis of fine chemicals.⁵ However, the direct use of visible light in organic reactions is limited owing to the ability of organic molecules to absorb photons in the visible spectra. In order to solve this long-standing problem, many photo-catalysts such as metals (Ru, Ir, Rh) and dyes have been exploited.⁶

⁴ PITRE, S. P.; MCTIERNAN, C. D.; SCAIANO, J. C. "Understanding the Kinetics and Spectroscopy of Photoredox Catalysis and Transition-Metal-Free Alternatives". *Acc. Chem. Res.*, **49**: 1320, 2016.

⁵ (a) HOFFMANN, N. "Photochemical Reactions as Key Steps in Organic Synthesis". *Chem. Rev.* **108**: 1052, 2008. (b) XUAN, J.; XIAO, W. J. "Visible-light photoredox catalysis". *Angew. Chem. Int. Ed.*, **51**: 6828, 2012. (c) CAREY, A. F.; SUNDBERG, R. J. *Advanced Organic Chemistry*, 5th ed., Springer, 2007.

⁶ (a) YOON, T. P.; ISCHAY, M.; DU, J. "Visible light photocatalysis as a greener approach to photochemical synthesis". *Nat. Chem.*, **2**: 527, 2010. (b) BRACHET, E.; GHOSH, T.; GHOSH, I.; KÖNIG, B. "Visible light C–H amidation of heteroarenes with benzoyl azides". *Chem. Sci.*, **6**: 987, 2015. (c) XIAO, Q. H.; JIA, R. C.; QIANG, W.; FENG, L. L.; QIAO, H. D.; ANDRÉ, M. B.; WEN, J. X. "Photocatalytic Generation of N-Centered Hydrazonyl Radicals: A Strategy for Hydroamination of β , γ -Unsaturated Hydrazones". *Angew. Chem. Int. Ed.*, **53**: 12163, 2014. (d) KARAKAYA, I.; PRIMER, D. N.; MOLANDER, G. A. "Photoredox Cross-Coupling: Ir/Ni Dual Catalysis for the Synthesis of Benzylic Ethers". *Org. Lett.*, **17**: 3294, 2015. (e) TUCKER, J. W.; NGUYEN, J. D.; NARAYANAM, J. M. R.; KRABBE, S. W.; STEPHENSON, C. R. J. "Tin-free radical cyclization reactions initiated by visible light photoredox catalysis". *Chem. Commun.*, **46**: 4985, 2010. (f) FARNEY, E. P.; YOON, T. P. "Visible-light sensitization of vinyl azides by transition-metal photocatalysis". *Angew. Chem. Int. Ed.*, **53**: 793, 2014. (g) YASU, Y.; ARAI, Y.; TOMITA, R.; KOIKE, T.; AKITA, M. "Highly regio- and diastereoselective synthesis of CF₃-substituted lactones via photoredox-catalyzed carbolactonization of alkenoic acids". *Org. Lett.*, **16**: 780, 2014.

A remarkable example and perhaps the earliest known photoreaction involving an organic compound is that of Santonin (**1**). Since its first exposure to sunlight in 1834 by Hermarin Trommsdorff, curious observations related to the changes in its physical properties have been made, showing the extent of the interaction between light and matter. This case triggered the interest of many researchers regarding the investigation of Santonin photoproducts. In this way, the Santonin photoproducts were completely understood and elucidated in 1950s and 1960s, completing the photochemical puzzle that dated back to the 1830s. The three photoproducts of this process, which are lumisantoinin (**2**), its isomer (**3**), and photosantoninic acid (**4**), are showed in Scheme 3.⁷

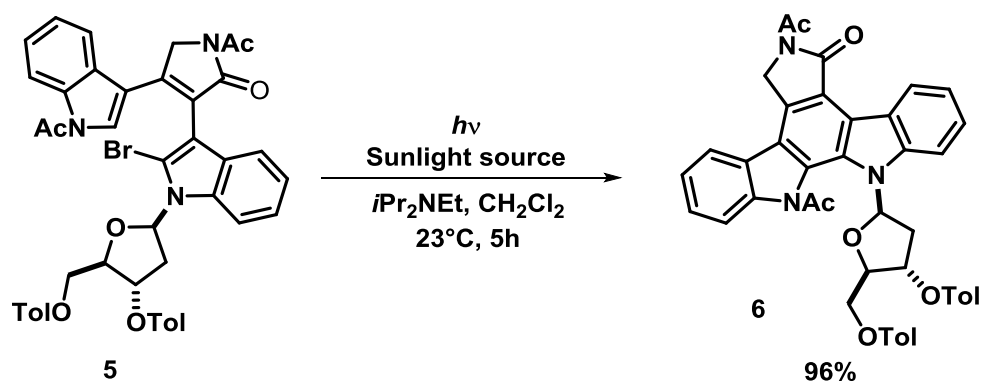


SCHEME 3: Santonin: Photochemical modifications.

The discovery of the photoproducts from Santonin was an important breakthrough in the course of organic photochemistry and paved the way for a variety of procedures that elucidated the interaction between matter and light. Fukuyama et.al, for instance, disclosed the photochemically induced cyclization reaction of the brominated indole (**5**) to achieve the product (**6**) in quantitative yield (Scheme 4).⁸

⁷ ROTH, H. D. "The Beginnings of Organic Photochemistry". *Angew. Chem. Int. Ed.*, **28**: 1193, 1989.

⁸ KOBAYASHI, Y.; FUJIMOTO, T.; FUKUYAMA, T. "Stereocontrolled total synthesis of (+)-K252a". *J. Am. Chem. Soc.*, **121**: 6501, 1999.



SCHEME 4: Cyclization reaction mediated by sunlight.

1.2 Excited States

Following the concepts of light-matter interaction, organic molecules may absorb light and reach electronically excited states. As a result of such excitation, the distribution of electrons in the molecule become significantly different when compared to its ground state. Consequently, molecules in the excited state present different properties than that of the ground state, particularly the reactivity; since the excited states characterize new energetic levels for the molecules, the generation of new reactive centers in the electronically excited species gives rise to a broadening in the reaction spectrum.⁵

The energy supplied by a particular wavelength of light can be calculated from the fundamental Planck's equation:

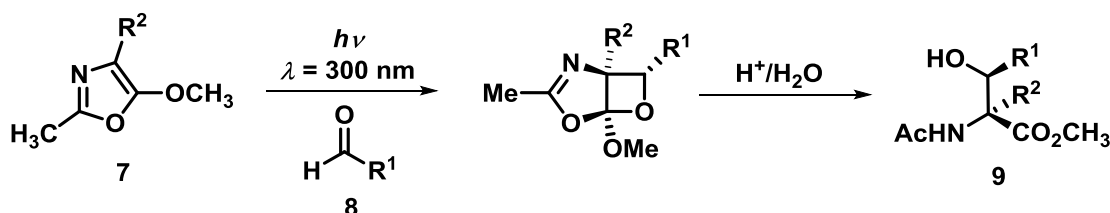
$$E = h\nu = h \frac{c}{\lambda}$$

In this equation, E is the energy of a light particle, the so-called photon, ν is the frequency of the radiation, h the Planck's constant, c the speed of light and λ the wavelength of the radiation. Replacing the constants h and c in the second form of the equation, the energy of the radiation can be easily calculated in kcal mol^{-1} using the following equation:

$$E = 2.86 \times 10^4 / \lambda$$

The electromagnetic radiation with wavelengths ranging from 800 nm (near infrared) to 150 nm (far UV) is the one primarily used in photochemistry, as this range corresponds to photon energies varying from 37 to 200 kcal mol⁻¹; for example, the light with a 254 nm wavelength affords 112.6 kcal mol⁻¹ of energy, which is enough to break most single bonds.⁵

In this context, several reports can be found in literature demonstrating how efficiently organic molecules interact with light and absorb it. A very interesting example of the application of this phenomena are [2+2] photocycloadditions, a class of reactions that affords cyclobutanes. The study of the intermediates as well as final products of this reaction are a very well developed field in organic synthesis.⁹ Lex et al., for instance, reported a photochemical protocol followed by a sequential hydrolysis step to achieve α -amino- β -hydroxy carboxylic esters (**9**) from 5-methoxyoxazoles (**7**), and aldehydes (**8**) as showed in Scheme 5.¹⁰



SCHEME 5: [2+2] Photocycloaddition reaction.

Since the reactivity of the molecules changes considerably when exposed to light irradiation, the comprehension of these excited species and their further transformations have become a very attractive subject. The fundamentals of this chemistry rely on important events e.g. light absorption, light emission (luminescence), and excited-state reactions (electron transfer, energy transfer, and bond breaking).^{5, 11}

⁹ (a) PATAI Series: *The Chemistry of Functional Groups*; Rappoport, Z., Series Ed.; Wiley: Chichester, 2005; *The Chemistry of Cyclobutanes Parts 1 and 2* (Rappoport, Z., LIEBMAN, J. F.). (b) NAMYSLO, J. C.; KAUFMANN, D. E. "The application of cyclobutane derivatives in organic synthesis". *Chem. Rev.*, **103**: 1485, 2003.

¹⁰ GRIESBECK, A. G.; BONDOCK, S.; LEX, J. "Synthesis of erythro- α -amino β -hydroxy carboxylic acid esters by diastereoselective photocycloaddition of 5-methoxyoxazoles with aldehydes". *J. Org. Chem.*, **68**: 9899, 2003.

¹¹ (a) COYLE, J. D. *Introduction to Organic Photochemistry*. John Wiley & Sons Ltd, 1989. (b) WARDLE, B. *Principles and Applications of Photochemistry*. John Wiley & Sons Ltd, 2009. (c) KLÁN, P.; WIRZ, J. *Photochemistry of Organic Compounds*. John Wiley & Sons Ltd, 2009. (d) PAVIA, D. L.; LAMPMAN, G. M.; KRIS, G. S.; VYVYAN, J. R. *Introduction to Spectroscopy*. 4^a ed., 2001 Brooks/Cole, Cengage Learning, 2009.

When a molecule absorbs light in the UV-Vis region, an electron is promoted from the highest-energy occupied molecular orbital (HOMO) to the lowest-energy unoccupied molecular orbital (LUMO), which results in an excited state molecule. One requirement for a molecule to absorb light is that the energy of the photon matches the energy difference between the orbitals, $\Delta E = E_{\text{photon}} = h\nu = hc/\lambda$; photons having insufficient energy will be transmitted. Therefore, the absorbance of light in different wavelengths provides invaluable experimental information about the energy difference and spacing between orbitals.¹¹

In the view that the molecules possess many occupied and unoccupied molecular orbitals, there are many possible transitions to promote an electron from a higher-energy occupied to lower-energy unoccupied orbital. However, only a few of these molecular orbitals are involved in light absorption events. Based on the frontier molecular orbitals, the lowest-energy photon corresponds to the transition of an electron from the highest occupied molecular orbital (HOMO) to the lowest unoccupied molecular orbital (LUMO). The HOMO-LUMO energy gap (ΔE) typically determines the color of light seen transmitted through a solution. Transitions of an electron from lower-energy occupied orbitals into higher-energy unoccupied orbitals necessarily require higher-energy photons. Figure 1 shows an example of a HOMO-LUMO excitation.¹¹

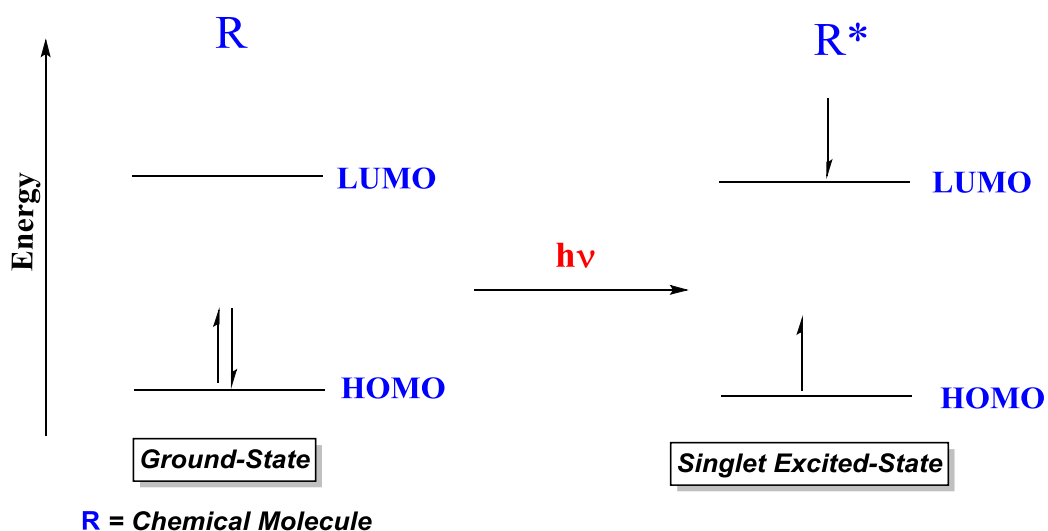


FIGURE 1: HOMO-LUMO diagram.

The second requirement for light absorption is that the electron spin remains unchanged. Most molecules possess an even number of electrons that are present in a paired form in the ground state (notably with the exceptions of O₂ and

many transition metal ions). The highest energy electrons occupy the HOMO and these electrons are paired with opposite spin ($+\frac{1}{2}$, $-\frac{1}{2}$), being the total spin of the electrons $S = 0$ and the multiplicity of the ground state a singlet.¹¹

The excitation of a photon having an energy that corresponds to the HOMO-LUMO energy gap would result in an excited state that is also a singlet. In a singlet excited state (S) the excited electrons retain opposite spins, while in triplet excited states (T) they have parallel spins. Thus, both excited states could happen during the electronic excitation. However, it is important to mention that the electrons do not undergo spin inversion at the time of the excitation, since it is forbidden by quantum mechanical selection rules, which state that there must be the conservation of spin during the excitation process. Subsequent spin state changes may occur, but as separate events from excitation. In the initial excited state, the unpaired electrons have opposite spins, and therefore, are in a singlet state (S). Thus, a very short time (10^{-15} s) is usually required for excitation, during which the molecule does not undergo any nuclear changes and there is also no change in the spin state of the promoted electron. After the excitation, however, these changes may occur rapidly.¹¹

When an electron excitation takes place, many events known as photophysical/chemical processes may occur. Such processes are related to the behavior of the electron when it goes back to the ground state after a photoexcitation. These pathways are explained below in the Jablonski diagram (Figure 2).^{11, 12}

The events in the diagram can be explained as follows:¹³

- I. A molecule in the S_1 state can cascade down through the vibrational levels of the S_0 state and thus return to the ground state by releasing its energy in small increments to the environment, though this process is generally very slow because of the large amount of energy. The process is called internal conversion (IC). As it is slow proceeds, most molecules in the S_1 state can adopt other returning pathways.

¹² ZIMMERMANN, J.; ZEUG, A.; RODER, B. "A generalization of the Jablonski diagram to account for polarization and anisotropy effects in time-resolved experiments". *Phys. Chem. Chem. Phys.*, **5**: 2964, 2003.

¹³ SMITH, M. B.; MARCH, J. *Advanced Organic Chemistry: Reactions, Mechanism, and Structure*. 5^a ed.; John Wiley & Sons Ltd, 2001.

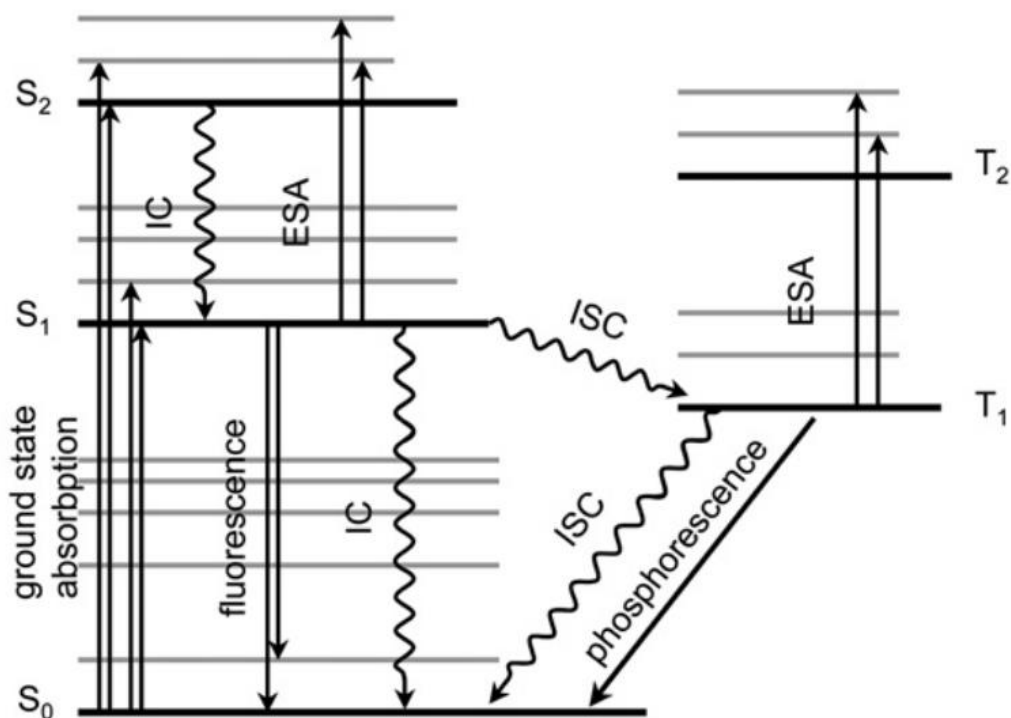
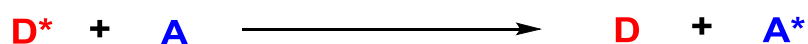


FIGURE 2: Energy level diagram and summary of photochemical processes (Jablonski diagram: IC – internal conversion, ESA – excited state absorption, ISC – intersystem crossing).

- II. A molecule in the S₁ state decrease to some low vibrational level of the S₀ state at once by releasing the absorbed energy in the form of light. This process, which generally happens within 10⁻⁹ s, is called fluorescence. Due to the possibility of fluorescence, either the chemical reaction of the S₁ state must take place very fast or fluorescence will occur before the reaction.
- III. Mostly molecules (not all) in the S₁ state can undergo an intersystem crossing (ISC) to the lowest state, the triplet T₁. The intersystem crossing from the singlet to the triplet state is a “forbidden” pathway on account of the angular momentum, but it often occurs by compensations elsewhere in the system. Since intersystem crossing occurs without loss of energy and the singlet state often has a higher energy than the corresponding triplet state, the energy must be somehow eliminated. The higher probability for this process to happen is when the S₁ molecule crosses to a T₁ state at a high vibrational level and then cascade down from the T₁ to its lowest vibrational level. This cascade process is very fast (10⁻¹² s). When T₂ or higher states are populated, they also rapidly cascade to the lowest vibrational level of T₁ state.

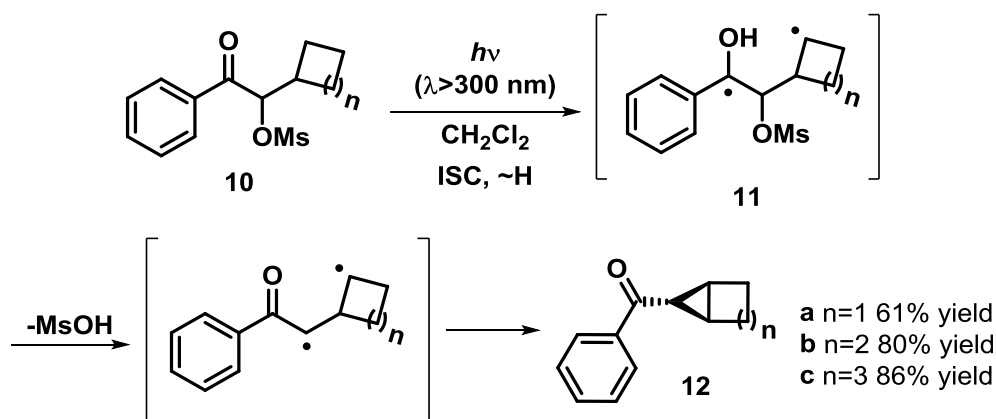
- IV. A molecule in the T_1 state may return to the S_0 state by releasing heat (intersystem crossing) or light, which is known as phosphorescence. It is well known that the angular momentum difficulty exists in this form in a way that both intersystem crossing and phosphorescence are very slow (approximately 10^{-3} – 10^{-1} s). This means that T_1 states generally have much longer lifetimes than S_1 states. When they occur in the same molecule, phosphorescence is found at lower frequencies than fluorescence (because of the higher difference in energy between S_1 and S_0 than between T_1 and S_0) and is longer lived (because of the longer lifetime of the T_1 state).
- V. If none of the above possibilities takes place, a molecule in an excited state (S_1 or T_1) may transfer its excess energy all at once to another molecule in the close environment, in a process called photosensitization. The excited molecule (D, for donor) thus drops to S_0 while other molecule (A, for acceptor) becomes excited:



Thus, there are two ways for a molecule to reach an excited state: (1) by absorption of a quantum of light or (2) by energy transfer from a previously excited molecule. The donor molecule D is also called a photosensitizer.

Scheme 6 shows an example of the use of intersystem crossing to promote a photochemical reaction. In this case, a route for the synthesis of cyclopropanes (**12**) from 2-cycloalkaneacetophenones (**10**) was reported; the reaction proceeds via the 1,4-biradical intermediate (**11**), which is formed from the irradiation of **10** with light through an intersystem crossing (ISC). Next, the elimination of the leaving group followed by a cyclization step yields the cyclopropane derivative as the final product.¹⁴

¹⁴ PRIV-DOZ, P. W.; MÜHLING, O. "A new photochemical route to cyclopropanes". *Angew. Chem. Int. Ed.*, **40**: 1064, 2001.



Scheme 6: Photochemical route to access cyclopropane systems.

The photochemical transformations always occur following the laws of photochemistry.¹¹ The two fundamental laws for photochemical reactions are given below:¹¹

1. 1st law of photochemistry: only the light absorbed by a molecule is responsible for promoting a photochemical modification in the molecule. Also known as Grotthuss-Draper law, it emphasizes the importance of the absorption of light by the molecule involved in the primary photo process, which may be a chemical reaction or a physical process involving directly excited species. All of the aspects and consequences of this law must be considered for the quantitative analysis of a photoreaction.¹¹
2. 2nd law of photochemistry: only one molecule is excited for each quantum of radiation absorbed. This law was formulated in the beginning of 20th century at the emerging time of quantum theory and is also known as Stark-Einstein law. In other words, it affirms that the absorption of light by a molecule is a one-photon process. Therefore, for a primary photo process, only one molecule reacts for each photon absorbed.¹¹

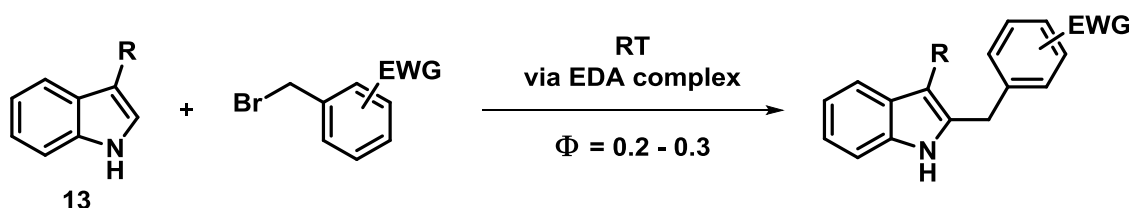
In this context, another very important concept in photochemistry is the quantum yield, which is related to photochemical kinetics. The quantum yield, also called the quantum efficiency, is defined as the number of events that occur per absorbed photon. These events might be related to physical processes that are responsible for energy dissipation and also to molecules formed upon photo irradiation. Generally, the (total) quantum yield of a photoreaction, Φ , is:¹¹

$$\Phi = \frac{\text{number of molecules undergoing the reaction of interest}}{\text{number of photons absorbed by the photoreactive substance}}$$

The above equation defines the quantum yield of product formation, Φ_p , but it can also be expressed in terms of rates if it is measured per units of time.¹¹

$$\Phi = \frac{\text{rate of the reaction of interest}}{\text{rate of light absorption by photoreactive substance}}$$

An interesting example of the application of this concept was reported by Melchiorre's group, which used quantum yield measurements to evaluate the photochemical alkylation of indoles **13** (Scheme 7). Their calculations showed that the process displayed a quantum yield (Φ) of 0.2 - 0.3 at 450 nm wavelength; in other words, between 20 – 30% of the molecules underwent photochemical transformations under the radiation incident in the system.¹⁵



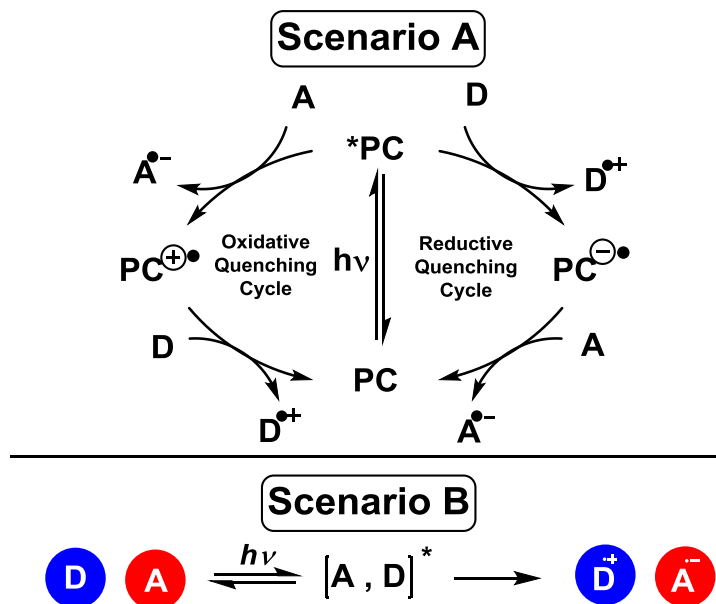
SCHEME 7: Photochemical alkylation of indoles driven by an EDA complex.

1.3 Electron Donor-Acceptor Complex

As previously discussed, the light-matter interaction has the potential of generating new electronically charged species by means of electron excitation prior to a chemical transformation. However, since organic molecules often do not absorb in the visible light region, there are two possible scenarios to achieve the formation of charged (or radical) species: (A) by using an external photocatalyst (e.g., metal complexes with polyheteroaryl ligands or organic dyes) and (B) by the formation of a

¹⁵ KANDUKURI, S. R.; BAHAMONDE, A.; CHATTERJEE, I.; JURBERG, I. D.; ESCUDERO-ADÁN, E. C.; MELCHIORRE, P. "X-ray characterization of an electron donor-acceptor complex that drives the photochemical alkylation of indoles". *Angew. Chem. Int. Ed.*, **54**: 1485, 2015.

diffusion-controlled ground-state association between an electron-rich species (the donor, D) and an electron-poor species (the acceptor, A), forming a complex known as EDA complex (also called charge-transfer, CT, complex), and in this case, the electron-transfer occurs without the need of an additional photocatalyst (Scheme 8).³



SCHEME 8: General representations for a photoinduced electron transfer mediated (A) a Photocatalyst and (B) Electron donor-acceptor (EDA complex).

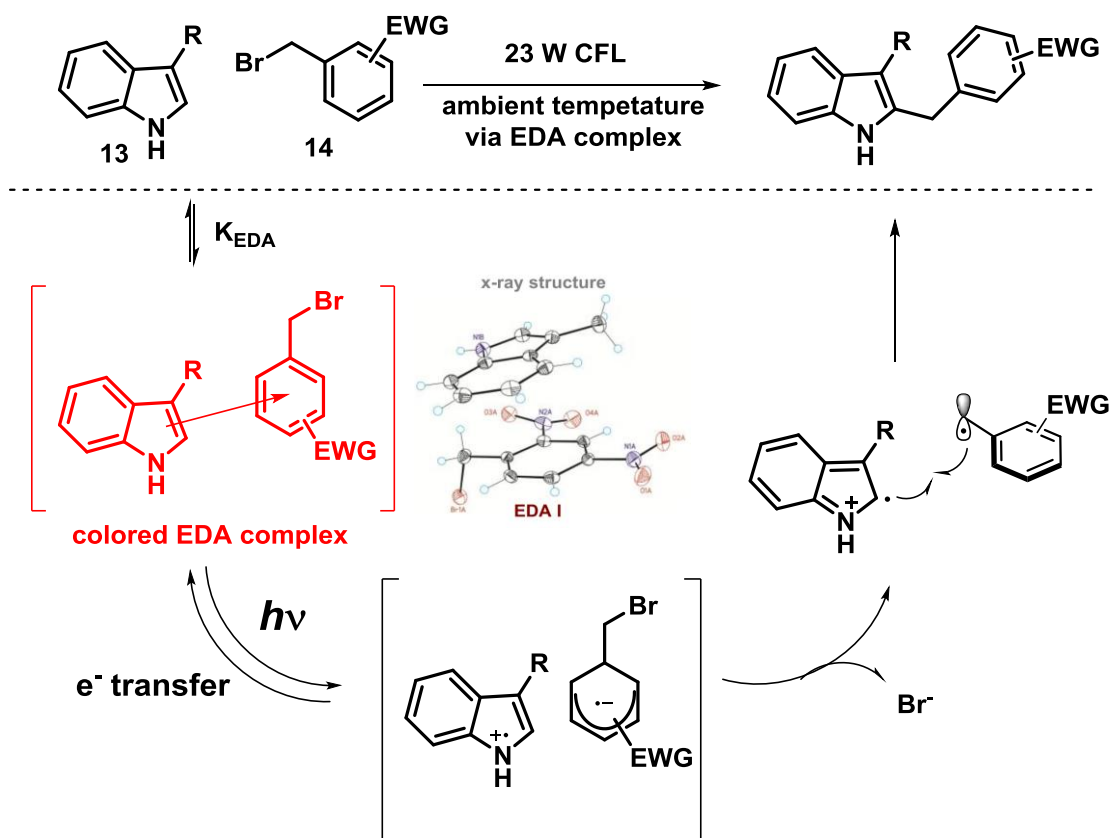
Electron donor-acceptor (EDA) complexes were introduced by Mulliken in the 1950s and are formed when molecules (or different parts of the same molecule) interact with each other in a manner where electrons are transferred from the donor to the acceptor.^{3,16} In these complexes, the resulting electrostatic attraction provides a stabilizing force for the molecular complex.³ This new molecular aggregation is generally associated with a marked color change and a new absorption band, the so-called charge-transfer band, which is not observed at the UV-vis absorption spectra of the individual components.

The formation of electron donor-acceptor complexes (or charge transfer complexes) happen because of a weak association of molecules or molecular subgroups. The association does not constitute a strong covalent bond and rely significantly on temperature, solvent and concentration.³

¹⁶ ROSOKHA, S. V.; KOCHI, J. K. "Fresh look at electron-transfer mechanisms via the donor/acceptor bindings in the critical encounter complex". *Acc. Chem. Res.* **41**: 641, 2008.

Although EDA complexes are considered key intermediates in several organic reactions, especially in single-electron transfer (SET) events, their use in organic synthesis is still rather limited, especially because electron transfers from donors to acceptors in EDA complexes are fast and reversible. However, some very interesting transformations have been achieved by the use of these complexes, e.g., the asymmetric alkylation, perfluoroalkylation and arylation of aromatic compounds.³
17

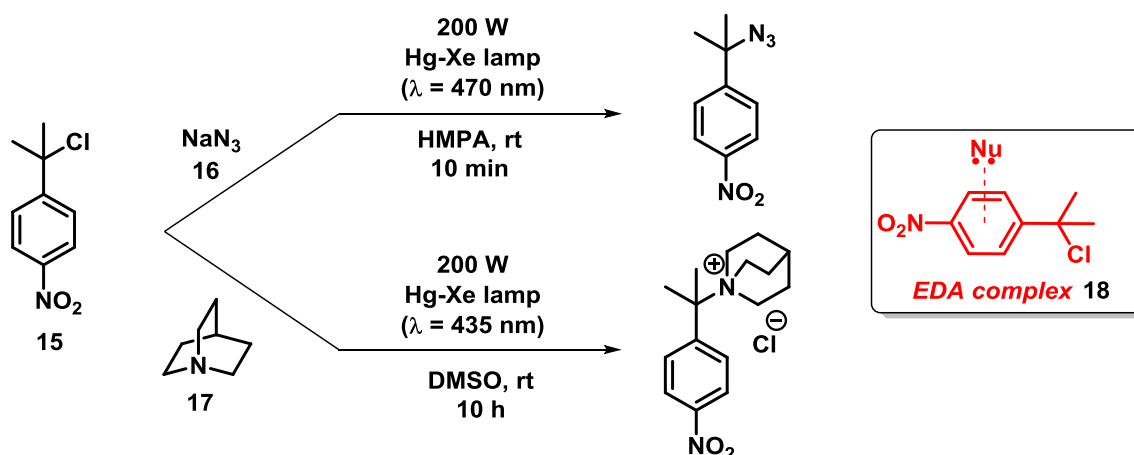
For example, the aforementioned photochemical alkylation of indoles (Scheme 9) consists on a metal-free strategy where an electron donor-acceptor complex generated upon association of substituted 1H-indoles (**13**) with electron-accepting benzyl and phenacyl bromides (**14**) promotes the reaction. Scheme 9 shows in detail the EDA complex that drives the alkylation, as well as the subsequent electron transfer between the species. Interestingly, the group was able to prove the existence of such complex by x-ray single crystal characterizations.¹⁵



SCHEME 9: Alkylation of indoles driven by an EDA complex.

¹⁷ CHENG, Y.; YUAN, X.; MA, J.; YU, S. "Direct Aromatic C-H Trifluoromethylation via an Electron-Donor-Acceptor Complex". *Chem. Eur. J.*, **21**: 8355, 2015.

One of the seminal reports on the synthetic applications of EDA complexes includes radical-nucleophilic substitution ($S_{RN}1$) reactions, which generally involves a mechanism with a radical chain propagation step. Scheme 10 shows the reaction between *p*-nitrocumyl chloride (**15**) and sodium azide (**16**) or quinoclidine (**17**), which occurs via a radical substitution reaction promoted by the photoexcitation of the EDA complex **18**).^{3, 18}



SCHEME 10: Radical-nucleophilic substitution reactions mediated by EDA complexes.

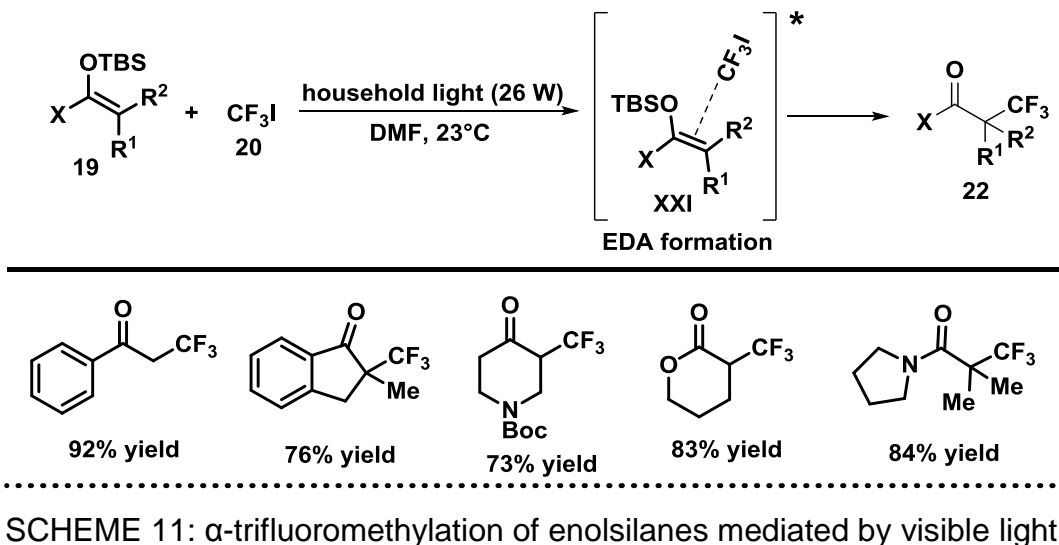
Another interesting application of EDA complexes was disclosed by MacMillan's group in 2011, in which enolsilanes, a very important class of reaction intermediates and precursors, were submitted to trifluoromethylation reactions. In this work, silylketene acetal (**19**) and CF_3I (**20**) were submitted to irradiation using a household light bulb, giving rise to the α -trifluoromethylated products (**22**) through the photoexcitation of EDA complex (**21**), as showed in Scheme 11.^{3, 19}

Chatani's group also reported an efficient methodology for the arylation of arenes and heteroarenes (**23**) using diaryliodonium salts (**24**) employing visible light. They observed that Ar_2I^+ could easily react in the presence of arenes and heteroarenes to form a new carbon-carbon bond under white LED irradiation. Interestingly, the reaction occurred even in the absence of a photocatalyst and in such conditions the pyrrole scaffold provided the best results; in order to explain the arylation reaction of

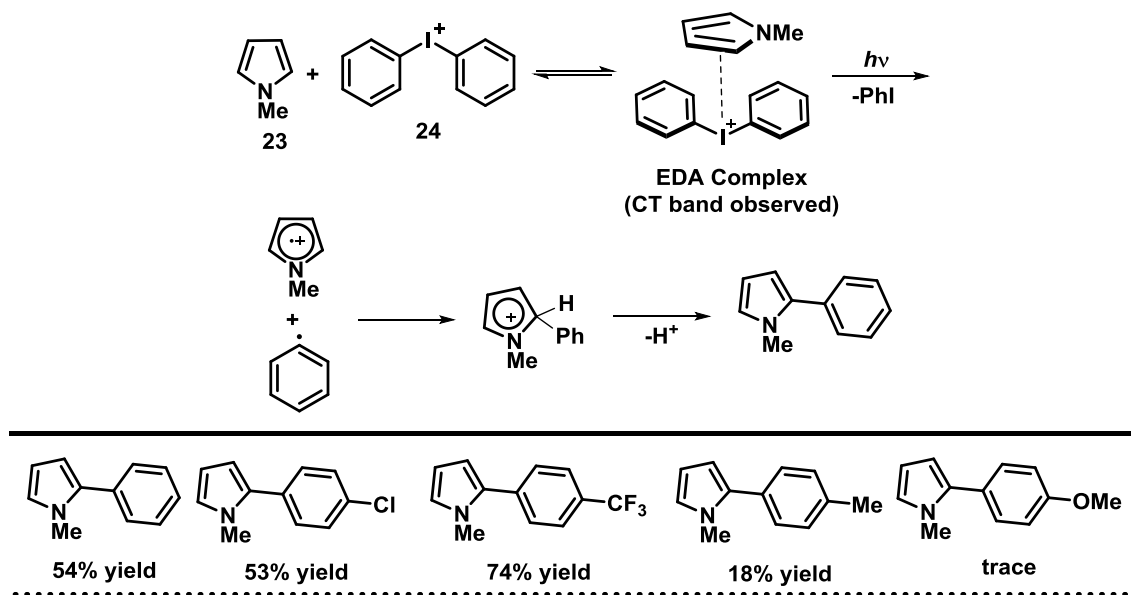
¹⁸ WADE, P. A.; MORRINSON, H. A.; KORNBLUM, N. "The Effect of Light on Electron-Transfer Substitution at a Saturated Carbon Atom". *J. Org. Chem.*, **52**: 3102, 1987.

¹⁹ PHAM, P. V.; NAGIB, D. A.; MACMILLAN, D. W. C. "Photoredox Catalysis: A Mild, Operationally Simple Approach to the Synthesis of α -Trifluoromethyl Carbonyl Compounds" *Angew. Chem. Int. Ed.*, **50**: 6119, 2011.

pyrrole with and without a photocatalyst, the authors proposed two possible mechanisms in which both lead to the product.



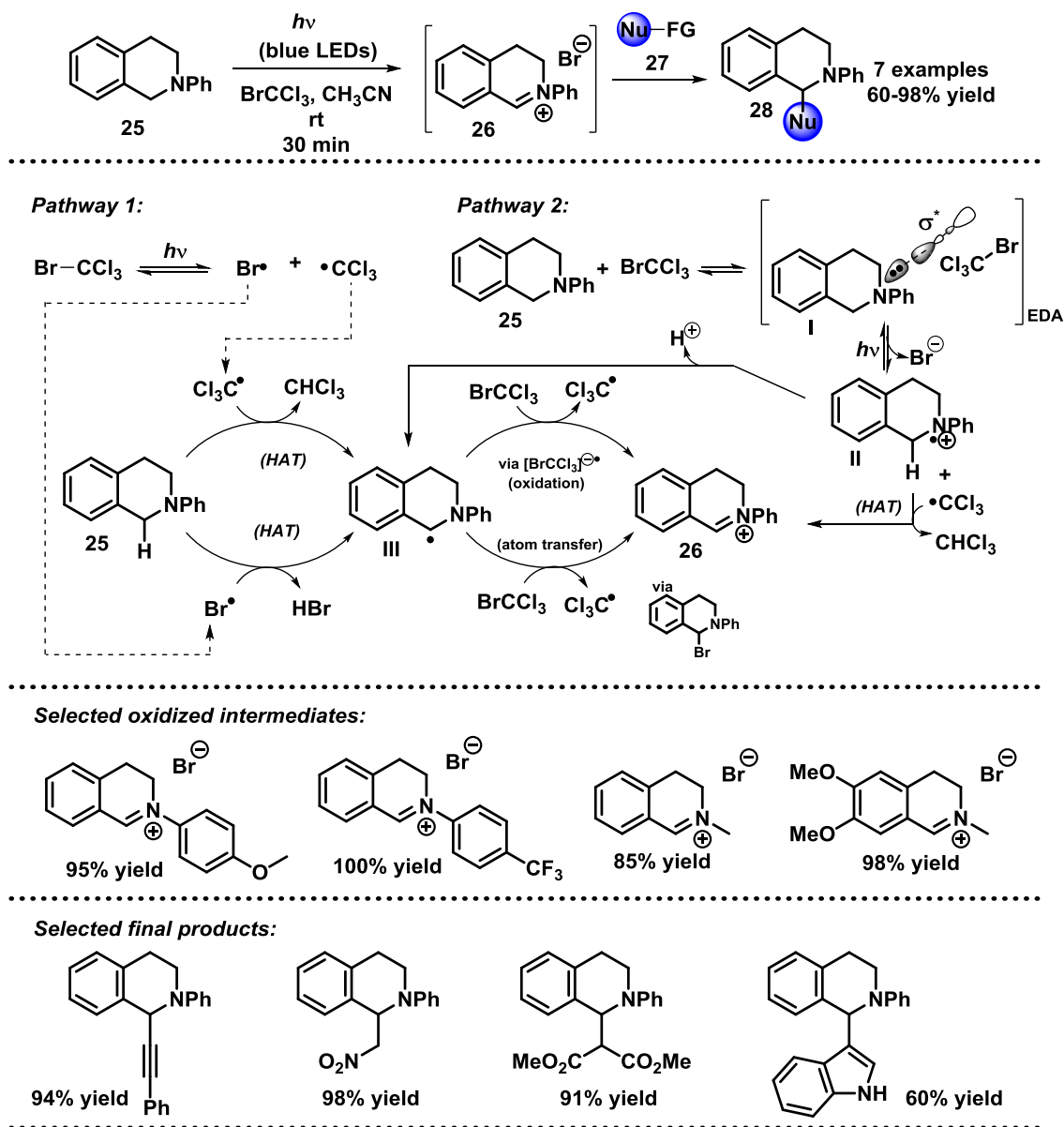
In this report, UV experiments of the reagents both separately and mixed were able to characterize the charge-transfer interaction between the molecules by the observation of a new absorption band in the UV-Vis spectrum. Therefore, the authors proposed a mechanism through an EDA complex (Scheme 12).^{3, 20}



SCHEME 12: Visible light-mediated direct arylation of heteroarenes using diaryliodonium salts in the absence of a photocatalyst.

²⁰ TOBISU, M.; FURUKAWA, T.; CHATANI, N. "Visible Light-mediated Direct Arylation of Arenes and Heteroarenes Using Diaryliodonium Salts in the Presence and Absence of a Photocatalyst" *Chem. Lett.*, **42**: 1203, 2013.

In order to extend the applications of EDA complexes as a tool in organic synthesis, Zeitler et al. reported the α -CH functionalization of tetrahydroisoquinolines (**25**) in the presence of BrCCl_3 . This methodology allowed the formation of an iminium ion intermediate (**26**) that can be trapped with different classes of nucleophiles (**27**) to produce the corresponding products (**28**).



SCHEME 13: Visible light mediated transformations with polyhalomethanes providing α -CH activation of tetrahydroisoquinoline.

Preliminary mechanistic experiments suggested two plausible pathways for this oxidation process: (i) firstly, the homolytic cleavage of BrCCl_3 under blue light irradiation (C-Br bond dissociation energy, BDE = 55.3 kcal.mol⁻¹), followed by a number of possible atom transfers/oxidations steps or (ii) an electron-transfer event

within the EDA complex (I) formed between BrCCl₃ and tetrahydroisoquinoline (characterized by a blue coloration and bathochromic shift in the UV-vis spectrum), to afford radical cation (II). This intermediate can either lose a proton to afford radical intermediate (III) which can undergo an atom-transfer or oxidation event to produce the compound (26), or it can undergo hydrogen atom transfer (HAT) to directly produce the same intermediate (26). Within these possible scenarios, chloroform was observed as a byproduct in the reaction mixture, pointing out that HAT must be operative in the present case (Scheme 13).^{3, 21}

1.4 Indole and Oxindole Synthesis

Nitrogen heterocycles are among the most significant structural units in pharmaceuticals the pharmaceutical industry.²² For instance, in a database built up by Njardarson's group of all U.S. FDA approved drugs,²³ up to 640 pharmaceuticals contained at least one nitrogen heterocycle. Remarkably, the indole scaffold was ranked in the ninth position among all the structures, which proves the importance of this core for biological applications. Scheme 14 shows some relevant structures containing the indole ring and their related activities.

Due to their marked pharmacological properties, since the first report on Fischer's indolization,²⁴ the synthesis and functionalization of indoles has been the focus of interest of many synthetic organic chemists, and therefore, numerous methods have been developed to this end. Key factors including starting material availability and functional group tolerance often drive which particular synthetic method is more suitable. In some cases, it may be difficult to control the specific substitution pattern in the indole ring by applying the standard indole-forming reactions; thus, new

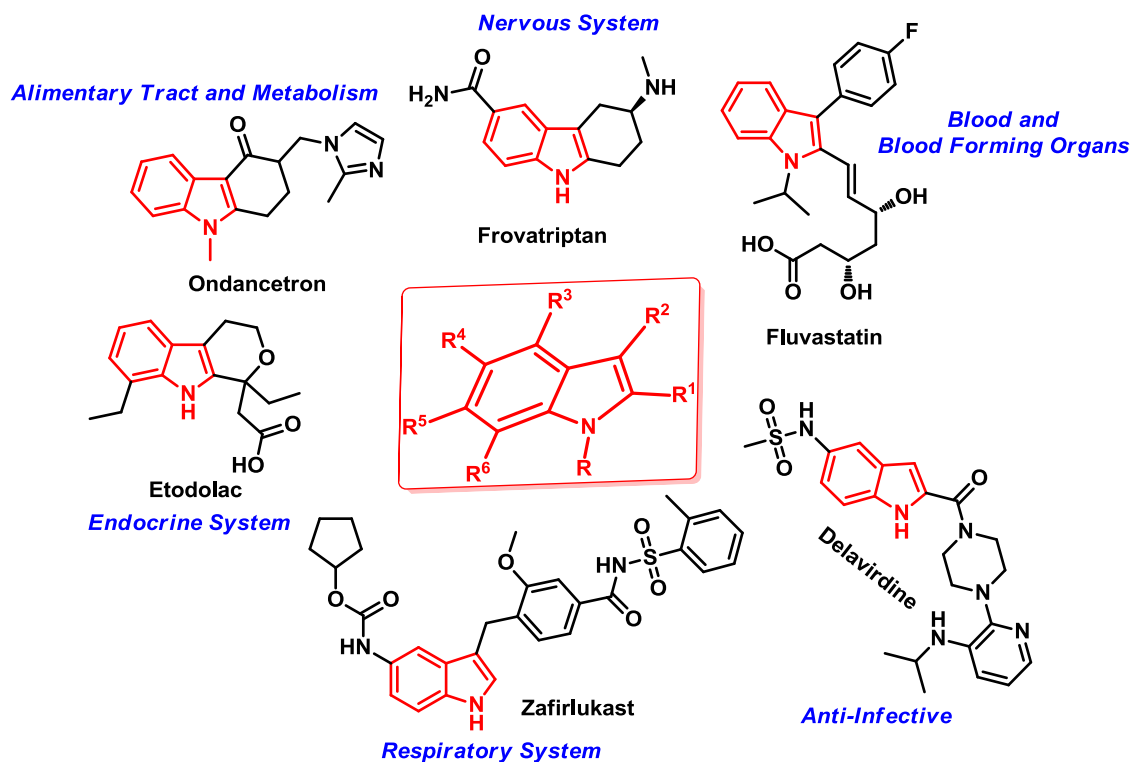
²¹ FRANZ, J. F.; KRAUS, W. B.; ZEITLER, K. "No photocatalyst required – versatile, visible light mediated transformations with polyhalomethanes" *Chem. Commun.*, **51**: 8280, 2015.

²² (a) TROFIMOV, B. A.; SOBENINA, L. N.; DEMENEV, A. P.; MIKHALEVA, A. I. "C-vinylpyrroles as pyrrole building blocks". *Chem. Rev.*, **104**: 2481, 2004. (b) BELINA, F.; ROSSI, R. "Synthesis and biological activity of pyrrole, pyrroline and pyrrolidine derivatives with two aryl groups on adjacent positions". *Tetrahedron*, **62**: 7213, 2006. (c) MARTINS, M. A. P.; FRIZZO, C. P.; MOREIRA, D. N.; ZANATTA, N.; BONACORSO, H. G. "Ionic liquids in heterocyclic synthesis". *Chem. Rev.*, **108**: 2015, 2008. (d) GULEVICH, A. V.; DUDNIK A. S.; CHERNYAK, N.; GEVORGYAN, V. "Transition Metal-Catalyzed Synthesis of Monocyclic Five-Membered Aromatic Heterocycles". *Chem. Rev.*, **113**: 3084, 2013.

²³ VITALU, E.; SMITH, D. T.; NJARDARSON, J. T. "Analysis of the structural diversity, substitution patterns, and frequency of nitrogen heterocycles among U.S. FDA approved pharmaceuticals". *J. Med. Chem.*, **57**: 10257, 2014.

²⁴ ROBINSON, B. "The Fischer indole synthesis". *Chem. Rev.*, **63**: 373, 1963.

methodologies are required to overcome this drawback. Additionally, it is worth mentioning that the indole ring is not only restricted to biological applications but also has application in other research areas, namely agrochemistry and material science.²⁵

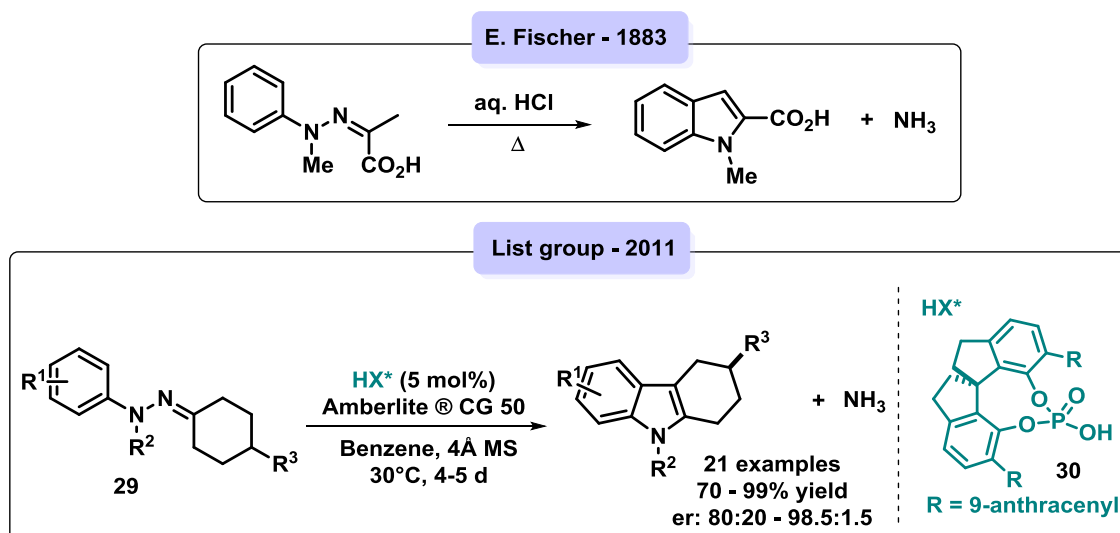


SCHEME 14: Pharmaceutical active compounds containing the indole scaffold.

Although various protocols have been reported in the last decades, the Fischer indolization is still one of the most widely used procedures for the synthesis of indoles. One of the most elegant methods for the indole synthesis was presented by List's group in 2011. They reported the first asymmetric catalytic Fischer indolization using 4-substituted cyclohexanone-derived phenylhydrazones (**29**) in the presence of 5 mol% of a novel spirocyclic phosphoric acid (**30**) using benzene as solvent (Scheme 15).²⁶

²⁵ VICENTE, R. "Recent advances in indole syntheses: New routes for a classic target". *Org. Biomol. Chem.*, **9**: 6469, 2011.

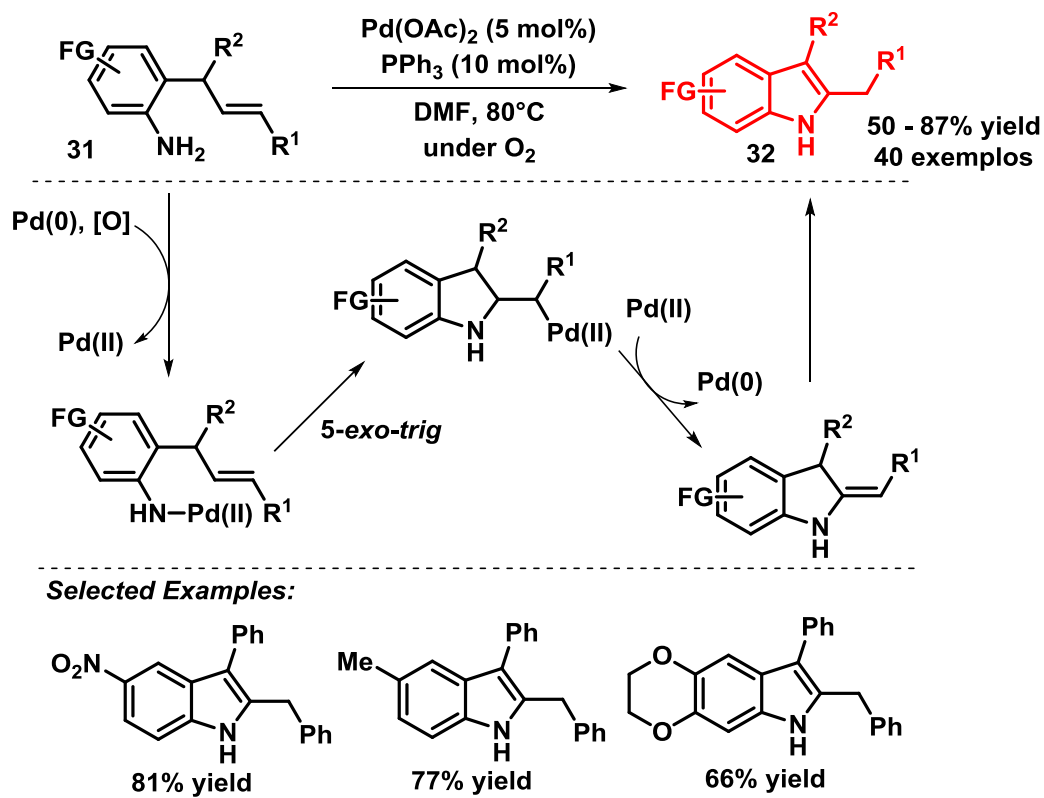
²⁶ MÜLLER, S.; WEBBER, M. J.; LIST, B. "The catalytic asymmetric Fischer indolization". *J. Am. Chem. Soc.*, **133**: 18534, 2011.



SCHEME 15: First catalytic asymmetric Fischer indolization.

Furthermore, the indole ring can be synthesized using catalytic organometallic compounds such as palladium, and copper complexes. In this scenario, Ghorai et. al. published in 2014 an efficient strategy for the synthesis of 3-substituted-2-benzylindoles (**32**) from *o*-allylanilines (**31**). The reaction occurred via a regioselective 5-*exo-trig* intramolecular oxidative cycloisomerization using Pd(OAc)₂ as catalyst and molecular oxygen as an oxidant (Scheme 16).²⁷

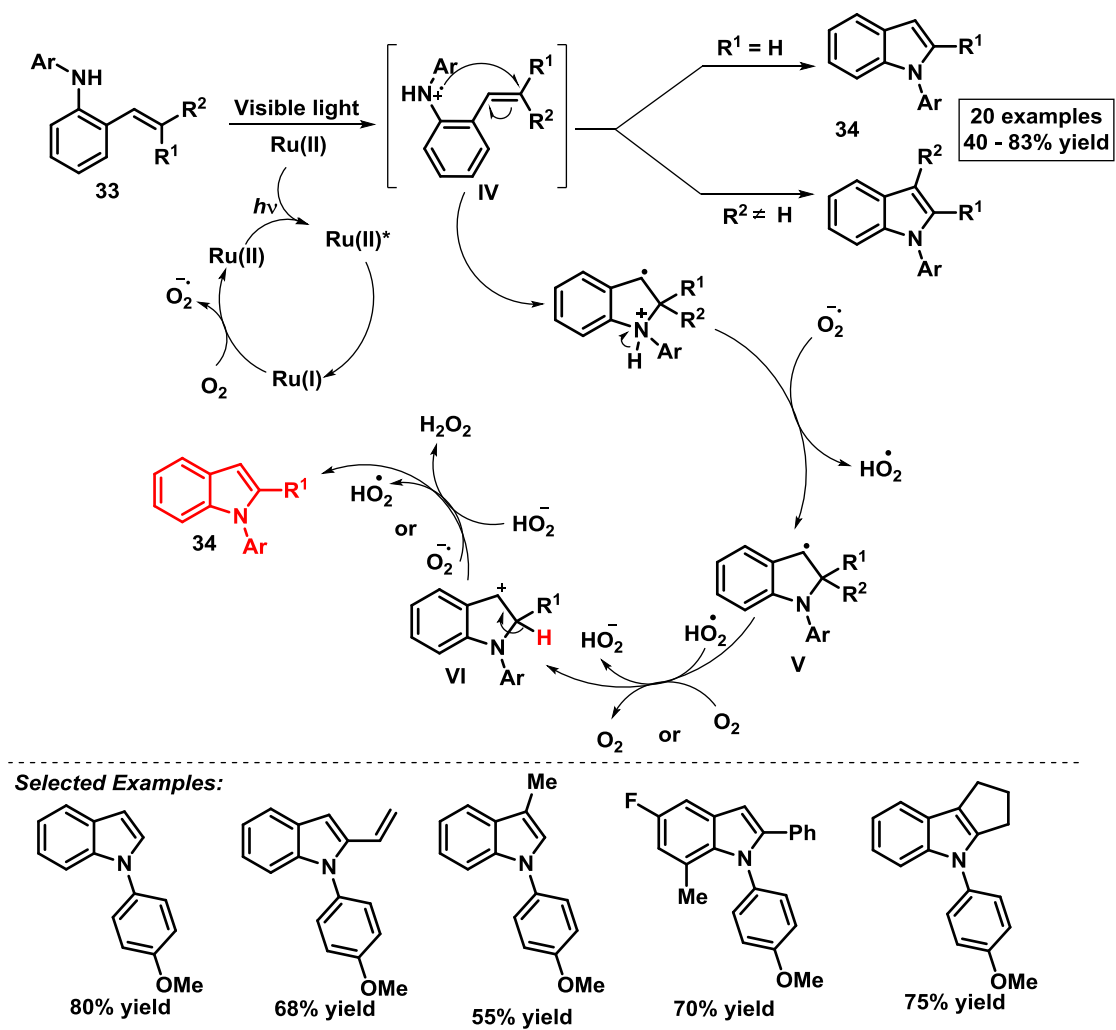
²⁷ NALLAGONDA, R.; REHAN, M.; GHORAI, P. "Synthesis of functionalized indoles via palladium-catalyzed aerobic oxidative cycloisomerization of *o*-allylanilines". *Org. Lett.*, **16**: 4786, 2014.



SCHEME 16: Synthesis of functionalized indoles via palladium-catalyzed aerobic oxidative cyclization.

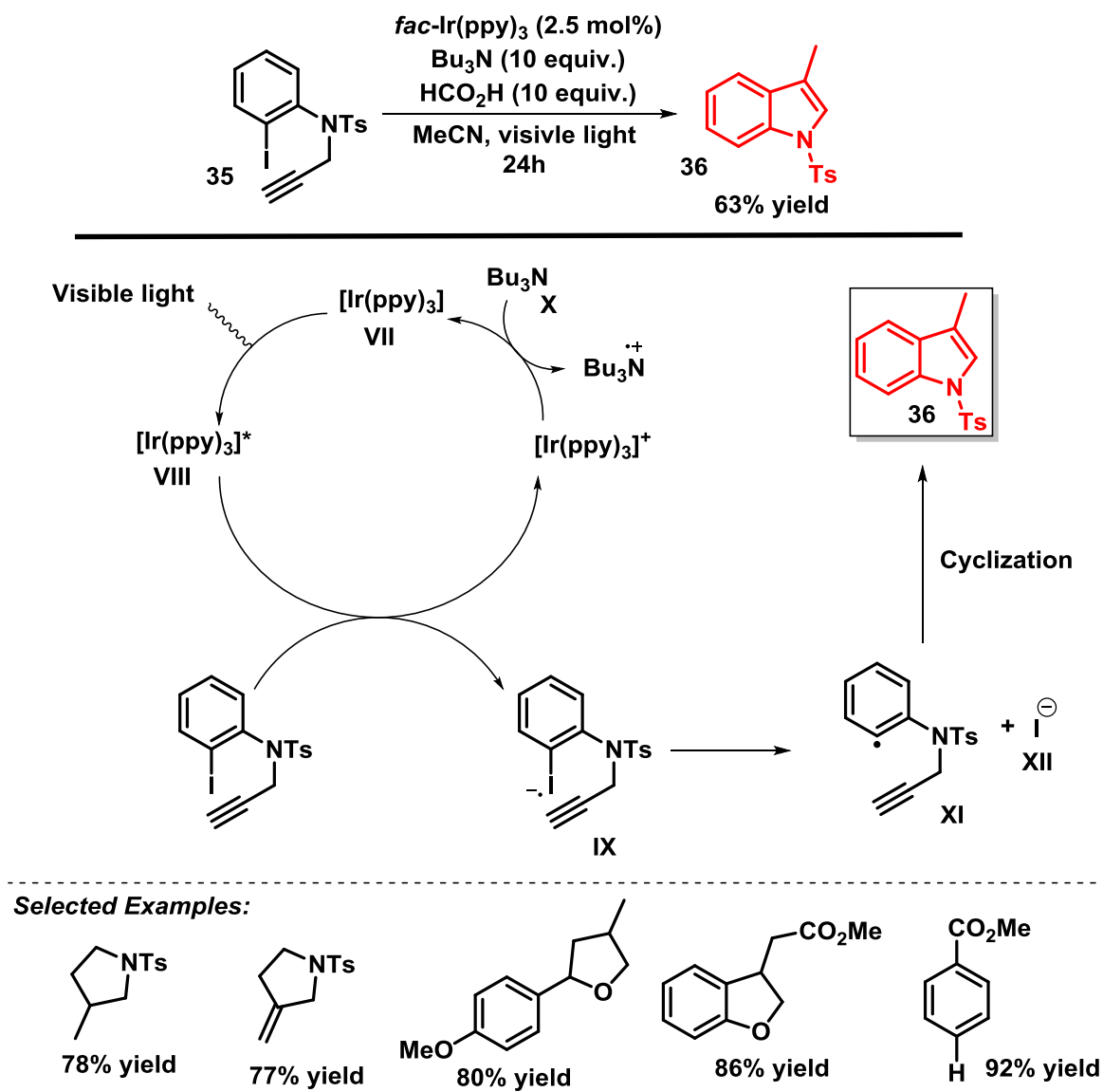
Another efficient approach was reported by Zheng et. al., which developed a visible-light photocatalysis strategy to achieve *N*-arylindoles (**34**) from styrylanilines (**33**) in a presence of ruthenium(II) as photocatalyst (Scheme 17). The main feature of this photocatalytic approach lies in the use of mild oxidative conditions to generate a nitrogen-centered radical cation (**IV**) from styryl anilines (**33**) using a photo-excited $[\text{Ru}(\text{bpz})_3](\text{PF}_6)_2$ complex. Next, the electrophilic addition of the nitrogen-centered radical cation (**IV**) to a tethered alkene generates the benzylic radical (**V**), which subsequently is oxidized to its corresponding benzylic cation (**VI**). The final step is the aromatization of the structure through deprotonation, forming indole (**34**).²⁸

²⁸ MAITY, S.; ZHENG, N. "A Visible-Light-Mediated Oxidative C-N Bond Formation/Aromatization Cascade: Photocatalytic Preparation of *N*-Arylindoles". *Angew. Chem. Int. Ed.*, **51**: 9562, 2012.



SCHEME 17: Proposed mechanism for the photocatalytic *N*-arylindoles synthesis.

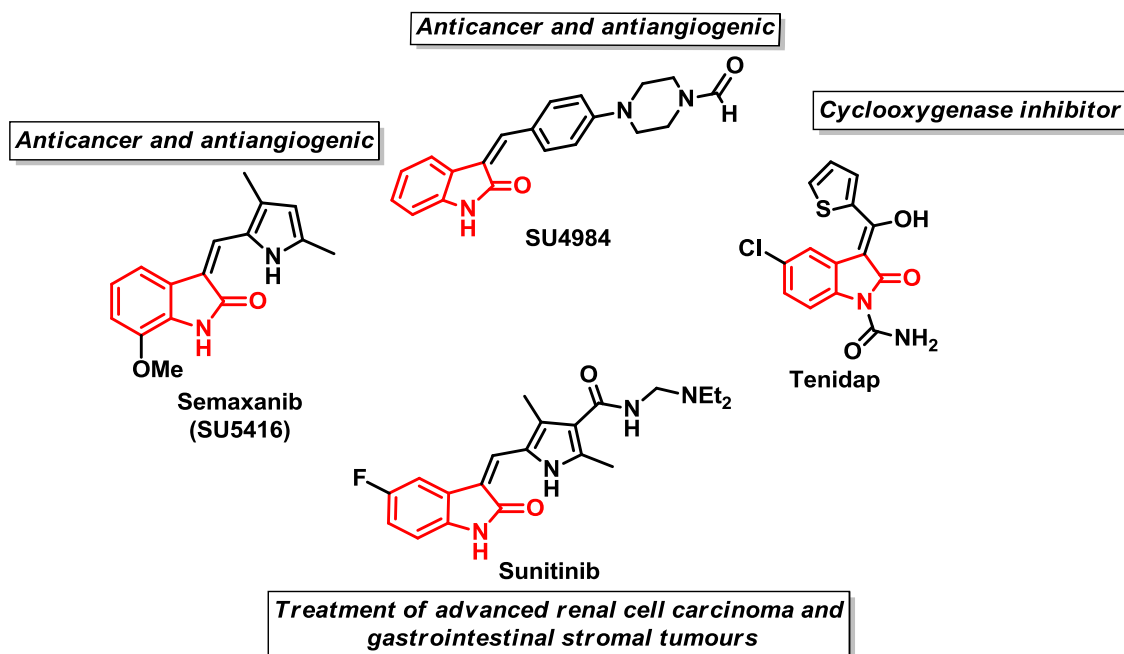
In a similar way, Stephenson's group has developed an attractive strategy to synthesize indoles (**36**) by using Ir(III) as a photocatalyst that generates radical species from the inactivated aryl iodides (**35**), as showed in Scheme 18.



Scheme 18: Reduction of aryl iodide and intramolecular reductive cyclization.

The proposed mechanism starts with the photoexcitation Ir(III) (**VII**) by visible light of which in its excited state (**VIII**) donates an electron to the carbon-iodine bond (**IX**) and reduced to its ground state (**VII**) by the tertiary amine (**X**). The carbon radical (**XI**) generated by the elimination of iodide (**XII**) undergoes a cyclization followed by abstraction of a hydrogen atom to give the cyclic product (**36**). This visible light photoredox-mediated radical reductive deiodination protocol was able to promote the reduction of alkyl, alkenyl and aryl iodides additionally to the discussed intramolecular reductive cyclization.¹ Although the methodology was applicable for several types of compounds, it has some lingering drawbacks, such as the dependence on a large excess of a tertiary amine as a sacrificial reagent.

Besides indoles, other *N*-heterocycle compounds such as oxindoles are also prominent structural motifs and have received great attention from the synthetic organic chemist's community, mostly because they can be found in numerous natural products and pharmaceutically active compounds (Scheme 19).²⁹

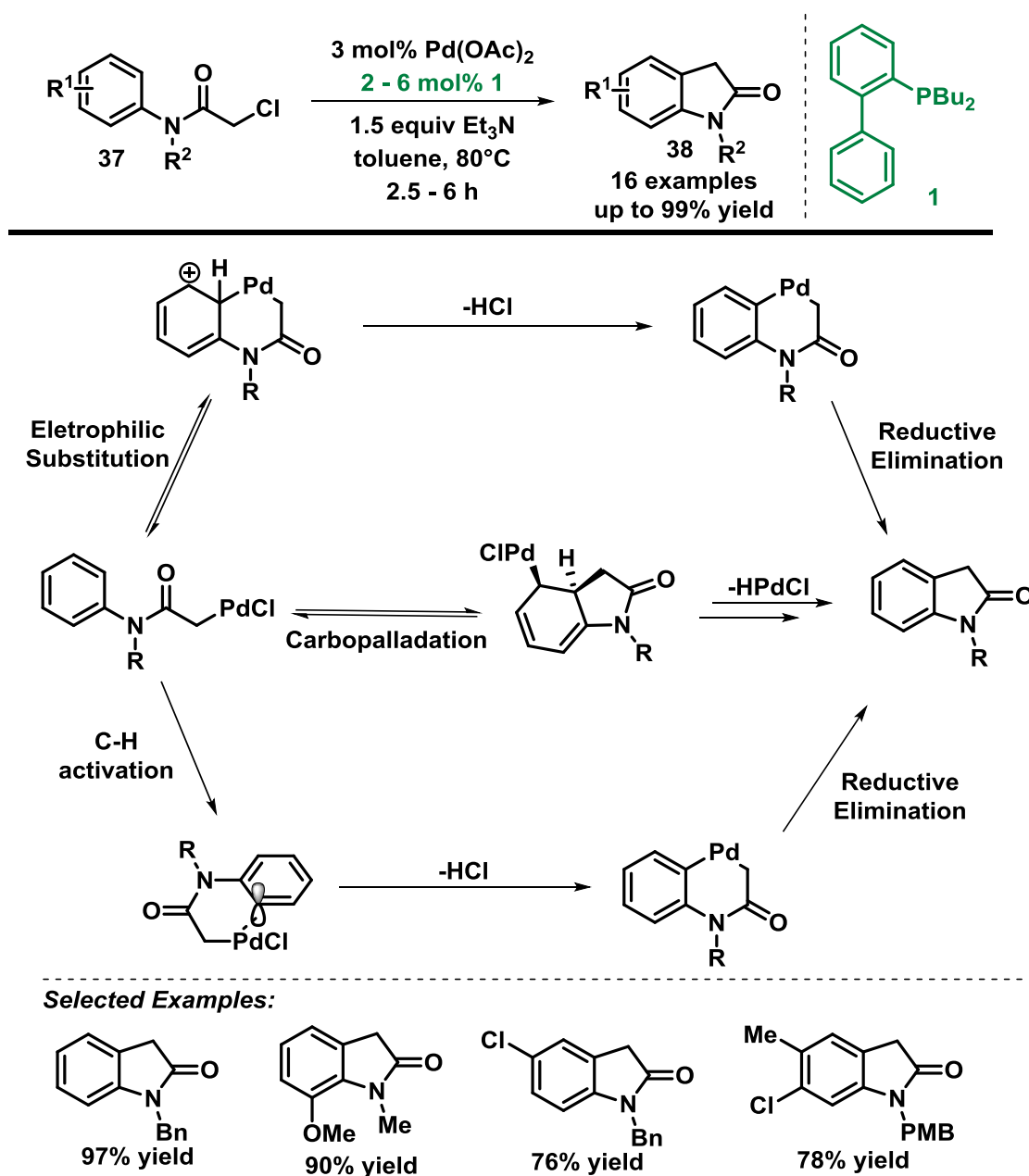


SCHEME 19: Pharmaceutically active oxindoles.

Relying on the importance of the oxindole ring system, the synthesis of these scaffolds has been widely investigated. For instance, Buchwald's group reported a palladium-catalyzed strategy for the synthesis of substituted oxindoles (**38**) from α -chloroacetanilides (**37**) via an intramolecular C-H activation. This protocol was applied to a broad substrate range, with 16 examples being obtained with yields from 76 to 99% (Scheme 20).³⁰

²⁹ (a) SUMPTER, W. C. "The chemistry of oxindole". *Chem. Rev.*, **37**: 443, 1946. (b) DA SILVA, J. F. M.; GARDEN, S. J.; PINTO, A. C. "The Chemistry of Isatins: A Review from 1975 to 1999". *J. Braz. Chem. Soc.*, **12**: 273, 2001. (c) KLEIN, J. E. M. N.; TAYLOR, R. J. K. "Transition-Metal-Mediated Routes to 3,3-Disubstituted Oxindoles through Anilide Cyclisation". *Eur. J. Org. Chem.*, **2011**: 6821, 2011. (d) MILLEMAGGI, A.; TAYLOR, R. J. K. "3-Alkenyl-oxindoles: Natural Products, Pharmaceuticals, and Recent Synthetic Advances in Tandem/Telescoped Approaches". *Eur. J. Org. Chem.*, **2010**: 4527, 2010. (e) DALPOZZO, R.; BARTOLI, G.; BENCIVENNI, G. "Recent advances in organocatalytic methods for the synthesis of disubstituted 2- and 3-indolinones". *Chem. Soc. Rev.*, **41**, 7247, 2012. (f) HONG, L.; WANG, R. "Recent Advances in Asymmetric Organocatalytic Construction of 3,3'-Spirocyclic Oxindoles". *Adv. Synth. Catal.*, **355**: 1023, 2013. (g) CHEN, G.; WENG, Q.; FU, L.; WANG, Z.; YU, P.; LIU, Z.; LI, X.; ZHANG, H.; LIANG, G. "Synthesis and biological evaluation of novel oxindole-based RTK inhibitors as anti-cancer agents". *Bioorganic Med. Chem.*, **22**: 6953, 2014.

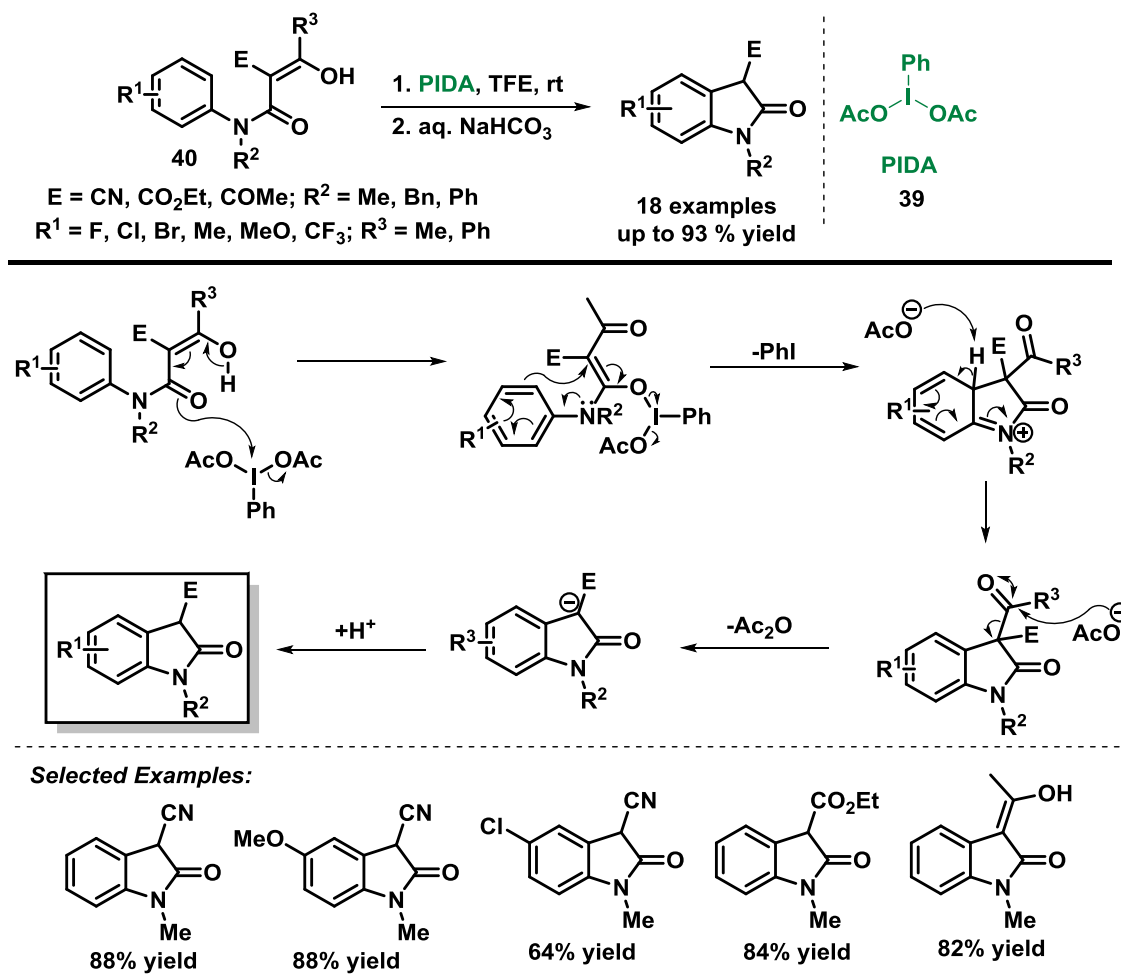
³⁰ HENNESSY, E. J.; BUCHWALD, S. L. "Synthesis of substituted oxindoles from α -chloroacetanilides via palladium-catalyzed C-H functionalization". *J. Am. Chem. Soc.*, **125**: 12084, 2003.



Scheme 20: Palladium-catalyzed oxindole synthesis and possible mechanistic pathways.

In consonance with the sustainability appeal, the application of metal-free methodologies has become a highly desired approach towards the synthesis of oxindoles. Based on these concepts, various efforts have been reported in this area. A recent example includes the work published by Zhao et al., which employed hypervalent iodine (**39**) to build a new C(sp²)-C(sp²) bond starting from anilidine (**40**).

Scheme 21 shows this novel approach along with the proposed mechanism for this transformation.³¹

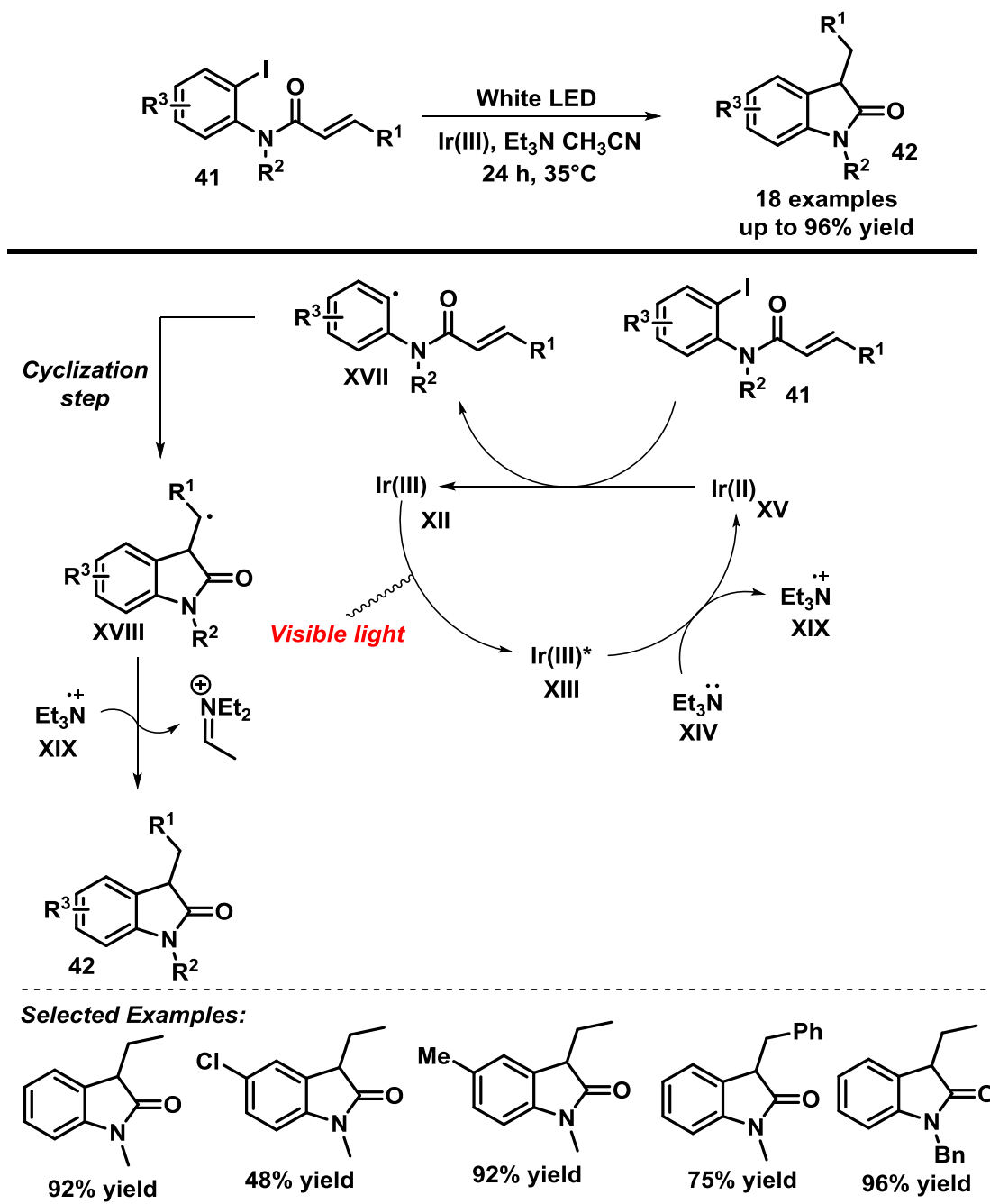


SCHEME 21: Metal-free synthesis of 2-oxindoles via $\text{PhI}(\text{OAc})_2$ -mediated oxidative C–C bond formation.

In 2015, Zhang's group used visible-light to induce a novel radical cyclization reaction for the preparation of oxindoles under mild reaction conditions. The radical cyclization reaction of o-iodophenylacrylamides (**41**) was achieved through an "anti-Michael" type addition of aryl radicals to give the corresponding oxindoles (**42**). The methodology was performed using the irradiation of a 12 W white LED strip in

³¹ JINGLEI, LV.; ZHANG-NEGRERIE, D.; DENG, J.; DU, Y.; ZHAO, K. "Metal-Free Synthesis of 2-Oxindoles via $\text{PhI}(\text{OAc})_2$ - Mediated Oxidative C–C Bond Formation". *J. Org. Chem.*, **79**: 1111, 2014.

combination with 0.1 mol % of an Ir(III) catalyst and 10 equivalents of Et₃N to induce the radical cyclization of **41** to achieve 3-substituted oxindoles **42** (Scheme 22).³²



SCHEME 22: Visible light induced radical cyclization of o-iodophenylacrylamides.

A plausible mechanism was proposed, and it begins with the excitation of the metal catalyst (XII) under visible-light to afford the excited Ir(III)* species (XIII),

³² DONG, W.; LIU, Y.; HU, B.; REN, K.; LI, Y.; XIE, X.; JIANG, Y.; ZHANG, Z. "Visible light induced radical cyclization of o-iodophenylacrylamides: a concise synthesis of indolin-2-one". *Chem. Commun.*, **51**: 4587, 2015.

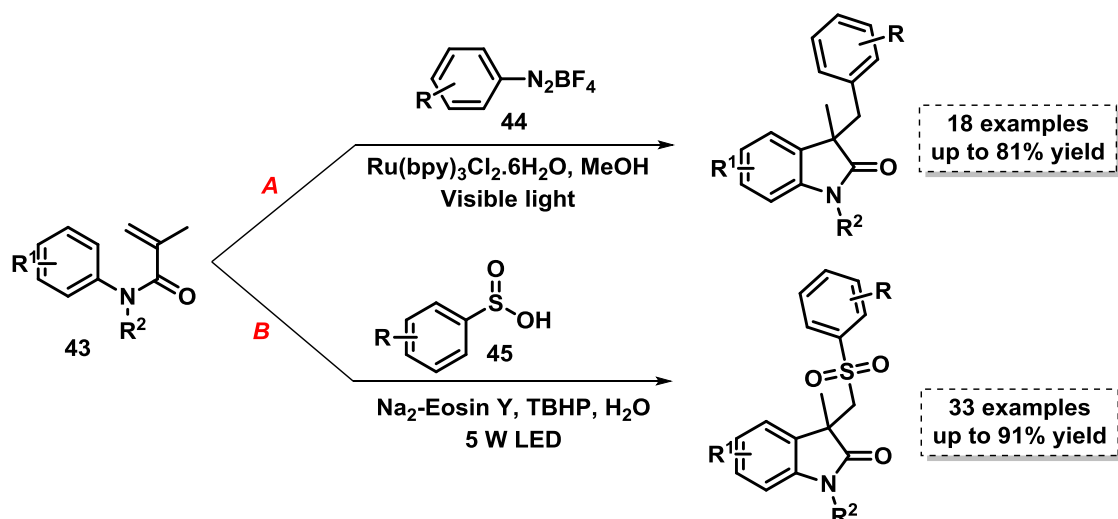
which oxidizes Et₃N (**XIV**) to give the reduced Ir(II) (**XV**) species along with the radical cation of the amine (**XVI**). The electron-rich metal complex Ir(II) (**XV**) then reduces the aryl iodide (**41**) to afford the key radical intermediate (**XVII**) and regenerate the photocatalyst Ir(III) (**XII**). The radical addition of intermediate (**XVII**) to the α,β -unsaturated amide forms radical (**XVIII**), which can be rapidly reduced by the abstraction of a hydrogen atom from the α -amino position of the iminium radical cation (**XIX**), giving the oxindole (**42**). The authors have presented 18 examples with variety of substituents with yields up to 96%.

In order to access functionalized oxindoles, two independent groups have published synthetic approaches starting from *N*-Acrylamides (**43**) in the presence of a photoactive catalyst. In the first approach, reported in 2013, Zou's group published a strategy using the aryl diazonium salts (**44**), with Ru(II) as catalyst and visible-light irradiation to achieve the desired oxindole system (Scheme 23A).³³ On the other hand, Wang's group approach was used to synthesize sulfonated oxindoles from *N*-acrylamides and arylsulfonic acid (**45**) using Eosin Y as a photoorganocatalyst (Scheme 23B).³⁴ It is worth mentioning that in both cases two new bonds were generated (Scheme 23).³⁵

³³ FU, W.; XU, F.; FU, Y.; ZHU, M.; YU, J.; XU, C.; ZOU, D. "Synthesis of 3,3-disubstituted oxindoles by visible-light-mediated radical reactions of aryl diazonium salts with *N*-arylacrylamides". *J. Org. Chem.*, **78**: 12202, 2013.

³⁴ XIA, D.; MIAO, T.; LI, P.; WANG, L. "Visible-Light Photoredox Catalysis: Direct Synthesis of Sulfonated Oxindoles from *N*-Arylacrylamides and Arylsulfonic Acids by Means of a Cascade C-S/C-C Formation Process". *Chem. Asian J.* **10**: 1919, 2015.

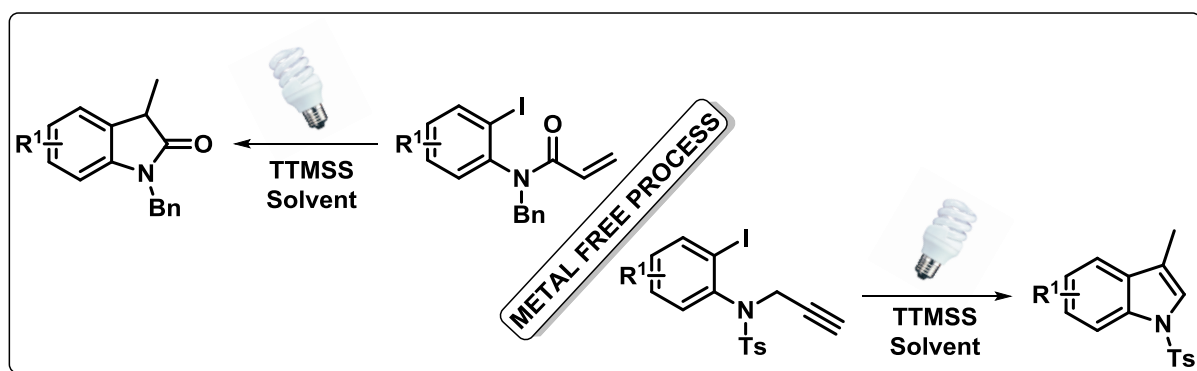
³⁵ For visible-light promoted oxindole synthesis, see: (a) JU, X.; LIANG, Y.; JIA, P.; LI, W.; YU, W. "Synthesis of oxindoles via visible light photoredox catalysis". *Org. Biomol. Chem.*, **10**: 498, 2012. (b) HONEKER, R.; GARZA-SANCHEZ, R. A.; HOPKINSON, M. N.; GLORIUS, F. "Visible-Light-Promoted Trifluoromethylthiolation of Styrenes by Dual Photoredox/Halide Catalysis". *Chem. Eur. J.*, **22**: 4395, 2016. (c) WEI, X.; WANG, L.; DU, S.; WU, L.; LIU, Q. "Visible-light photoredox intramolecular difluoroacetamidation: facile synthesis of 3,3-difluoro-2-oxindoles from bromodifluoroacetamides". *Org. Biomol. Chem.*, **14**: 2195, 2016. (d) TANG, Q.; LIU, X.; LIU, S.; XIE, H.; LIU, W.; ZENG, J.; CHENG, P. "*N*-(Acyloxy)phthalimides as tertiary alkyl radical precursors in the visible light photocatalyzed tandem radical cyclization of *N*-arylacrylamides to 3,3-dialkyl substituted oxindoles". *RSC Adv.*, **5**: 89009, 2015. (e) ZHENG, L.; YANG, C.; XU, Z.; GAO, F.; XIA, W. "Difunctionalization of alkenes via the visible-light-induced trifluoromethylarylation/1,4-Aryl shift/desulfonylation cascade reactions". *J. Org. Chem.*, **80**: 5730, 2015. (f) ZHENG, L.; HUANG, H.; YANG, C.; XIA, W. "UV light-mediated difunctionalization of alkenes through aroyl radical addition/1,4-/1,2-Aryl shift cascade reactions". *Org. Lett.*, **17**: 1034, 2015. (g) XIA, X. D.; REN, Y.-L.; CHEN, J.-R.; YU, X.-L.; LU, L.-Q.; ZOU, Y.-Q.; WAN, J.; XIAO, W.-J. "Phototandem catalysis: Efficient synthesis of 3-ester-3-hydroxy-2-oxindoles by a visible light-induced cyclization of diazoamides through an aerobic oxidation sequence". *Chem. Asian J.* **10**: 124, 2015. (h) FU, W.; ZHU, M.; ZOU, G.; XU, C.; WANG, Z. "Visible-Light-Mediated Radical Aryldifluoroacetylation of *N*-Arylacrylamides to give Difluoroacetylated Oxindoles". *Asian J. Org. Chem.*, **3**: 1273, 2014. (i) FU, W.; ZHU, M.; ZOU, G.; XU, C.; WANG, Z. "Visible-Light-Mediated Trifluoroethylation of *N*-Arylacrylamides with Trifluoroethyl Iodide: Synthesis of CF₃-Containing Oxindoles". *SYNLETT*, **25**: 2513, 2014. (j) XIE, J.; XU, P.; LI, H.; XUE, Q.; JIN, H.; CHENG, Y.; ZHU, C. "A room temperature



SCHEME 23: Oxindole synthesis. (A) Synthesis of 3,3-disubstituted oxindoles by visible-light-mediated radical reaction of aryl diazonium salts with *N*-arylacrylamides. (B) Direct synthesis of sulfonated oxindoles from *N*-arylacrylamides and arylsulfonic acids using visible light by means of a cascade C-S/C-C formation process.

2 Project Goals

- ✓ Development of a new metal-free strategy to the synthesis of indoles and oxindoles rings by using a mild condition mediated by visible light irradiation;
- ✓ Methodology with broad functional group tolerance;



SCHEME 24: Project goal

- ✓ Search for a new radical pathway through the Electron Donor-Acceptor (EDA) concept;
- ✓ Investigation of the reaction mechanism.

3 Results and Discussion

3.1 Optimization Studies

Tris(trimethylsilyl)silane [TTMSS, (TMS)₃SiH] has been used in many transformations in the last few years, especially in radical chain reactions. In organic chemistry, more specifically, TTMSS has received great attention in its use as a radical-based reagent. Numerous examples of the successful use of TTMSS in radical reductions, hydrosilylation, and radical cyclizations have been published. In this regard, TTMSS has proven to be an useful hydride and radical source that can be combined with various initiation methods (e.g. AIBN and heating, light irradiation and oxygen dosing).³⁶ Scheme 24 summarizes some examples of the use of TTMSS in radical chemistry which involve reactions such as intermolecular C-C bond formation,³⁷ hydrosilylation of alkynes,³⁸ silyldesulfonylation,³⁹ carbocycles construction,⁴⁰ construction of nitrogen heterocycle,⁴¹ and radical reduction.⁴²

³⁶ CHATGILIALOGLU, C.; LALEVÉE, J. "Recent Applications of the (TMS)₃SiH Radical-Based Reagent". *Molecules*, **17**: (2012), 527.

³⁷ CRICH, D.; RAHAMAN, M. Y. "Thiomaleic anhydride: A convenient building block for the synthesis of α -substituted γ - and δ -lactones through free-radical addition, nucleophilic ring opening, and subsequent thiocarboxylate manipulation". *J. Org. Chem.*, **74**: 6792, 2009.

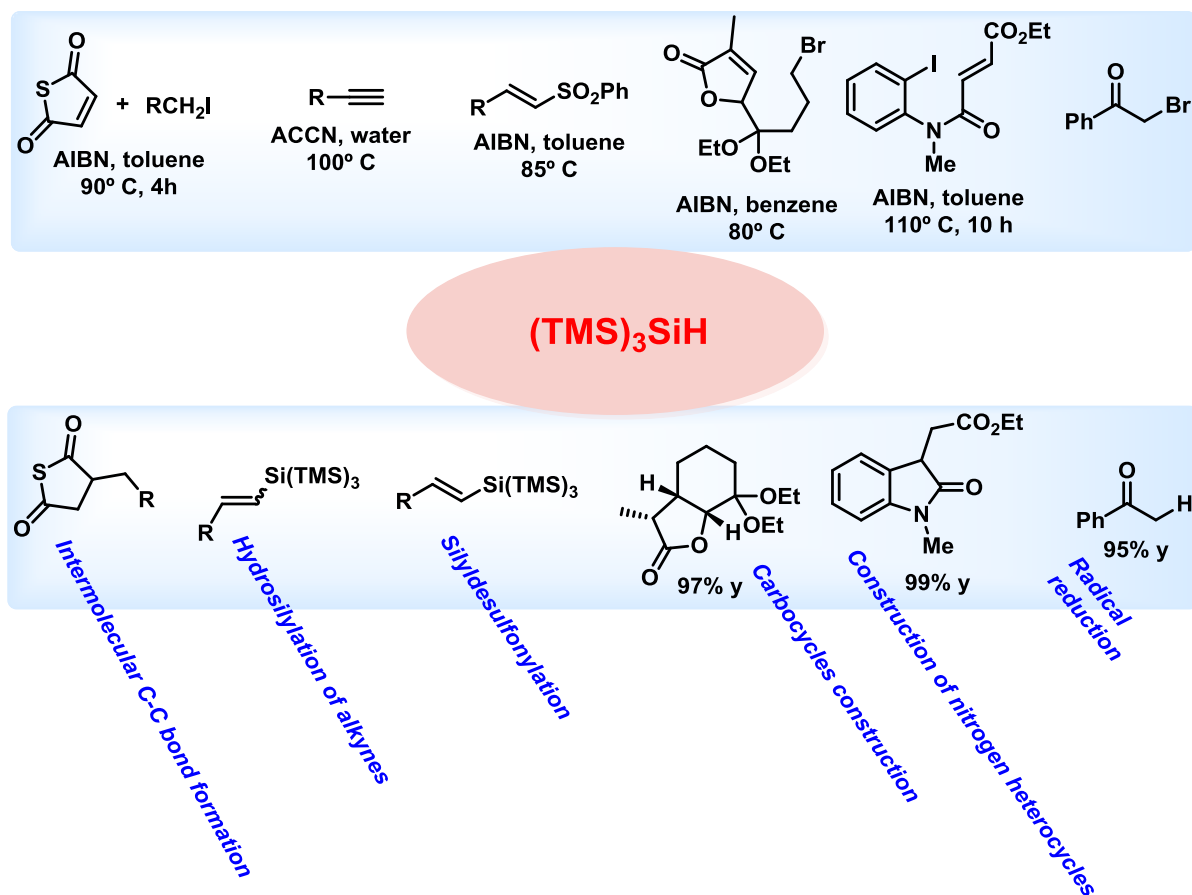
³⁸ POSTIGO, A.; KOPSOV, S.; ZLOTSKY, S. S.; FERRERI, C.; CHATGILIALOGLU, C. "Hydrosilylation of C-C multiple bonds using (Me₃Si)₃SiH in water. Comparative study of the radical initiation step". *Organometallics*, **28**: 3282, 2009.

³⁹ (a) WNUK, S. F.; GARCIA, P. I.; WANG, Z. "Germyldesulfonylation of Vinyl and (α -Fluoro) vinyl Sulfones: Application of Tris(trimethylsilyl)silanes and Tris(trimethylsilyl)germanes in Pd-Catalyzed Couplings". *Org. Lett.*, **2**: 1995, 2004. (b) WANG, Z.; PITTLELOUD, J. P.; MONTES, L.; RAPP, M.; DERANE, D.; WNUK, S. F. "Vinyl tris(trimethylsilyl)silanes: substrates for Hiyama coupling". *Tetrahedron*, **64**: 5322, 2008.

⁴⁰ MAULIDE, N.; MARKÓ, I. E. "Stereoselective synthesis of bicyclic lactones by annelation with functionalized orthoesters". *Chem. Commun.*, 1200, 2006. N. Maulide, I. E. Markó, *Chem. Commun.* **2006**, 1200.

⁴¹ PUDLO, M.; GÉRARD, S.; MIRAND, C.; SAPI, J. "A tandem radical cyclization approach to 3-(2-oxopyrrolidin-3-yl)indolin-2-ones, potential intermediates toward complex indole-heterocycles". *Tetrahedron Lett.*, **49**: 1066, 2008.

⁴² JIANG, H.; BAK, J. R.; LOPEZ-DELGADO, F. J.; JØRGENSEN, K. A. "Practical metal- and additive-free methods for radical-mediated reduction and cyclization reactions". *Green Chem.*, **15**: 3355, 2013.

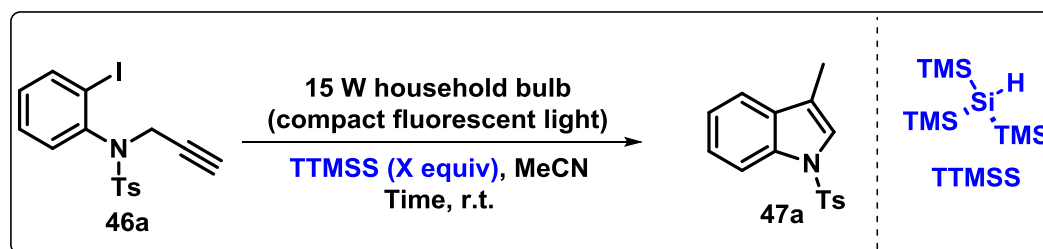


Scheme 25: Tris(trimethylsilyl)silane as a radical promoter.

Considering TTMSS's known properties in radical reactions, we began our investigation on the dehalogenation of substrate **46a** followed by an 5-exo-dig cyclization reaction by evaluating the effect of different parameters on the reaction conditions, namely the amount of TTMSS (Table 1), solvents and halide substituents (Tables 2 and 3), and *N*-protecting groups (Table 4).

To test the feasibility of the outlined plan, the ability of TTMSS to promote the photochemical cyclization process of *N*-tosyl-propargyl aniline (**46a**) towards the formation of indole ring system (**47a**) was investigated. The use of 1 equivalent of TTMSS in CH₃CN at room temperature for 24 hours led to the desired product with 58% of isolated yield (Table 1, entry 1). Next, the excess of TTMSS as a radical promoter was examined, and it was possible to notice that the yields were considerably higher as the amount of TTMSS was increased (Table 1, entries 2 and 3); the use of 1.5 and 2 equivalents of TTMSS led to 76% and 99% isolated yields, respectively. However, when 2 equivalents of TTMSS were used, the reaction achieved completion in 2 hours.

TABLE 1: Optimization studies: Effect of the TTMSS loading.



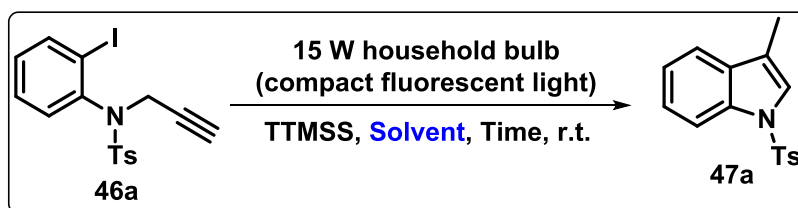
Entry	(X equiv)	Time (h)	Yield ^b (%)
1	1	24	58
2	1.5	24	76
3	2	2	99
4	0	24	nr
5 ^c	2	24	40

^a Reactions were carried out on a 0,1 mmol scale using 1 equiv. of TTMSS and 0,4 mL of MeCN. ^b Yield determined after chromatography column. ^c Reaction performed at 40°C in the absence of light.

Interestingly, the absence of the TTMSS reagent resulted in no observable reaction (Table 1, entry 4), and the starting material was fully recovered. It has long been established that TTMSS reacts via thermal conditions as a source of radicals; based on that knowledge, we set up an experiment at 40° C for 24 hours in the absence of light. The isolated yield in this case was 40%, which showed that a thermal pathway is also possible, though it seems to be less efficient than the one mediated by light.

Considering that solvents play an important role in governing the rates of chemical transformations, the reaction was performed in several other solvents at the same temperature (Table 2). Apolar or low-polarity solvents (with low dielectric constant), such as dichloromethane (DCM), toluene, tetrahydrofuran (THF), and ethyl acetate (EtOAc) were able to provide the desired product with moderate to good yields (57%, 64%, 53%, and 76%, respectively - Table 2, entries 2, 3, 4 and 5). The yields dropped significantly with the utilization of aprotic polar solvents such as dimethylsulfoxide (DMSO), and *N,N*-dimethylformamide (DMF) (5% and 12%, respectively - Table 2, entries 6 and 7). When acetone was used, though, the reaction took place with an 89% yield (Table 2, entry 8), which may be related to the low viscosity of this solvent when compared to DMSO or DMF.

TABLE 2: Optimization studies: Solvent screening.



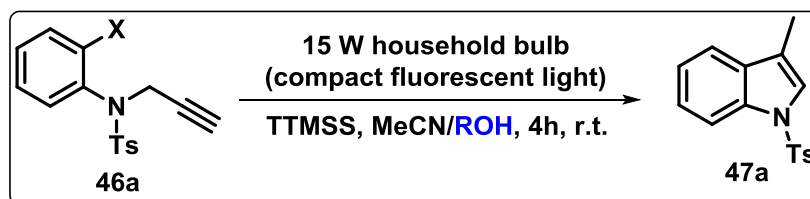
Entry ^a	Solvent	Time (h)	Yield (%) ^b
1	MeCN	2	99
2	DCM	24	57
3	Toluene	24	64
4	THF	24	53
5	EtOAc	24	76
6	DMSO	24	5
7	DMF	24	12
8	Acetone	6	89
9	EtOH	24	88
10	EtOH	4	90
11	H ₂ O	24	nr

^a Reactions were carried out on a 0,1 mmol scale using 2 equiv of TTMSS and 0,4 mL of MeCN. ^b Yield determined after chromatography column.

A more promising result was obtained in ethanol (EtOH), a protic polar solvent, which afforded great results both in terms of yield and reaction time, since an 88% could be achieved in 4h of reaction (Table 2, entry 10). To complete the screening of solvents, the reaction was performed in water, and the low solubility of the reagents in this medium kept the reaction from occurring (Table 2, entry 11).

The analysis of Table 2 shows that the best solvents for the reaction were acetonitrile and ethanol. On the basis of the outcomes obtained from the solvents investigation, we decided to study the possibility of protic solvents to act as a proton sources in the reaction (Table 3), which would enable a decrease in the amount of TTMSS used. In that way, different quantities of EtOH were employed (Table 3, entries 1, 2 and 3) and the best result was obtained when 5 equivalents were used, providing the desired product with 92% of yield (Table 3, entry 3). Other protic solvents such as, methanol (MeOH) and isopropanol (*i*-PrOH) were also tested, but afforded lower yields (75% and 76%, respectively - Table 3, entries 4 and 5).

TABLE 3: Optimization studies: Additional proton source.



Entry ^a	X	Alcohol	(X Equiv)	Yield ^b (%)
1	I	EtOH	1	82
2	I	EtOH	3,5	80
3	I	EtOH	5	92
4	I	MeOH	5	75
5	I	<i>i</i> -PrOH	5	76
6	Br	EtOH	5	85
7 ^c	I	EtOH	5	87

^a Reactions were carried out on a 0,1 mmol scale using 1 equiv of TTMSS and 0,4 mL of MeCN. ^bYield after chromatography column. ^c Reaction performed in a 5 mmol scale.

Having established the best reaction conditions so far, the next factor evaluated was influence of the halogen atom attached to the aromatic ring of the starting materials. Remarkably, when the halogen atom was changed from iodine to bromine the desired product was still achieved in a very good yield (82%, Table 3, entry 6). This occurrence can be justified on account of the weak bond between C_(sp²)-Br, which is approximately 80 kcal mol⁻¹, similar to the one between C_(sp²)-I (65 kcal mol⁻¹). With the aim of demonstrating the potential scalability of this photochemical approach for the synthesis of indoles, the reaction to produce indole 47a was performed on a 5 mmol scale, with the desired product being isolated in 87% yield (Table 3, entry 7).

In order to complete the optimization studies, the effect of *N*-protecting group for the cyclization reaction was next investigated (Table 4) and the tosyl group proved to be the best one for this reaction (Table 4, entry 1). When *N*-protecting groups like acetyl and isobutyryl were used, the results showed that these groups were not suitable for this transformation, since very low yields were obtained (13 and 14%, respectively - Table 4, entries 2 and 3). In summary, the results showed that both the nature of the solvent and the amount of TTMSS were critical to obtain the indole

product in high yields (under the optimized reaction conditions, product **47a** was obtained in 92% yield, table 3, entry 3). From all of these results, it is possible to conclude that the optimal reaction conditions for this reaction were achieved when using 1.0 equivalent of TTMSS, a mixture of CH₃CN/EtOH as solvent, and tosyl as *N*-protecting group.

TABLE 4: Optimization studies: Effect of the structure – *N*-protecting group.

Entry ^a	R	Time (h)	Yield ^b (%)
1	Tosyl	4	92
2	Acetyl	24	13
3	Isobutyryl	24	14

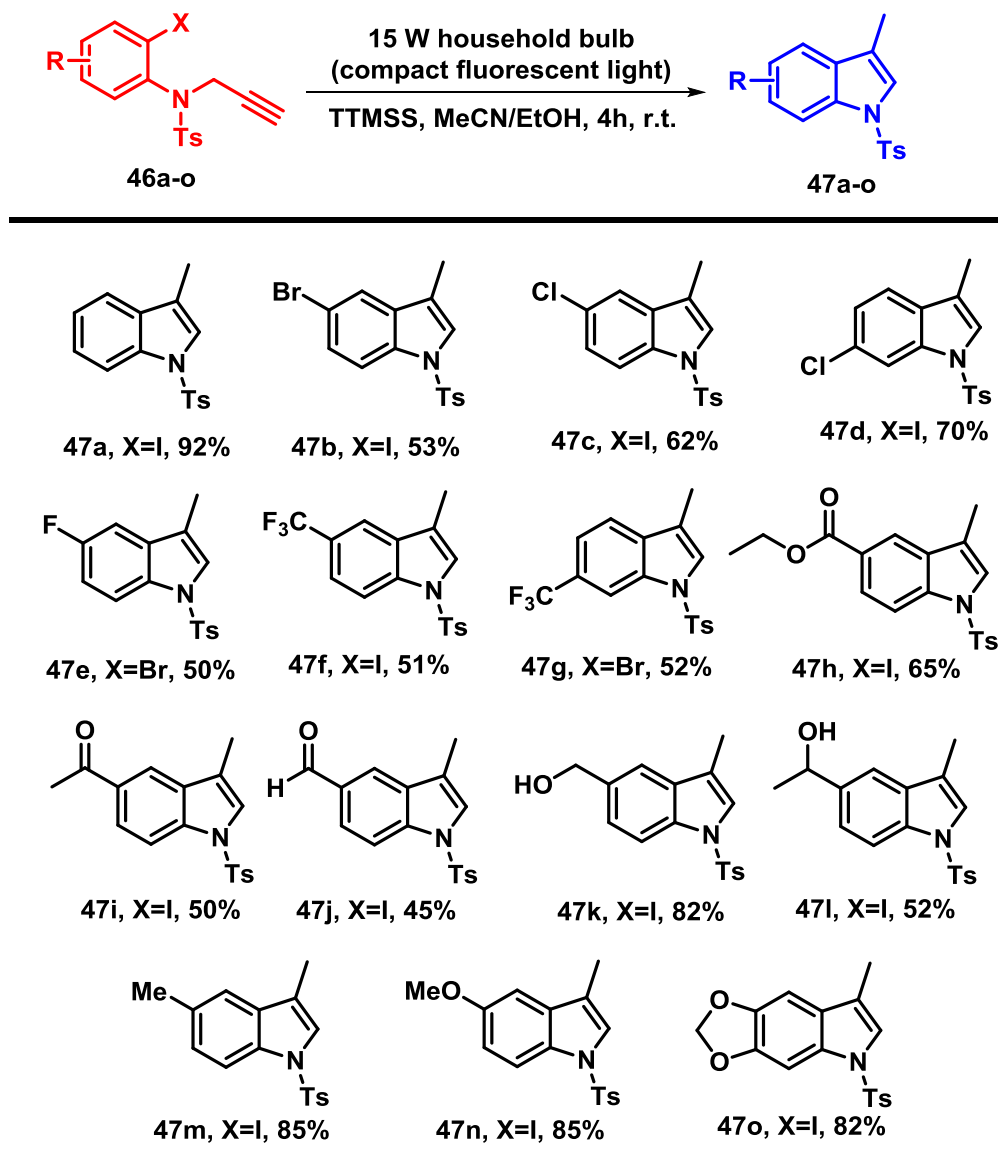
^a Reactions were carried out on a 0,1 mmol scale using 1 equiv of TTMSS, 0,4 mL of MeCN, and 5 equiv of EtOH. ^b Yield after purification by chromatography column.

In terms of reaction mechanism, which will be further discussed, we believe that the use of ethanol as a protic solvent helps in a termination step and, therefore, allow us to decrease the amount of TTMSS. As for the *N*-protecting group, it probably has a pivotal role in the conformation adopted by the starting material favoring the cyclization process.

3.2 Scope Evaluation

Having the optimized conditions in hand, we next turned our attention to the investigation of the scope and generality of this method by subjecting a wide range of substituted 2-halobenzenesulfonamides **46a–o** containing terminal alkynes to the optimized reaction conditions. Substrates bearing either electron-withdrawing or electron-donating groups furnished the desired indoles **47a–o** in moderate to excellent yields (45–85%). Electron-donating groups at different positions of the aromatic ring affording higher yields than those bearing electron-withdrawing groups (Scheme 25). It should be noted that besides the isolated products, the unreacted starting materials could be easily recovered. As seen in Scheme 25, substrates bearing additional

halogens such as Br and Cl, functionalities that allow subsequent functionalization by transition metal-mediated cross-coupling reactions,⁴³ underwent smoothly in the optimized reaction conditions affording the corresponding products in moderate yields (53% and 62%, respectively).



SCHEME 26: Substrate scope for the visible-light-mediated indole synthesis.

Due to the interesting properties of fluorine atoms and the trifluoromethyl (CF_3) moiety in medicinal chemistry, agrochemical and intelligent materials,⁴⁴ the

⁴³ CARIN, C. C.; SEECHURN, J.; KITCHING, M. O.; COLACOT, T. J.; SNIICKUS, V. "Palladium-catalyzed cross-coupling: A historical contextual perspective to the 2010 nobel prize". *Angew. Chem. Int. Ed.*, **51**: 5062, 2012.

⁴⁴ (a) PURSER, S.; MOORE, P. R.; SWALLOW, S.; GOUVERNEUR, V. "Fluorine in medicinal chemistry". *Chem. Soc. Rev.*, **37**: 320, 2008. (b) HAGMANN, W. K. "The many roles for fluorine in

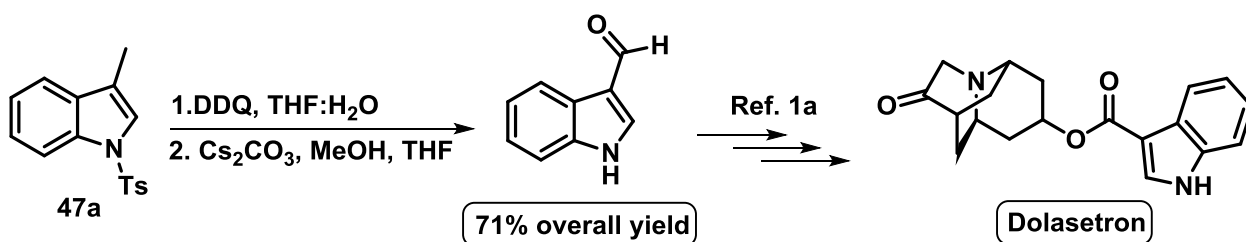
synthesis of the indole scaffolds containing these important subunits was conducted using the developed protocol. The reaction of the fluoro derivative led the product **47e** in 50% isolated yield, while the one bearing the trifluoromethyl group **47f** similarly gave 51% yield. Furthermore, the feasibility of the cyclization process showed no dependence on the substitution patterns (e.g., para-, meta-) of the aromatic ring of the substrates (compare **47f** vs. **47g**). Notably, this process was also compatible with ester, ketone and aldehyde functional groups attached to the aromatic ring (compare **47h** vs. **47i** vs. **47j**), and interestingly, unprotected alcohols could also be readily employed with no great effect on the yield (**47k** and **47l**).

With the aim of demonstrating the potential scalability of this photochemical approach for the synthesis of indoles, the reaction was performed on a 5 mmol scale and the desired product was isolated in 87% yield. Having in mind the high degree of functionalization displayed by product **47a**, further manipulations were briefly explored in order to demonstrate its synthetic utility. In order to accomplish that, initially 3-methylindole **47a** was treated with DDQ in aqueous THF to obtain the corresponding aldehyde in 75% yield.⁴⁵ Next, the *N*-tosyl protecting group was further removed through a simple known procedure, affording the structure bearing a free amino group in 95% yield.⁴⁶ Thus, after two simple synthetic manipulations it was possible to isolate 1H-indole-3-carboxaldehyde (71% overall yield), which could be a valuable precursor for the synthesis of several FDA approved drugs, particularly Dolasetron (trade name Anzemet) which is a serotonin 5-HT₃ receptor antagonist used to treat nausea and vomiting associated to chemotherapy (Scheme 26).

medicinal chemistry". *J. Med. Chem.*, **51**: 4359, 2008. (c) JIANG, H.; FALCICCHIO, A.; JENSEN, K. L.; PAIXÃO, M. W.; BERTELSEN, S.; JØRGENSEN, K. A. "Target-directed organocatalysis: A direct asymmetric catalytic approach to chiral propargylic and allylic fluorides". *J. Am. Chem. Soc.*, **131**: 7153, 2009. (d) NAGID, D. A.; MACMILLAN, D. W. C. "Trifluoromethylation of arenes and heteroarenes by means of photoredox catalysis". *Nature*, **480**: 224, 2011.

⁴⁵ AMIR-HEIDARI, B.; MICKFIELD, J. "NMR confirmation that tryptophan dehydrogenation occurs with syn stereochemistry during the biosynthesis of CDA in *Streptomyces coelicolor*". *J. Org. Chem.*, **72**: 8950, 2007.

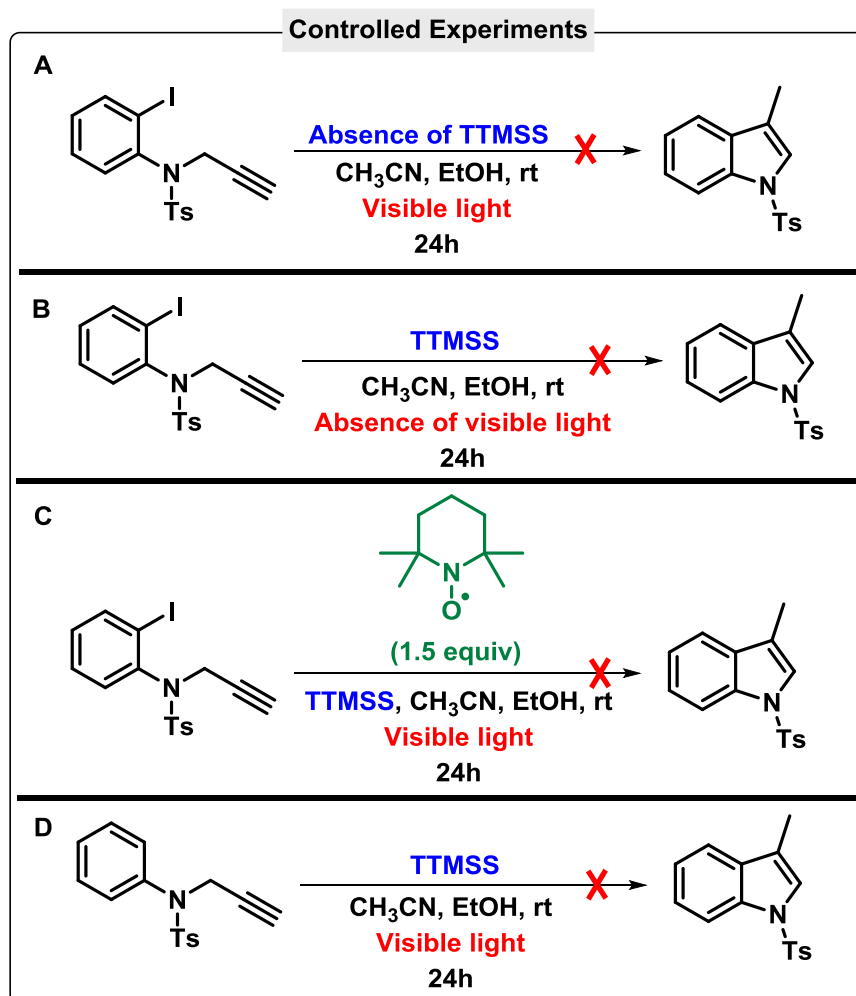
⁴⁶ BAJWA, J. S.; CHEN, G. P.; PRASAD, K.; REPIČ, O.; BLACKLOCK, T. J. "Deprotection of *N*-tosylated indoles and related structures using cesium carbonate". *Tetrahedron Lett.*, **47**: 6425, 2006.



SCHEME 27: Formal synthesis of Dolasetron.

3.3 Mechanistic Insights

Aiming to gain further insights into the mechanism of this visible-light-induced reaction, we performed additional controlled experiments (Scheme 27).



SCHEME 28: Controlled experiments.

The mechanistic investigations were started with the reaction of aryl iodide **46a** in the absence of TTMSS under optimized reaction conditions, and, as expected, no conversion to indole **47a** was observed (Scheme 27, equation A). The reaction performed in the absence of light also did not afford the desired product, while the starting material being fully recovered (Scheme 27, equation B). Considering that a C-centered radical is likely the key intermediate of the process, the presence of a radical scavenger should inhibit the intramolecular reductive cyclization process. As expected, when a radical quencher such as 2,2,6,6-tetramethyl-1-piperidinyloxy (TEMPO) was added to the system, a complete inhibition of the reductive reaction was observed, once again strongly suggesting a radical pathway for this transformation (Scheme 27, equation C). To complete our set of control experiments, a reaction using the halogen-free at 2-position of the aromatic ring was made, and as expected the reaction did not occur (Scheme 27, equation D). These experiments allowed us to reach the conclusion that continuous visible-light irradiation and the silicon reagent are required to yield the indole scaffold via a radical reaction mechanism.

The controlled experiments afforded insights on the reaction mechanism, and based on the EDA complex concepts, it is believed that the key step in the mechanism involves the formation of a highly-organized EDA complex. This critical intermediate probably plays an important role in the reactivity. In order to investigate the transient formation of a ground-state EDA aggregation, we measured both the optical absorption spectra of each reaction component separately, and the reaction components together (Figure 3). After mixing the starting material **46a** with TTMSS in acetonitrile (in the same reaction conditions), a marked yellow color developed, while the optical absorption spectrum showed a hypsochromic shift in the visible region, which may be a diagnostic of an EDA complex formation (green line in the Figure 3).

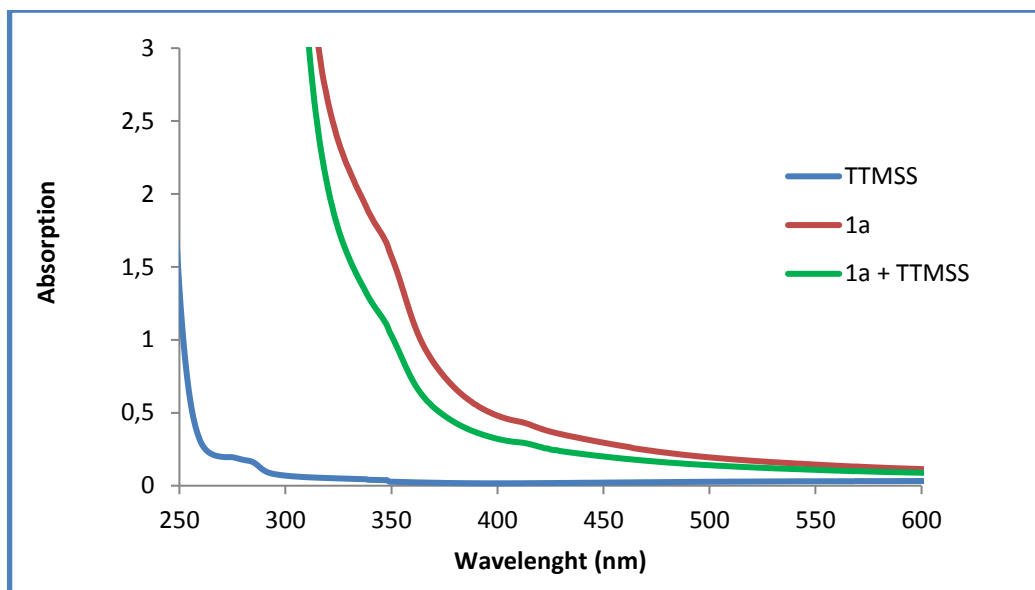


FIGURE 3: Absorption spectra of the separated reagents of the model reaction, and the reaction mixture.

In addition, experiments with successive intervals of irradiation and dark periods were carried out, which showed the total interruption of the reaction progress in the absence of light and the recuperation the of reactivity under further illumination (Figure 4). These results demonstrate that light is a necessary component of this photochemical process. Although such results do not definitively rule out a radical-chain mechanism,⁴⁷ the data shows that any chain-propagation process must be short-lived and also indicates the necessity of light to carry out the reaction by means to generate the excited state of reagents.

⁴⁷ CISMESIA, M. A.; Yoon, T. P. "Characterizing chain processes in visible light photoredox catalysis". *Chem. Sci.*, **6**: 5426, 2015.

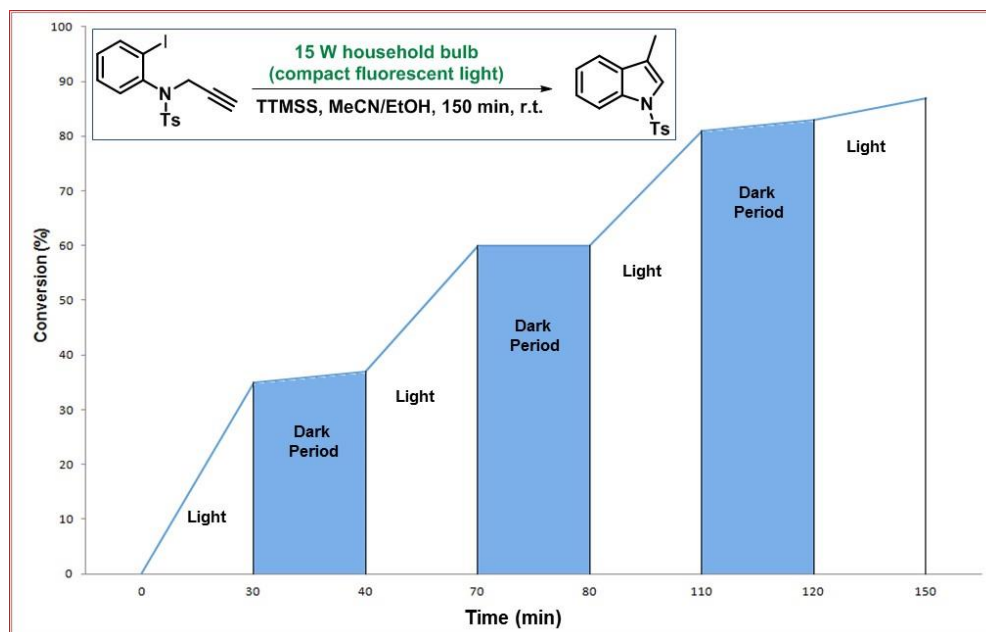


FIGURE 4: Successive intervals of irradiation and dark periods for the model reaction.

To further identify the hydrogen atom source in this process, labeling studies using MeOD (5 equiv.) in the reaction were performed, and the desired product was obtained with partial deuterium incorporation (D/H, 7:3) as showed in Figure 5. From this results, it was possible to conclude that the methanol (protic solvent) helps in the termination step of the reaction pathway.

3.4 Kinetic Studies

Aiming to analyze which of the reagents are involved in the rate-determining step of the reaction, kinetic studies were performed.⁴⁸ The kinetic study was conducted for the reaction between substrate **46a** and the TTMSS having acetonitrile as solvent (standard reaction under the optimized conditions).

⁴⁸ BLACKMOND, D. G. "Reaction progress kinetic analysis: A powerful methodology for mechanistic studies of complex catalytic reactions". *Angew. Chem. Int. Ed.*, **44**: 4302, 2005.

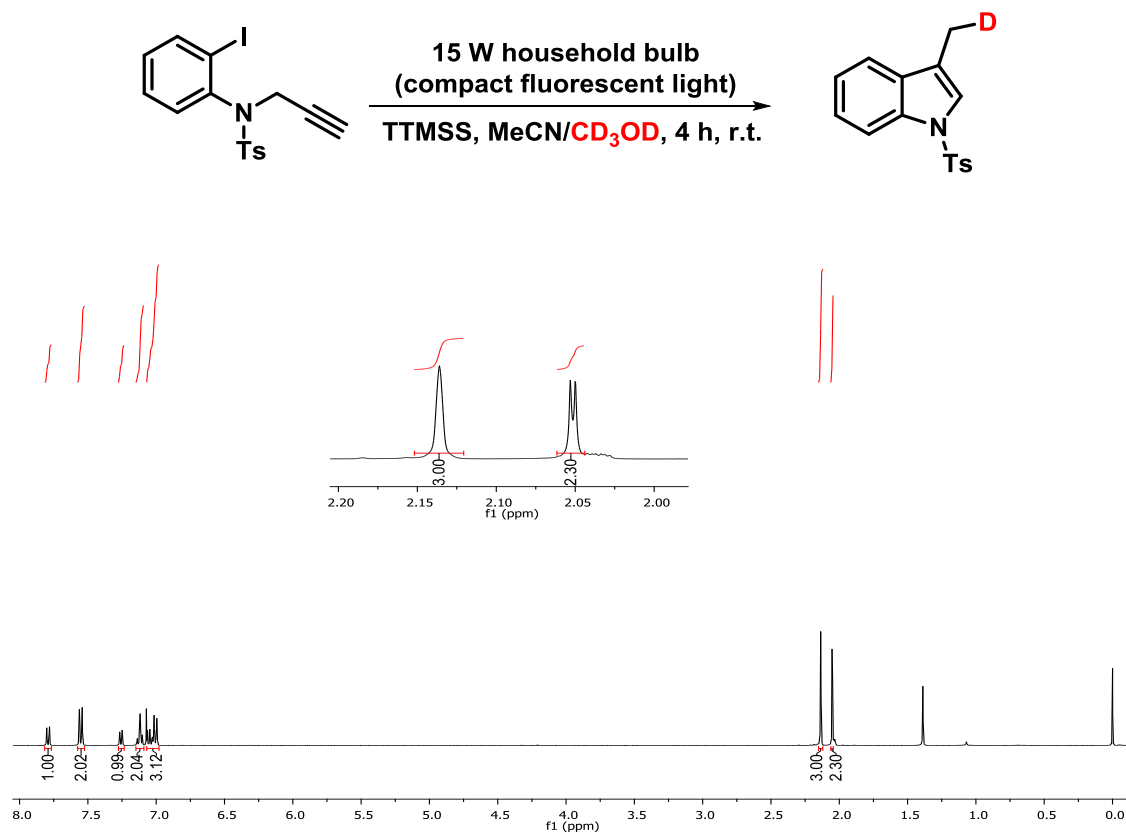


FIGURE 5: ¹H NMR spectra of deuterated labelled compound.

Experimental kinetic data can provide detailed insights into the reaction mechanism. The rates of a reaction can be determined by following the disappearance of the reactants or appearance of the product, which can be monitored by several methods like spectroscopy, spectrometry, pH and conductance, among others. In general, any property that can be measured and quantitatively related to the concentration of a reactant or a product can be used to determine a reaction rate. Therefore, the kinetic study provides an informative tool to investigate a reaction; a complete exploration allows the reaction to be described by a rate expression or rate law, which is an algebraic formula containing one or more rate constants as well as terms for the concentration of all reactant species that are involve in the rate-determining and prior steps. The overall kinetic order of the reaction is the sum of all the exponents in the rate expression and the mathematical form of the rate expression for a reaction depends on the order of the reaction. In this way, using $[A_0]$, $[B_0]$, $[C_0]$,

etc, for the initial time ($t = 0, t_0$) concentrations and [A], [B], [C], etc, as the reactant concentrations at time t , the following expressions are given:⁴⁹

First Order:

$$\text{Rate} = k[A]$$

Integrated form:

$$\ln\left(\frac{[A]_0}{[A]}\right) = kt \text{ or } [A] = A_0 e^{-kt}$$

Second Order/One reagent:

$$\text{Rate} = k[A]^2$$

Integrated form:

$$kt = \left(\frac{1}{A}\right) - \left(\frac{1}{A_0}\right)$$

Second order/two reagents:

$$\text{Rate} = k[A][B]$$

Integrated form:

$$kt = \left(\frac{1}{[B]_0 - [A]_0}\right) \ln\left(\frac{[A]_0[B]}{[B]_0[A]}\right)$$

Each expression showed above represents a kinetic model and can be plotted into a graph that can be used to determine the order of the reagents and also the kinetic constant. Graphically, a straight line is required in order to determine these factors. Moreover, in order to relate quantitatively the concentration of any reagent in a reaction with respect to any spectroscopic or spectrometric method, it is necessary

⁴⁹ (a) CLAYDEN, J.; GREEVES, N.; WARREN, S.; *Organic Chemistry*, *Organic Chemistry*, 2^a Ed., Oxford University Press, 2012. (b) CAREY, A. F.; SUNDBERG, R. J. *Advanced Organic Chemistry*, 5^a ed., Springer, 2007.

to build a calibration curve or use an internal standard. Considering these concepts, kinetic studies were conducted to investigate the developed photocatalyzed reaction.

Initially, calibration curves of the concentration versus time were built for the two reagents involved in the reaction (Tables 5 and 6; Figure 6 and 7) using a GC-MS equipment. The detailed data is given below:

TABLE 5: Kinetics studies: Area x Concentration of *N*-tosyl-propargyl aniline.

Area	Concentration (mol L ⁻¹)
91815816	0,25
69517837	0,20
51359099	0,15
40214411	0,10
22798302	0,05

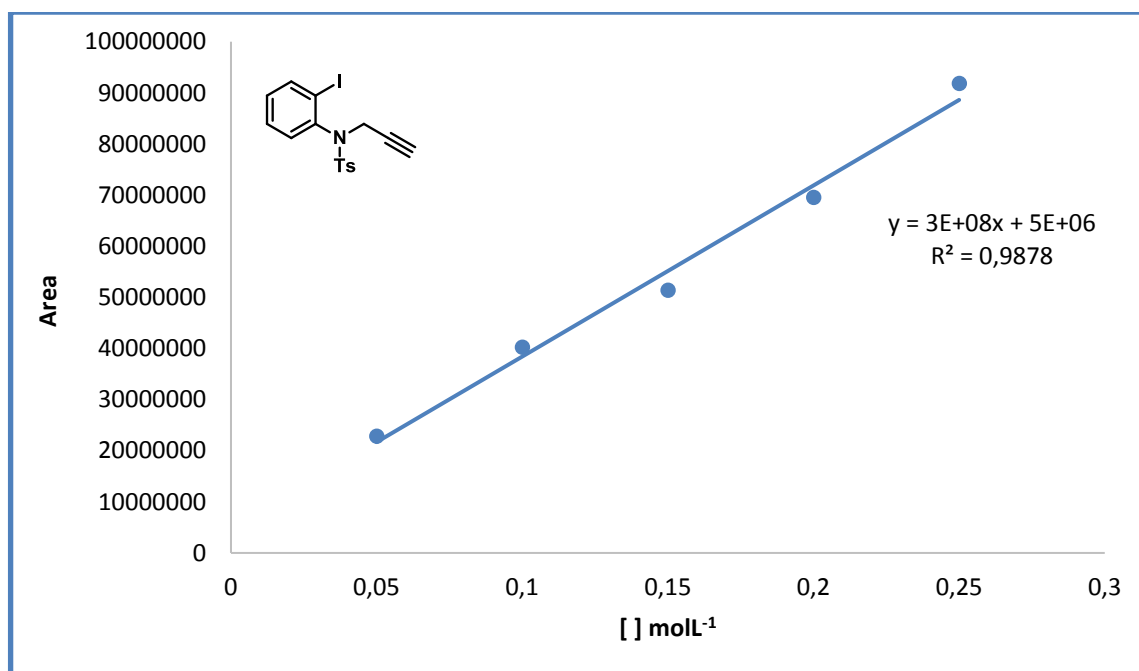


FIGURE 6: Calibration curve of *N*-tosyl-propargyl aniline.

TABLE 6: Kinetics studies: Area x Concentration of TTMSS.

Area	Concentration (molL ⁻¹)
49180772	0,25
44050000	0,20
37400191	0,15
27549983	0,10
14418184	0,05

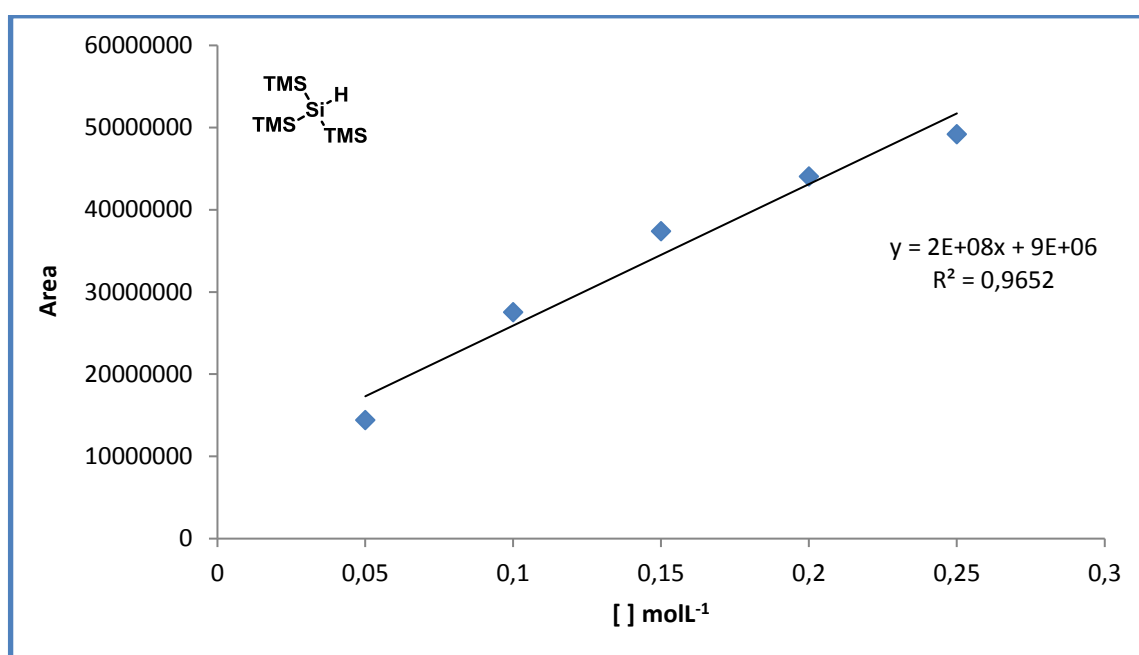


FIGURE 7: Calibration curve of TTMSS.

After the construction of the calibration curve, the progress of the reaction was investigated by monitoring the change in the concentration of the reaction versus time after every 30 minutes break by using GC-MS. The data obtained was used in the rate expressions to plot the respective graphs.

First the data was fitted considering the expression of first order for each of the reagents separately as given in the following expression:

$$\ln\left(\frac{[A]_0}{[A]}\right) = kt$$

The graphs for each reagent are showed in the Figures 8 and 9.

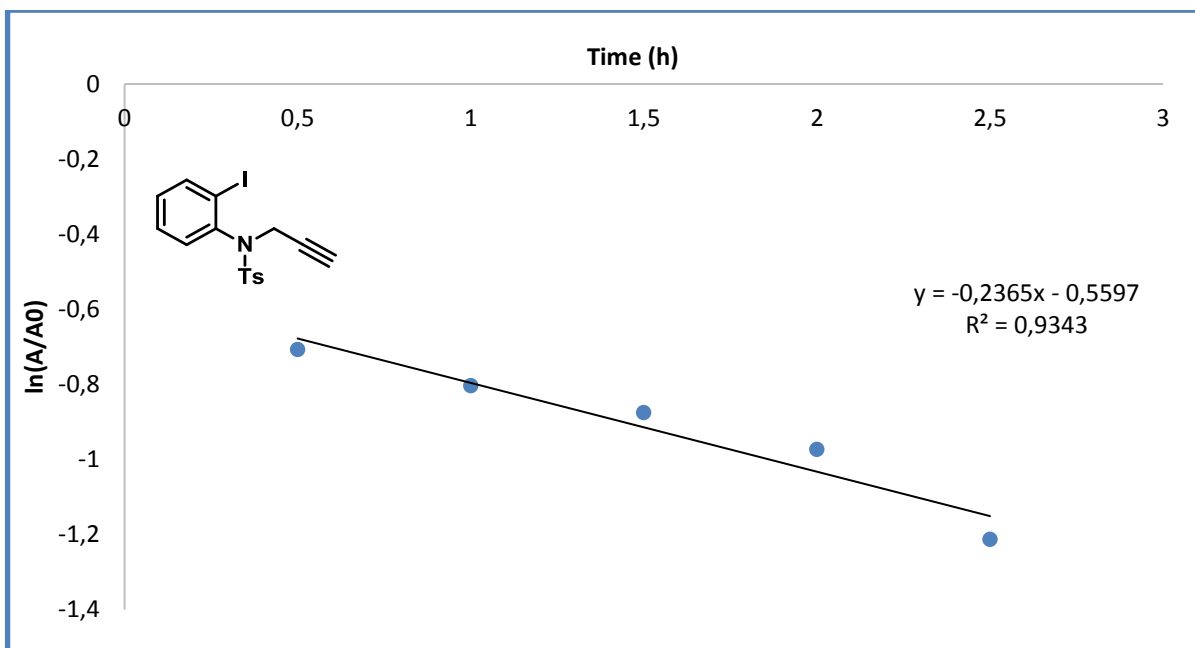


FIGURE 8: First order applied to *N*-tosyl-propargyl aniline.

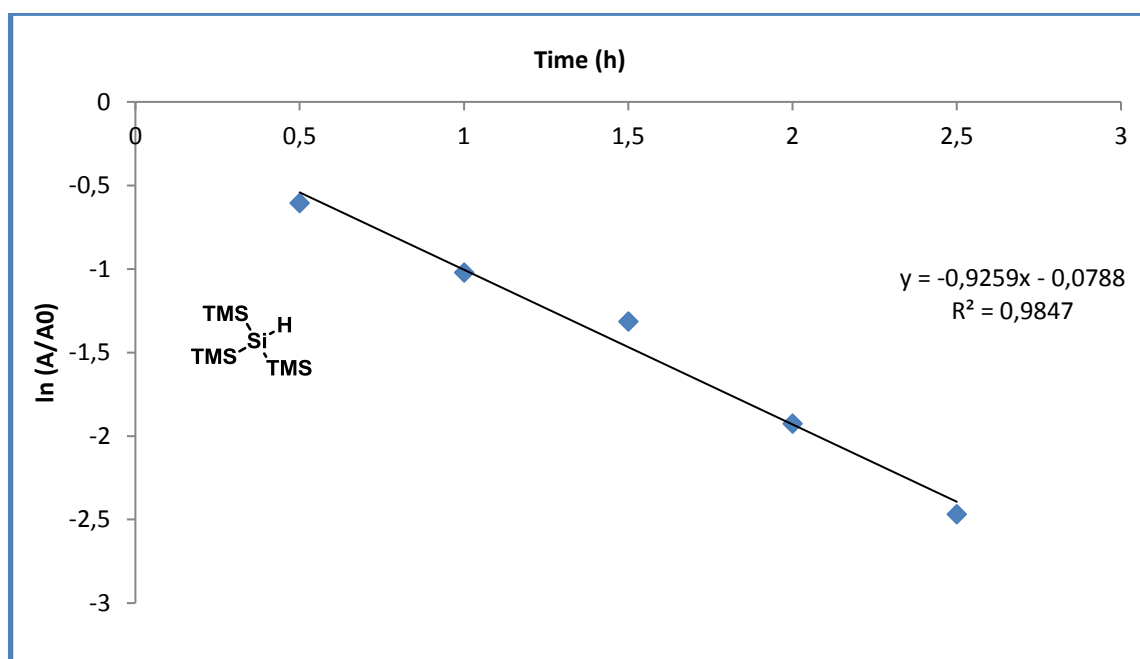


FIGURE 9: First order applied to TTMSS.

Next, the data as fitted using second order expression for each reagents separately, as give in the following equation:

$$kt = \left(\frac{1}{A}\right) - \left(\frac{1}{A_0}\right)$$

The s obtained graphs are depicted in Figures 10 and 11.

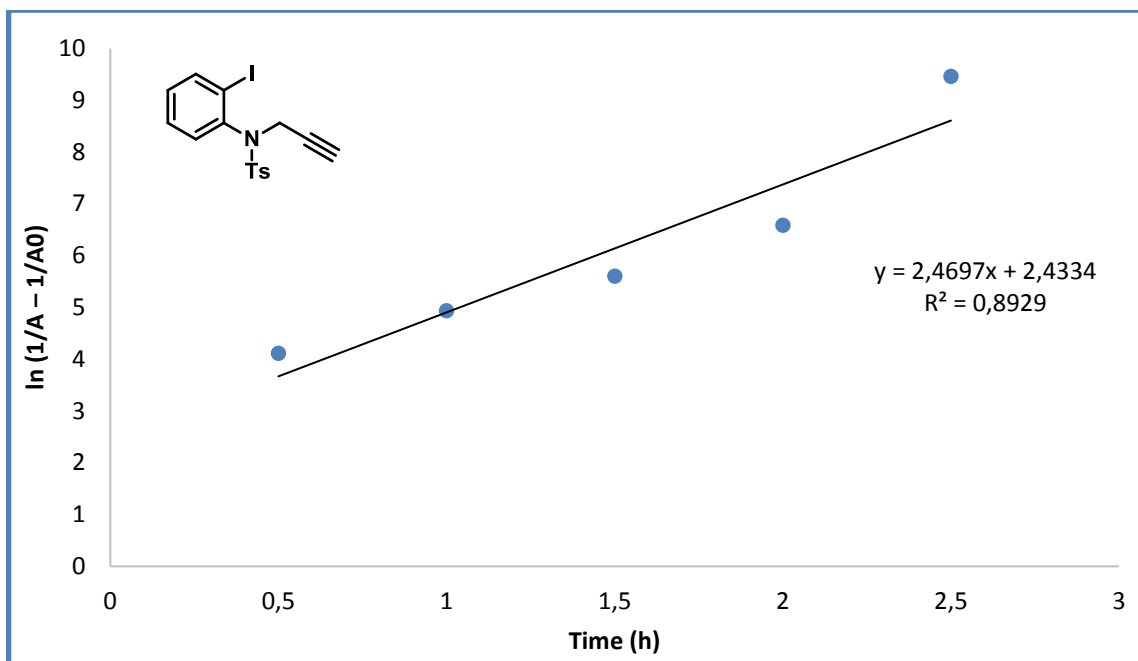


FIGURE 10: Second order applied to *N*-tosyl-propargyl aniline.

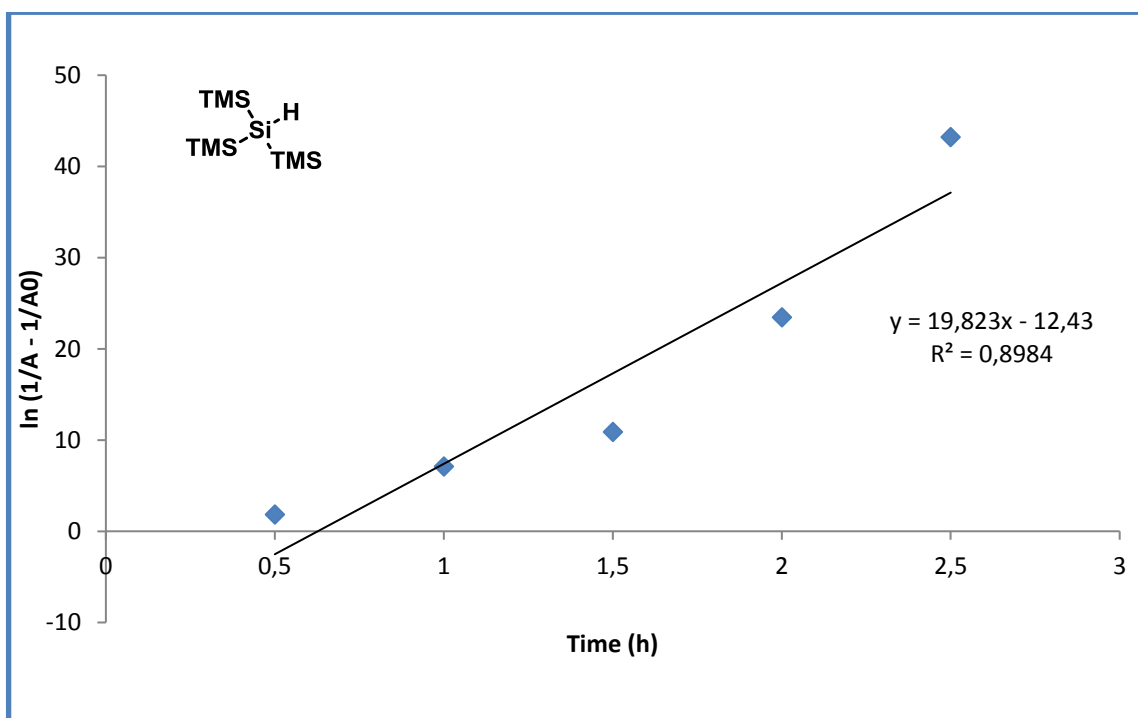


FIGURE 11: Second order applied to TTMSS.

The analysis of the graphs in Figures 8-11 it is clear that both the reagents follow first order, since the graph was well-adjusted to a straight line. Another possibility was evaluated by applying the data to another expression that relates the two reagents together, that is:

$$kt = \left(\frac{1}{[B]_0 - [A]_0} \right) \ln \left(\frac{[A]_0[B]}{[B]_0[A]} \right)$$

Fitting the data obtained using the above expression, it is possible to say that the reaction is overall second order but first order for each reagent (Figure 12).

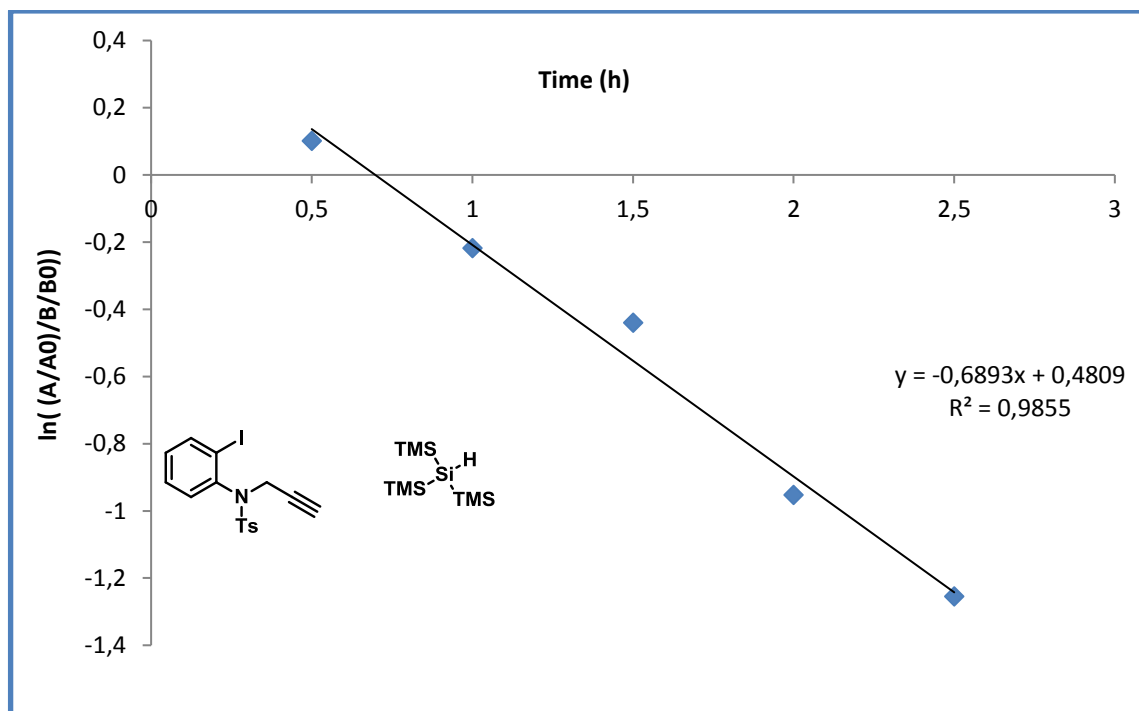
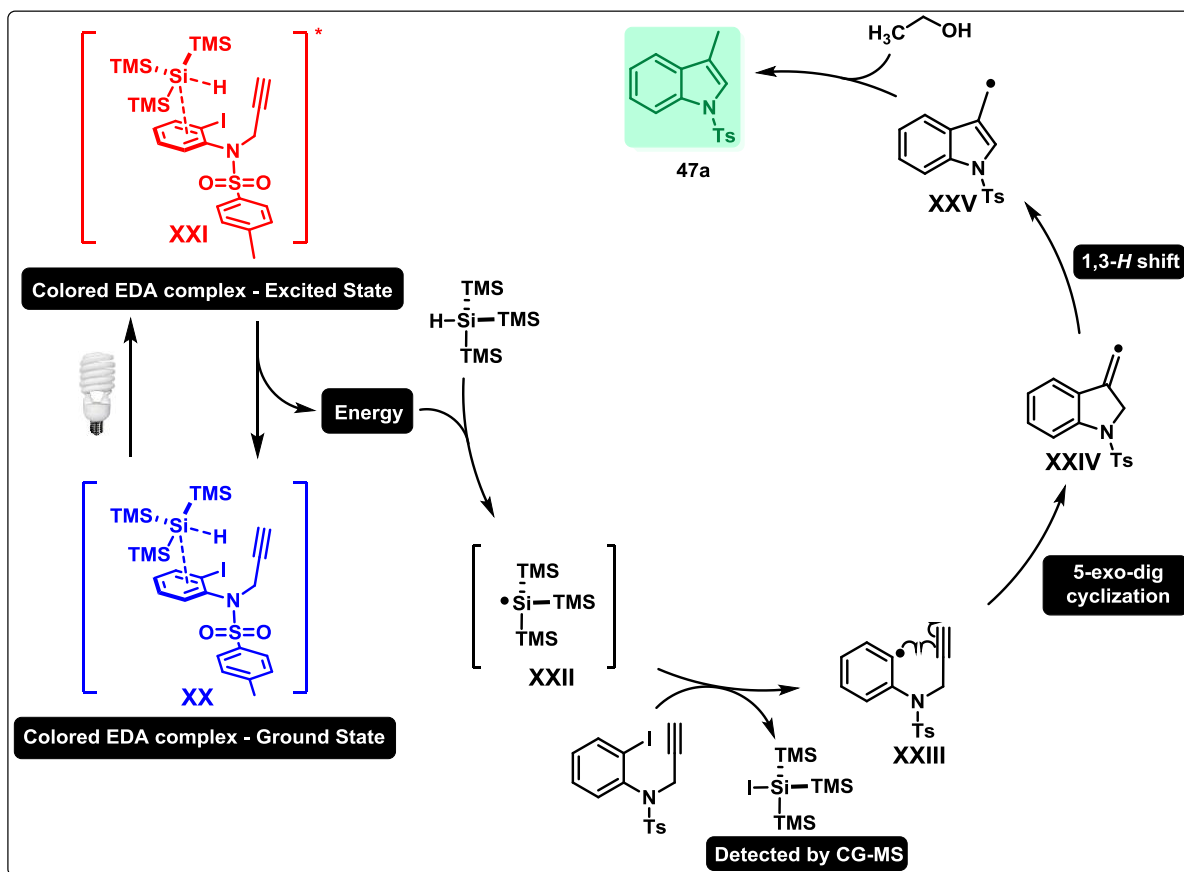


FIGURE 12: Second order overall – first order with respect to each reagent.

The kinetic study provided a virtuous interpretation of this photo-catalyzed reaction. Since the best adjustment of the curve was achieved using the last expression, the one which correlates both reagents in the same expression, it is possible to conclude that the overall reaction order is two (first order in each reagent). In that way, using the all of the above investigation, it is possible to infer that both reagents are involved in the rate determining step of the reaction or prior steps, which would require a high activation energy to reach the transition state and continue the photo-process up to the product.⁵⁰

Based on the aforementioned results and on previous reports, a plausible reaction mechanism was proposed (Scheme 28).

⁵⁰ ZHANG, S. L.; LANG, M. J.; GOODMAN, S.; DURNELL, C.; FIDLAR, V.; FLEMING, G. R.; YANG, N. C. "Donor-acceptor interaction and photochemistry of polymethylene-linked bichromophores in solution". *J. Am. Chem. Soc.*, **118**: 9042, 1996.



SCHEME 29: Proposed mechanism for the visible-light-mediated indole synthesis.

In the proposed mechanism, a silyl-centered radical ($(\text{Me}_3\text{Si})_3\text{Si}^*$) is initially generated under visible-light irradiation.⁵¹ The formation of the silyl radical may occur through a sequence of events that consists firstly of the formation of a donor-acceptor complex (EDA) by photon-absorbing electron through the association of the aryl substrate with TTMSS (**XX**)⁵² followed by the visible-light-promoted excitation of

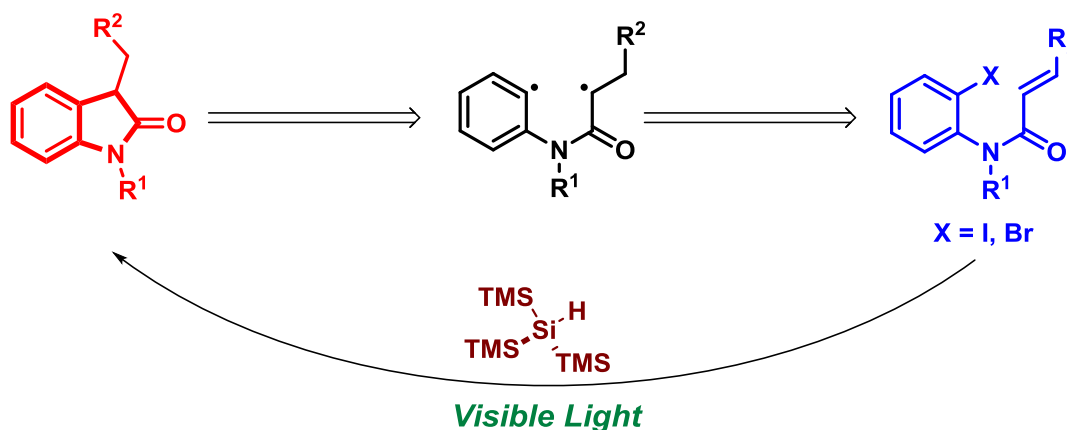
⁵¹ (a) CURRAN, D. P.; KELLER, A. I. "Radical additions of aryl iodides to arenes are facilitated by oxidative rearomatization with dioxygen". *J. Am. Chem. Soc.*, **128**: 13706, 2006. (b) KIM, J. G.; MISHRA, M. K.; JANG, D. O. "Synthesis of sterically hindered ketones from aldehydes via O-silyl oximes". *Tetrahedron Lett.*, **53**: 3527, 2012. (c) TEHFE, M. A.; LALEVÉE, J.; ALIONAS, X.; FOUASSIER, J. P. "Long wavelength cationic photopolymerization in aerated media: A remarkable titanocene/tris(trimethylsilyl)silane/onium salt photoinitiating system". *Macromolecules*, **42**: 8669, 2009. (d) HIEROLD, J.; LUPTON, D. W. "Synthesis of spirocyclic γ -lactones by cascade Beckwith-Dowd ring expansion/cyclization". *Org. Lett.*, **14**: 3412, 2012. (e) Hasegawa, E.; OGAWA, Y.; KAKINUMA, K.; TSUCHIDA, H.; TOSAKA, E.; TAKIZAWA, S.; MURAOKA, H.; SAIKAWA, T. "Tris(trimethylsilyl)silane promoted radical reaction and electron-transfer reaction in benzotrifluoride". *Tetrahedron*, **64**: 7724, 2008. (f) POSTIGO, A.; KOPSOV, S.; ZLOTSKY, S. S.; FERRERI, C.; CHATGILIALOGLU, C. "Hydrosilylation of C-C multiple bonds using $(\text{Me}_3\text{Si})_3\text{SiH}$ in water. Comparative study of the radical initiation step". *Organometallics*, **28**: 3282, 2009. (g) LALEVÉE, J.; BLANCHARD, N.; GRAFF, B.; ALLONAS, X.; FOUASSIER, J. P. "Tris(trimethylsilyl)silyl versus tris(trimethylsilyl)germyl: Radical reactivity and oxidation ability". *J. Organomet. Chem.*, **693**: 3643, 2008.

⁵² (a) FOSTER, R. "Electron donor-acceptor complexes". *J. Phys. Chem.*, **84**: 2135, 1980. (b) ROSOKHA, S. V.; KOCHI, J. K. "Fresh look at electron-transfer mechanisms via the donor/acceptor bindings in the critical encounter complex". *Acc. Chem. Res.* **41**: 641, 2008.

(XX), giving rise to (XXI). After an energy-transfer step, the Si-based radical (XXII) is formed⁵³ and subsequently promotes the single-electron reduction of the iodide substrate, generating the aryl radical (XXIII). Next, a kinetically favored 5-exo-dig cyclization occurs, leading to the formation of a vinyl radical (XXIV). Finally, an aromatization step via a 1,3-H shift produces an allylic radical (XXV), which further undergoes the proton abstraction of EtOH, yielding the corresponding heterocyclic product 47a.

3.5 Oxindole Synthesis

In light of the encouraging results for the synthesis of indoles, we envisioned that the visible-light-induced photochemical strategy could also be employed for the synthesis of oxindoles. As mentioned previously, the oxindole is an important class of heterocyclic compounds.⁵⁴ For this propose, *N*-protected 2-halophenylacrylamides and TTMSS were employed as starting materials under visible-light irradiation (Scheme 29).



SCHEME 30: Simplified retrosynthetic analysis.

Remarkably, a similar procedure to the one developed for the synthesis of indoles worked well for the synthesis of the oxindole scaffold and after a short optimization, the use of 2 equivalents of the TTMSS and benzyl as a *N*-protecting group

⁵³ ARCEO, E.; MONTRONI, E.; MELCHIORRE, P. "Photo-Organocatalysis of Atom-Transfer Radical Additions to Alkenes". *Angew. Chem. Int. Ed.*, **53**: 12064, 2014.

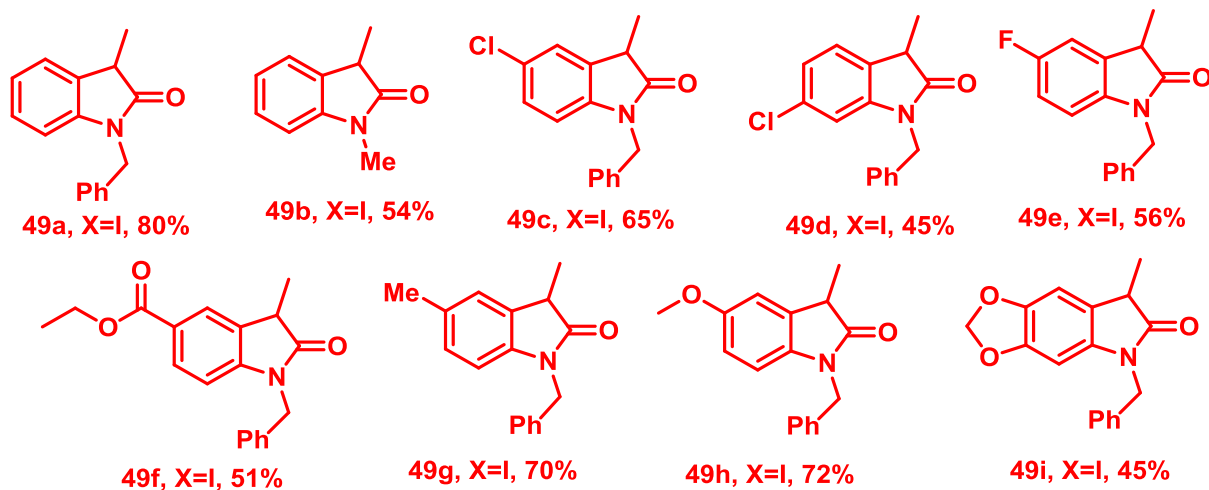
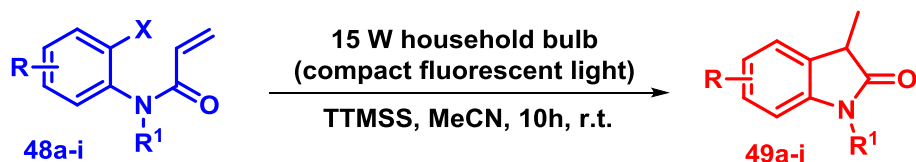
⁵⁴ SILVA, R. C.; CHATTERJEE, I.; ADÁN, E. E.; PAIXÃO, M. W.; MELCHIORRE, P. "Synthesis of Cyclopropane Spirooxindoles by means of a Vinylogous Organocatalytic Cascade". *Asian J. Org. Chem.*, **3**: 466, 2014.

in acetonitrile was found to be appropriate to obtain the desired product with a good yield (Table 7).

TABLE 7: Optimization studies – Synthesis of oxindole

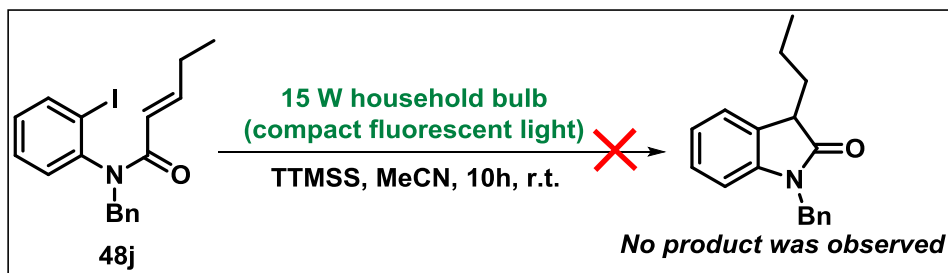
Entry	N-protecting group	TTMSS (Equiv.)	EtOH (Equiv.)	Time (h)	Yield (%)
1	Tosyl	1	5	10	nr
2	Benzyl	1	5	10	42
3	Benzyl	2	-	10	80

Having identified the optimal conditions, an evaluation of the reaction scope and limitations was conducted, starting with the effect of different alkyl groups attached to the nitrogen atom on the substrate (Scheme 30). On the basis of this study, it was possible to observe that the substrate containing an *N*-benzyl moiety afforded the 5-exo-trig cyclization product in higher yields when compared to its *N*-methyl analogue (**49a** vs. **49b**, 80% and 54% yield, respectively). Interestingly, substrates bearing halogen atoms on the aromatic ring such as Cl and F were tolerated under the reaction conditions, giving the desired products in 45–65% yield (**49c**, **49d** and **49e**). We then explored the scope of the reaction towards the presence of a sensitive and strong electron-withdrawing group, and, gratifyingly, product **49f** bearing an ester moiety afforded the desired product in 51% yield. Substrates containing electron donating groups reacted smoothly under the visible-light conditions, giving rise to the corresponding oxindoles **49g** and **49h** in 70% and 72% yield, respectively. Furthermore, the reaction of substrate **48i** revealed that the insertion of a second electron-donating group on the aromatic ring has a negative effect in terms of the chemical outcome (**49i** was obtained in 45% yield).



SCHEME 31: Substrate scope for the visible-light-mediated oxindole synthesis.

Next, the methodology was applied to substituted alkenes, but unfortunately when the substrate **48j** was used as starting material, the desired product could not be achieved (Scheme 31), and the starting material was fully recovered.



SCHEME 32: Scope limitation of the methodology.

4 Conclusion

In conclusion, we have developed a straightforward and highly efficient photochemical protocol leading to the formation of nitrogen-containing heterocycles. This metal- and additive free protocol is carried out by allying visible-light irradiation from simple household fluorescent light bulbs with the use of tris(trimethylsilyl)silane (TTMSS) as a carbon-radical promoter. The high functional-group tolerance, employment of readily available starting materials and scalability of the reaction substantiate the versatility of this method, making it attractive for both academia and industry. Further studies focused on the application of this transformation towards the synthesis of other heterocyclic compounds, as well as a thorough mechanistic study of this protocol, are underway and will be the topic of another master investigation of our group.

5 References

1. NGUYEN, J. D.; D'AMATO, E. M.; NARAYANAM, J. M. R.; STEPHENSON, C. R. J. "Engaging unactivated alkyl, alkenyl and aryl iodides in visible-light-mediated free radical reactions". *Nat. Chem.*, **4**: 854, 2012.
2. SILVA, G. P.; ALI, A.; SILVA, R. C.; JIANG, H.; PAIXÃO, M. W. "Tris(trimethylsilyl)silane and visible-light irradiation: a new metal- and additive-free photochemical process for the synthesis of indoles and oxindoles". *Chem. Commun.*, **51**: 15110, 2015.
3. LIMA, C. G. S.; LIMA, T. D. M.; DUARTE, M.; JURBERG, I. D.; PAIXÃO, M. W. "Organic Synthesis Enabled by Light-Irradiation of EDA Complexes: Theoretical Background and Synthetic Applications". *ACS Catal.*, **6**: 1389, 2016.
4. PITRE, S. P.; MCTIERNAN, C. D.; SCAIANO, J. C. "Understanding the Kinetics and Spectroscopy of Photoredox Catalysis and Transition-Metal-Free Alternatives". *Acc. Chem. Res.*, **49**: 1320, 2016.
5. (a) HOFFMANN, N. "Photochemical Reactions as Key Steps in Organic Synthesis". *Chem. Rev.* **108**: 1052, 2008. b) XUAN, J.; XIAO, W. J. "Visible-light photoredox catalysis". *Angew. Chem. Int. Ed.*, **51**: 6828, 2012. (c) CAREY, A. F.; SUNDBERG, R. J. *Advanced Organic Chemistry*, 5^a ed., Springer, 2007.
6. (a) YOON, T. P.; ISCHAY, M.; DU, J. "Visible light photocatalysis as a greener approach to photochemical synthesis". *Nat. Chem.*, **2**: 527, 2010. (b) BRACHET, E.; GHOSH, T.; GHOSH, I.; KÖNIG, B. "Visible light C–H amidation of heteroarenes with benzoyl azides". *Chem. Sci.*, **6**: 987, 2015. (c) XIAO, Q. H.; JIA, R. C.; QIANG, W.; FENG, L. L.; QIAO, H. D.; ANDRÉ, M. B.; WEN, J. X. "Photocatalytic Generation of N-Centered Hydrazonyl Radicals: A Strategy for Hydroamination of β , γ -Unsaturated Hydrazones". *Angew. Chem. Int. Ed.*, **53**: 12163, 2014. (d) KARAKAYA, I.; PRIMER, D. N.; MOLANDER, G. A. "Photoredox Cross-Coupling: Ir/Ni Dual Catalysis for the Synthesis of Benzylic Ethers". *Org. Lett.*, **17**: 3294, 2015. (e) TUCKER, J. W.; NGUYEN, J. D.; NARAYANAM, J. M. R.; KRABBE, S. W.; STEPHENSON, C. R. J. "Tin-free radical cyclization reactions initiated by visible light photoredox catalysis". *Chem. Commun.*, **46**: 4985, 2010. (f) FARNEY, E. P.; YOON, T. P. "Visible-light sensitization of vinyl azides by transition-metal photocatalysis". *Angew. Chem. Int. Ed.*, **53**: 793, 2014. (g) YASU, Y.; ARAI, Y.; TOMITA, R.; KOIKE, T.; AKITA, M. "Highly regio- and diastereoselective synthesis of CF₃-substituted lactones via photoredox-catalyzed carbolactonization of alkenoic acids". *Org. Lett.*, **16**: 780, 2014.
7. ROTH, H. D. "The Beginnings of Organic Photochemistry". *Angew. Chem. Int. Ed.*, **28**: 1193, 1989.
8. KOBAYASHI, Y.; FUJIMOTO, T.; FUKUYAMA, T. "Stereocontrolled total synthesis of (+)-K252a". *J. Am. Chem. Soc.*, **121**: 6501, 1999.

9. (a) PATAI Series: *The Chemistry of Functional Groups*; Rappoport, Z., Series Ed.; Wiley: Chichester, 2005; *The Chemistry of Cyclobutanes Parts 1 and 2* (Rappoport, Z., LIEBMAN, J. F.). (b) NAMYSLO, J. C.; KAUFMANN, D. E. "The application of cyclobutane derivatives in organic synthesis". *Chem. Rev.*, **103**: 1485, 2003.
10. GRIESBECK, A. G.; BONDOCK, S.; LEX, J. "Synthesis of erythro- α -amino beta-hydroxy carboxylic acid esters by diastereoselective photocycloaddition of 5-methoxyoxazoles with aldehydes". *J. Org. Chem.*, **68**: 9899, 2003.
11. (a) COYLE, J. D. *Introduction to Organic Photochemistry*. John Wiley & Sons Ltd, 1989. (b) WARDLE, B. *Principles and Applications of Photochemistry*. John Wiley & Sons Ltd, 2009. (c) KLÁN, P.; WIRZ, J. *Photochemistry of Organic Compounds*. John Wiley & Sons Ltd, 2009. (d) PAVIA, D. L.; LAMPMAN, G. M.; KRIS, G. S.; VYVYAN, J. R. *Introduction to Spectroscopy*. 4th ed., 2001 Brooks/Cole, Cengage Learning, 2009.
12. ZIMMERMANN, J.; ZEUG, A.; RODER, B. "A generalization of the Jablonski diagram to account for polarization and anisotropy effects in time-resolved experiments". *Phys. Chem. Chem. Phys.*, **5**: 2964, 2003.
13. SMITH, M. B.; MARCH, J. *Advanced Organic Chemistry: Reactions, Mechanism, and Structure*. 5th ed.; John Wiley & Sons Ltd, 2001.
14. PRIV-DOZ, P. W.; MÜHLING, O. "A new photochemical route to cyclopropanes". *Angew. Chem. Int. Ed.*, **40**: 1064, 2001.
15. KANDUKURI, S. R.; BAHAMONDE, A.; CHATTERJEE, I.; JURBERG, I. D.; ESCUDERO-ADÁN, E. C.; MELCHIORRE, P. "X-ray characterization of an electron donor-acceptor complex that drives the photochemical alkylation of indoles". *Angew. Chem. Int. Ed.*, **54**: 1485, 2015.
16. ROSOKHA, S. V.; KOCHI, J. K. "Fresh look at electron-transfer mechanisms via the donor/acceptor bindings in the critical encounter complex". *Acc. Chem. Res.* **41**: 641, 2008.
17. CHENG, Y.; YUAN, X.; MA, J.; YU, S. "Direct Aromatic C-H Trifluoromethylation via an Electron-Donor–Acceptor Complex". *Chem. Eur. J.*, **21**: 8355, 2015.
18. WADE, P. A.; MORRINSON, H. A.; KORNBLUM, N. "The Effect of Light on Electron-Transfer Substitution at a Saturated Carbon Atom". *J. Org. Chem.*, **52**: 3102, 1987.
19. PHAM, P. V.; NAGIB, D. A.; MACMILLAN, D. W. C. "Photoredox Catalysis: A Mild, Operationally Simple Approach to the Synthesis of α -Trifluoromethyl Carbonyl Compounds" *Angew. Chem. Int. Ed.*, **50**: 6119, 2011.
20. TOBISU, M.; FURUKAWA, T.; CHATANI, N. "Visible Light-mediated Direct Arylation of Arenes and Heteroarenes Using Diaryliodonium Salts in the Presence and Absence of a Photocatalyst" *Chem. Lett.*, **42**: 1203, 2013.

21. FRANZ, J. F.; KRAUS, W. B.; ZEITLER, K. "No photocatalyst required -versatile, visible light mediated transformations with polyhalomethanes" *Chem. Commun.*, **51**: 8280, 2015.
22. (a) TROFIMOV, B. A.; SOBENINA, L. N.; DEMENEV, A. P.; MIKHALEVA, A. I. "C-vinylpyrroles as pyrrole building blocks". *Chem. Rev.*, **104**: 2481, 2004. (b) BELINA, F.; ROSSI, R. "Synthesis and biological activity of pyrrole, pyrroline and pyrrolidine derivatives with two aryl groups on adjacent positions". *Tetrahedron*, **62**: 7213, 2006. (c) MARTINS, M. A. P.; FRIZZO, C. P.; MOREIRA, D. N.; ZANATTA, N.; BONACORSO, H. G. "Ionic liquids in heterocyclic synthesis". *Chem. Rev.*, **108**: 2015, 2008. (d) GULEVICH, A. V.; DUDNIK A. S.; CHERNYAK, N.; GEVORGYAN, V. "Transition Metal-Catalyzed Synthesis of Monocyclic Five-Membered Aromatic Heterocycles". *Chem. Rev.*, **113**: 3084, 2013.
23. VITALU, E.; SMITH, D. T.; NJARDARSON, J. T. "Analysis of the structural diversity, substitution patterns, and frequency of nitrogen heterocycles among U.S. FDA approved pharmaceuticals". *J. Med. Chem.*, **57**: 10257, 2014.
24. ROBINSON, B. "The Fischer indole synthesis". *Chem. Rev.*, **63**: 373, 1963.
25. VICENTE, R. "Recent advances in indole syntheses: New routes for a classic target". *Org. Biomol. Chem.*, **9**: 6469, 2011.
26. MÜLLER, S.; WEBBER, M. J.; LIST, B. "The catalytic asymmetric Fischer indolization". *J. Am. Chem. Soc.*, **133**: 18534, 2011.
27. NALLAGONDA, R.; REHAN, M.; GHORAI, P. "Synthesis of functionalized indoles via palladium-catalyzed aerobic oxidative cycloisomerization of o-allylanilines". *Org. Lett.*, **16**: 4786, 2014.
28. MAITY, S.; ZHENG, N. "A Visible-Light-Mediated Oxidative C-N Bond Formation/Aromatization Cascade: Photocatalytic Preparation of N-Arylindoles". *Angew. Chem. Int. Ed.*, **51**: 9562, 2012.
29. (a) SUMPTER, W. C. "The chemistry of oxindole". *Chem. Rev.*, **37**: 443, 1946. (b) DA SILVA, J. F. M.; GARDEN, S. J.; PINTO, A. C. "The Chemistry of Isatins: A Review from 1975 to 1999". *J. Braz. Chem. Soc.*, **12**: 273, 2001. (c) KLEIN, J. E. M. N.; TAYLOR, R. J. K. "Transition-Metal-Mediated Routes to 3,3-Disubstituted Oxindoles through Anilide Cyclisation". *Eur. J. Org. Chem.*, **2011**: 6821, 2011. (d) MILLEMAGGI, A.; TAYLOR, R. J. K. "3-Alkenyl-oxindoles: Natural Products, Pharmaceuticals, and Recent Synthetic Advances in Tandem/Telescoped Approaches". *Eur. J. Org. Chem.*, **2010**: 4527, 2010. (e) DALPOZZO, R.; BARTOLI, G.; BENCIVENNI, G. "Recent advances in organocatalytic methods for the synthesis of disubstituted 2- and 3-indolinones". *Chem. Soc. Rev.*, **41**, 7247, 2012. (f) HONG, L.; WANG, R. "Recent Advances in Asymmetric Organocatalytic Construction of 3,3'-Spirocyclic Oxindoles". *Adv. Synth. Catal.*, **355**: 1023, 2013. (g) CHEN, G.; WENG, Q.; FU, L.; WANG, Z.; YU, P.; LIU, Z.; LI, X.; ZHANG, H.; LIANG, G. "Synthesis and biological evaluation of novel oxindole-based RTK inhibitors as anti-cancer agents". *Bioorganic Med. Chem.*, **22**: 6953, 2014.

30. HENNESSY, E. J.; BUCHWALD, S. L. "Synthesis of substituted oxindoles from alpha-chloroacetanilides via palladium-catalyzed C-H functionalization". *J. Am. Chem. Soc.*, **125**: 12084, 2003.
31. JINGLEI, LV.; ZHANG-NEGRERIE, D.; DENG, J.; DU, Y.; ZHAO, K. "Metal-Free Synthesis of 2-Oxindoles via PhI(OAc)₂ - Mediated Oxidative C-C Bond Formation". *J. Org. Chem.*, **79**: 1111, 2014.
32. DONG, W.; LIU, Y.; HU, B.; REN, K.; LI, Y.; XIE, X.; JIANG, Y.; ZHANG, Z. "Visible light induced radical cyclization of o-iodophenylacrylamides: a concise synthesis of indolin-2-one". *Chem. Commun.*, **51**: 4587, 2015.
33. FU, W.; XU, F.; FU, Y.; ZHU, M.; YU, J.; XU, C.; ZOU, D. "Synthesis of 3,3-disubstituted oxindoles by visible-light-mediated radical reactions of aryl diazonium salts with N-arylacrylamides". *J. Org. Chem.*, **78**: 12202, 2013.
34. XIA, D.; MIAO, T.; LI, P.; WANG, L. "Visible-Light Photoredox Catalysis: Direct Synthesis of Sulfonated Oxindoles from N-Arylacrylamides and Arylsulfinic Acids by Means of a Cascade C-S/C-C Formation Process". *Chem. Asian J.* **10**: 1919, 2015.
35. (a) JU, X.; LIANG, Y.; JIA, P.; LI, W.; YU, W. "Synthesis of oxindoles via visible light photoredox catalysis". *Org. Biomol. Chem.*, **10**: 498, 2012. (b) HONEKER, R.; GARZA-SANCHEZ, R. A.; HOPKINSON, M. N.; GLORIUS, F. "Visible-Light-Promoted Trifluoromethylthiolation of Styrenes by Dual Photoredox/Halide Catalysis". *Chem. Eur. J.*, **22**: 4395, 2016. (c) WEI, X.; WANG, L.; DU, S.; WU, L.; LIU, Q. "Visible-light photoredox intramolecular difluoroacetamidation: facile synthesis of 3,3-difluoro-2-oxindoles from bromodifluoroacetamides". *Org. Biomol. Chem.*, **14**: 2195, 2016. (d) TANG, Q.; LIU, X.; LIU, S.; XIE, H.; LIU, W.; ZENG, J.; CHENG, P. "N-(Acyloxy)phthalimides as tertiary alkyl radical precursors in the visible light photocatalyzed tandem radical cyclization of N-arylacrylamides to 3,3-dialkyl substituted oxindoles". *RSC Adv.*, **5**: 89009, 2015. (e) ZHENG, L.; YANG, C.; XU, Z.; GAO, F.; XIA, W. "Difunctionalization of alkenes via the visible-light-induced trifluoromethylarylation/1,4-Aryl shift/desulfonylation cascade reactions". *J. Org. Chem.*, **80**: 5730, 2015. (f) ZHENG, L.; HUANG, H.; YANG, C.; XIA, W. "UV light-mediated difunctionalization of alkenes through aroyl radical addition/1,4-/1,2-Aryl shift cascade reactions". *Org. Lett.*, **17**: 1034, 2015. (g) XIA, X. D.; REN, Y-L.; CHEN, J-R.; YU, X-L.; LU, L-Q.; ZOU, Y-Q.; WAN, J.; XIAO, W-J. "Phototandem catalysis: Efficient synthesis of 3-ester-3-hydroxy-2-oxindoles by a visible light-induced cyclization of diazoamides through an aerobic oxidation sequence". *Chem. Asian J.* **10**: 124, 2015. (h) FU, W.; ZHU, M.; ZOU, G.; XU, C.; WANG, Z. "Visible-Light-Mediated Radical Aryldifluoroacetylation of N-Arylacrylamides to give Difluoroacetylated Oxindoles". *Asian J. Org. Chem.*, **3**: 1273, 2014. (i) FU, W.; ZHU, M.; ZOU, G.; XU, C.; WANG, Z. "Visible-Light-Mediated Trifluoroethylation of N-Arylacrylamides with Trifluoroethyl Iodide: Synthesis of CF₃-Containing Oxindoles". *SYNLETT*, **25**: 2513, 2014. (j) XIE, J.; Xu, P.; LI, H.; XUE, Q.; JIN, H.; CHENG, Y.; ZHU, C. "A room temperature decarboxylation/C-H functionalization cascade by visible-light photoredox catalysis". *Chem. Commun.* **49**: 5674, 2013.
36. CHATGILIALOGLU, C.; LALEVÉE, J. "Recent Applications of the (TMS)₃SiH Radical-Based Reagent". *Molecules*, **17**: (2012), 527.

37. CRICH, D.; RAHAMAN, M. Y. "Thiomaleic anhydride: A convenient building block for the synthesis of α -substituted γ - and δ -lactones through free-radical addition, nucleophilic ring opening, and subsequent thiocarboxylate manipulation". *J. Org. Chem.*, **74**: 6792, 2009.
38. POSTIGO, A.; KOPSOV, S.; ZLOTSKY, S. S.; FERRERI, C.; CHATGILIALOGLU, C. "Hydrosilylation of C-C multiple bonds using $(\text{Me}_3\text{Si})_3\text{SiH}$ in water. Comparative study of the radical initiation step". *Organometallics*, **28**: 3282, 2009.
39. (a) WNUK, S. F.; GARCIA, P. I.; WANG, Z. "Germyledesulfonylation of Vinyl and (a-Fluoro) vinyl Sulfones: Application of Tris(trimethylsilyl)silanes and Tris(trimethylsilyl)germanes in Pd-Catalyzed Couplings". *Org. Lett.*, **2**: 1995, 2004. (b) WANG, Z.; PITTLELOU, J. P.; MONTES, L.; RAPP, M.; DERANE, D.; WNUK, S. F. "Vinyl tris(trimethylsilyl)silanes: substrates for Hiyama coupling". *Tetrahedron*, **64**: 5322, 2008.
40. MAULIDE, N.; MARKÓ, I. E. "Stereoselective synthesis of bicyclic lactones by annelation with functionalized orthoesters". *Chem. Commun.*, 1200, 2006.
41. PUDLO, M.; GÉRARD, S.; MIRAND, C.; SAPI, J. "A tandem radical cyclization approach to 3-(2-oxopyrrolidin-3-yl)indolin-2-ones, potential intermediates toward complex indole-heterocycles". *Tetrahedron Lett.*, **49**: 1066, 2008.
42. JIANG, H.; BAK, J. R.; LOPEZ-DELGADO, F. J.; JØRGENSEN, K. A. "Practical metal- and additive-free methods for radical-mediated reduction and cyclization reactions". *Green Chem.*, **15**: 3355, 2013.
43. CARIN, C. C.; SEECHURN, J.; KITCHING, M. O.; COLACOT, T. J.; SNIECKUS, V. "Palladium-catalyzed cross-coupling: A historical contextual perspective to the 2010 nobel prize". *Angew. Chem. Int. Ed.*, **51**: 5062, 2012.
44. (a) PURSER, S.; MOORE, P. R.; SWALLOW, S.; GOUVERNEUR, V. "Fluorine in medicinal chemistry". *Chem. Soc. Rev.*, **37**: 320, 2008. (b) HAGMANN, W. K. "The many roles for fluorine in medicinal chemistry". *J. Med. Chem.*, **51**: 4359, 2008. (c) JIANG, H.; FALCICCHIO, A.; JENSEN, K. L.; PAIXÃO, M. W.; BERTELSEN, S.; JØRGENSEN, K. A. "Target-directed organocatalysis: A direct asymmetric catalytic approach to chiral propargylic and allylic fluorides". *J. Am. Chem. Soc.*, **131**: 7153, 2009. (d) NAGID, D. A.; MACMILLAN, D. W. C. "Trifluoromethylation of arenes and heteroarenes by means of photoredox catalysis". *Nature*, **480**: 224, 2011.
45. AMIR-HEIDARI, B.; MICKFIELD, J. "NMR confirmation that tryptophan dehydrogenation occurs with syn stereochemistry during the biosynthesis of CDA in *Streptomyces coelicolor*". *J. Org. Chem.*, **72**: 8950, 2007.
46. BAJWA, J. S.; CHEN, G. P.; PRASAD, K.; REPIČ, O.; BLACKLOCK, T. J. "Deprotection of N-tosylated indoles and related structures using cesium carbonate". *Tetrahedron Lett.*, **47**: 6425, 2006.

47. CISMESIA, M. A.; YOON, T. P. "Characterizing chain processes in visible light photoredox catalysis". *Chem. Sci.*, **6**: 5426, 2015.
48. BLACKMOND, D. G. "Reaction progress kinetic analysis: A powerful methodology for mechanistic studies of complex catalytic reactions". *Angew. Chem. Int. Ed.*, **44**: 4302, 2005.
49. (a) CLAYDEN, J.; GREEVES, N.; WARREN, S.; Organic Chemistry., *Organic Chemistry*, 2^a Ed., Oxford University Press, 2012. (b) CAREY, A. F.; SUNDBERG, R. J. *Advanced Organic Chemistry*, 5^a ed., Springer, 2007.
50. ZHANG, S. L.; LANG, M. J.; GOODMAN, S.; DURNELL, C.; FIDLAR, V.; FLEMING, G. R.; YANG, N. C. "Donor-acceptor interaction and photochemistry of polymethylene-linked bichromophores in solution". *J. Am. Chem. Soc.*, **118**: 9042, 1996.
51. (a) CURRAN, D. P.; KELLER, A. I. "Radical additions of aryl iodides to arenes are facilitated by oxidative rearomatization with dioxygen". *J. Am. Chem. Soc.*, **128**: 13706, 2006. (b) KIM, J. G.; MISHRA, M. K.; JANG, D. O. "Synthesis of sterically hindered ketones from aldehydes via O-silyl oximes". *Tetrahedron Lett.*, **53**: 3527, 2012. (c) TEHFE, M. A.; LALEVÉE, J.; ALIONAS, X.; FOUASSIER, J. P. "Long wavelength cationic photopolymerization in aerated media: A remarkable titanocene/tris(trimethylsilyl)silane/onium salt photoinitiating system". *Macromolecules*, **42**: 8669, 2009. (d) HIEROLD, J.; LUPTON, D. W. "Synthesis of spirocyclic γ -lactones by cascade Beckwith-Dowd ring expansion/cyclization". *Org. Lett.*, **14**: 3412, 2012. (e) Hasegawa, E.; OGAWA, Y.; KAKINUMA, K.; TSUCHIDA, H.; TOSAKA, E.; TAKIZAWA, S.; MURAOKA, H.; SAIKAWA, T. "Tris(trimethylsilyl)silane promoted radical reaction and electron-transfer reaction in benzotrifluoride". *Tetrahedron*, **64**: 7724, 2008. (f) POSTIGO, A.; KOPSOV, S.; ZLOTSKY, S. S.; FERRERI, C.; CHATGILIALOGLU, C. "Hydrosilylation of C-C multiple bonds using $(\text{Me}_3\text{Si})_3\text{SiH}$ in water. Comparative study of the radical initiation step". *Organometallics*, **28**: 3282, 2009. (g) LALEVÉE, J.; BLANCHARD, N.; GRAFF, B.; ALLONAS, X.; FOUASSIER, J. P. "Tris(trimethylsilyl)silyl versus tris(trimethylsilyl)germyl: Radical reactivity and oxidation ability". *J. Organomet. Chem.*, **693**: 3643, 2008.
52. (a) FOSTER, R. "Electron donor-acceptor complexes". *J. Phys. Chem.*, **84**: 2135, 1980. (b) ROSOKHA, S. V.; KOCHI, J. K. "Fresh look at electron-transfer mechanisms via the donor/acceptor bindings in the critical encounter complex". *Acc. Chem. Res.* **41**: 641, 2008.
53. ARCEO, E.; MONTRONI, E.; MELCHIORRE, P. "Photo-Organocatalysis of Atom-Transfer Radical Additions to Alkenes". *Angew. Chem. Int. Ed.*, **53**: 12064, 2014.
54. SILVA, R. C.; CHATTERJEE, I.; ADÁN, E. E.; PAIXÃO, M. W.; MELCHIORRE, P. "Synthesis of Cyclopropane Spirooxindoles by means of a Vinylogous Organocatalytic Cascade". *Asian J. Org. Chem.*, **3**: 466, 2014.
55. BRESSY, C.; ALBERICO, D.; LAUTENS, M. "A route to annulated indoles via a palladium-catalyzed tandem alkylation/direct arylation reaction". *J. Am. Chem. Soc.*, **127**: 13148, 2005.

56. LUO, Q. L.; LV, L.; LI, Y.; TAN, P.; NAN, W.; HUI, Q. "An Efficient Protocol for the Amidation of Carboxylic Acids Promoted by Trimethyl Phosphite and Iodine". *Eur. J. Org. Chem.*, **34**: 6916, 2011.

57. LIU, X.; MA, X.; HUANG, Y.; GU, Z. "Pd-catalyzed Heck-type cascade reactions with N-tosyl hydrazones: An efficient way to alkenes via in situ generated alkylpalladium". *Org. Lett.* **15**: 4814, 2013.

6 Experimental Section

6.1 General Experimental Information

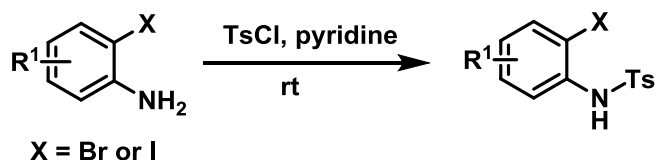
All solvents were dried and distilled prior to use by standard procedures and chemicals were either used as received or purified according to the procedures outlined in Purification of Common Laboratory Chemicals. Glassware used was dried in oven or flame dried under vacuum and cooled under inert atmosphere. Reactions were monitored by TLC and visualized by a dual short wave/long wave UV lamp and stained with an ethanolic solution of potassium permanganate or vanillin. Column flash chromatography was performed using gel 60 (230–400 mesh), and analytical thin-layer chromatography (TLC) was performed using silica gel aluminum sheets. Yields refer to chromatographically and spectroscopically pure compounds, unless otherwise noted.

^1H NMR and ^{13}C NMR spectra were recorded at 400 MHz. for ^1H and 100 MHz for ^{13}C , respectively. Chemical shifts (δ) are reported in parts per million relative to tetramethylsilane (TMS), and coupling constants (J) are reported in hertz. All signals are reported in ppm with the internal reference of 7.26 ppm or 77.0 ppm for chloroform. Data are presented as follows: multiplicity (s = singlet, d = doublet, t = triplet, q = quartet, quint = quintet, m = multiplet, br = broad, dd = doublet of doublet, dt = doublet of triplet), coupling constant (J/Hz) and integration.

6.2 General Experimental Procedures

6.2.1 Preparation of the starting materials

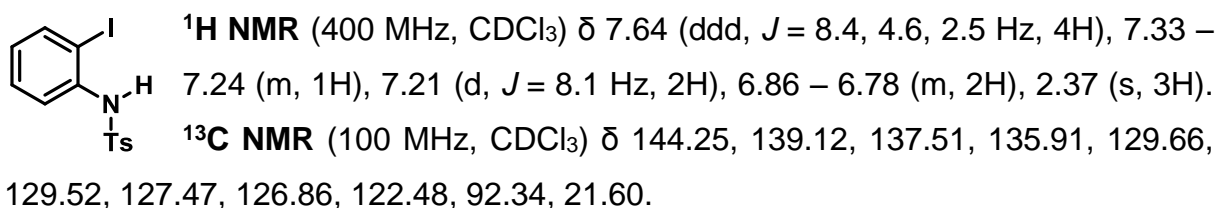
6.2.1.1 Preparation of the *N*-tosyl-protected aniline⁵⁵



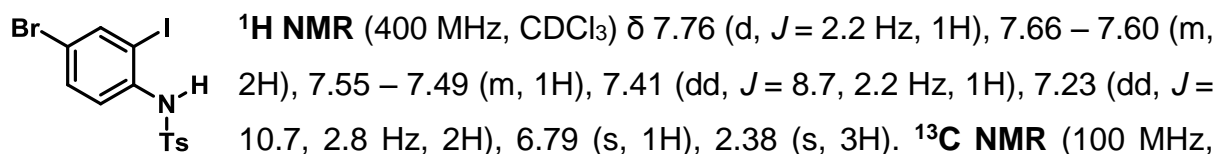
SCHEME 33: Synthesis of *N*-tosyl-protected aniline.

To a solution of 2-iodoaniline (4.50 mmol, 1 equiv) in pyridine (10 mL) was added in one portion *p*-toluenesulfonyl chloride (4.70 mmol, 1.05 equiv). The reaction was stirred at rt for 1.5 h then quenched with water (10 mL). The solution was extracted with CH_2Cl_2 (3 time) and the combined organic extracts were washed with a 10% aqueous CuSO_4 (2 time), dried over anhydrous Na_2SO_4 , filtered and concentrated under vacuum. The crude mixture was purified by flash chromatography (hexane/EtOAc) to afford the corresponding tosyl-protected aniline.

N-(2-iodophenyl)-4-methylbenzenesulfonamide



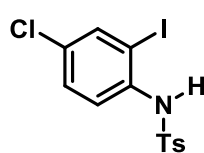
N-(4-bromo-2-iodophenyl)-4-methylbenzenesulfonamide



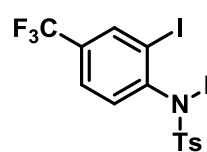
⁵⁵ BRESSY, C.; ALBERICO, D.; LAUTENS, M. "A route to annulated indoles via a palladium-catalyzed tandem alkylation/direct arylation reaction". *J. Am. Chem. Soc.*, **127**: 13148, 2005.

CDCl₃) δ 144.53, 140.88, 136.86, 135.66, 132.53, 129.82, 127.45, 123.46, 118.88, 92.83, 21.64.

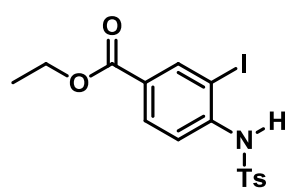
***N*-(4-chloro-2-iodophenyl)-4-methylbenzenesulfonamide**

 **¹H NMR** (400 MHz, CDCl₃) δ 7.65 – 7.60 (m, 7H), 7.58 (s, 1H), 7.29 (dd, *J* = 8.7, 2.4 Hz, 2H), 7.25 – 7.21 (m, 4H), 6.73 (s, 2H), 2.40 (s, 6H). **¹³C NMR** (100 MHz, CDCl₃) δ 144.50, 138.22, 136.38, 135.66, 131.35, 129.78, 129.63, 127.45, 123.12, 92.36, 21.61.

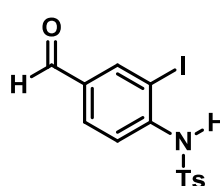
***N*-(2-iodo-4-(trifluoromethyl)phenyl)-4-methylbenzenesulfonamide**

 **¹H NMR** (400 MHz, CDCl₃) δ 7.90 (t, *J* = 2.4 Hz, 2H), 7.74 – 7.68 (m, 6H), 7.54 (dd, *J* = 8.6, 1.7 Hz, 2H), 7.29 – 7.24 (m, 5H), 7.08 (s, 2H), 2.39 (s, 6H). **¹³C NMR** (100 MHz, CDCl₃) δ 144.84, 140.80, 136.16, 135.61, 129.96, 127.40, 126.64, 126.61, 120.29, 90.19, 21.61.

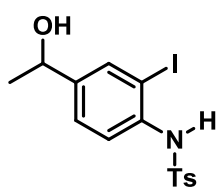
Ethyl 3-iodo-4-((4-methylphenyl)sulfonamido)benzoate

 **¹H NMR** (400 MHz, CDCl₃) δ 8.31 (dd, *J* = 4.8, 1.9 Hz, 2H), 8.03 – 7.76 (m, 3H), 7.74 – 7.61 (m, 5H), 7.26 – 7.16 (m, 5H), 4.33 (q, *J* = 7.0 Hz, 4H), 2.36 (s, 5H), 1.35 (t, *J* = 7.1 Hz, 6H). **¹³C NMR** (100 MHz, CDCl₃) δ 164.41, 144.67, 141.36, 140.47, 135.63, 130.75, 129.87, 127.41, 119.73, 90.13, 61.38, 21.59, 14.30.

***N*-(4-formyl-2-iodophenyl)-4-methylbenzenesulfonamide**

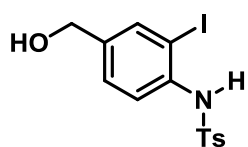
 **¹H NMR** (400 MHz, CDCl₃) δ 9.82 (s, 1H), 8.20 (d, *J* = 1.5 Hz, 1H), 7.79 (tt, *J* = 3.2, 1.6 Hz, 1H), 7.77 – 7.73 (m, 3H), 7.31 – 7.26 (m, 2H), 2.41 (s, 3H).

***N*-(4-(1-hydroxyethyl)-2-iodophenyl)-4-methylbenzenesulfonamide**



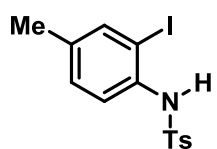
¹H NMR (400 MHz, CDCl₃) δ 7.88 (d, *J* = 8.3 Hz, 3H), 7.69 (d, *J* = 1.9 Hz, 2H), 7.64 (d, *J* = 8.3 Hz, 4H), 7.60 – 7.57 (m, 2H), 7.34 (t, *J* = 7.1 Hz, 4H), 7.31 – 7.26 (m, 3H), 7.22 (d, *J* = 8.0 Hz, 4H), 6.82 (s, 2H), 4.79 (dd, *J* = 6.4, 2.4 Hz, 2H), 2.39 (s, 6H), 2.13 (d, *J* = 2.8 Hz, 2H), 1.43 (d, *J* = 6.5 Hz, 6H). ¹³C NMR (100 MHz, CDCl₃) δ 149.40, 145.40, 144.68, 144.26, 137.92, 136.05, 132.89, 129.70, 129.53, 127.45, 126.70, 125.76, 122.44, 103.30, 92.53, 68.91, 25.23, 21.78, 21.60.

***N*-(4-(hydroxymethyl)-2-iodophenyl)-4-methylbenzenesulfonamide**



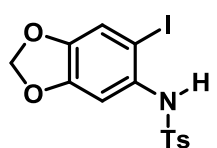
¹H NMR (400 MHz, CDCl₃) δ 7.86 – 7.76 (m, 1H), 7.60 (d, *J* = 1.8 Hz, 1H), 7.55 (ddd, *J* = 8.3, 3.7, 1.7 Hz, 3H), 7.29 – 7.19 (m, 1H), 7.14 (dd, *J* = 8.6, 0.6 Hz, 2H), 6.72 (s, 1H), 4.52 (s, 2H), 2.31 (s, 3H), 1.71 (bs, 1H). ¹³C NMR (100 MHz, CDCl₃) δ 144.28, 139.66, 137.38, 136.74, 135.86, 129.69, 128.00, 127.46, 122.37, 92.40, 63.66, 21.60.

***N*-(2-iodo-4-methylphenyl)-4-methylbenzenesulfonamide**



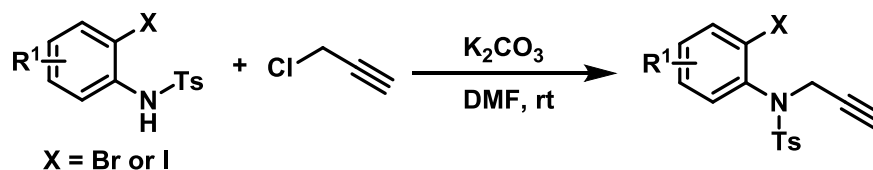
¹H NMR (400 MHz, CDCl₃) δ 7.64 – 7.58 (m, 2H), 7.44 – 7.39 (m, 2H), 7.26 (dd, *J* = 5.6, 5.0 Hz, 1H), 6.87 – 6.82 (m, 2H), 3.12 (s, 3H), 2.42 (s, 3H).

***N*-(6-iodobenzo[d][1,3]dioxol-5-yl)-4-methylbenzenesulfonamide**



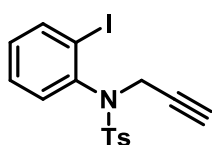
¹H NMR (400 MHz, CDCl₃) δ 7.63 – 7.57 (m, 2H), 7.26 – 7.18 (m, 3H), 7.01 (s, 1H), 6.52 (s, 1H), 5.98 (d, *J* = 5.1 Hz, 2H), 2.39 (d, *J* = 3.2 Hz, 3H). ¹³C NMR (100 MHz, CDCl₃) δ 149.04, 144.18, 135.78, 131.61, 129.62, 127.56, 127.31, 117.21, 108.90, 105.55, 102.20, 81.71, 21.62.

6.2.1.2 Preparation of the *N*-tosyl-propargyl aniline (Compounds 46a-o)¹

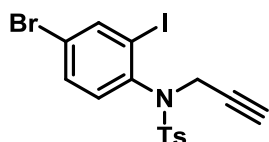


SCHEME 34: Synthesis of *N*-tosyl-propargyl aniline.

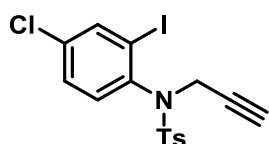
To a solution of *N*-tosyl protected 2-iodoaniline (1.0 mmol, 1 equiv) in DMF (5 mL) was added K_2CO_3 (3.0 mmol, 3 equiv) and propargyl chloride (2.0 mmol, 2 equiv). The reaction was stirred at rt for 3 h then quenched with water (5 mL). The aqueous layer was extracted with ether (3 x 10mL) and the combined organic phase were dried over anhydrous Na_2SO_4 , filtered and concentrated. The crude mixture was purified by flash chromatography (hexane/EtOAc) to afford *N*-tosyl-propargyl aniline.



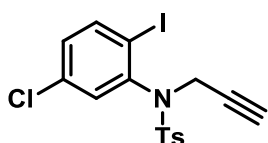
Compound 46a: $^1\text{H NMR}$ (400 MHz, CDCl_3) δ 7.91 (dd, $J = 7.9, 1.4$ Hz, 1H), 7.71 (d, $J = 8.3$ Hz, 2H), 7.31 – 7.26 (m, 3H), 7.14 (dd, $J = 7.9, 1.6$ Hz, 1H), 7.06 (td, $J = 7.9, 1.6$ Hz, 1H), 4.77 (dd, $J = 18.2, 2.5$ Hz, 1H), 4.12 (dd, $J = 18.2, 2.5$ Hz, 1H), 2.44 (s, 3H), 2.16 (t, $J = 2.5$ Hz, 1H). $^{13}\text{C NMR}$ (100 MHz, CDCl_3) δ 143.96, 140.68, 140.29, 136.64, 131.25, 130.46, 129.45, 128.75, 128.34, 102.57, 77.69, 74.06, 40.66, 21.63.



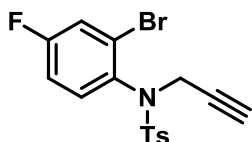
Compound 46b: $^1\text{H NMR}$ (400 MHz, CDCl_3) δ 8.05 (d, $J = 2.2$ Hz, 1H), 7.72 – 7.66 (m, 2H), 7.41 (dd, $J = 8.5, 2.3$ Hz, 1H), 7.33 – 7.27 (m, 2H), 6.99 (d, $J = 8.5$ Hz, 1H), 4.73 (dd, $J = 18.2, 2.3$ Hz, 1H), 4.09 (dd, $J = 18.2, 2.4$ Hz, 1H), 2.45 (s, 3H), 2.18 (t, $J = 2.5$ Hz, 1H). $^{13}\text{C NMR}$ (100 MHz, CDCl_3) δ 144.25, 142.35, 139.88, 136.27, 132.01, 129.59, 128.29, 123.76, 103.51, 74.41, 40.55, 21.66.



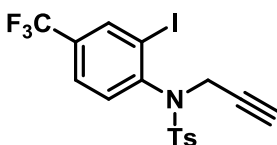
Compound 46c: $^1\text{H NMR}$ (400 MHz, CDCl_3) δ 7.90 (d, $J = 2.3$ Hz, 1H), 7.70 (d, $J = 8.2$ Hz, 2H), 7.35 – 7.24 (m, 3H), 7.05 (d, $J = 8.5$ Hz, 1H), 4.81 – 4.69 (m, 1H), 4.16 – 4.02 (m, 1H), 2.45 (s, 3H), 2.18 (t, $J = 2.4$ Hz, 1H). $^{13}\text{C NMR}$ (100 MHz, CDCl_3) δ 144.22, 139.64, 139.38, 136.29, 135.53, 131.47, 129.58, 129.00, 128.30, 103.02, 74.37, 40.60, 21.65.



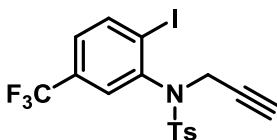
Compound 46d: $^1\text{H NMR}$ (400 MHz, CDCl_3) δ 7.84 (d, $J = 8.5$ Hz, 1H), 7.74 (d, $J = 8.3$ Hz, 2H), 7.34 (d, $J = 8.0$ Hz, 2H), 7.11 (dt, $J = 8.4, 2.3$ Hz, 2H), 4.74 (dd, $J = 18.2, 2.1$ Hz, 1H), 4.12 (dd, $J = 18.2, 2.2$ Hz, 1H), 2.48 (s, 3H), 2.22 (t, $J = 2.5$ Hz, 1H). $^{13}\text{C NMR}$ (100 MHz, CDCl_3) δ 144.37, 141.83, 140.74, 136.13, 134.44, 131.42, 130.73, 129.60, 128.32, 100.07, 77.13, 74.56, 40.57, 21.66.



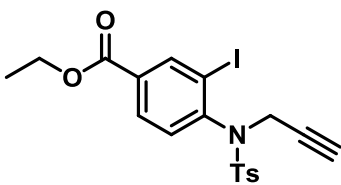
Compound 46e: $^1\text{H NMR}$ (400 MHz, CDCl_3) δ 7.72 – 7.66 (m, 2H), 7.37 (dd, $J = 7.9, 2.9$ Hz, 1H), 7.29 (dd, $J = 11.5, 3.5$ Hz, 2H), 7.21 (dd, $J = 8.8, 5.6$ Hz, 1H), 6.99 (ddd, $J = 8.8, 7.6, 2.9$ Hz, 1H), 4.76 (d, $J = 17.9$ Hz, 1H), 4.16 – 4.06 (m, 1H), 2.44 (s, 3H), 2.19 (t, $J = 2.5$ Hz, 1H).



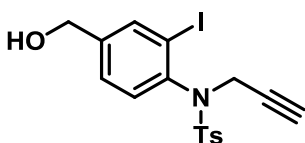
Compound 46f: $^1\text{H NMR}$ (400 MHz, CDCl_3) δ 8.05 (d, $J = 1.5$ Hz, 1H), 7.62 – 7.56 (m, 2H), 7.47 – 7.43 (m, 1H), 7.20 (d, $J = 8.0$ Hz, 2H), 7.14 (dd, $J = 5.9, 2.3$ Hz, 1H), 4.63 (d, $J = 18.2$ Hz, 1H), 4.08 – 3.99 (m, 1H), 2.32 (s, 3H), 2.09 (t, $J = 2.5$ Hz, 1H). $^{13}\text{C NMR}$ (100 MHz, CDCl_3) δ 145.78, 144.44, 137.21, 136.15, 131.41, 129.68, 129.53, 128.30, 125.84, 102.75, 77.13, 74.60, 40.51, 21.65.



Compound 46g: $^1\text{H NMR}$ (400 MHz, CDCl_3) δ 7.79 (d, $J = 8.0$ Hz, 1H), 7.69 (d, $J = 8.2$ Hz, 2H), 7.48 (d, $J = 6.8$ Hz, 1H), 7.37 (s, 1H), 7.32 (d, $J = 7.9$ Hz, 2H), 4.75 (s, 1H), 4.18 (s, 1H), 2.46 (s, 3H), 2.19 (t, $J = 2.4$ Hz, 1H).

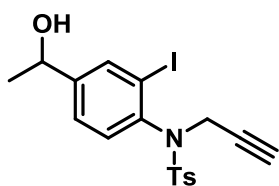


Compound 46h: $^1\text{H NMR}$ (400 MHz, CDCl_3) δ 8.56 (d, $J = 1.9$ Hz, 1H), 7.98 – 7.94 (m, 1H), 7.73 – 7.68 (m, 2H), 7.33 – 7.29 (m, 2H), 7.23 – 7.19 (m, 1H), 4.75 (d, $J = 18.1$ Hz, 1H), 4.38 (q, $J = 7.1$ Hz, 2H), 4.22 – 4.09 (m, 1H), 2.45 (s, 3H), 2.19 (t, $J = 2.5$ Hz, 1H), 1.40 (t, $J = 7.1$ Hz, 3H). $^{13}\text{C NMR}$ (100 MHz, CDCl_3) δ 164.36, 144.31, 141.21, 136.22, 132.18, 130.92, 129.88, 129.61, 129.53, 128.30, 102.27, 77.26, 74.50, 61.64, 40.53, 21.65, 14.29.

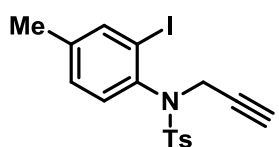


Compound 46k: $^1\text{H NMR}$ (400 MHz, CDCl_3) δ 7.94 – 7.90 (m, 1H), 7.74 – 7.68 (m, 2H), 7.31 – 7.27 (m, 3H), 7.13 – 7.07 (m, 1H), 4.75 (dd, $J = 18.2, 2.4$ Hz, 1H), 4.66 (d, $J = 2.3$ Hz, 2H), 4.15 – 4.07 (m, 1H), 2.44 (s, 3H), 2.16 (t, $J = 2.5$ Hz, 1H), 1.96 (bs, 1H). $^{13}\text{C NMR}$ (100

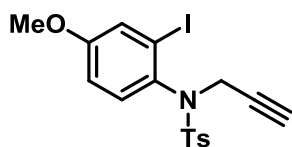
MHz, CDCl₃) δ 144.02, 143.53, 139.72, 138.30, 136.57, 130.99, 129.70, 128.31, 126.99, 102.64, 77.65, 74.13, 63.64, 40.67, 21.64.



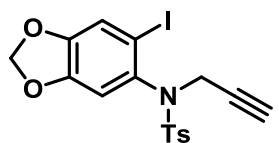
Compound 46l: ¹H NMR (400 MHz, CDCl₃) δ 7.84 (d, *J* = 6.2 Hz, 1H), 7.80 (d, *J* = 8.3 Hz, 1H), 7.64 (d, *J* = 8.3 Hz, 2H), 7.22 (d, *J* = 8.0 Hz, 2H), 7.01 (d, *J* = 8.0 Hz, 1H), 4.83 – 4.73 (m, 1H), 4.72 – 4.63 (m, 1H), 4.02 (dd, *J* = 18.3, 2.3 Hz, 1H), 2.37 (s, 3H), 2.08 (t, *J* = 2.4 Hz, 1H), 1.96 (bs, 1H), 1.40 (d, *J* = 6.5 Hz, 3H). ¹³C NMR (100 MHz, CDCl₃) δ 148.37, 143.99, 139.60, 137.24, 136.66, 130.95, 129.49, 128.30, 125.86, 102.62, 77.70, 74.11, 69.08, 40.70, 25.22, 21.63.



Compound 46m: ¹H NMR (400 MHz, CDCl₃) δ 7.74 (d, *J* = 1.2 Hz, 1H), 7.71 (d, *J* = 8.3 Hz, 2H), 7.29 (d, *J* = 8.0 Hz, 2H), 7.07 (dd, *J* = 8.1, 1.3 Hz, 1H), 7.00 (d, *J* = 8.0 Hz, 1H), 4.74 (dd, *J* = 18.2, 2.4 Hz, 1H), 4.10 (dd, *J* = 18.2, 2.4 Hz, 1H), 2.44 (s, 3H), 2.31 (s, 3H), 2.15 (t, *J* = 2.5 Hz, 1H).

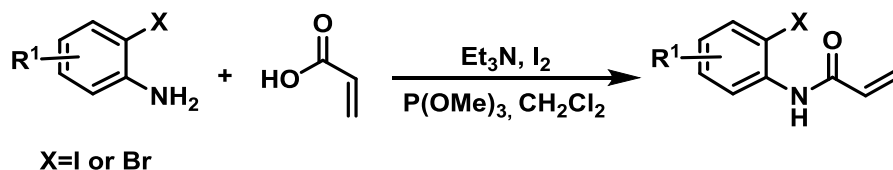


Compound 46n: ¹H NMR (400 MHz, CDCl₃) δ 7.73 (s, 2H), 7.43 (s, 1H), 7.31 (s, 2H), 7.04 (s, 1H), 6.82 (s, 1H), 4.78 (d, *J* = 16.8 Hz, 1H), 4.11 (d, *J* = 16.9 Hz, 1H), 3.81 (s, 3H), 2.47 (s, 3H), 2.19 (s, 1H). ¹³C NMR (100 MHz, CDCl₃) δ 159.87, 143.84, 136.68, 133.28, 131.22, 129.42, 128.31, 125.03, 114.44, 103.05, 77.91, 73.97, 55.68, 40.84, 21.63.



Compound 46o: ¹H NMR (400 MHz, CDCl₃) δ 7.75 – 7.70 (m, 2H), 7.30 (d, *J* = 7.9 Hz, 2H), 7.27 (s, 1H), 6.67 (s, 1H), 6.03 – 5.99 (m, 2H), 4.73 (dd, *J* = 18.2, 2.5 Hz, 1H), 4.05 (dd, *J* = 18.2, 2.5 Hz, 1H), 2.44 (d, *J* = 2.9 Hz, 3H), 2.19 (dt, *J* = 4.9, 2.5 Hz, 1H). ¹³C NMR (100 MHz, CDCl₃) δ 148.82, 144.03, 136.56, 129.51, 128.30, 127.90, 118.52, 112.05, 111.22, 110.00, 102.45, 91.81, 77.75, 74.22, 40.72, 21.64.

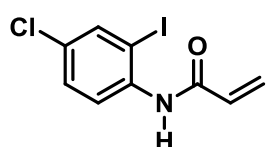
6.2.1.3 Preparation of the *N*-acrylamides⁵⁶



SCHEME 35: Synthesis of *N*-acrylamides.

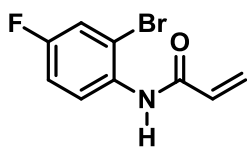
A solution of P(OMe)₃ (0.35 mL, 3.0 mmol) in dichloromethane (15 mL) was cooled to 0° C, using an ice bath, then I₂ (760 mg, 3.0 mmol) was added. After the solid iodine was completely dissolved, acrylic acid (204.7 μL, 3.0 mmol) and Et₃N (0.70 mL, 5.0 mmol) were added in sequential order, and the solution was stirred for 10 min in a cooling bath. After this period, substituted aniline (2.0 mmol) was added and the mixture was stirred for 10 min. After removing the cooling bath, the reaction mixture was stirred for 3 h at room temperature (reaction monitored by TLC), then diluted with saturated aqueous NaHCO₃ and extracted with dichloromethane (3 x 30 mL). The combined organic layer was sequentially washed with water, HCl 1M, water, and brine, dried with anhydrous Na₂SO₄, and then purified by flash chromatography (hexane/EtOAc) to afford substituted *N*-acrylamide.

N-(4-chloro-2-iodophenyl)acrylamide



¹H NMR (400 MHz, CDCl₃) δ 8.27 (d, *J* = 8.8 Hz, 1H), 7.77 (t, *J* = 3.1 Hz, 1H), 7.65 – 7.52 (m, 1H), 7.37 – 7.31 (m, 1H), 6.47 (dd, *J* = 16.9, 1.1 Hz, 1H), 6.31 (dd, *J* = 16.9, 10.2 Hz, 1H), 5.85 (dd, *J* = 10.2, 1.1 Hz, 1H). ¹³C NMR (100 MHz, CDCl₃) δ 163.43, 137.88, 136.85, 130.99, 130.11, 129.33, 128.52, 122.36, 89.87.

N-(2-bromo-4-fluorophenyl)acrylamide

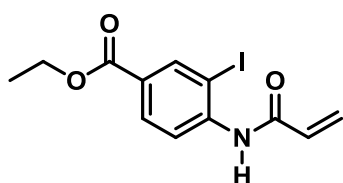


¹H NMR (400 MHz, CDCl₃) δ 8.46 – 8.33 (m, 1H), 7.67 (s, 1H), 7.31 (dd, *J* = 7.8, 2.9 Hz, 1H), 7.11 – 7.03 (m, 1H), 6.46 (dd, *J* = 16.9, 1.2 Hz, 1H), 6.31 (dd, *J* = 16.9, 10.2 Hz, 1H), 5.84 (dd, *J* = 10.2,

⁵⁶ LUO, Q. L.; LV, L.; LI, Y.; TAN, P.; NAN, W.; HUI, Q. "An Efficient Protocol for the Amidation of Carboxylic Acids Promoted by Trimethyl Phosphite and Iodine". *Eur. J. Org. Chem.*, **34**: 6916, 2011.

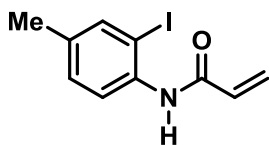
1.2 Hz, 1H). ^{13}C NMR (100 MHz, CDCl_3) δ 163.39, 159.85, 157.38, 132.01, 130.95, 128.38, 123.16, 119.48, 119.22, 115.38, 115.16, 113.66.

Ethyl 4-acrylamido-3-iodobenzoate



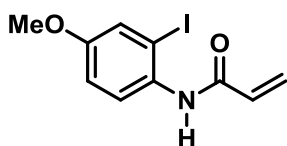
^1H NMR (400 MHz, CDCl_3) δ 8.48 – 8.44 (m, 1H), 8.43 (d, J = 1.8 Hz, 1H), 8.00 (ddd, J = 8.6, 1.9, 0.4 Hz, 1H), 7.81 (s, 1H), 6.47 (dd, J = 16.9, 1.1 Hz, 1H), 6.33 (dd, J = 16.9, 10.2 Hz, 1H), 5.86 (dd, J = 10.2, 1.1 Hz, 1H), 4.35 (q, J = 7.1 Hz, 2H), 1.38 (t, J = 7.1 Hz, 3H). ^{13}C NMR (100 MHz, CDCl_3) δ 164.64, 163.48, 141.79, 140.14, 131.05, 130.77, 128.89, 127.51, 120.33, 88.69, 61.27, 14.32.

N-(2-iodo-4-methylphenyl)acrylamide



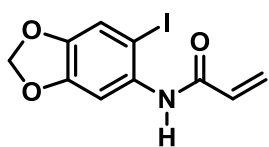
^1H NMR (400 MHz, CDCl_3) δ 8.18 (s, 1H), 7.64 (s, 1H), 7.53 (s, 1H), 7.18 (dd, J = 8.3, 0.7 Hz, 1H), 6.46 (dd, J = 16.9, 1.2 Hz, 1H), 6.31 (dd, J = 16.9, 10.2 Hz, 1H), 5.83 (dd, J = 10.2, 1.0 Hz, 1H), 2.31 (s, 3H). ^{13}C NMR (100 MHz, CDCl_3) δ 163.40, 139.03, 136.21, 135.55, 131.34, 130.00, 127.88, 121.78, 90.19, 20.36.

N-(2-iodo-4-methoxyphenyl)acrylamide



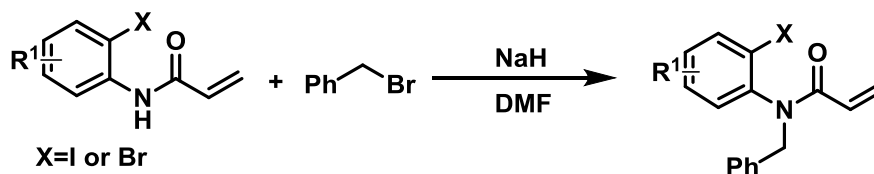
^1H NMR (400 MHz, CDCl_3) δ 8.12 (d, J = 8.7 Hz, 1H), 7.46 – 7.38 (m, 1H), 7.35 (d, J = 2.8 Hz, 1H), 6.94 (dd, J = 9.0, 2.8 Hz, 1H), 6.49 – 6.41 (m, 1H), 6.31 (dd, J = 17.0, 10.2 Hz, 1H), 5.81 (d, J = 10.8 Hz, 1H), 3.80 (s, 3H).

N-(6-iodobenzo[d][1,3]dioxol-5-yl)acrylamide



^1H NMR (400 MHz, CDCl_3) δ 7.88 (s, 1H), 7.42 (s, 1H), 7.20 (s, 1H), 6.45 (dd, J = 16.9, 1.1 Hz, 1H), 6.29 (dd, J = 17.0, 10.2 Hz, 1H), 6.01 (s, 2H), 5.82 (dd, J = 10.2, 0.9 Hz, 1H). ^{13}C NMR (100 MHz, CDCl_3) δ 163.37, 148.67, 145.41, 132.41, 131.21, 127.96, 117.13, 104.12, 101.99, 78.23.

6.2.1.4 Preparation of the *N*-benzyl-acrylamides (Compounds 48a-i)⁵⁷

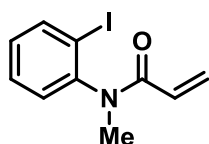


SCHEME 36: Synthesis of *N*-benzyl-acrylamides.

NaH (30 mg, 60% in mineral oil, 0.75 mmol, 1.5 eq) was added in portions to a solution of substituted *N*-(2-iodophenyl) acrylamide (0.50 mmol, 1.0 eq) in DMF (2.0 ml) at 0 °C. After stirring for 20 min, BnBr (70 μ l, 0.60 mmol, 1.2 eq) was added dropwise and the reaction mixture was allowed to warm to room temperature and stirred overnight. The reaction was quenched with water and THF was removed by evaporation. The residue was extracted with ethyl acetate twice, and the organic phase was washed with brine, dried over Na₂SO₄, filtered and concentrated. The residue was purified by column chromatography (hexane/EtOAc) to afford the desired product. All spectroscopy data are accordance with seminal literature.

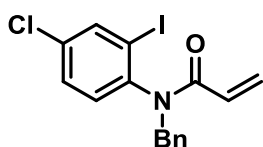


Compound 48a: ¹H NMR (400 MHz, CDCl₃) δ 7.87 (dd, J = 7.9, 1.4 Hz, 1H), 7.22 – 7.13 (m, 5H), 6.99 – 6.94 (m, 1H), 6.65 (dd, J = 7.8, 1.6 Hz, 1H), 6.39 (dd, J = 16.7, 2.0 Hz, 1H), 5.75 (dd, J = 16.7, 10.3 Hz, 1H), 5.62 (d, J = 14.2 Hz, 1H), 5.48 (dd, J = 10.3, 2.0 Hz, 1H), 3.98 (d, J = 14.2 Hz, 2H).

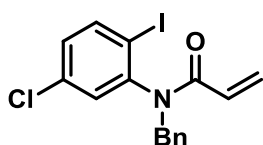


Compound 48b: ¹H NMR (400 MHz, CDCl₃) δ 7.90 – 7.84 (m, 1H), 7.39 – 7.31 (m, 1H), 7.22 – 7.15 (m, 1H), 7.08 – 6.96 (m, 1H), 6.32 (dd, J = 16.7, 2.0 Hz, 1H), 5.77 (dd, J = 16.7, 10.3 Hz, 1H), 5.45 (dd, J = 10.3, 2.0 Hz, 1H), 3.18 (s, 3H). ¹³C NMR (100 MHz, CDCl₃) δ 165.48, 145.51, 140.18, 129.88, 129.37, 128.13, 127.97, 99.65, 36.14.

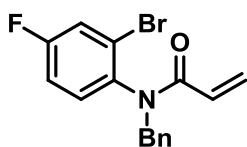
⁵⁷ LIU, X.; MA, X.; HUANG, Y.; GU, Z. "Pd-catalyzed Heck-type cascade reactions with *N*-tosyl hydrazones: An efficient way to alkenes via in situ generated alkylpalladium". *Org. Lett.* **15**: 4814, 2013.



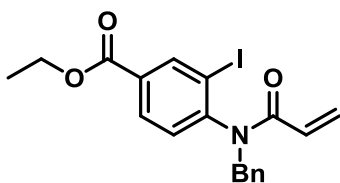
Compound 48c: $^1\text{H NMR}$ (400 MHz, CDCl_3) δ 7.93 (d, $J = 2.3$ Hz, 1H), 7.31 – 7.25 (m, 3H), 7.22 (dt, $J = 8.9, 2.3$ Hz, 2H), 7.18 (d, $J = 2.4$ Hz, 1H), 6.66 – 6.60 (m, 1H), 6.48 (dd, $J = 16.7, 1.9$ Hz, 1H), 5.83 (dd, $J = 16.7, 10.3$ Hz, 1H), 5.69 (d, $J = 14.2$ Hz, 1H), 5.58 (dd, $J = 10.3, 1.9$ Hz, 1H), 4.03 (d, $J = 14.2$ Hz, 2H). $^{13}\text{C NMR}$ (100 MHz, CDCl_3) δ 165.12, 142.06, 139.50, 136.45, 134.86, 131.53, 129.53, 129.35, 129.20, 128.54, 127.87, 127.80, 100.99, 77.35, 51.71.



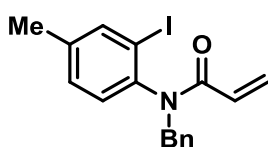
Compound 48d: $^1\text{H NMR}$ (400 MHz, CDCl_3) δ 7.77 (d, $J = 8.5$ Hz, 1H), 7.25 – 7.18 (m, 3H), 7.17 – 7.11 (m, 2H), 6.98 (dd, $J = 8.5, 2.4$ Hz, 1H), 6.66 (d, $J = 2.4$ Hz, 1H), 6.41 (dd, $J = 16.6, 1.9$ Hz, 1H), 5.75 (dd, $J = 16.6, 10.3$ Hz, 1H), 5.58 – 5.50 (m, 2H), 4.02 (d, $J = 14.3$ Hz, 2H). $^{13}\text{C NMR}$ (100 MHz, CDCl_3) δ 164.99, 144.58, 140.75, 136.21, 134.94, 131.23, 130.20, 129.47, 129.36, 128.56, 127.88, 127.82, 98.07, 51.83.



Compound 48e: $^1\text{H NMR}$ (400 MHz, CDCl_3) δ 7.42 (dd, $J = 7.8, 2.8$ Hz, 1H), 7.30 – 7.19 (m, 5H), 6.90 (ddd, $J = 8.7, 7.6, 2.8$ Hz, 1H), 6.75 (dd, $J = 8.8, 5.5$ Hz, 1H), 6.46 (dd, $J = 16.7, 1.9$ Hz, 1H), 5.86 (dd, $J = 16.7, 10.3$ Hz, 1H), 5.66 (d, $J = 14.2$ Hz, 1H), 5.60 – 5.54 (m, 1H), 4.11 (d, $J = 14.2$ Hz, 2H). $^{13}\text{C NMR}$ (100 MHz, CDCl_3) δ 165.47, 162.93, 160.41, 136.57, 132.55, 132.47, 129.41, 129.01, 128.48, 127.71, 124.65, 124.55, 121.09, 120.84, 115.49, 115.27, 51.57.

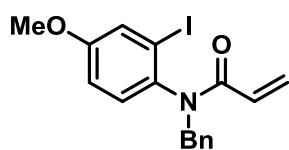


Compound 48f: $^1\text{H NMR}$ (400 MHz, CDCl_3) δ 8.51 (dd, $J = 6.2, 1.9$ Hz, 1H), 7.85 – 7.72 (m, 1H), 7.18 – 7.13 (m, 3H), 7.13 – 7.08 (m, 2H), 6.68 (dd, $J = 8.2, 2.9$ Hz, 1H), 6.38 (dt, $J = 16.6, 2.2$ Hz, 1H), 5.69 (ddd, $J = 16.1, 10.3, 5.8$ Hz, 1H), 5.59 (d, $J = 14.3$ Hz, 1H), 5.47 (dt, $J = 10.3, 2.1$ Hz, 1H), 4.28 (q, $J = 7.1$ Hz, 2H), 4.00 (d, $J = 14.2$, 2H), 1.29 (t, $J = 7.1$ Hz, 3H). $^{13}\text{C NMR}$ (100 MHz, CDCl_3) δ 164.80, 147.19, 141.24, 136.34, 130.93, 130.24, 129.53, 129.22, 128.52, 127.93, 127.82, 100.35, 77.37, 61.69, 51.63, 14.30.

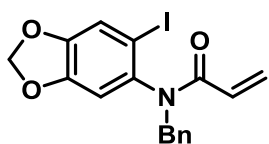


Compound 48g: $^1\text{H NMR}$ (400 MHz, CDCl_3) δ 7.78 (dd, $J = 1.8, 0.6$ Hz, 1H), 7.33 – 7.22 (m, 5H), 7.06 – 6.98 (m, 1H), 6.65 – 6.57 (m, 1H), 6.47 (dd, $J = 16.7, 2.0$ Hz, 1H), 5.87 (dd, $J = 16.7, 10.3$

Hz, 1H), 5.70 (d, $J = 14.2$ Hz, 1H), 5.56 (dd, $J = 10.3, 2.0$ Hz, 1H), 4.04 (d, $J = 14.2$ Hz, 2H), 2.33 (d, $J = 2.6$ Hz, 3H).



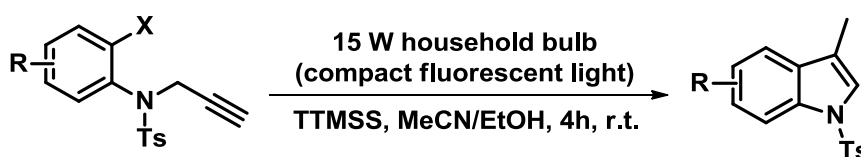
Compound 48h: $^1\text{H NMR}$ (400 MHz, CDCl_3) δ 7.45 (d, $J = 2.8$ Hz, 1H), 7.32 – 7.20 (m, 5H), 6.74 (dd, $J = 8.7, 2.8$ Hz, 1H), 6.61 (d, $J = 8.7$ Hz, 1H), 6.46 (dd, $J = 16.7, 2.0$ Hz, 1H), 5.89 (dd, $J = 16.7, 10.3$ Hz, 1H), 5.70 (d, $J = 14.2$ Hz, 1H), 5.57 (dd, $J = 10.3, 2.0$ Hz, 1H), 4.03 (d, $J = 14.2$ Hz, 2H), 3.80 (s, 3H). $^{13}\text{C NMR}$ (100 MHz, CDCl_3) δ 165.76, 159.39, 136.91, 136.12, 131.11, 129.55, 128.49, 128.39, 128.21, 127.54, 124.86, 114.67, 100.74, 55.69, 51.97.



Compound 48i: $^1\text{H NMR}$ (400 MHz, CDCl_3) δ 7.22 (s, 1H), 7.21 – 7.15 (m, 5H), 6.38 (ddd, $J = 16.8, 6.1, 2.0$ Hz, 1H), 6.16 (d, $J = 3.7$ Hz, 1H), 5.92 (s, 2H), 5.84 (dd, $J = 16.7, 10.3$ Hz, 1H), 5.58 (d, $J = 14.2$ Hz, 1H), 5.51 (dd, $J = 10.3, 2.0$ Hz, 1H), 3.93 (d, $J = 14.2$ Hz, 1H). $^{13}\text{C NMR}$ (100 MHz, CDCl_3) δ 165.66, 148.63, 137.11, 136.76, 129.46, 128.75, 128.49, 128.11, 127.65, 118.27, 111.05, 102.45, 89.30, 51.97.

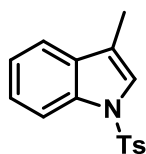
6.2.1.5 General procedure for the photochemical intramolecular cyclization reaction

6.2.1.5.1 Indole Synthesis

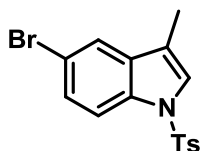


To a 5 mL vial equipped with a Teflon-coated magnetic stirring bar was added the N-tosyl-propargyl aniline (0.1 mmol, 1 equiv.), 0.4 ml acetonitrile (0.25 M), 29.2 μL (5 equiv) ethanol and TTMSS (0.1 mmol, 1 equiv). The reaction mixture was positioned approximately 5 cm away from the light source, and stirred at room temperature. After complete consumption of the starting material (followed by TLC), the reaction was quenched with 2 mL water, then aqueous layer was extracted with DCM (3x10 mL) and the combined organic layers were dried over Na_2SO_4 . After

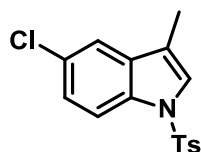
vacuum removal of solvents, the crude product was purified by flash column chromatography (SiO₂, n-Hexane/EtOAc (9:1)).



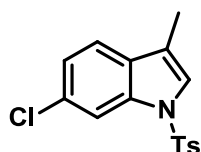
Compound 47a: The title compound was synthesized according to the general procedure in 92% (26,2 mg) isolated yield as a yellow solid (m.p.: 102-103° C). **¹H NMR** (400 MHz, CDCl₃) δ 7.86 (d, *J* = 8.3 Hz, 1H), 7.61 (d, *J* = 8.4 Hz, 2H), 7.32 (d, *J* = 7.3 Hz, 1H), 7.23 – 7.00 (m, 5H), 2.19 (s, 3H), 2.11 (d, *J* = 1.2 Hz, 3H). **¹³C NMR** (100 MHz, CDCl₃) δ 144.6, 135.4, 135.2, 131.7, 129.7, 126.7, 124.5, 123.0, 122.9, 119.3, 118.5, 113.6, 21.5, 9.6. **HRMS:** calculated for C₁₆H₁₆NO₂S (M-H)⁺ 286.0902; found 286.0802.



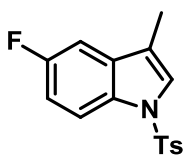
Compound 47b: The title compound was synthesized according to the general procedure in 53% (19,2 mg) isolated yield viscous oil. **¹H NMR** (400 MHz, CDCl₃) δ 7.72 (d, *J* = 8.8 Hz, 1H), 7.62 – 7.55 (m, 2H), 7.46 – 7.42 (m, 1H), 7.29 – 7.24 (m, 1H), 7.17 (d, *J* = 1.2 Hz, 1H), 7.11 – 7.05 (m, 2H), 2.21 (s, 3H), 2.07 (d, *J* = 1.3 Hz, 3H). **¹³C NMR** (100 MHz, CDCl₃) δ 144.9, 135.1, 133.9, 133.5, 129.8, 127.4, 126.7, 124.2, 122.2, 117.9, 116.5, 115.1, 21.5, 9.5. **HRMS:** calculated for C₁₆H₁₅BrNO₂S (M-H)⁺ 364.0007; found 364.0013.



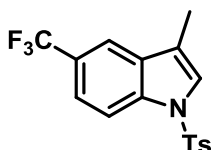
Compound 47c: The title compound was synthesized according to the general procedure in 62% (19,8 mg) isolated yield as a yellow solid (m.p.: 111-113 °C). **¹H NMR** (400 MHz, CDCl₃) δ 7.89 (d, *J* = 8.8 Hz, 1H), 7.71 (d, *J* = 8.3 Hz, 2H), 7.40 (m, 1H), 7.26 (m, 4H), 2.34 (s, 3H), 2.20 (d, *J* = 1.2 Hz, 3H). **¹³C NMR** (100 MHz, CDCl₃) 144.9, 135.1, 133.6, 133.0, 129.8, 128.9, 126.7, 124.7, 124.4, 119.2, 118.0, 114.7, 21.5, 9.5 ppm. **HRMS:** calculated for C₁₆H₁₅ClNO₂S (M-H)⁺ 320.0512; found 320.0528.



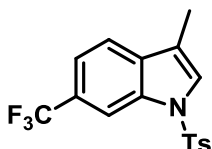
Compound 47d: The title compound was synthesized according to the general procedure in 70% (22,3 mg) isolated yield as yellow solid (m.p.: 168 – 170 °C). **¹H NMR** (400 MHz, CDCl₃) δ 7.81 (d, *J* = 1.6 Hz, 1H), 7.55 (d, *J* = 8.4 Hz, 2H), 7.15 (d, *J* = 8.4 Hz, 1H), 7.11 – 6.98 (m, 4H), 2.16 (s, 3H), 2.02 (d, *J* = 1.2 Hz, 3H). **¹³C NMR** (100 MHz, CDCl₃) δ 145.0, 135.5, 135.2, 130.6, 130.2, 129.9, 126.7, 123.6, 123.5, 120.2, 118.3, 113.8, 21.5, 9.6. **HRMS:** calculated for C₁₆H₁₅ClNO₂S (M-H)⁺ 320.0512; found 320.0523.



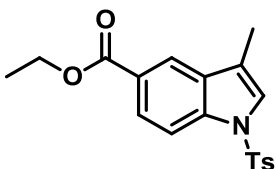
Compound 47e: The title compound was synthesized according to the general procedure in 50% (15,2 mg) isolated yield as a yellow solid (m.p: 98-100 °C). **¹H NMR** (400 MHz, CDCl₃) δ 7.76 – 7.69 (m, 1H), 7.56 – 7.49 (m, 2H), 7.17 – 7.12 (m, 1H), 7.05 – 6.99 (m, 2H), 6.93 – 6.80 (m, 2H), 2.15 (s, 3H), 2.01 (d, *J* = 1.3 Hz, 3H). **¹³C NMR** (100 MHz, CDCl₃) δ 144.8, 135.1, 129.8, 126.7, 124.7, 118.4, 114.7, 114.6, 112.5, 112.3, 105.2, 104.9, 21.5, 9.6. **HRMS:** calculated for C₁₆H₁₅FNO₂S (M-H)⁺ 304.0808; found 304.0802.



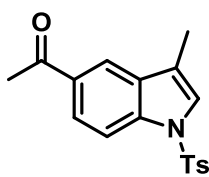
Compound 47f: The title compound was synthesized according to the general procedure in 51% (18,0 mg) isolated yield as a yellow solid (m.p: 117-119 °C). **¹H NMR** (400 MHz, CDCl₃) δ 7.88 (d, *J* = 8.7 Hz, 1H), 7.59 – 7.51 (m, 3H), 7.36 (d, *J* = 8.7, 1H), 7.23 (d, *J* = 1.2 Hz, 1H), 7.10 – 7.00 (m, 2H), 2.16 (s, 3H), 2.09 (d, *J* = 1.3 Hz, 3H). **¹³C NMR** (100 MHz, CDCl₃) δ 145.8, 137.3, 135.7, 132.0, 130.5, 127.3, 125.2, 121.9, 121.9, 119.1, 117.6, 117.6, 114.4, 22.1, 10.1. **HRMS:** calculated for C₁₇H₁₅F₃NO₂S (M + H)⁺ 354.0776; found 354.0767.



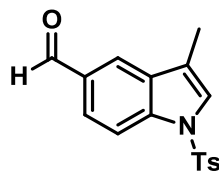
Compound 47g: The title compound was synthesized according to the general procedure in 52% (18,4 mg) isolated yield as a yellow solid (m.p: 131-133 °C). **¹H NMR** (400 MHz, CDCl₃) δ 8.26 (s, 1H), 7.75 (d, *J* = 8.4 Hz, 2H), 7.58 – 7.41 (m, 3H), 7.23 (d, *J* = 8.1 Hz, 2H), 2.34 (s, 3H), 2.26 (d, *J* = 1.2 Hz, 3H). **¹³C NMR** (100 MHz, CDCl₃) δ 145.2, 135.0, 134.4, 134.2, 130.0, 126.8, 125.5, 119.9, 119.8, 119.7, 118.2, 111.1, 111.0, 21.6, 9.6. **HRMS:** calculated for C₁₇H₁₅O₂F₃NS (M + H)⁺ 354.0776; found 354.0766.



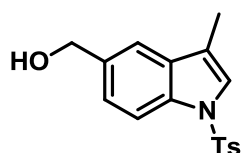
Compound 47h: The title compound was synthesized according to the general procedure in 65% (23,2 mg) isolated yield as an off brown solid (m.p: 115-117 °C). **¹H NMR** (400 MHz, CDCl₃) δ 8.10 (t, *J* = 1.2 Hz, 1H), 7.95 – 7.89 (m, 2H), 7.66 (d, 8,6 Hz, 2H), 7.28 (q, *J* = 1.1 Hz, 1H), 7.12 (d, *J* = 8.6, 2H), 4.31 (q, *J* = 7.1 Hz, 2H), 2.24 (s, 3H), 2.19 (d, *J* = 1.3 Hz, 3H), 1.32 (t, *J* = 7.1 Hz, 3H). **¹³C NMR** (100 MHz, CDCl₃) δ 166.8, 145.1, 137.7, 135.2, 131.6, 129.9, 126.7, 125.8, 125.4, 124.2, 121.7, 119.0, 113.3, 60.9, 21.6, 14.4, 9.6. **HRMS:** calculated for C₁₉H₂₀O₄NS (M + H)⁺ 358.1113; found 358.1110.



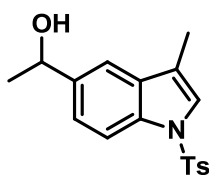
Compound 47i: The title compound was synthesized according to the general procedure in 50% (16,3 mg) isolated yield as a yellow solid (m.p: 143-145 °C). **¹H NMR** (400 MHz, CDCl₃) δ 7.93 (dd, *J* = 1.7, 0.6 Hz, 1H), 7.86 (dd, *J* = 8.7, 0.6 Hz, 1H), 7.77 (dd, *J* = 8.7, 1.7 Hz, 1H), 7.59 (d, *J* = 8.5 Hz, 2H), 7.21 (d, *J* = 1.3 Hz, 1H), 7.06 (d, *J* = 8.5 Hz, 2H), 2.49 (s, 3H), 2.18 (s, 3H), 2.13 (d, *J* = 1.3 Hz, 3H). **¹³C NMR** (100 MHz, CDCl₃) δ 197.8, 145.2, 137.8, 135.1, 132.5, 131.7, 129.9, 126.8, 124.9, 124.4, 120.5, 119.2, 113.4, 26.8, 21.6, 9.6. **HRMS:** calculated for C₁₈H₁₈O₃NS. (M + H)⁺ 328.1007, found 328.0996.



Compound 47j: The title compound was synthesized according to the general procedure in 45% (14,1 mg) isolated yield as a yellow solid (m.p: 138-140 °C). **¹H NMR** (400 MHz, CDCl₃) δ 9.98 (s, 1H), 8.03 (d, *J* = 8.6 Hz, 1H), 7.93 (d, *J* = 1.0 Hz, 1H), 7.77 (dd, *J* = 8.6, 1.5 Hz, 1H), 7.69 (dd, *J* = 8.5, 1.9 Hz, 2H), 7.34 (d, *J* = 1.2 Hz, 1H), 7.18 ((d, *J* = 8.5 Hz, 2H) 2.28 (s, 3H), 2.23 (d, *J* = 1.3 Hz, 3H). **¹³C NMR** (100 MHz, CDCl₃) δ 191.9, 145.3, 138.6, 135.1, 131.9, 130.0, 127.0, 126.8, 125.7, 124.7, 122.4, 119.0, 113.9, 21.6, 9.6. **HRMS:** calculated for C₁₇H₁₆O₃NS (M + H)⁺ 314.0851; found 314.0857.

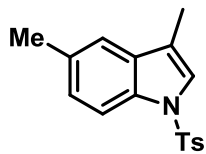


Compound 47k: The title compound was synthesized according to the general procedure in 82% (25,8 mg) isolated yield as a yellow solid (m.p: 60-62° C). **¹H NMR** (400 MHz, CDCl₃) δ 7.87 (d, *J* = 8.5 Hz, 1H), 7.63 (d, *J* = 8.6, 2H), 7.38 – 7,37 (m, 1H), 7.25 – 7.20 (m, 2H), 7.11 (d, *J* = 8.6, 2H), 4.67 (s, 2H), 2.24 (s, 3H), 2.15 (d, *J* = 1.3 Hz, 3H). **¹³C NMR** (100 MHz, CDCl₃) δ 144.7, 135.8, 135.3, 134.8, 132.0, 129.8, 126.7, 123.9, 123.6, 118.6, 118.0, 113.8, 65.5, 21.5, 9.7. **HRMS:** calculated for C₁₇H₁₈NO₃S (M+H)⁺ 316.1007; found 316.1002.

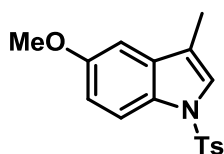


Compound 47l: The title compound was synthesized according to the general procedure in 52% (17, 1 mg) isolated yield as a yellow solid (m.p: 81-83 °C). **¹H NMR** (400 MHz, CDCl₃) ¹H NMR (400 MHz, CDCl₃) δ 7.73 - 7.72 (m, 1H), 7.69 (d, *J* = 8.3 Hz, 1H), 7.45 – 7.41 (m, 1H), 7.38 (d, *J* = 8.0 Hz, 1H), 7.31 (s, 1H), 7.18 (d, *J* = 8.6, 2H), 7.05 – 7.00 (m, 1H), 6.81 (d, *J* = 8.6, 2H) ,4.95 (q, *J* = 6.5 Hz), 2.34 (s, 3H), 2.18 (d, *J* = 1.3 Hz, 3H), 1.49

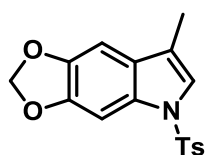
(d, $J = 6.5$ Hz, 3H). **^{13}C NMR** (100 MHz, CDCl_3) δ 147.7, 145.0, 144.1, 131.9, 131.4, 128.9, 128.8, 128.4, 127.2, 126.4, 124.6, 122.4, 69.8, 25.5, 21.7, 21.4. **HRMS:** calculated for $\text{C}_{18}\text{H}_{20}\text{NO}_3\text{S}$ ($\text{M}+\text{H}$) $^+$ 330.1164; found 330.1028.



Compound 47m: The title compound was synthesized according to the general procedure in 85% (25,4 mg) isolated yield as a yellow solid (m.p: 64-66 °C). **^1H NMR** (400 MHz, CDCl_3) ^1H NMR (400 MHz, CDCl_3) δ 7.66 (d, $J = 8.4$ Hz, 1H), 7.56 (d, $J = 8.6$ Hz, 2H), 7.07 – 7.02 (m, 2H), 6.99 (d, $J = 8.6$ Hz, 2H), 6.93 (dd, $J = 8.4, 1.6$ Hz, 1H), 2.22 (s, 3H), 2.12 (s, 3H), 2.01 (d, $J = 1.3$ Hz, 3H). **^{13}C NMR** (100 MHz, CDCl_3) δ 145.1, 136.0, 134.1, 133.2, 132.6, 130.3, 127.3, 126.5, 123.8, 119.9, 119.1, 113.9, 22.1, 21.9, 10.2. **HRMS:** calculated for $\text{C}_{17}\text{H}_{18}\text{NO}_2\text{S}$ ($\text{M}+\text{H}$) $^+$ 300.1058; found 300.1028.

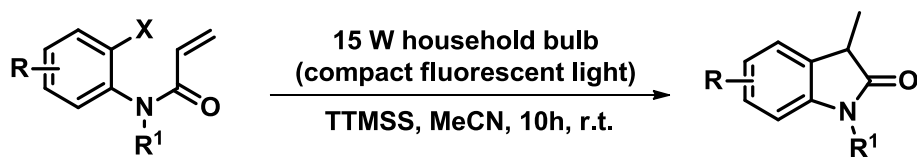


Compound 47n: The title compound was synthesized according to the general procedure in 85% (26,8 mg) isolated yield as a white solid (m.p: 111-113° C). **^1H NMR** (400 MHz, CDCl_3) δ 7.79 (d, $J = 8.9$ Hz, 1H), 7.63 (d, $J = 8.3$ Hz, 2H), 7.17 (s, 1H), 7.11 (d, $J = 8.0$ Hz, 2H), 6.88 – 6.74 (m, 2H), 3.75 (s, 3H), 2.25 (s, 3H), 2.12 (d, $J = 1.1$ Hz, 3H). **^{13}C NMR** (100 MHz, CDCl_3) δ 156.4, 144.5, 135.4, 132.8, 129.9, 129.7, 126.7, 123.9, 118.7, 114.6, 113.4, 101.9, 55.7, 21.5, 9.8. **HRMS:** calculated for $\text{C}_{17}\text{H}_{18}\text{NO}_3\text{S}$ ($\text{M}+\text{H}$) $^+$ 316.1007; found 316.0995.

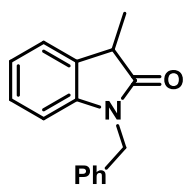


Compound 47o: The title compound was synthesized according to the general procedure in 82% (27 mg) isolated yield as a white viscous oil. **^1H NMR** (400 MHz, CDCl_3) δ 7.70 (d, $J = 8.6$ Hz, 2H), 7.49 (m, 1H), 7.20 (d, $J = 8.6$ Hz, 2H), 7.18 (m, 1H), 6.81 – 6.75 (m, 1H), 5.96 (s, 2H), 2.34 (s, 3H), 2.15 (d, $J = 1.2$ Hz, 3H). **^{13}C NMR** (100 MHz, CDCl_3) δ 146.4, 144.9, 144.6, 135.3, 130.0, 129.8, 126.7, 126.1, 122.08, 118.8, 101.3, 98.3, 95.5, 21.6, 9.8. **HRMS:** calculated for $\text{C}_{17}\text{H}_{16}\text{NO}_4\text{S}$ ($\text{M}+\text{H}$) $^+$ 330.0800; found 330.0791.

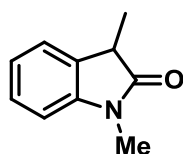
6.2.1.5.2 Oxindole Synthesis



To a 5 mL vial equipped with a Teflon-coated magnetic stirring bar was added the N-benzyl-acrylamides (0.1 mmol, 1 equiv.), 0.4 ml acetonitrile (0.25 M) and TTMSS (0.2 mmol, 2 equiv). The reaction mixture was positioned approximately 5 cm away from the light source, and stirred at room temperature. After complete consumption of the starting material (followed by TLC), the reaction was quenched with 2 mL water, then aqueous layer was extracted with DCM (3x10 mL) and the combined organic layers were dried over Na₂SO₄. After vacuum removal of solvents, the crude product was purified by flash column chromatography (SiO₂, n-Hexane/EtOAc (9:1)).

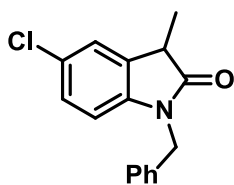


Compound 49a: The title compound was synthesized according to the general procedure in 80% (19 mg) isolated yield as white solid. ¹H NMR (400 MHz, CDCl₃) δ 7.52 – 7.40 (m, 6H), 7.35 – 7.30 (m, 1H), 7.21 – 7.16 (m, 1H), 6.89 (d, *J* = 7.8 Hz, 1H), 5.08 (s, 2H), 3.71 (q, *J* = 7.6 Hz, 1H), 1.71 (d, *J* = 7.6 Hz, 3H). ¹³C NMR (100 MHz, CDCl₃) δ 178.8, 143.1, 135.9, 130.6, 128.7, 127.8, 127.6, 127.3, 123.6, 122.4, 108.9, 43.7, 40.6, 15.6. **HRMS:** calculated for C₁₆H₁₆NO (M+H)⁺ 238.1232; found 238.1223.

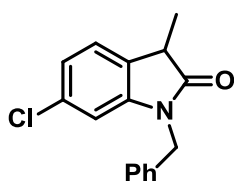


Compound 49b: The title compound was synthesized according to the general procedure in 54% (8,7 mg) isolated yield as yellow solid.⁵⁸ ¹H NMR (400 MHz, CDCl₃) δ 7.16 – 7.07 (m, 2H), 6.94 – 6.89 (m, 1H), 6.68 (d, *J* = 7.8 Hz, 1H), 3.29 (q, *J* = 7.6 Hz, 1H), 3.06 (s, 3H), 1.33 (d, *J* = 7.6 Hz, 3H). ¹³C NMR (100 MHz, CDCl₃) δ 178.7, 127.9, 123.5, 123.2, 122.4, 108.5, 107.9, 40.6, 26.2, 15.3. **HRMS:** calculated for C₁₀H₁₂NO (M+H)⁺ 162.0919; found 162.0863.

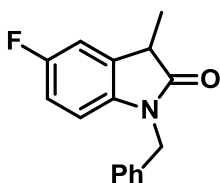
⁵⁸ B. Li, Y. Park, S. Chang, *J. Am. Chem. Soc.* **2014**, 136, 1125.



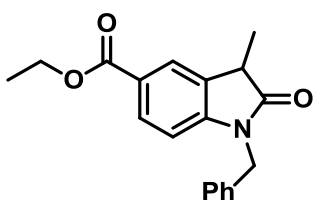
Compound 49c: The title compound was synthesized according to the general procedure in 65% (17,6 mg) isolated yield as yellow oil. **¹H NMR** (400 MHz, CDCl₃) δ 7.24 – 7.07 (m, 6H), 7.03 – 6.94 (m, 1H), 6.48 (d, *J* = 8.3 Hz, 1H), 4.76 (s, 2H), 3.41 (q, *J* = 7.6 Hz, 1H), 1.40 (d, *J* = 7.6 Hz, 3H). **¹³C NMR** (100 MHz, CDCl₃) δ 178.2, 142.8, 141.6, 135.5, 132.3, 128.8, 127.9, 127.7, 127.2, 124.2, 109.9, 43.8, 40.6, 15.5. **HRMS:** calculated for C₁₆H₁₅ClNO (M+H)⁺ 272.0842; found 272.0867.



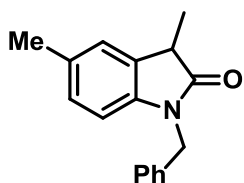
Compound 49d: The title compound was synthesized according to the general procedure in 45% (12,2 mg) isolated yield as yellow oil. **¹H NMR** (400 MHz, CDCl₃) δ 7.25 – 7.12 (m, 5H), 7.02 (dd, *J* = 7.9, 0.9 Hz, 1H), 6.87 (dd, *J* = 7.9, 1.8 Hz, 1H), 6.58 (d, *J* = 1.8 Hz, 1H), 4.75 (s, 2H), 3.38 (q, *J* = 7.6 Hz, 1H), 1.40 (d, *J* = 7.6 Hz, 3H). **¹³C NMR** (100 MHz, CDCl₃) δ 178.6, 144.2, 135.4, 133.5, 128.9, 128.5, 127.8, 127.2, 124.4, 122.3, 109.5, 43.7, 40.1, 15.5. **HRMS:** calculated for C₁₆H₁₅ClNO (M+H)⁺ 272.0842; found 272.0823.



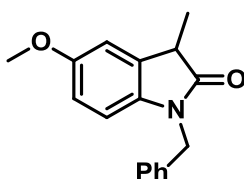
Compound 49e: The title compound was synthesized according to the general procedure in 56% (14,3 mg) isolated yield as yellow oil. **¹H NMR** (400 MHz, CDCl₃) δ 7.50 – 7.35 (m, 5H), 7.16 – 7.08 (m, 1H), 7.04 – 6.91 (m, 1H), 6.74 (dd, *J* = 8.5, 4.2 Hz, 1H), 5.01 (s, 2H), 3.67 (q, *J* = 7.7 Hz, 1H), 1.73 (s, 3H), 1.67 (d, *J* = 7.7 Hz, 3H). **¹³C NMR** (100 MHz, CDCl₃) δ 178.4, 158.0, 135.7, 128.8, 127.7, 127.2, 114.1, 113.8, 111.9, 111.6, 109.4, 43.8, 40.9, 15.5. **HRMS:** calculated for C₁₆H₁₅FNO (M+H)⁺ 256.1138; found 256.1107.



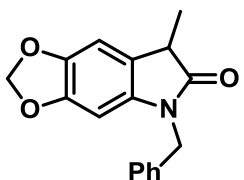
Compound 49f: The title compound was synthesized according to the general procedure in 51% (15,6 mg) isolated yield as oil. **¹H NMR** (400 MHz, CDCl₃) δ 7.85 – 7.77 (m, 2H), 7.3 – 7.2 (m, 5H), 6.7 (d, *J* = 8.7 Hz, 1H), 4.8 (s, 2H), 4.25 (q, *J* = 7.1 Hz, 2H), 3.5 (q, *J* = 7.6 Hz, 1H), 1.5 (d, *J* = 7.6 Hz, 3H), 1.3 (t, *J* = 7.1 Hz, 3H). **¹³C NMR** (100 MHz, CDCl₃) δ 178.9, 166.4, 147.1, 135.4, 130.5, 130.5, 128.9, 128.9, 127.8, 127.2, 124.8, 108.4, 60.8, 43.8, 40.3, 15.5, 14.4. **HRMS:** calculated for C₁₉H₂₀NO₃ (M+H)⁺ 310.1453; found 310.1447.



Compound 49g: The title compound was synthesized according to the general procedure in 70% (17,8 mg) isolated yield as yellow oil. **¹H NMR** (400 MHz, CDCl₃) δ 7.49 – 7.36 (m, 5H), 7.22 (m, 1H), 7.13 – 7.06 (m, 1H), 6.75 (d, *J* = 7.9 Hz, 1H), 5.05 (s, 2H), 3.66 (q, *J* = 7.6 Hz, 1H), 2.46 (s, 3H), 1.68 (d, *J* = 7.6 Hz, 3H). **¹³C NMR** (100 MHz, CDCl₃) δ 178.8, 140.6, 136.1, 131.9, 130.7, 128.7, 127.9, 127.5, 127.2, 124.5, 108.7, 43.7, 40.6, 21.0, 15.7. **HRMS:** calculated for C₁₇H₁₈NO (M+H)⁺ 252.1388; found 252.1369.



Compound 49h: The title compound was synthesized according to the general procedure in 72% (19,2 mg) isolated yield as yellow oil. **¹H NMR** (400 MHz, CDCl₃) δ 7.26 – 7.13 (m, 5H), 6.82 – 6.77 (m, 1H), 6.61 - 6.59 (m, 1H), 6.52 (d, *J* = 8.5 Hz, 1H), 4.81 (s, 2H), 3.68 (s, 3H), 3.45 (q, *J* = 7.6 Hz, 1H), 1.45 (d, *J* = 7.6 Hz, 3H). **¹³C NMR** (100 MHz, CDCl₃) δ 178.4, 155.9, 136.5, 136.0, 132.0, 128.8, 127.5, 127.3, 111.9, 111.2, 109.3, 55.8, 43.7, 40.9, 15.7. **HRMS:** calculated for C₁₇H₁₈NO₂ (M+H)⁺ 268.1338; found 268.1356.



Compound 49h: The title compound was synthesized according to the general procedure in 45% (12,6 mg) isolated yield as oil. **¹H NMR** (400 MHz, CDCl₃): δ 7.30 – 7.12 (m, 5H), 6.68 (s, 1H), 6.22 (s, 1H), 5.82 (s, 2H), 4.79 (s, 2H), 3.39 (q, *J* = 7.5 Hz, 1H), 1.42 (d, *J* = 7.5 Hz, 3H). **¹³C NMR** (100 MHz, CDCl₃) δ 179.0, 146.9, 143.2, 137.1, 135.8, 128.8, 127.6, 127.2, 122.5, 105.3, 100.9, 93.0, 43.8, 40.8, 15.9. **HRMS:** calculated for C₁₇H₁₆NO₃ (M+H)⁺ 282.1130; found 282.1

7 Appendix

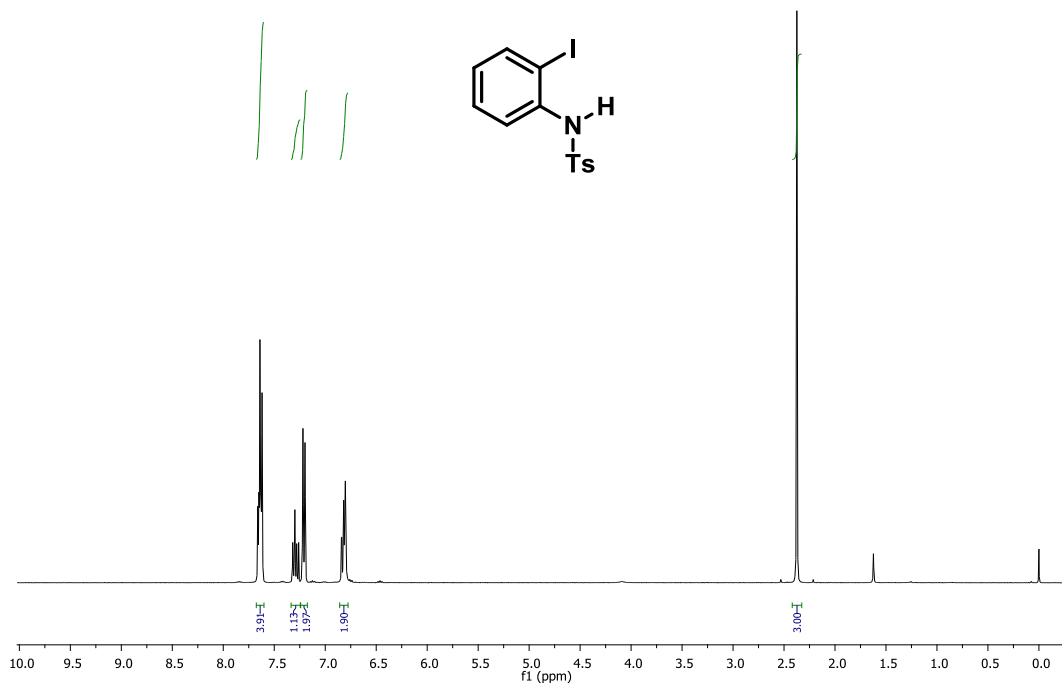


FIGURE 13: ¹H NMR spectrum of 46a precursor, 400 MHz, CDCl₃.

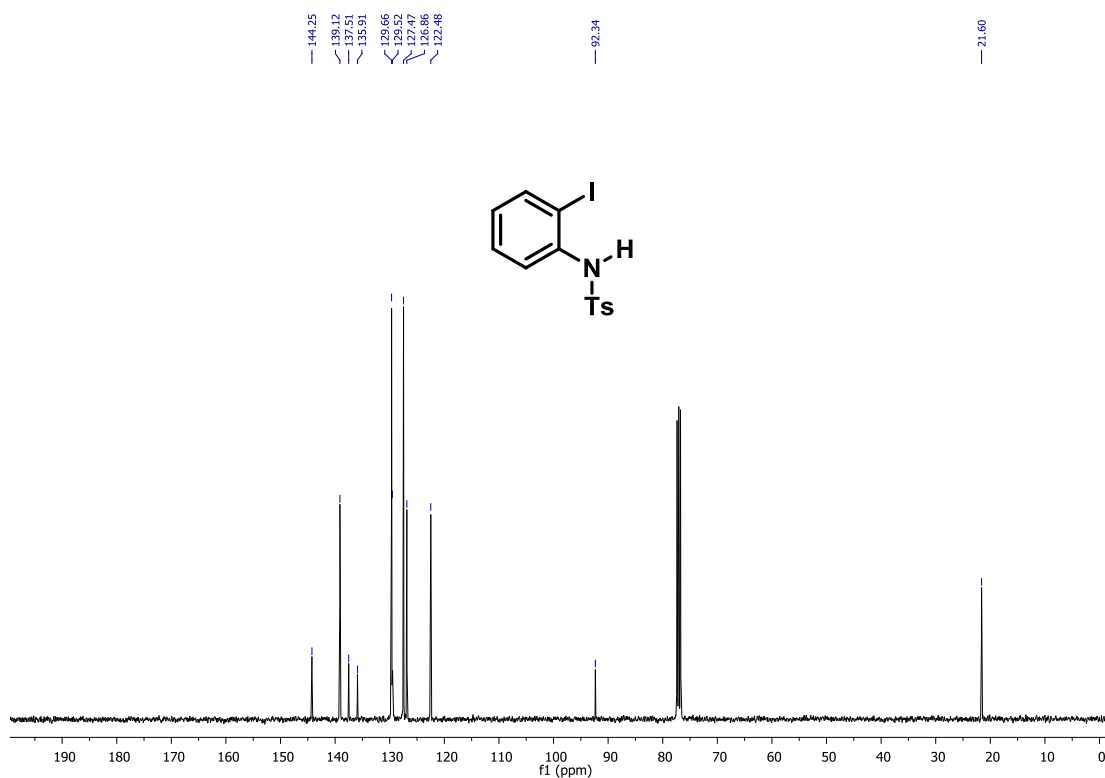


FIGURE 14: ¹³C NMR spectrum of 46a precursor, 100 MHz, CDCl₃.

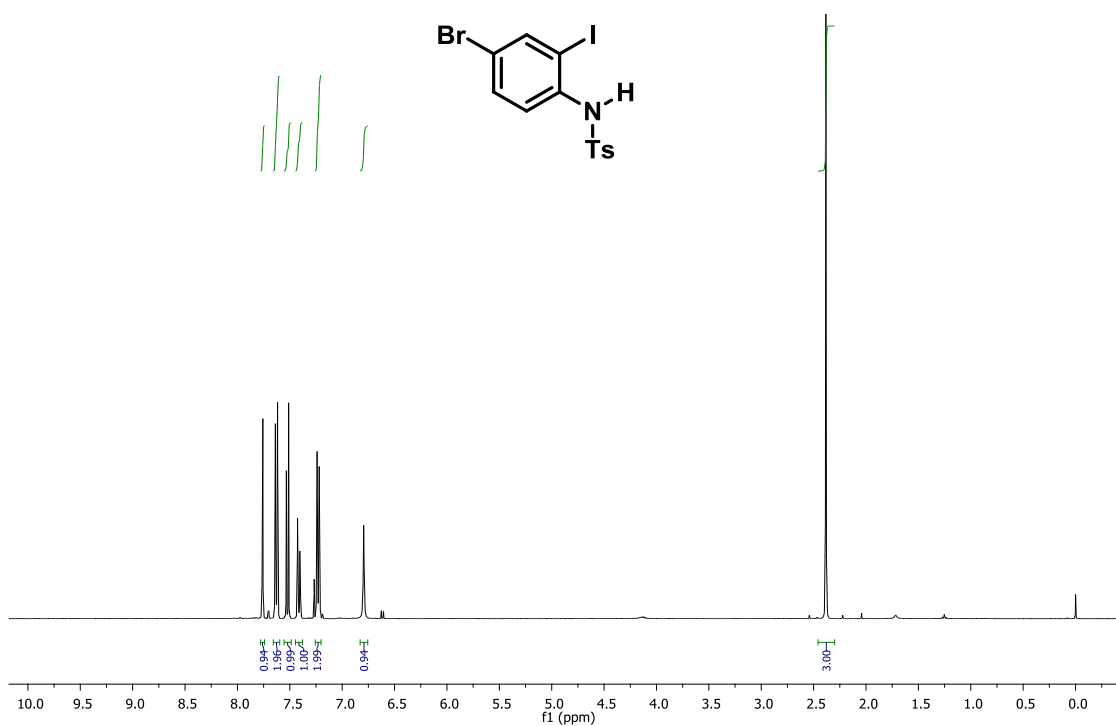


FIGURE 15: $^1\text{H NMR}$ spectrum of 46b precursor, 400 MHz, CDCl_3 .

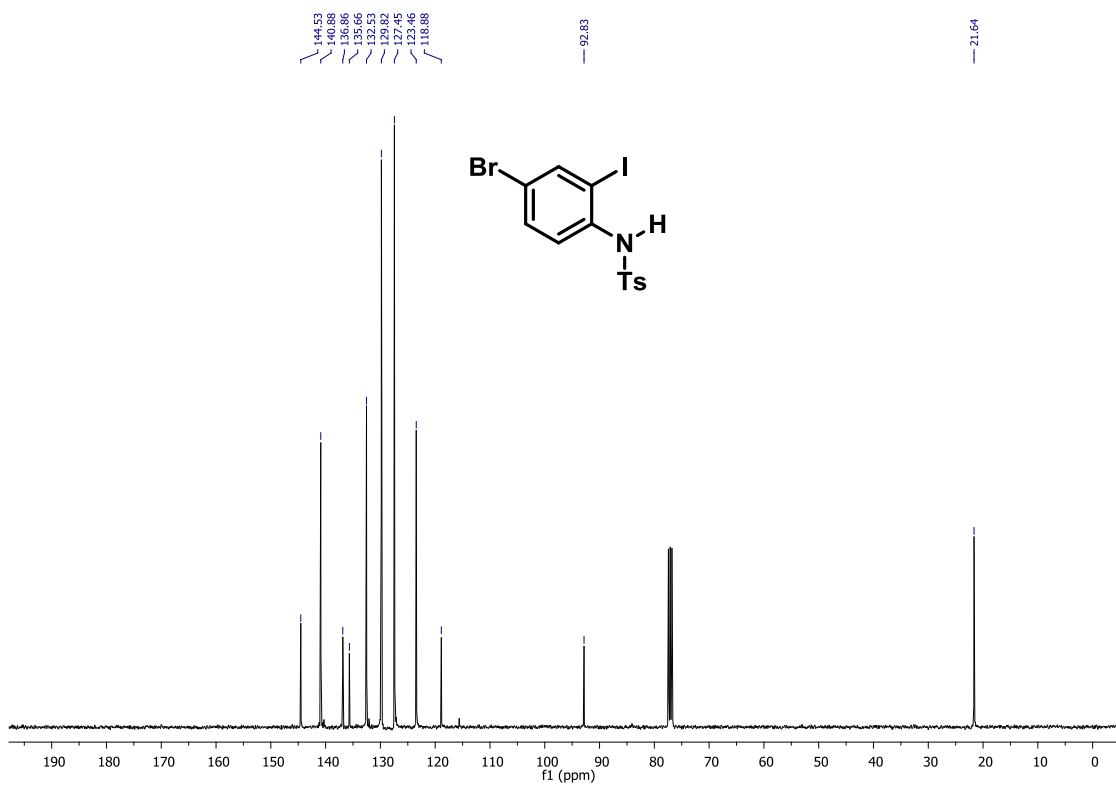


FIGURE 16: $^{13}\text{C NMR}$ spectrum of 46b precursor, 100 MHz, CDCl_3 .

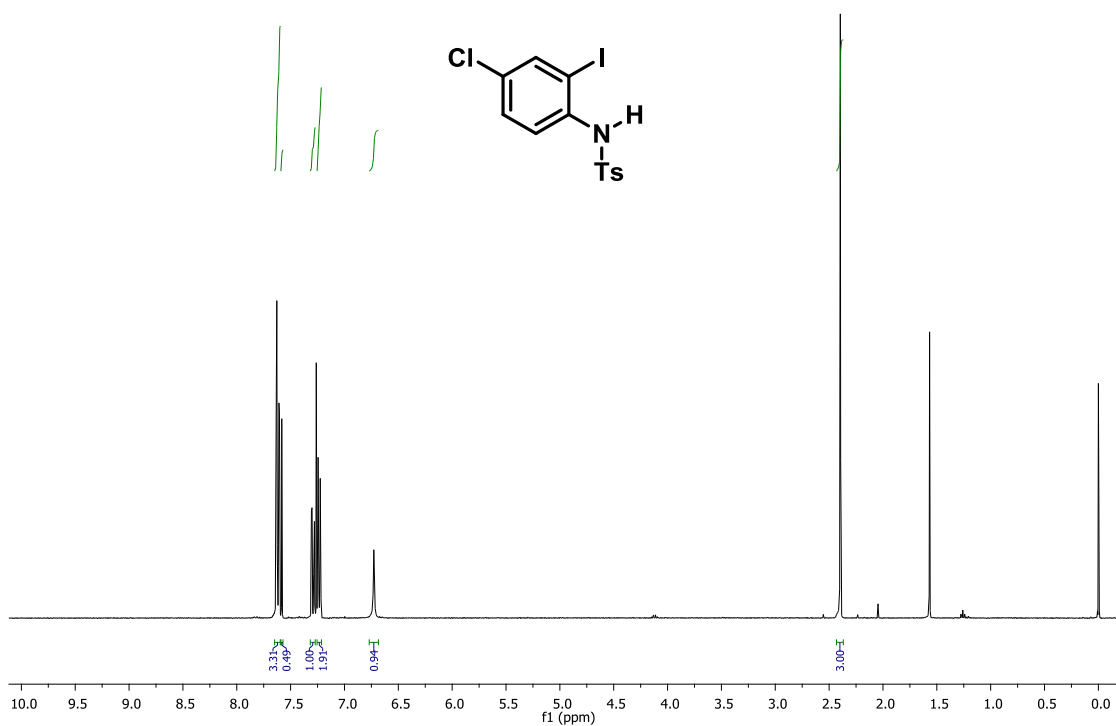


FIGURE 17: ^1H NMR spectrum of 46c precursor, 400 MHz, CDCl_3 .

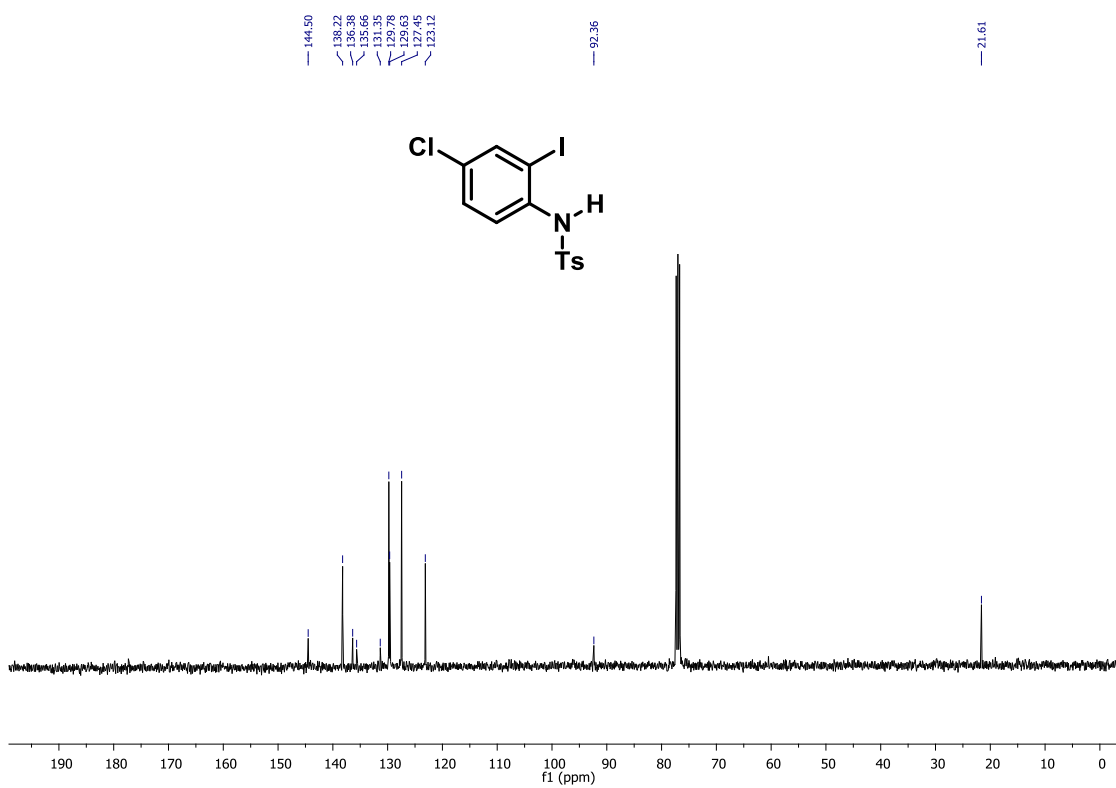


FIGURE 18: ^{13}C NMR spectrum of 46c precursor, 100 MHz, CDCl_3 .

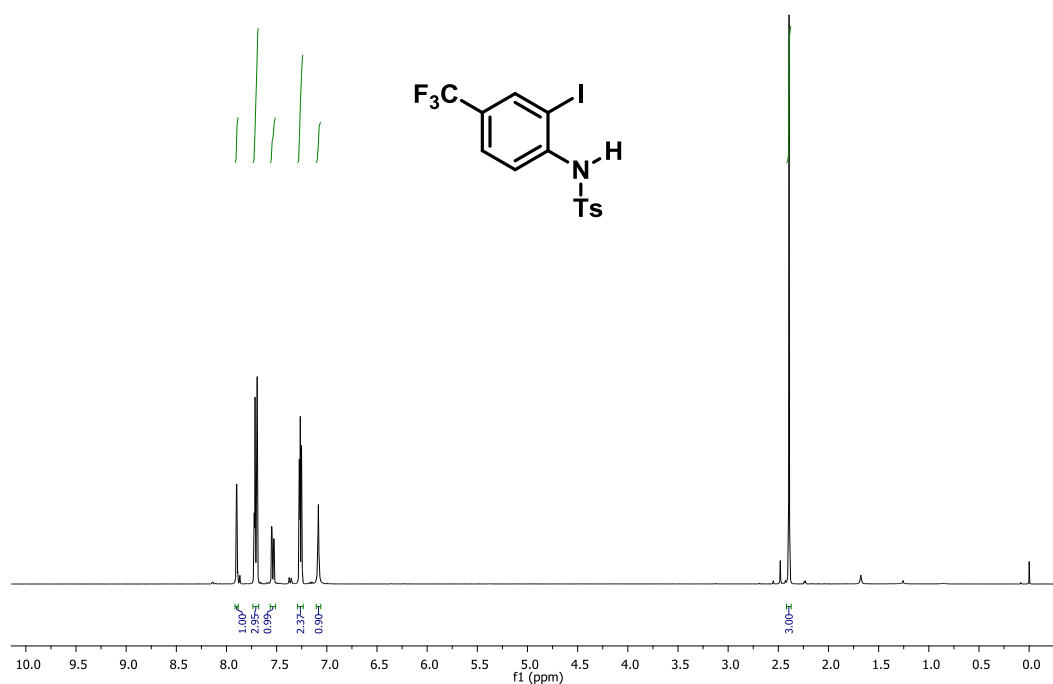


FIGURE 19: ^1H NMR spectrum of 46f precursor, 400 MHz, CDCl_3 .

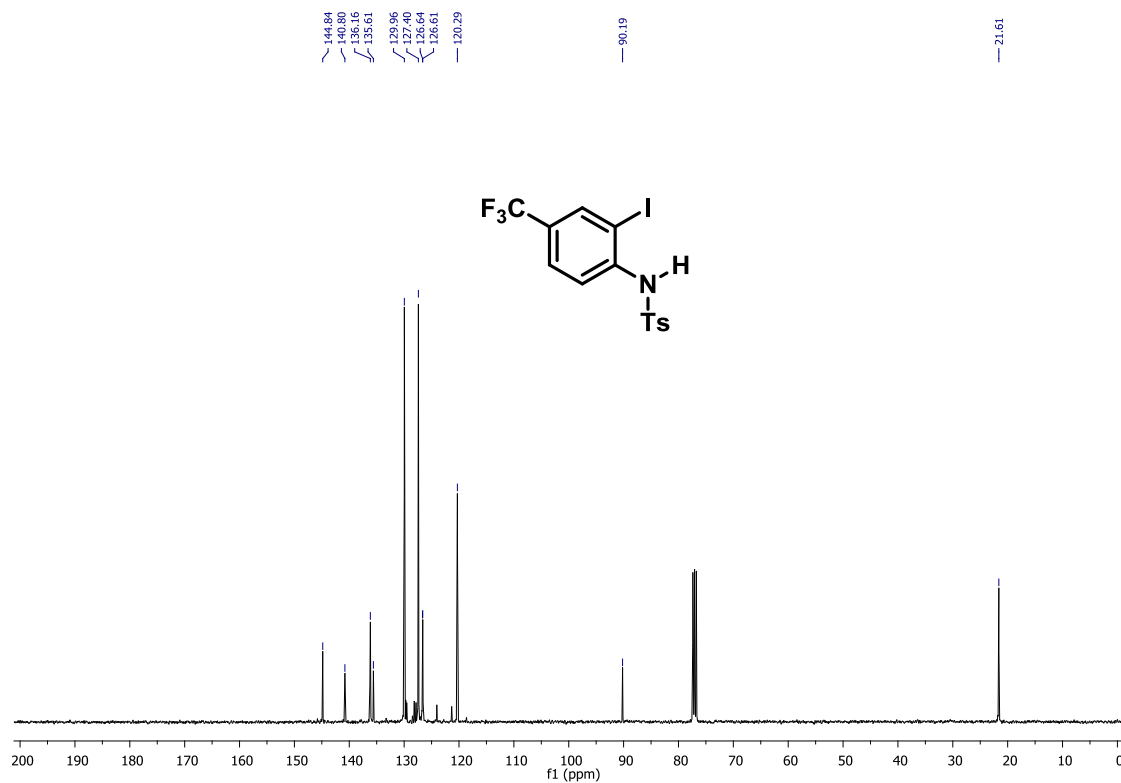


FIGURE 20: ^{13}C NMR spectrum of 46f precursor, 100 MHz, CDCl_3 .

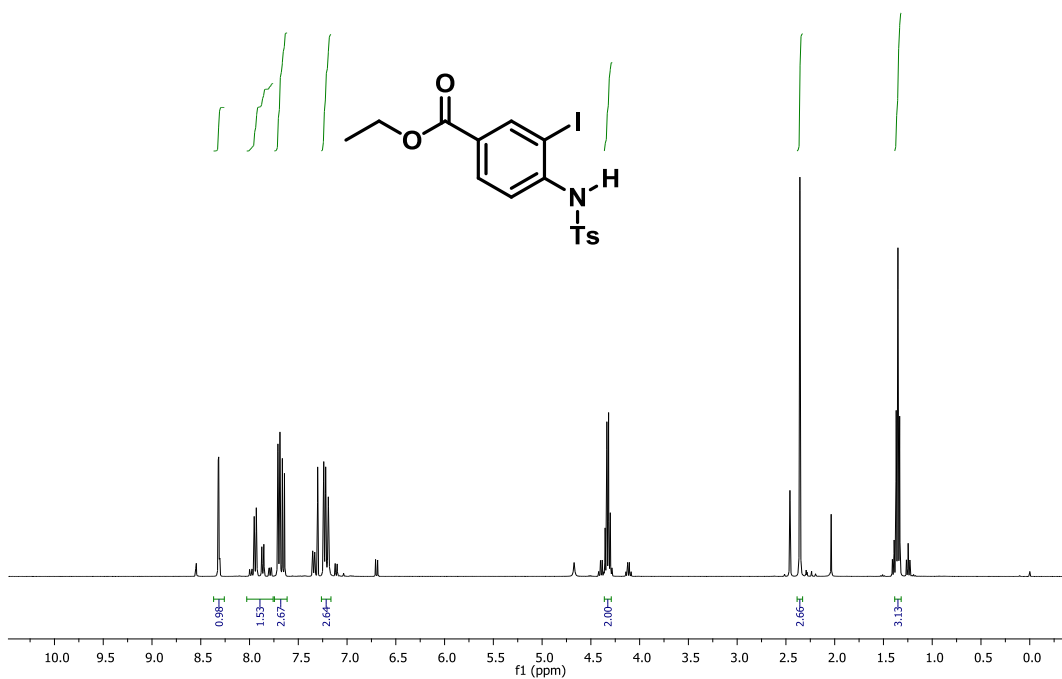


FIGURE 21: ¹H NMR spectrum of 46h precursor, 400 MHz, CDCl₃.

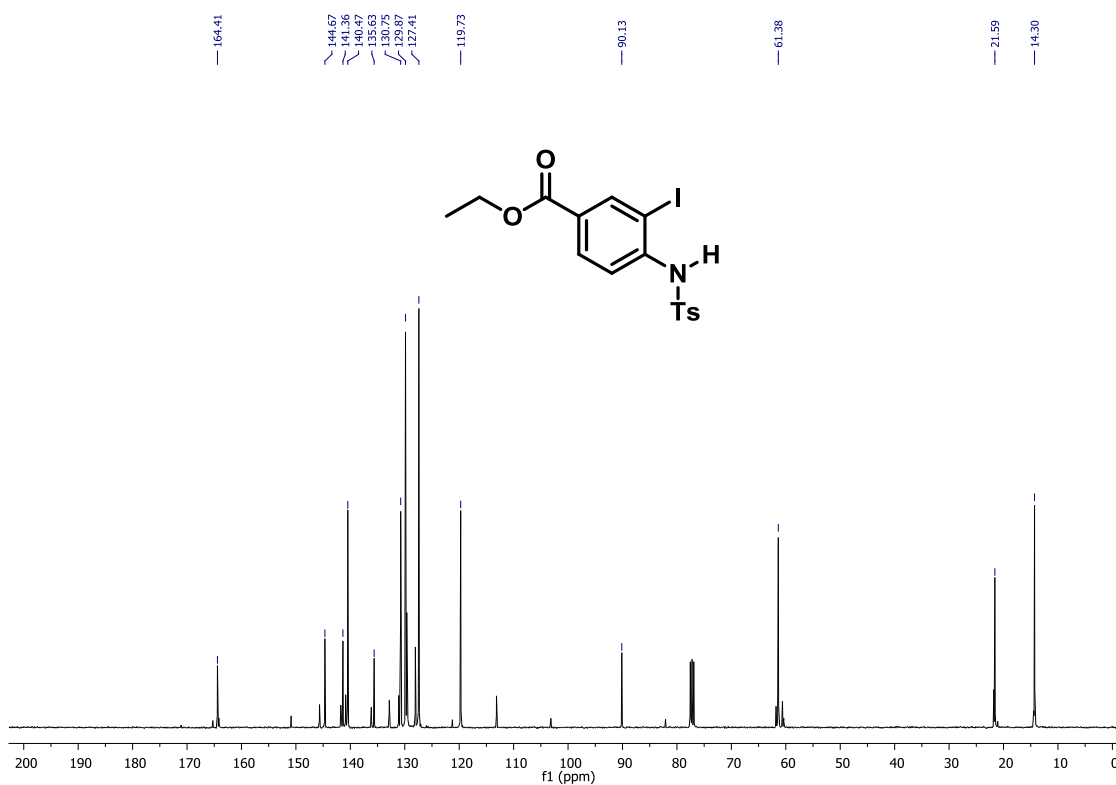


FIGURE 22: ¹³C NMR spectrum of 46h precursor, 100 MHz, CDCl₃.

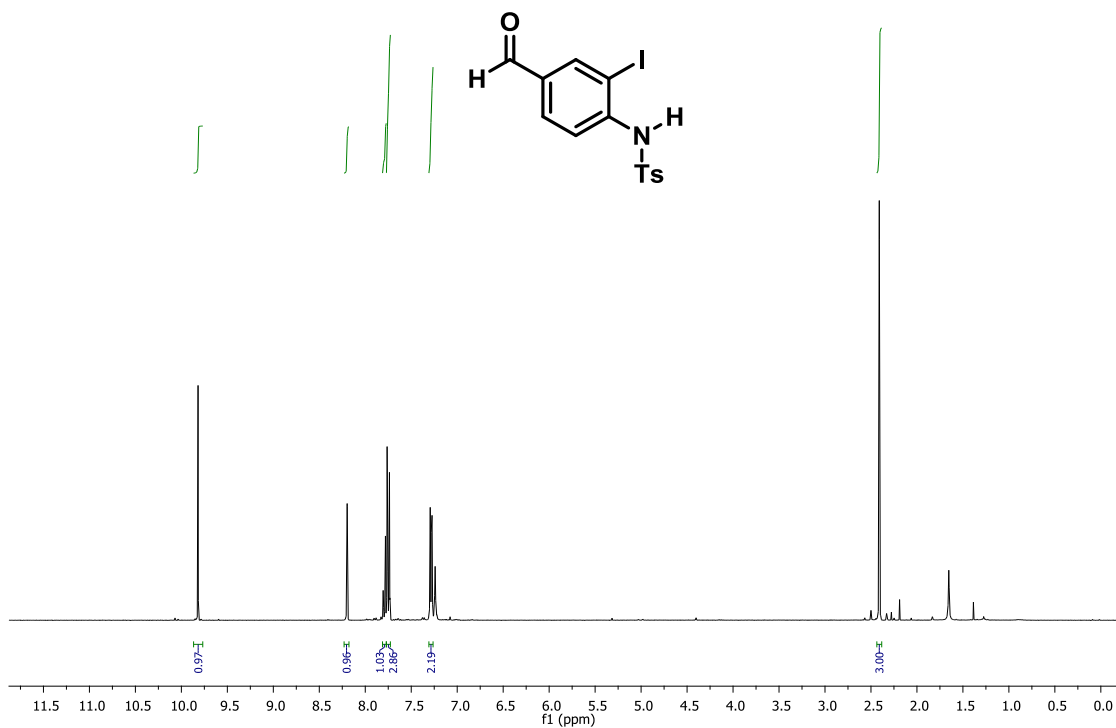


FIGURE 23: ¹H NMR spectrum of 46j precursor, 400 MHz, CDCl₃.

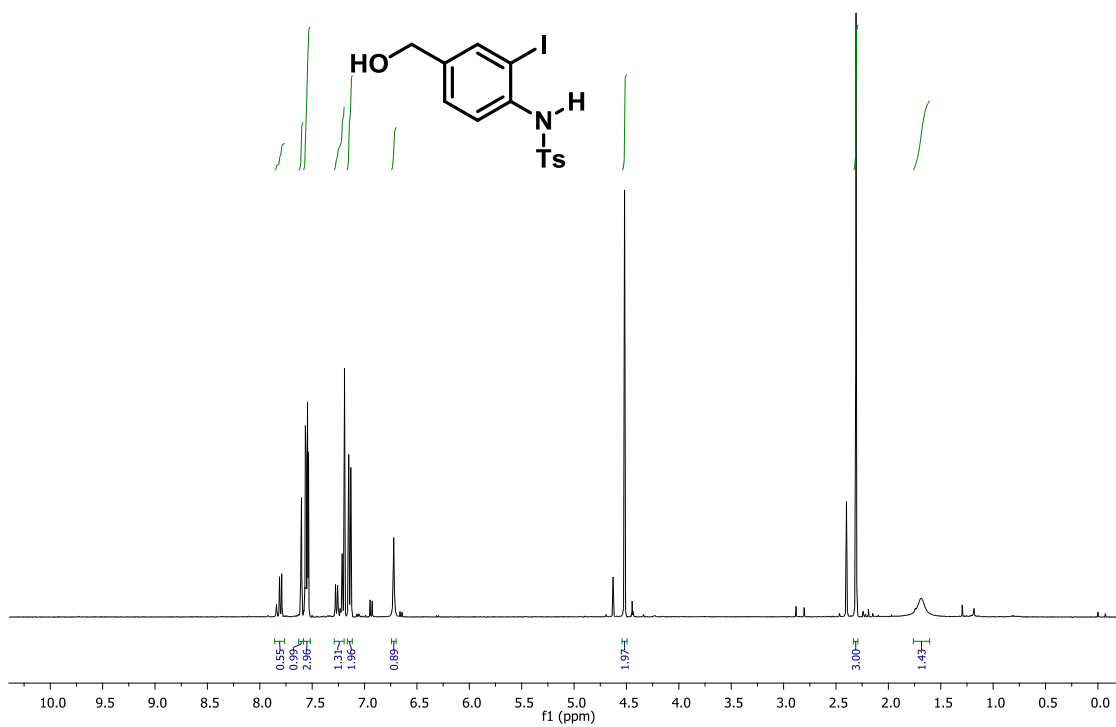


FIGURE 24: ¹H NMR spectrum of 46k precursor, 400 MHz, CDCl₃.

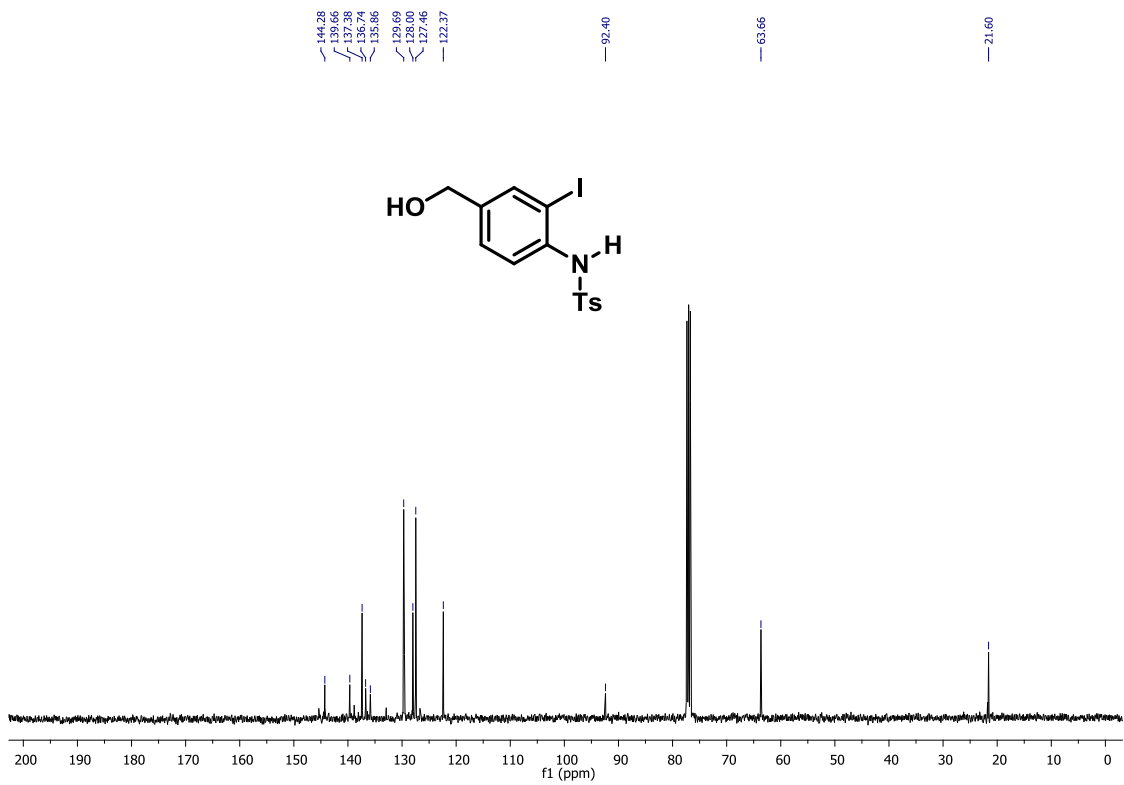


FIGURE 25: ¹³C NMR spectrum of 46k precursor, 100 MHz, CDCl₃.

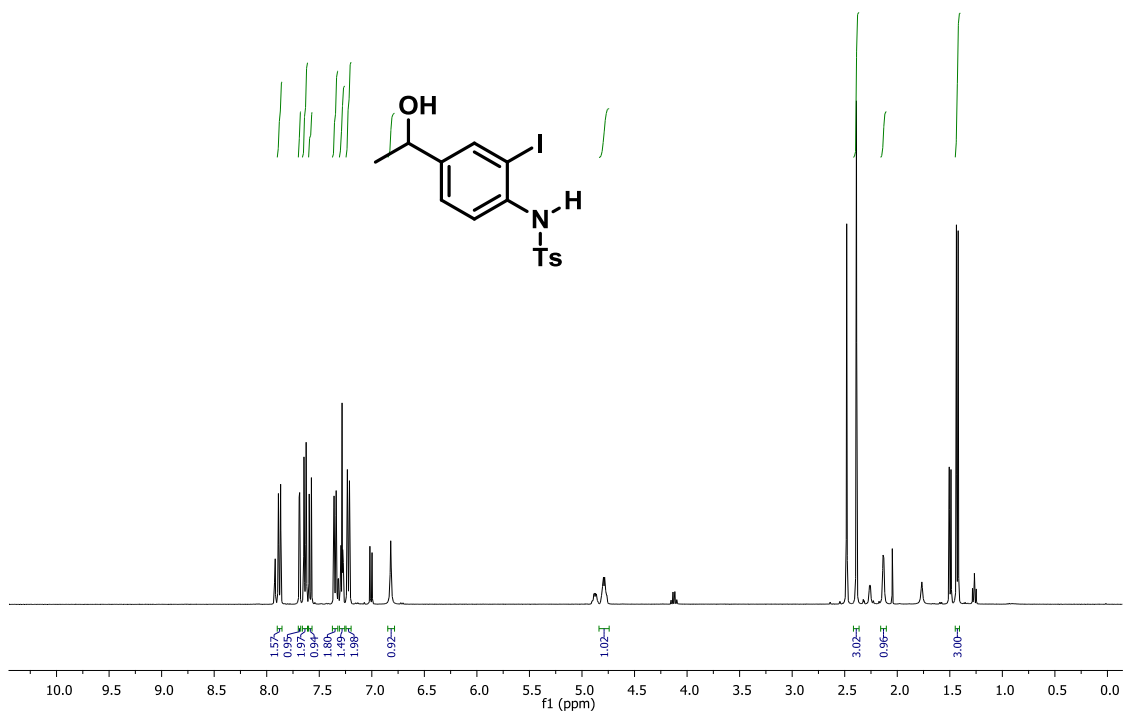


FIGURE 26: ¹H NMR spectrum of 46l precursor, 400 MHz, CDCl₃.

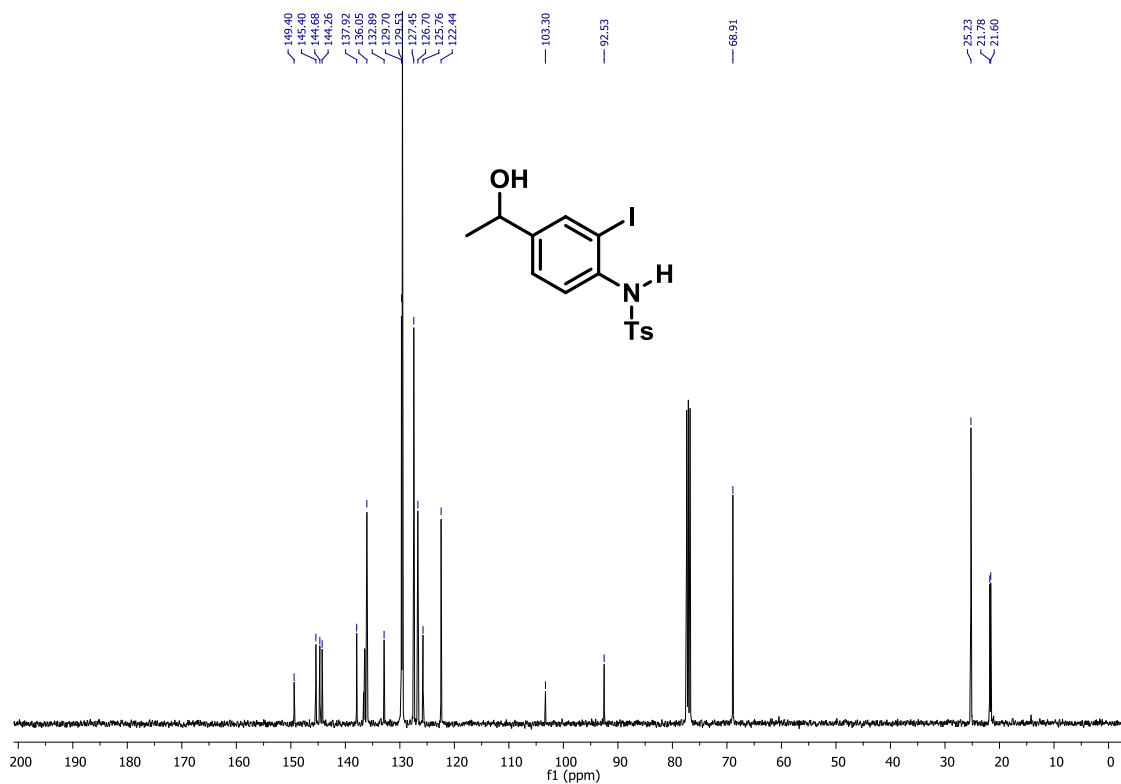


FIGURE 27: ¹³C NMR spectrum of 46l precursor, 100 MHz, CDCl₃.

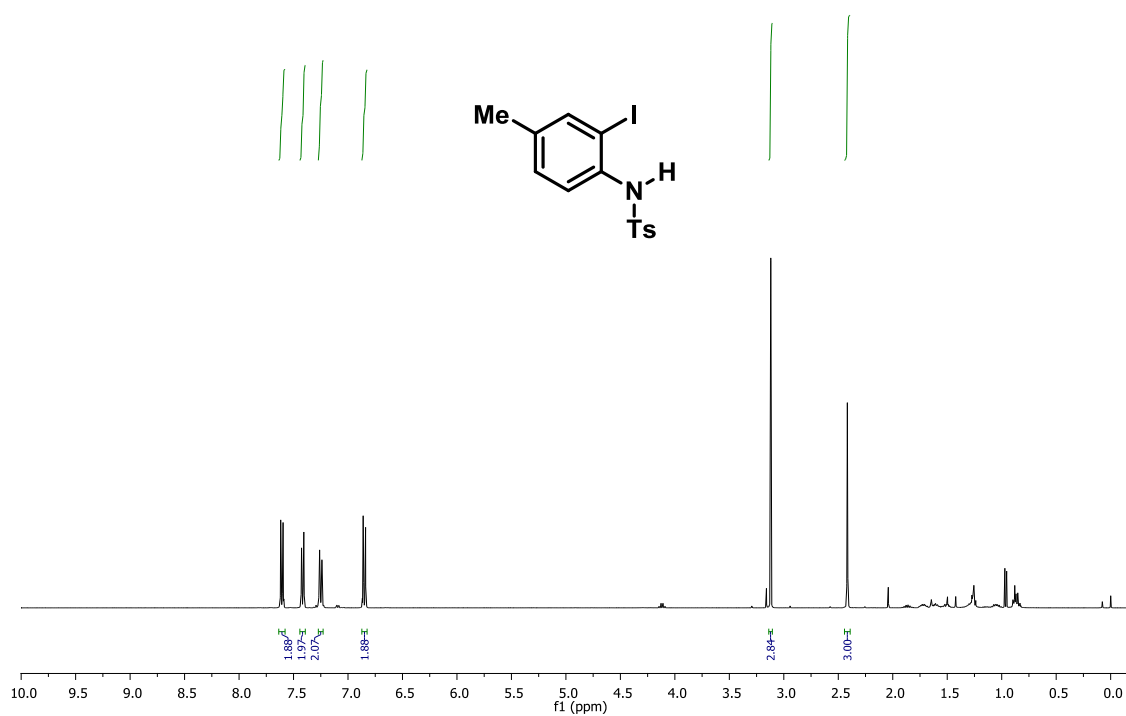


FIGURE 28: ¹H NMR spectrum of 46m precursor, 400 MHz, CDCl₃.

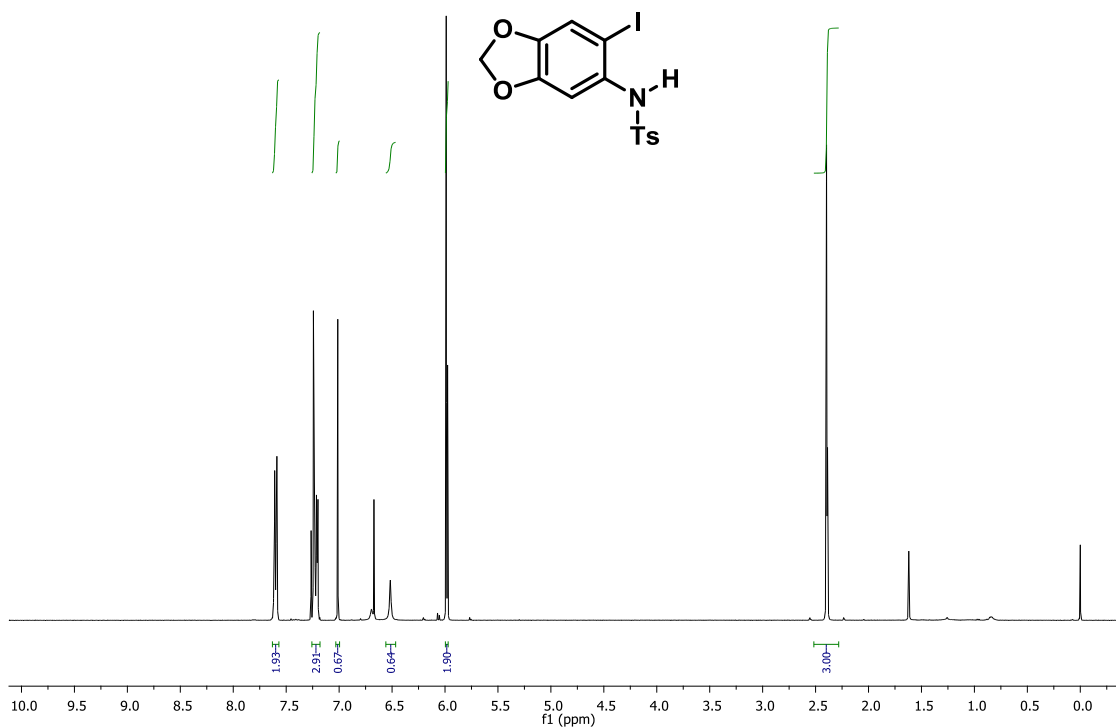


FIGURE 29: ^1H NMR spectrum of 46o precursor, 400 MHz, CDCl_3 .

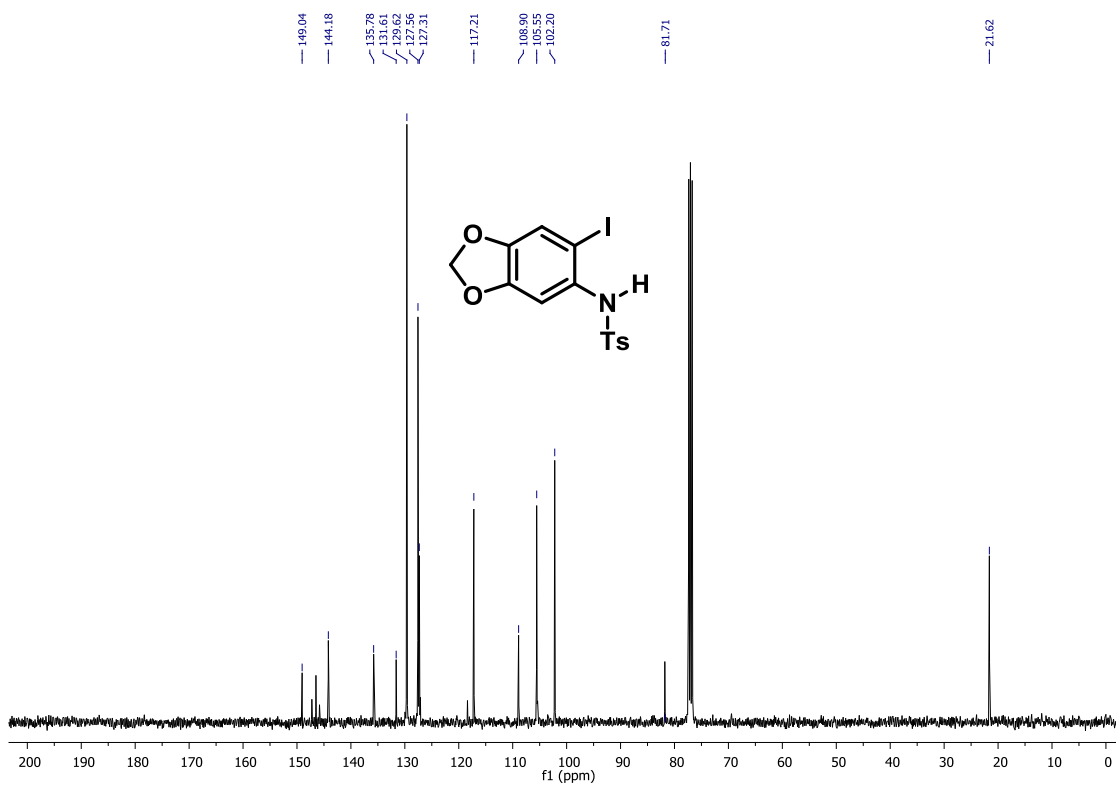


FIGURE 30: ^{13}C NMR spectrum of 46o precursor, 100 MHz, CDCl_3 .

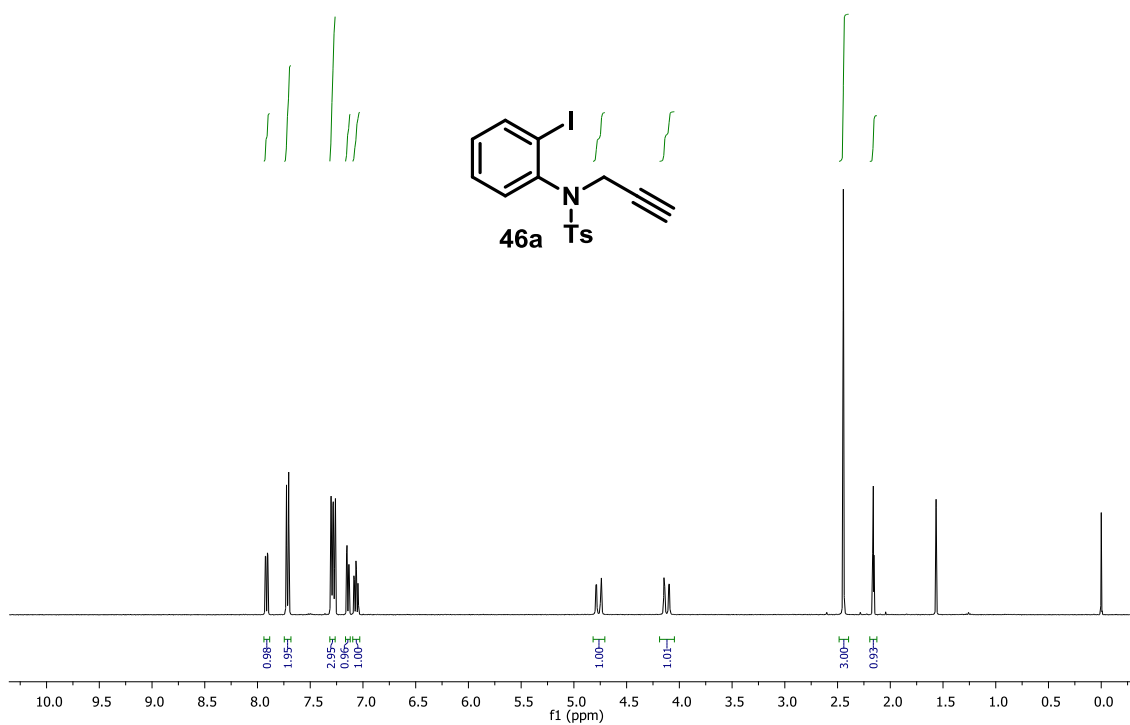


FIGURE 31: ¹H NMR spectrum of 46a, 400 MHz, CDCl₃.

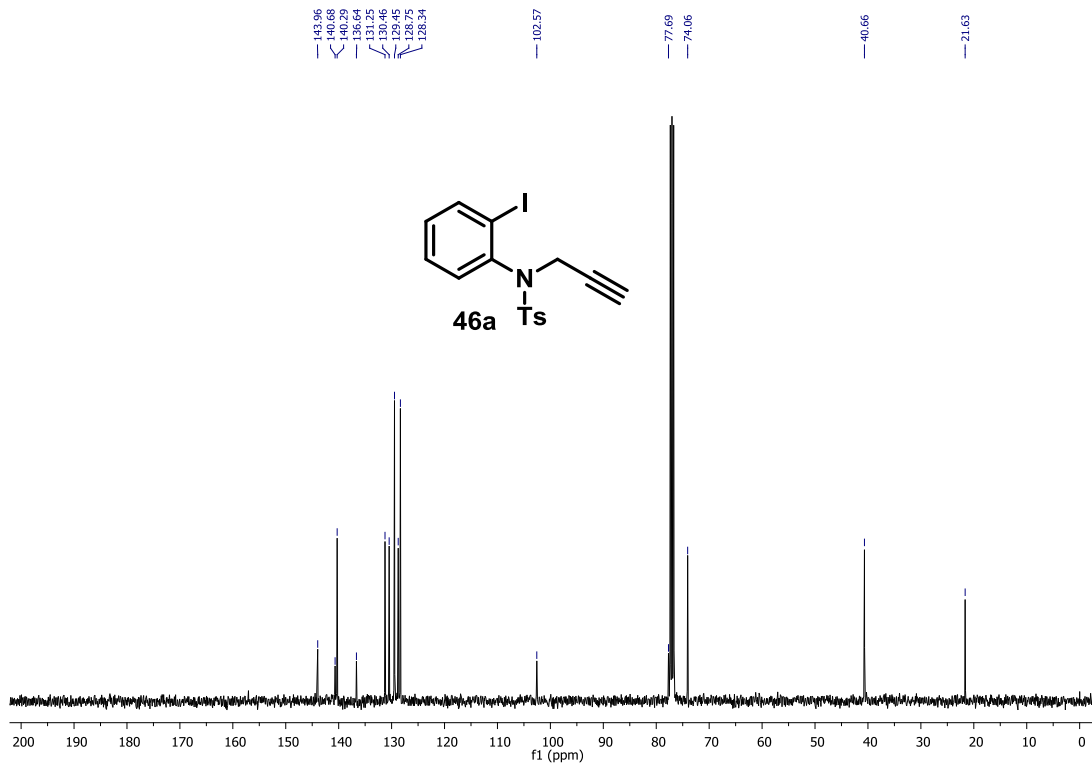


FIGURE 32: ¹³C NMR spectrum of 46a, 100 MHz, CDCl₃.

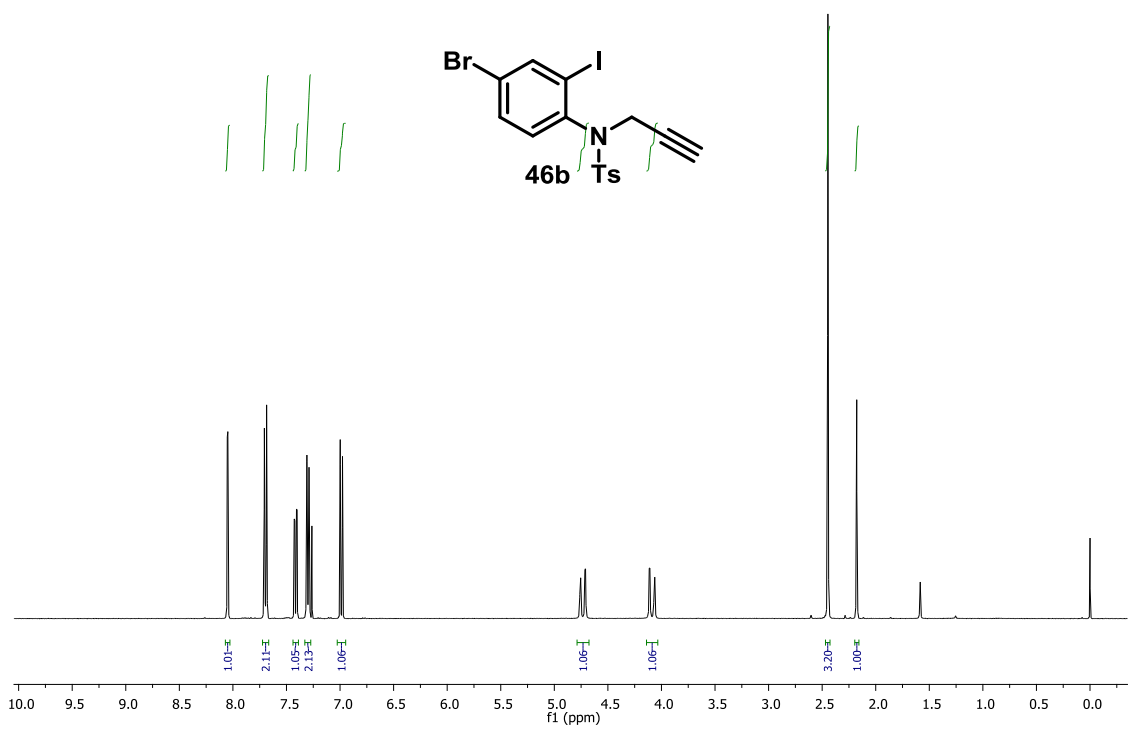


FIGURE 33: ¹H NMR spectrum of 46b, 400 MHz, CDCl₃.

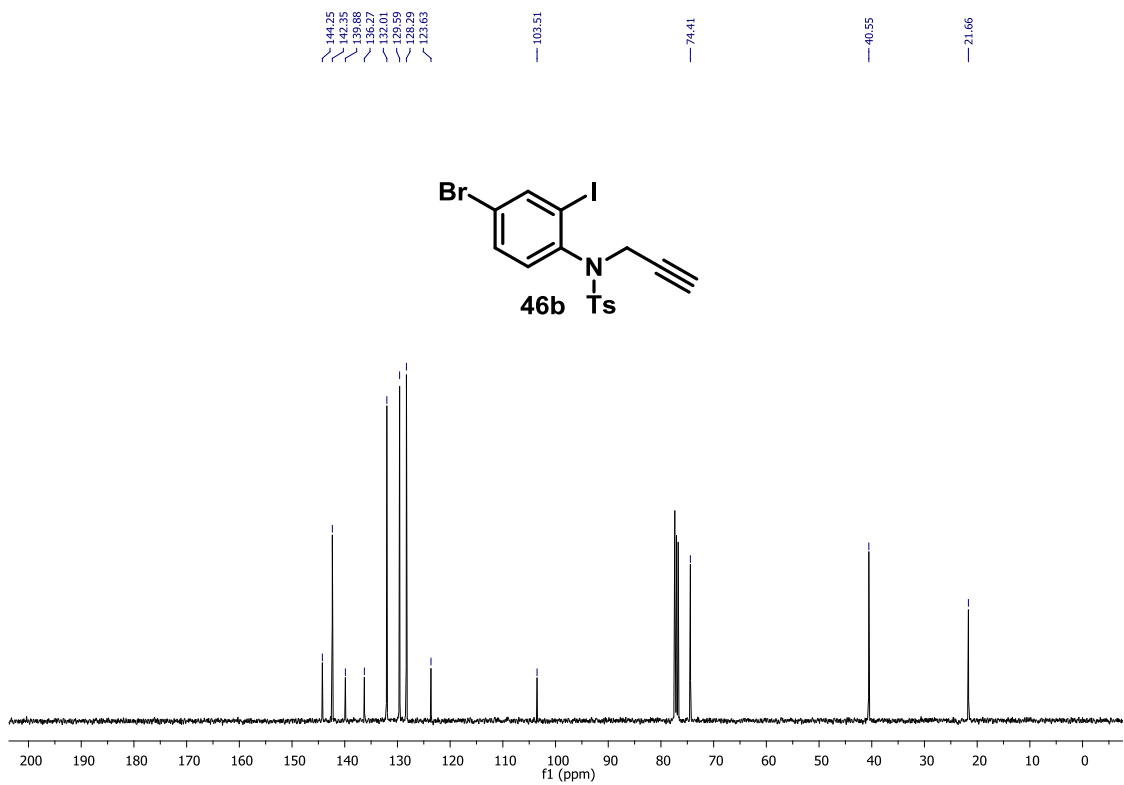


FIGURE 34: ¹³C NMR spectrum of 46b, 100 MHz, CDCl₃.

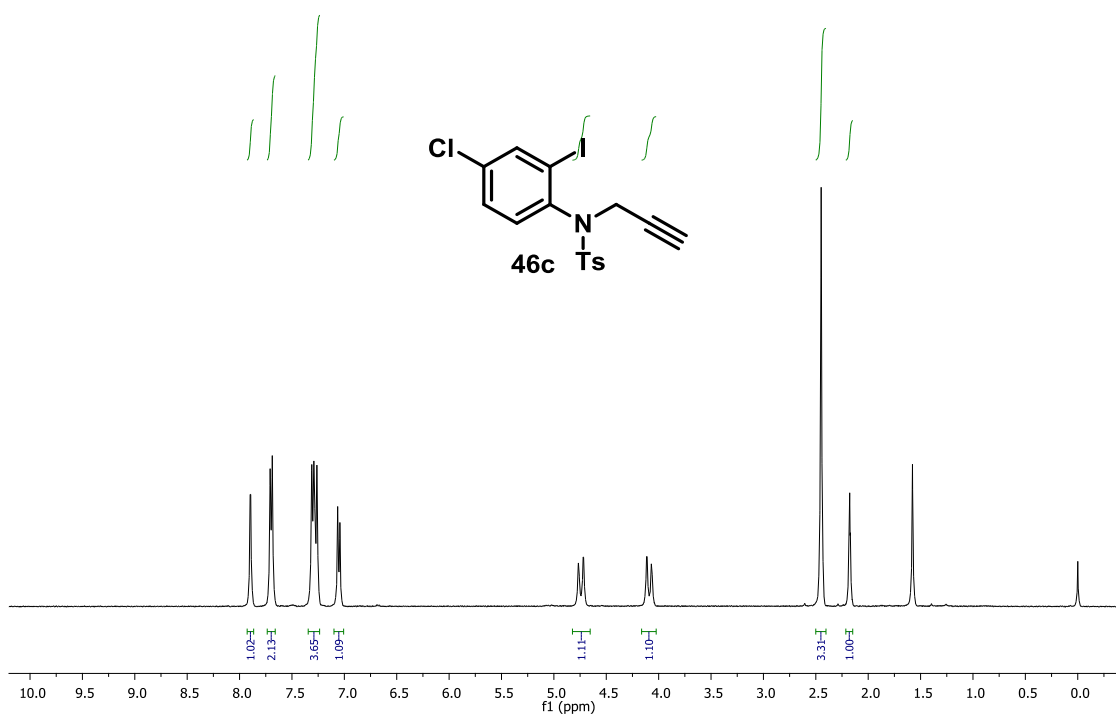


FIGURE 35: ¹H NMR spectrum of 46c, 400 MHz, CDCl₃.

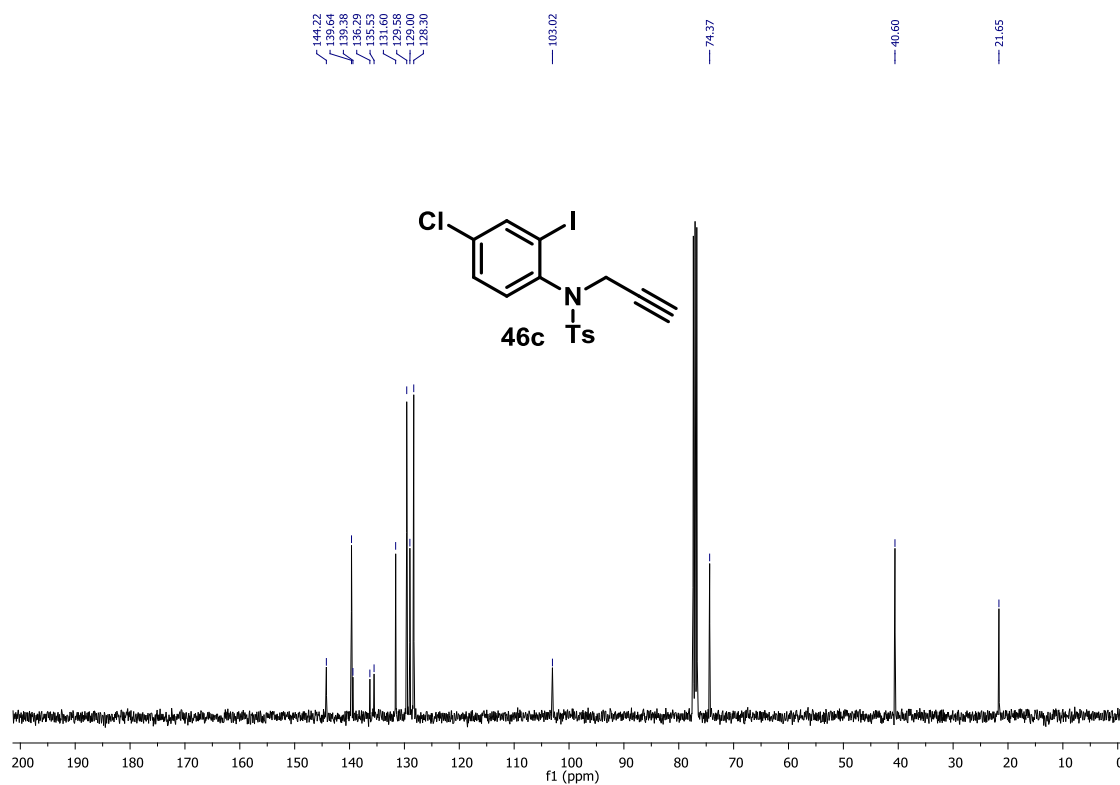


FIGURE 36: ¹³C NMR spectrum of 46c, 100 MHz, CDCl₃.

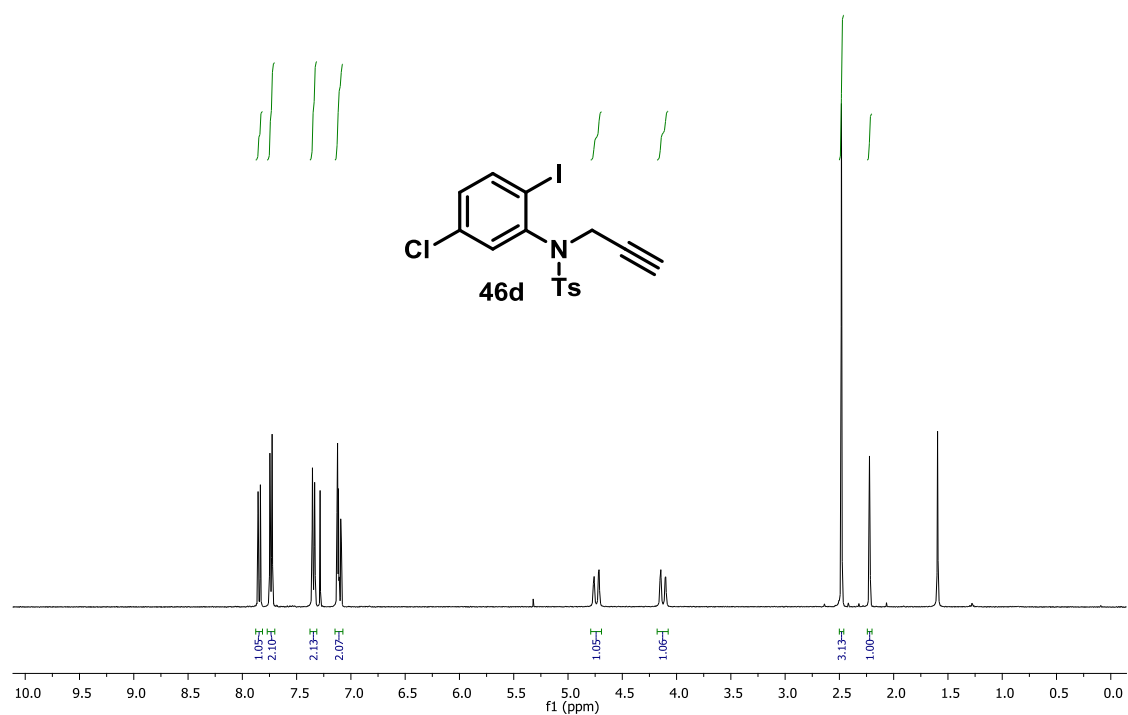


FIGURE 37: ¹H NMR spectrum of 46d, 400 MHz, CDCl₃.

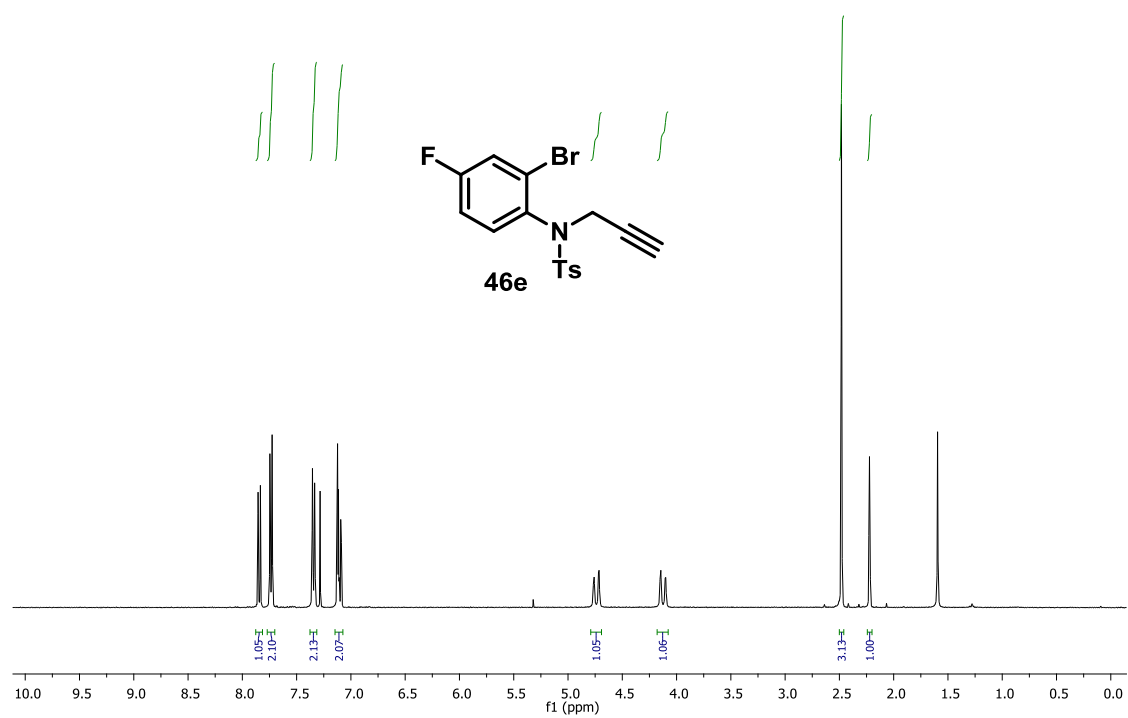


FIGURE 38: ¹H NMR spectrum of 46e, 400 MHz, CDCl₃.

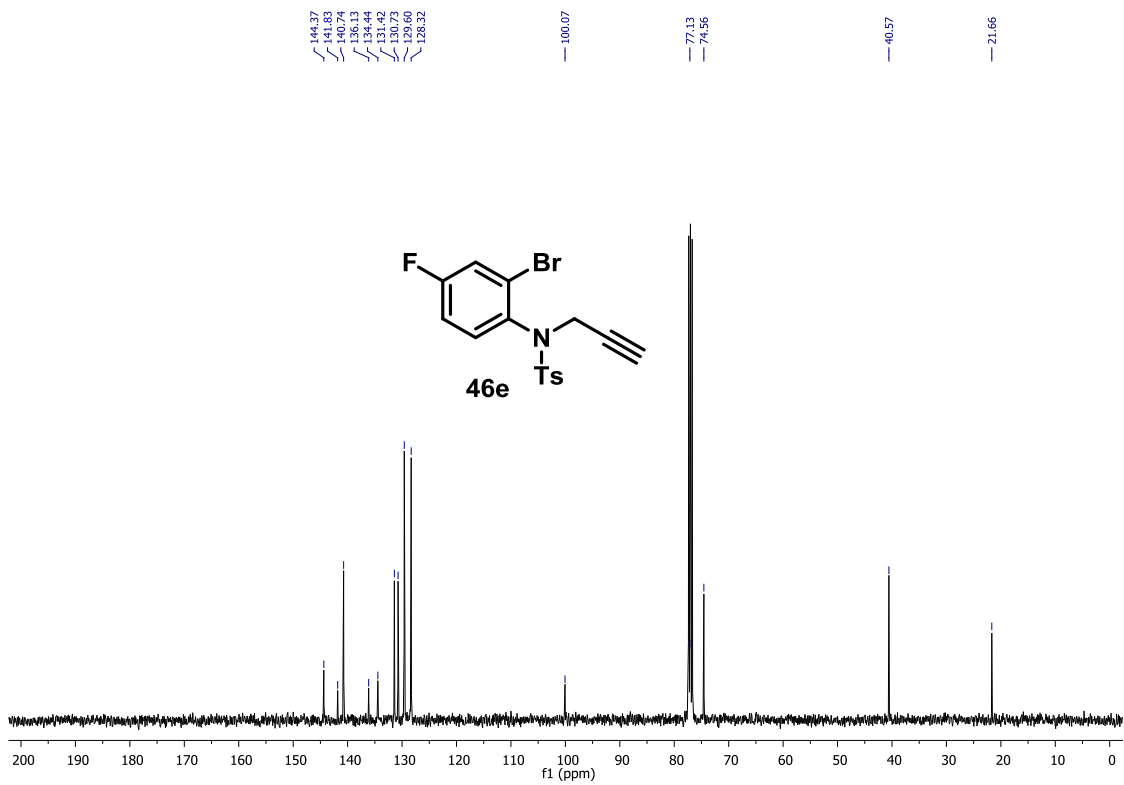


FIGURE 39: ¹³C NMR spectrum of 46e, 100 MHz, CDCl₃.

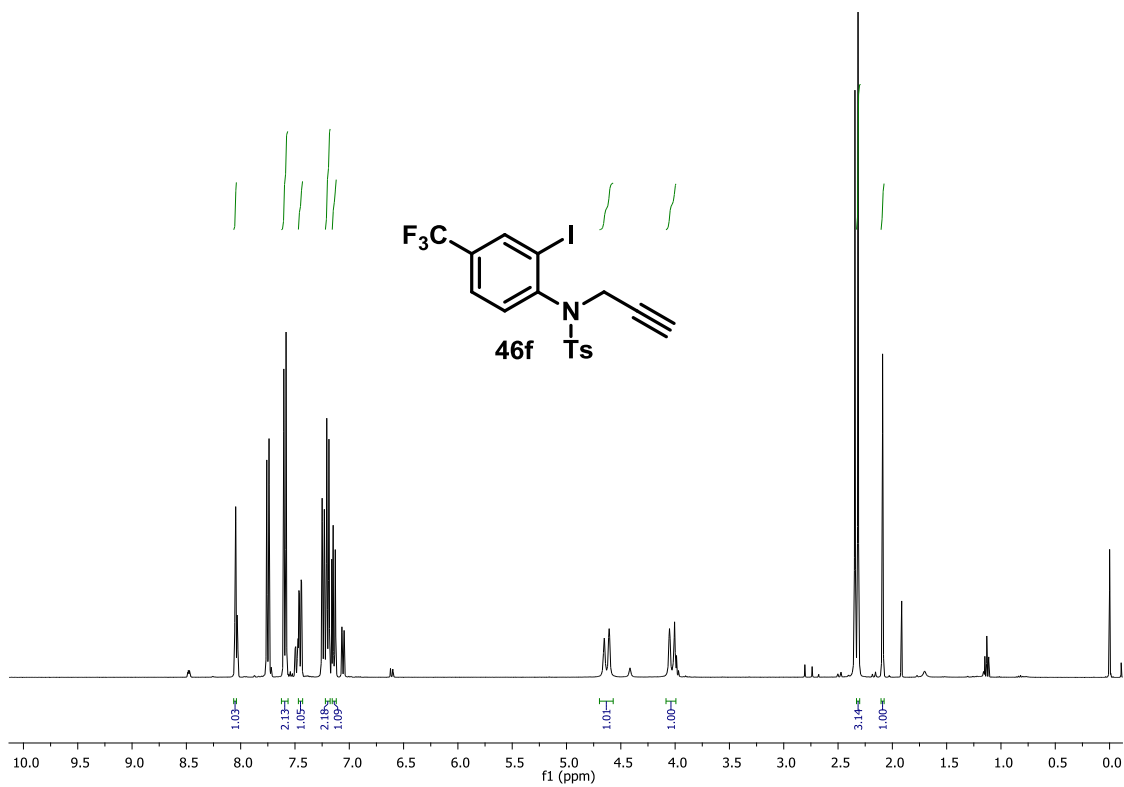


FIGURE 40: ¹H NMR spectrum of 46f, 400 MHz, CDCl₃.

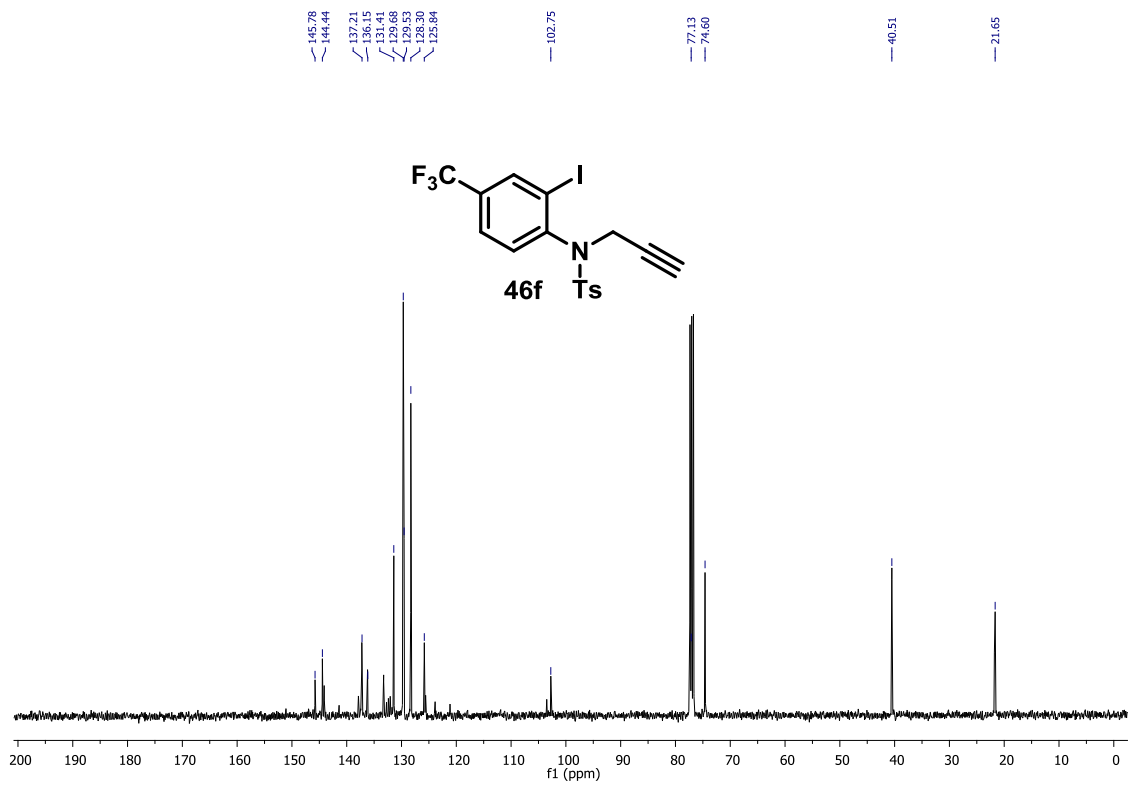


FIGURE 41: ¹³C NMR spectrum of 46f, 100 MHz, CDCl₃.

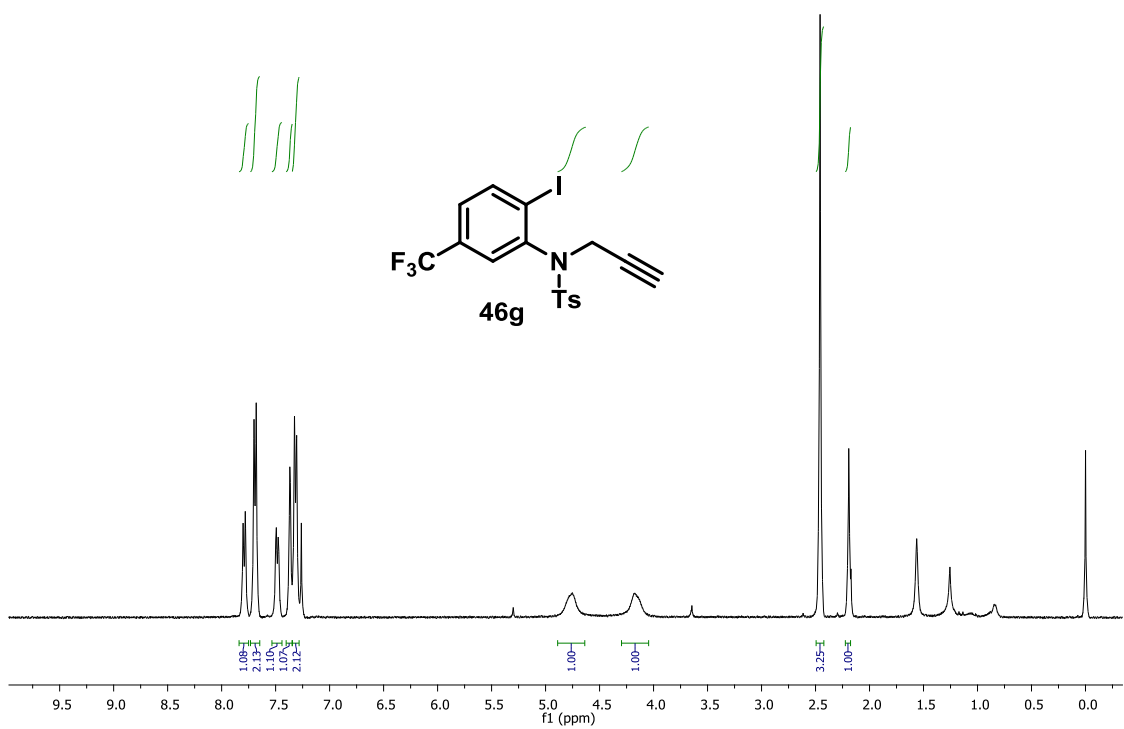


FIGURE 42: ¹H NMR spectrum of 46g, 400 MHz, CDCl₃.

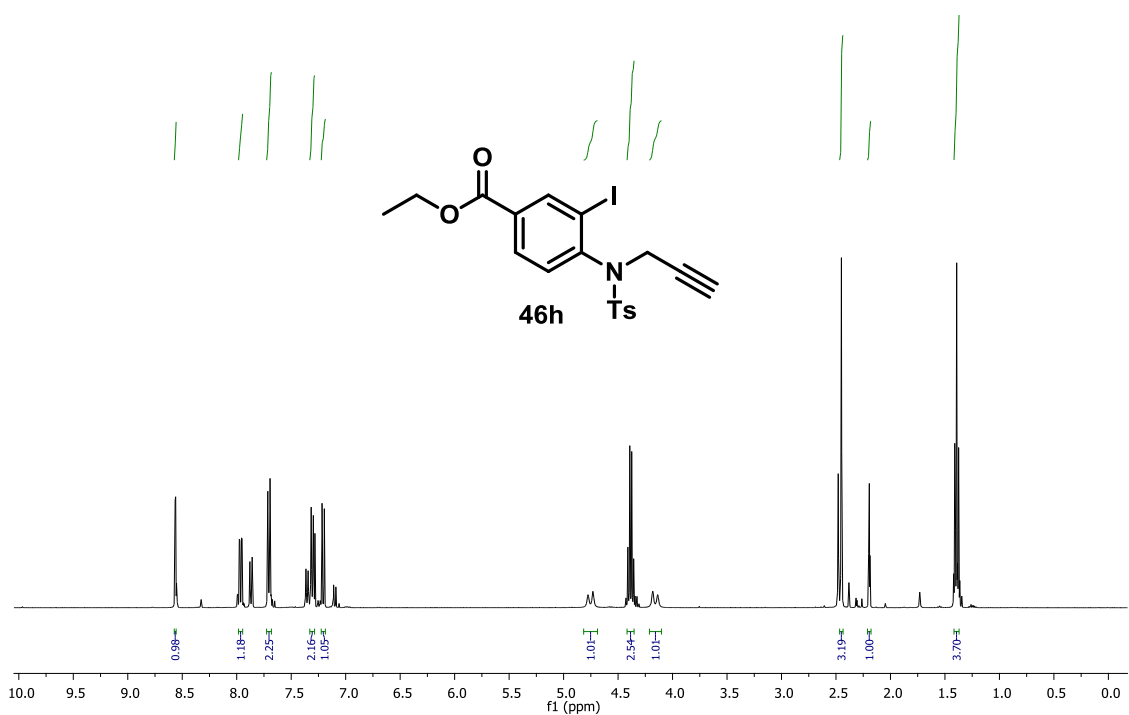


FIGURE 43: ¹H NMR spectrum of 46h, 400 MHz, CDCl₃.

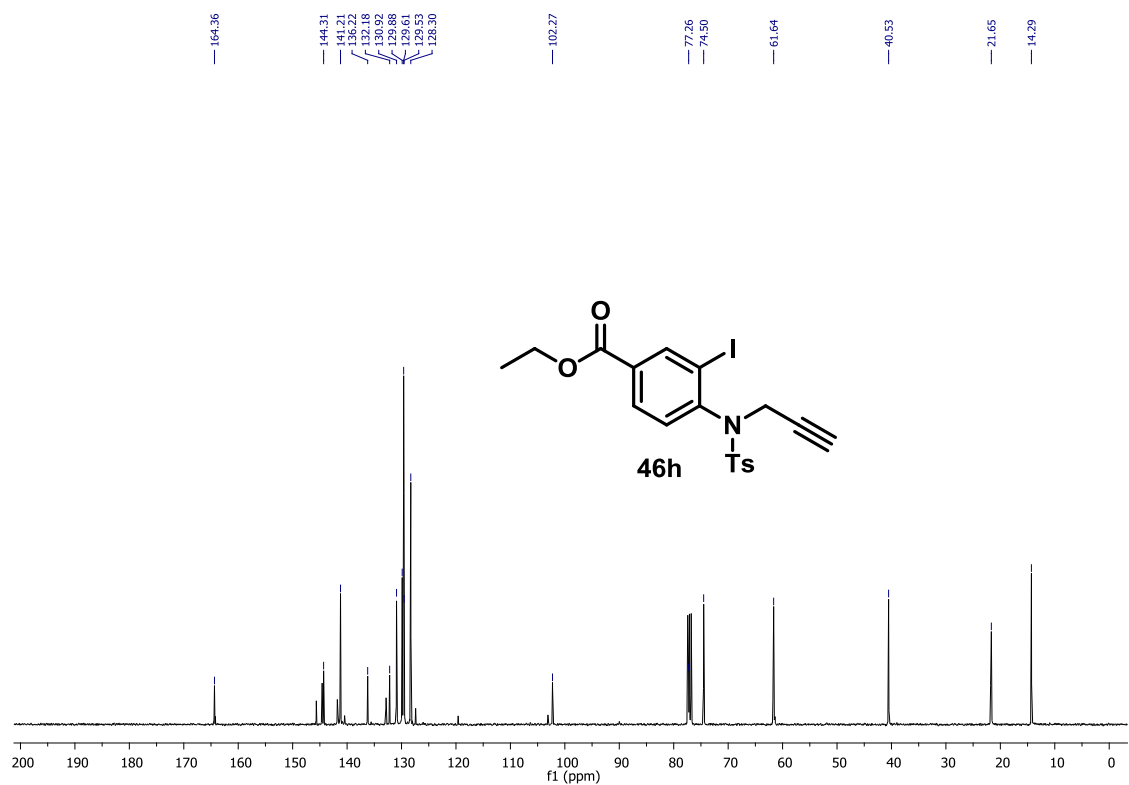


FIGURE 44: ¹³C NMR spectrum of 46h, 100 MHz, CDCl₃.

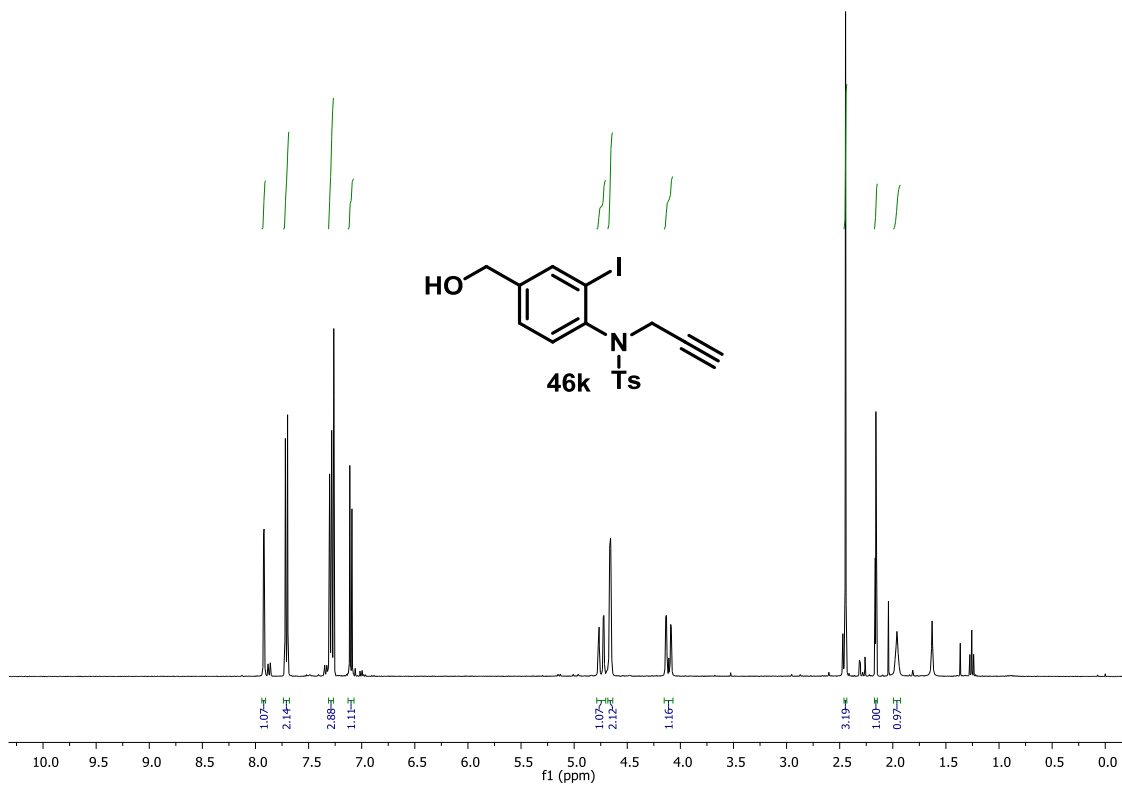


FIGURE 45: ¹H NMR spectrum of 46k, 400 MHz, CDCl₃.

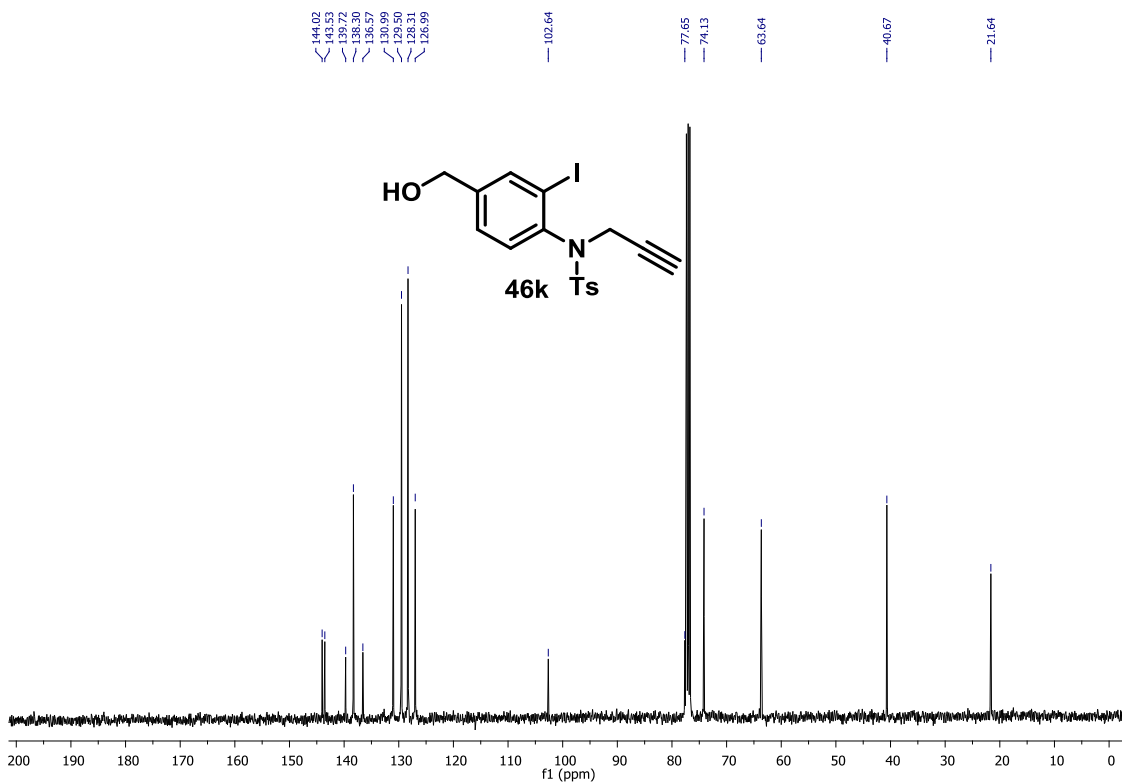


FIGURE 46: ¹³C NMR spectrum of 46k, 100 MHz, CDCl₃.

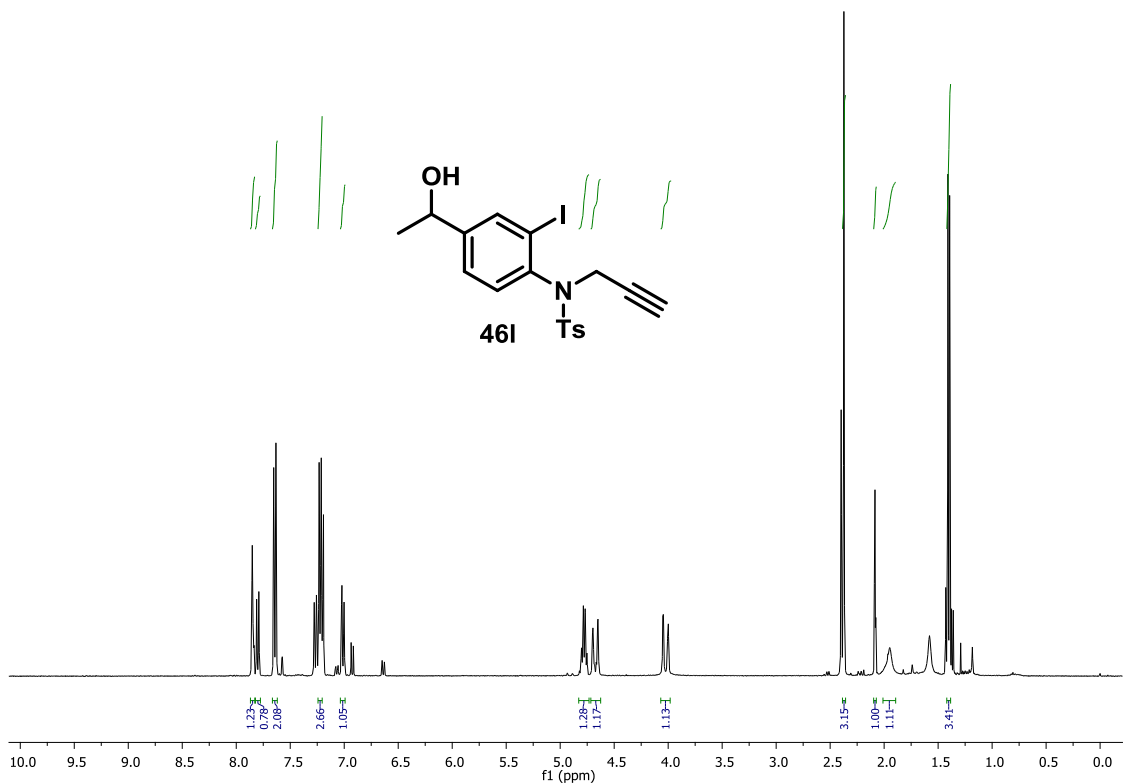


FIGURE 47: ¹H NMR spectrum of 46l, 400 MHz, CDCl₃.

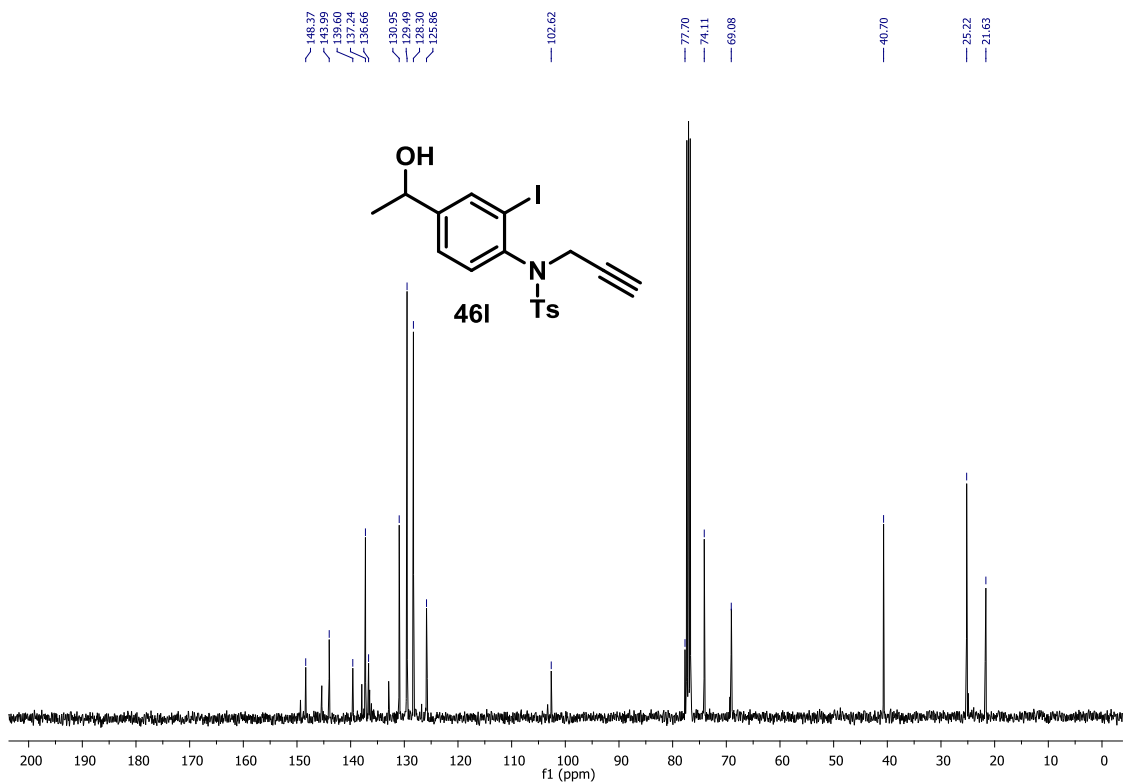


FIGURE 48: ¹³C NMR spectrum of 46l, 100 MHz, CDCl₃.

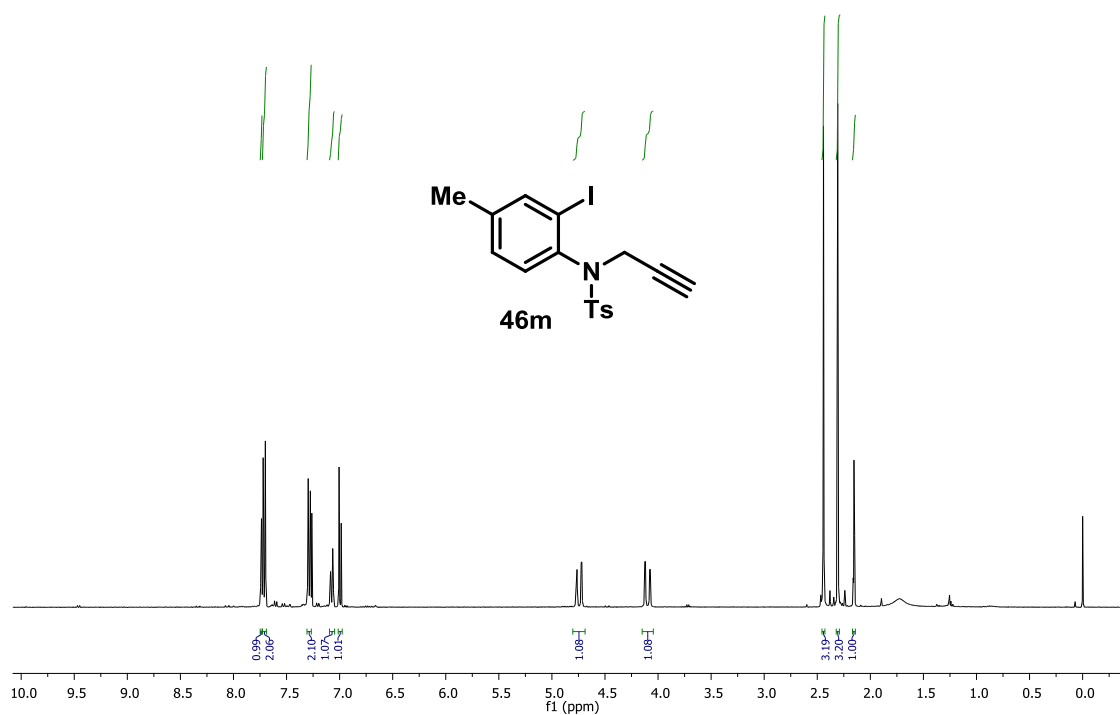


FIGURE 49: ¹H NMR spectrum of 46m, 400 MHz, CDCl₃.

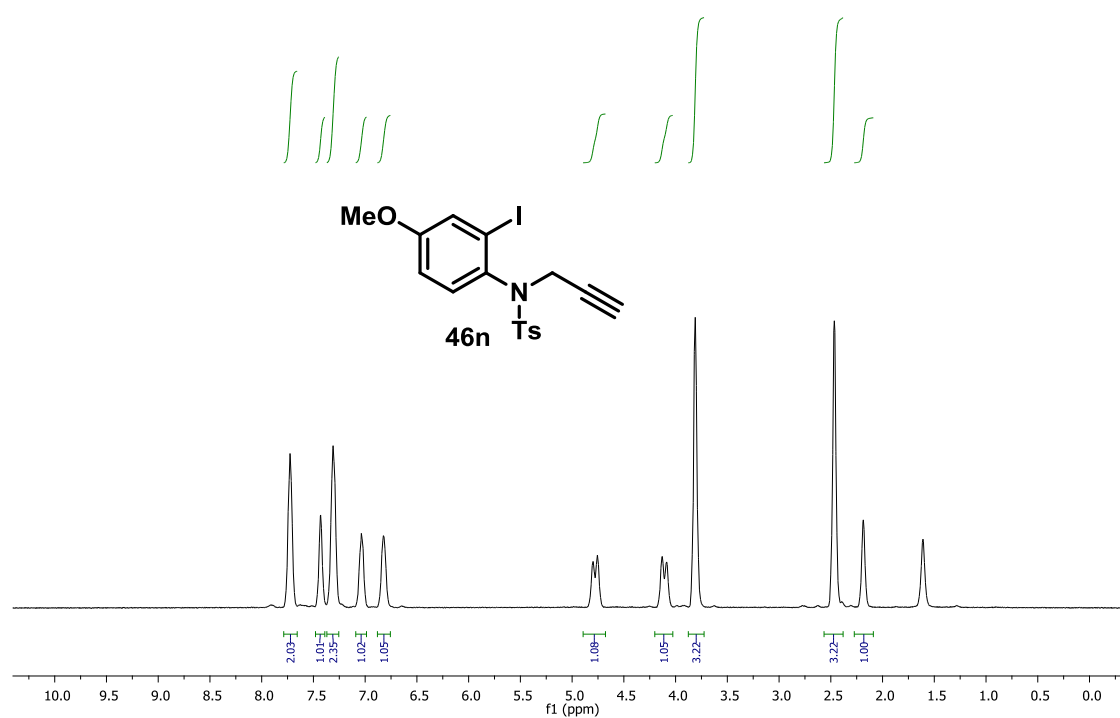


FIGURE 50: ¹H NMR spectrum of 46n, 400 MHz, CDCl₃.

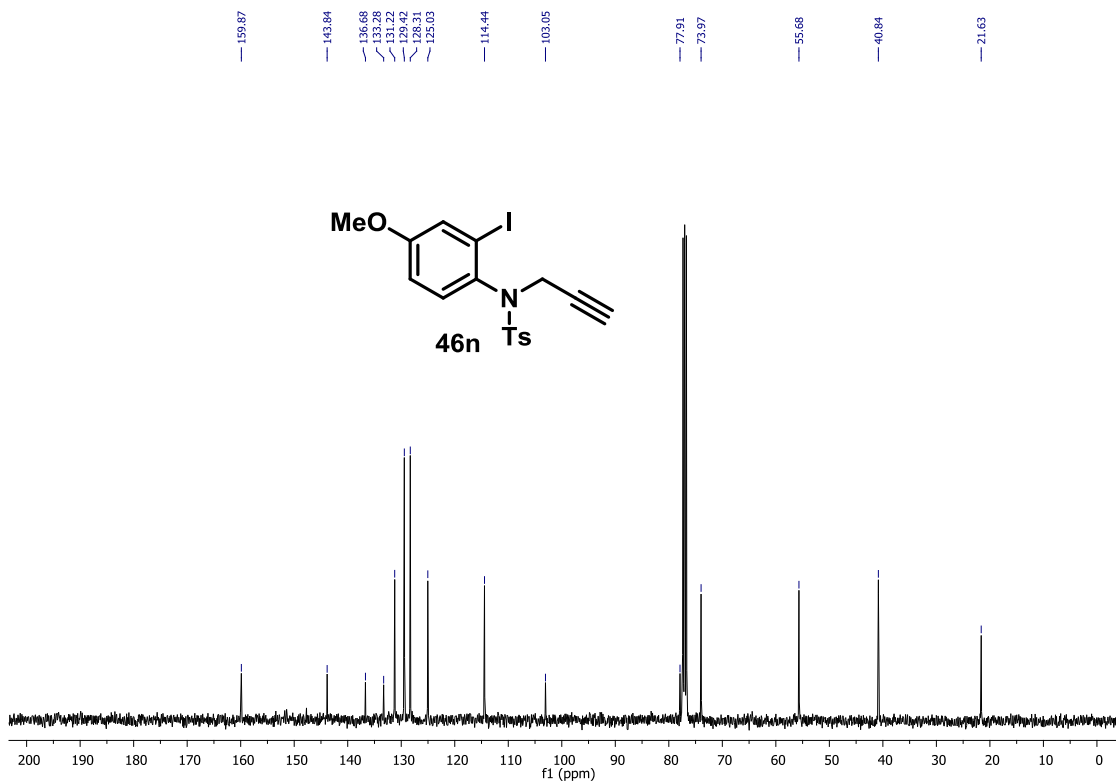


FIGURE 51: ^{13}C NMR spectrum of 46n, 100 MHz, CDCl_3 .

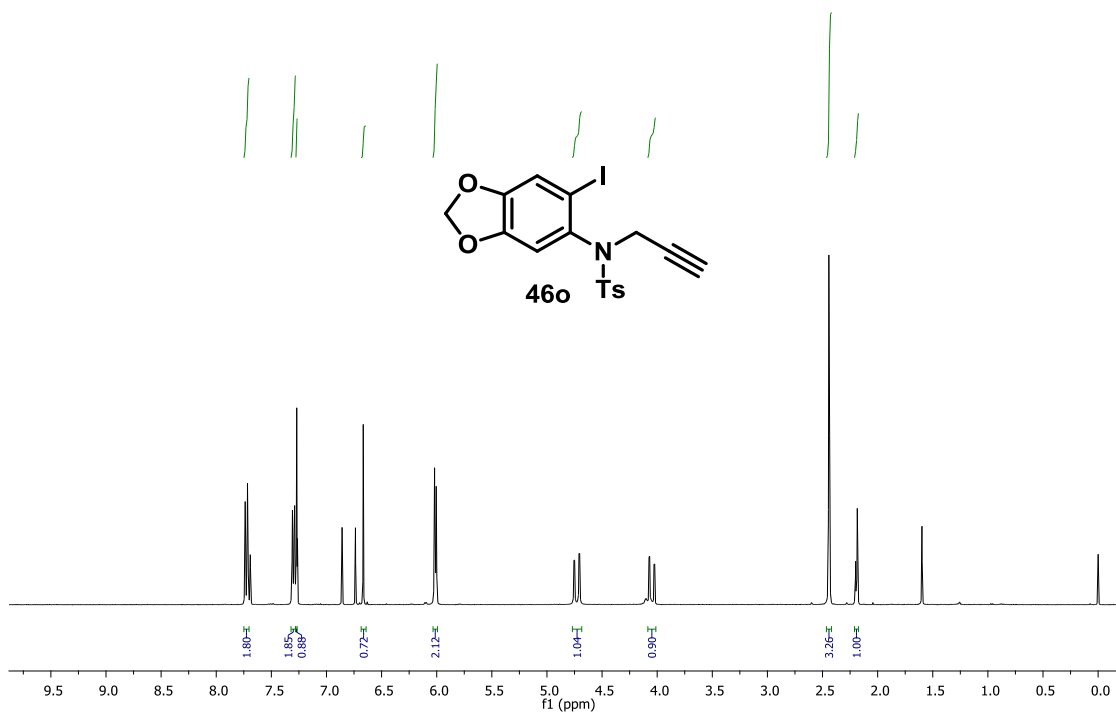


FIGURE 52: ^1H NMR spectrum of 46o, 400 MHz, CDCl_3 .

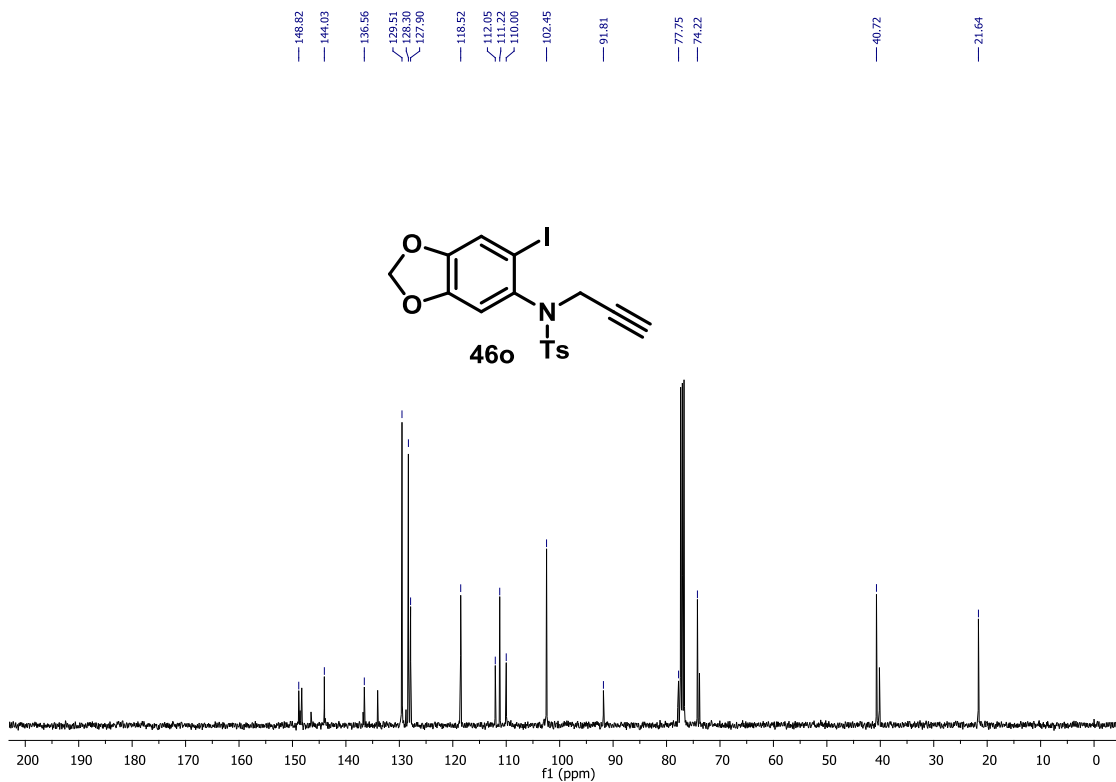


FIGURE 53: ^{13}C NMR spectrum of 46o, 100 MHz, CDCl_3 .

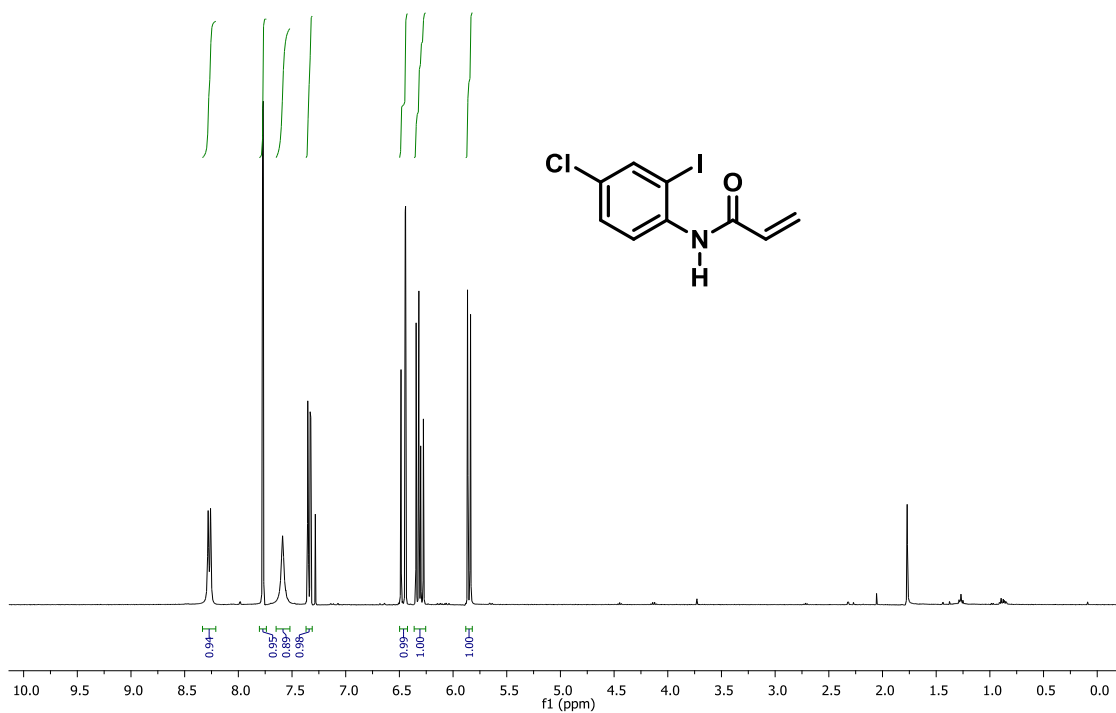


FIGURE 54: ^1H NMR spectrum of 48c precursor, 400 MHz, CDCl_3 .

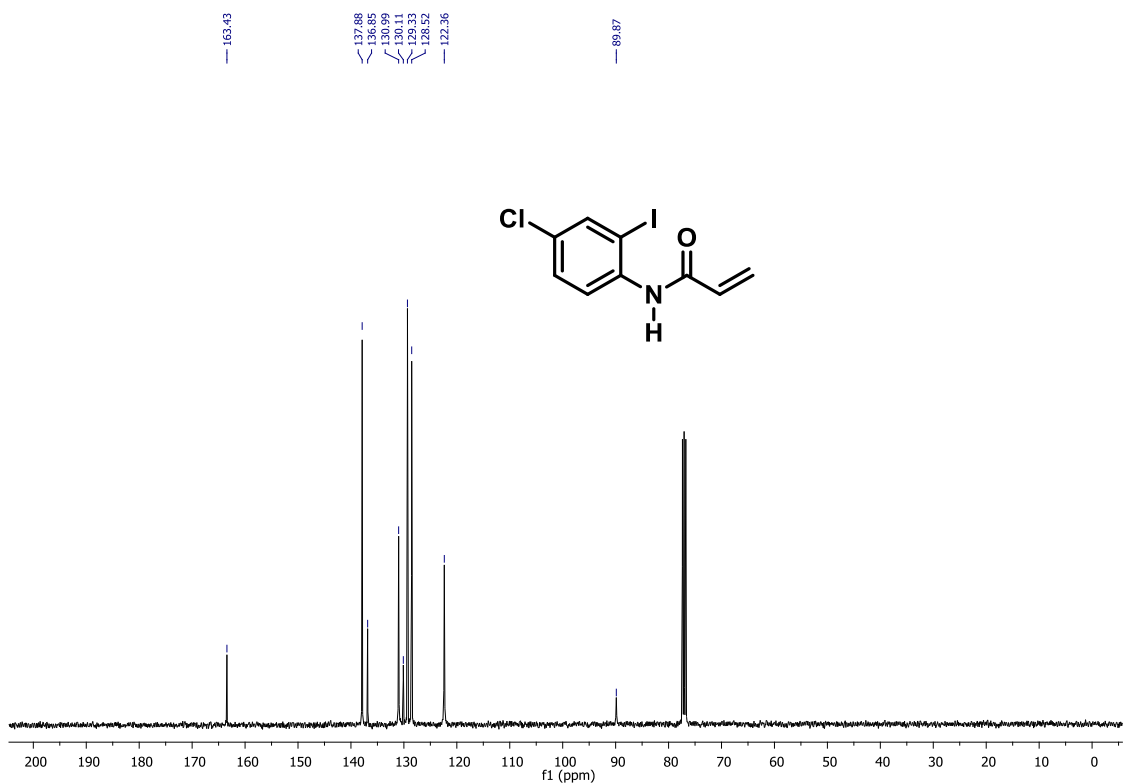


FIGURE 55: ¹³C NMR spectrum of 48c precursor, 100 MHz, CDCl₃.

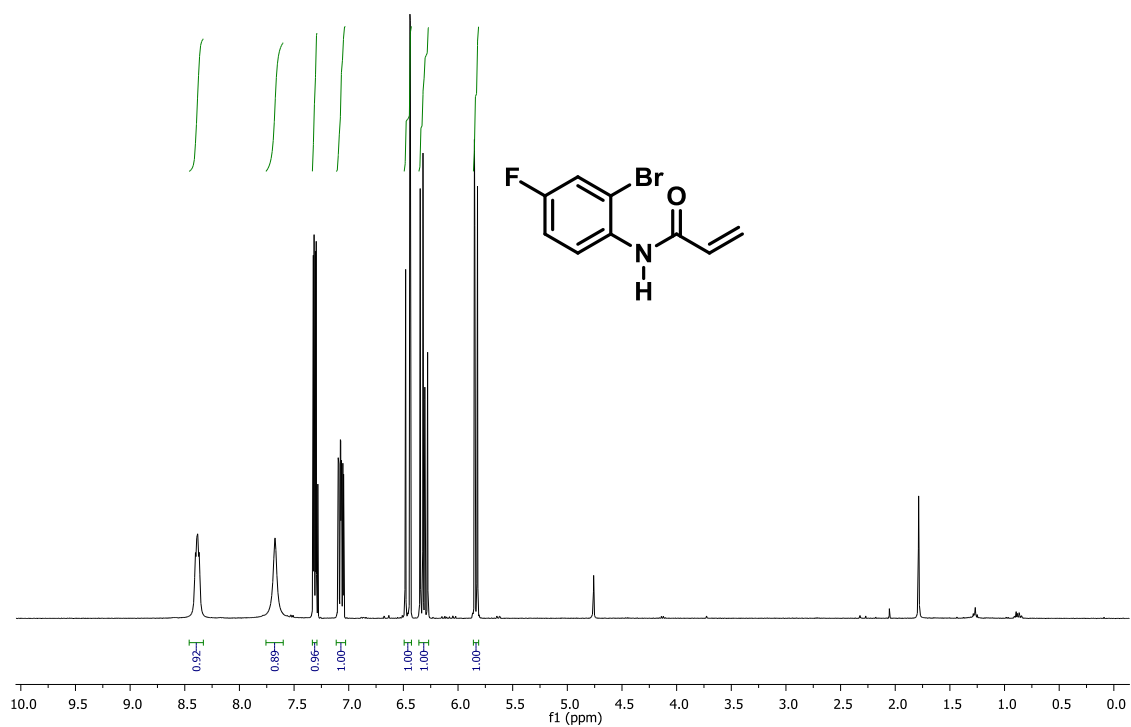


FIGURE 56: ¹H NMR spectrum of 48e precursor, 400 MHz, CDCl₃.

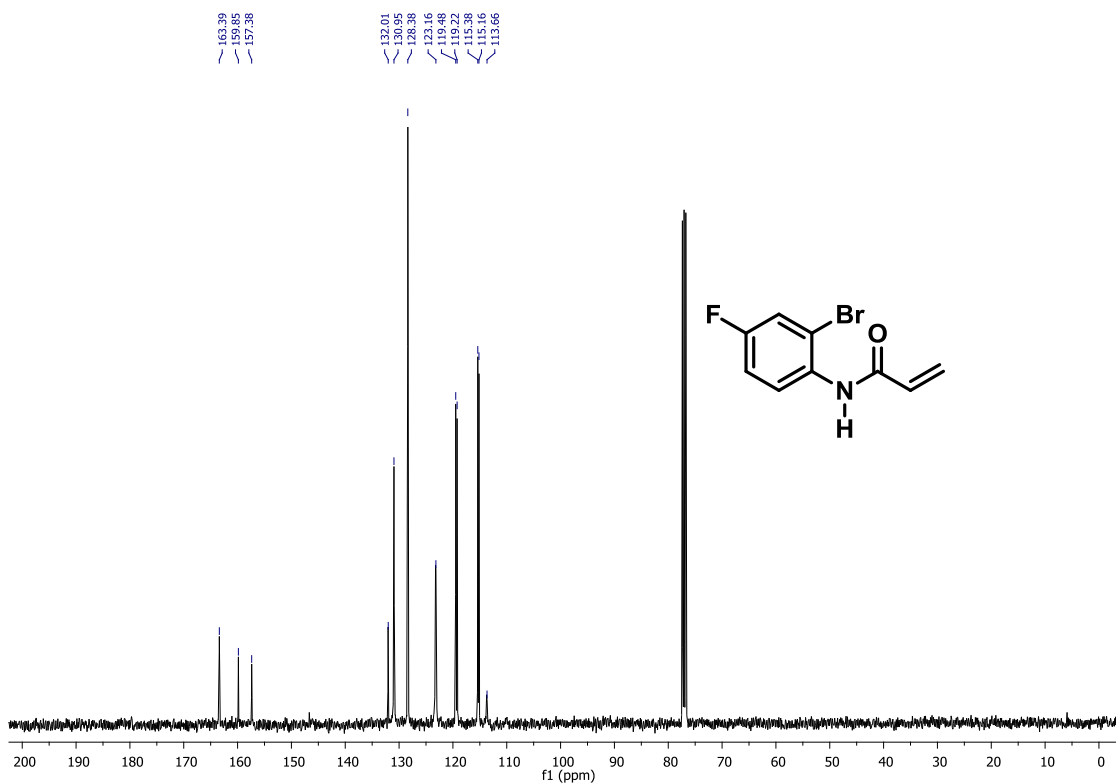


FIGURE 57: ¹³C NMR spectrum of 48e precursor, 100 MHz, CDCl₃.



FIGURE 58: ¹H NMR spectrum of 48f precursor, 400 MHz, CDCl₃.

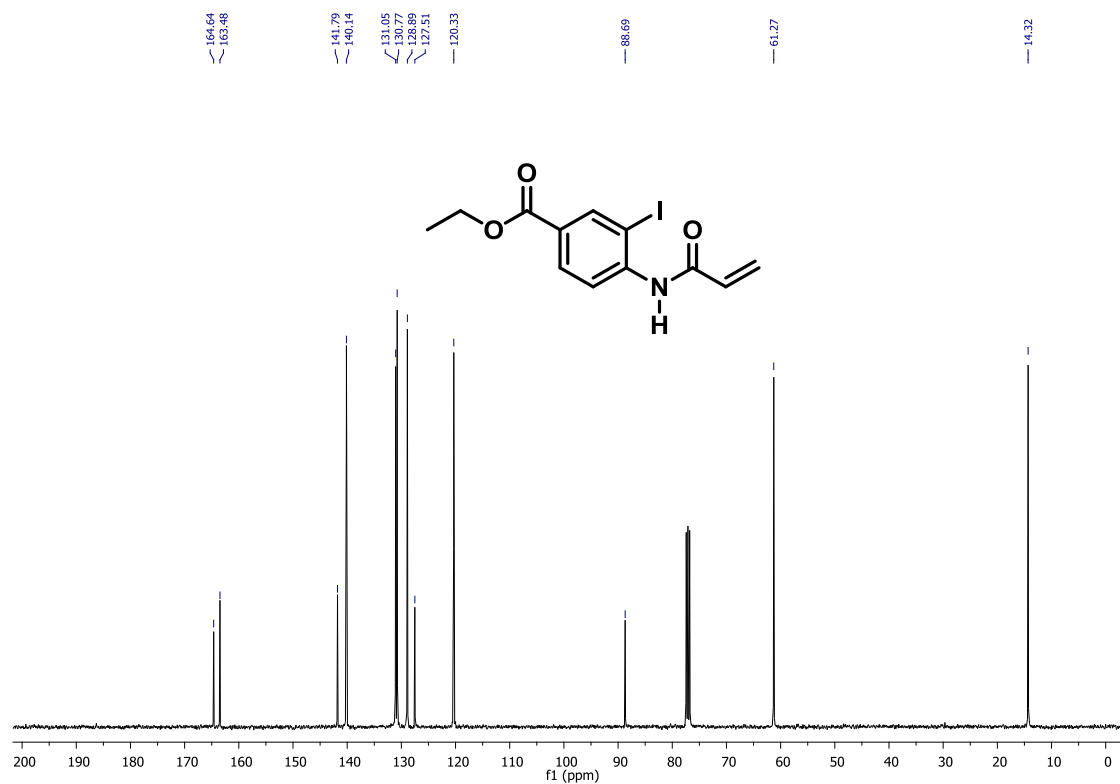


FIGURE 59: ^{13}C NMR spectrum of 48f precursor, 100 MHz, CDCl_3 .

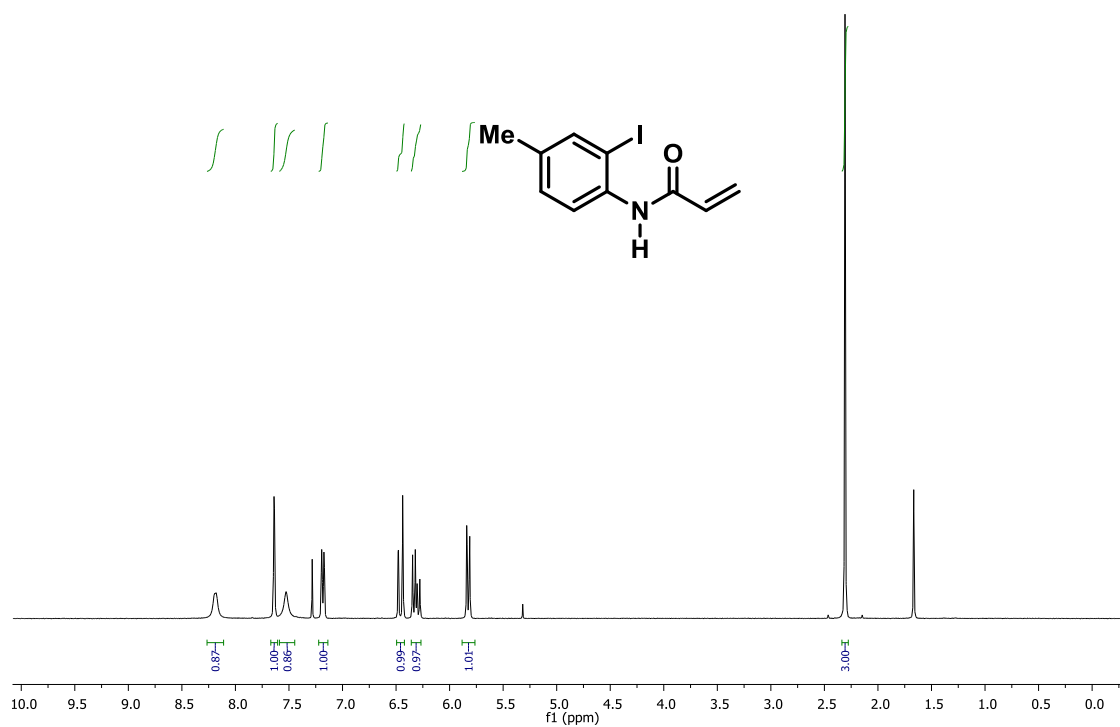


FIGURE 60: ^1H NMR spectrum of 48g precursor, 400 MHz, CDCl_3 .

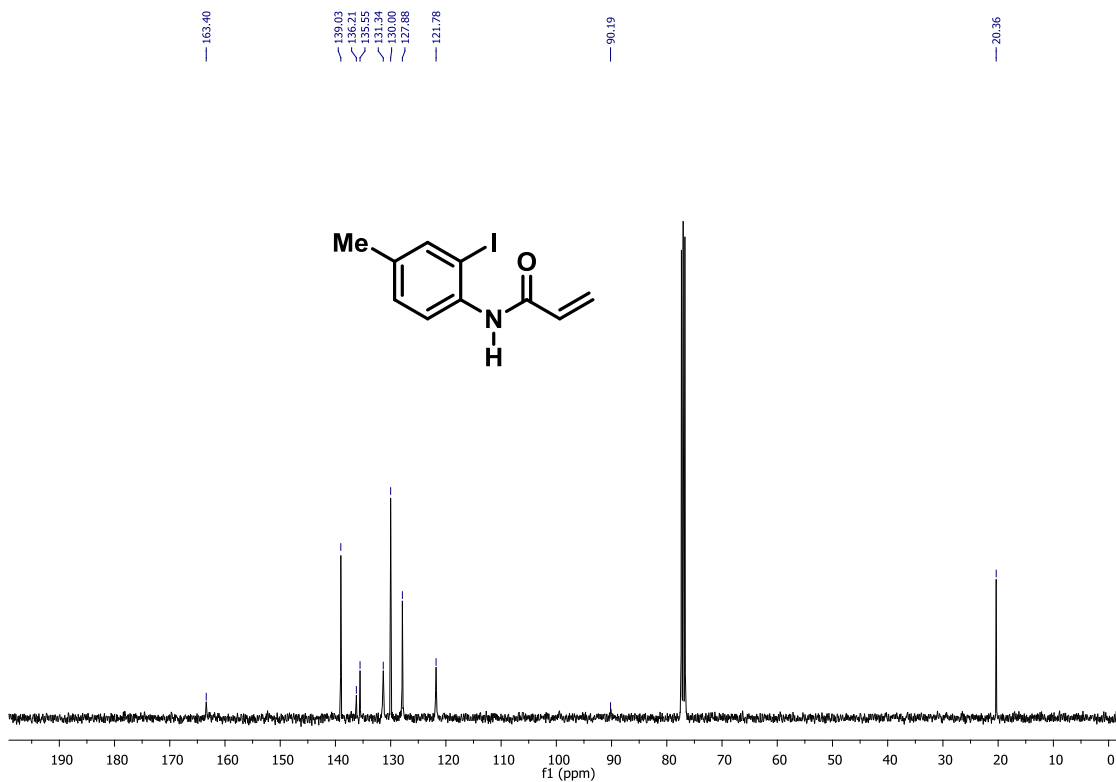


FIGURE 61: ¹³C NMR spectrum of 48g precursor, 100 MHz, CDCl₃.

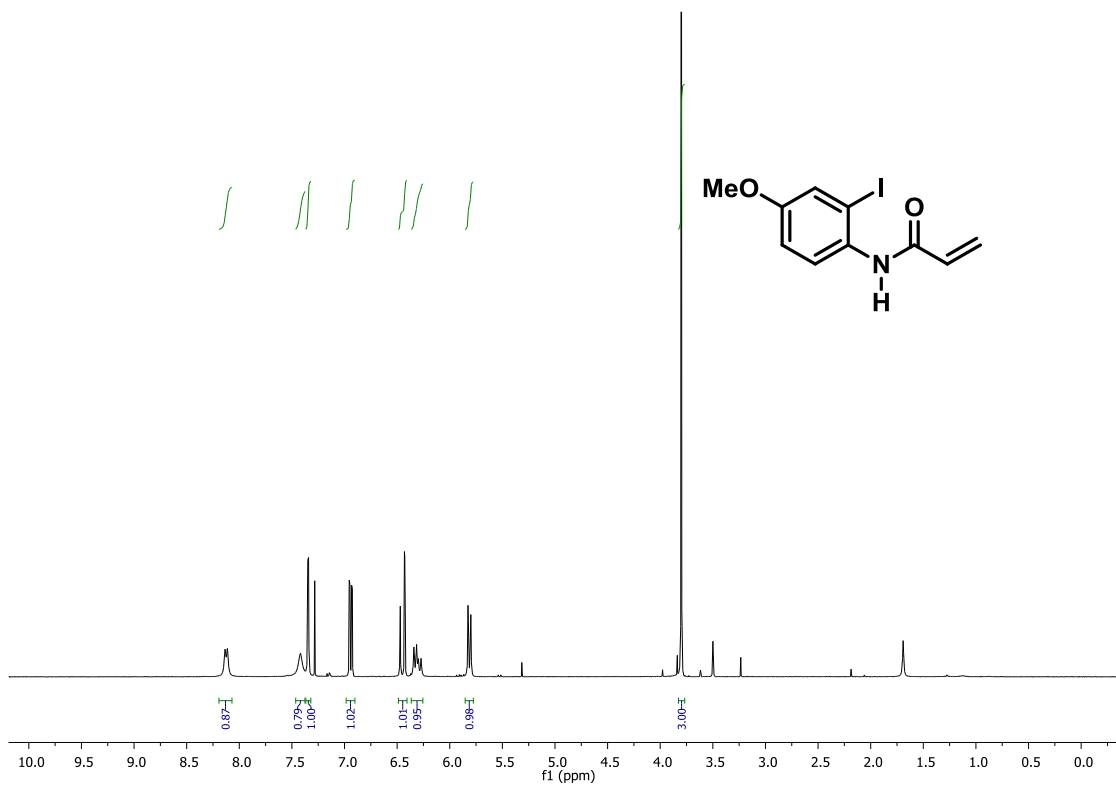


FIGURE 62: ¹H NMR spectrum of 48h precursor, 400 MHz, CDCl₃.

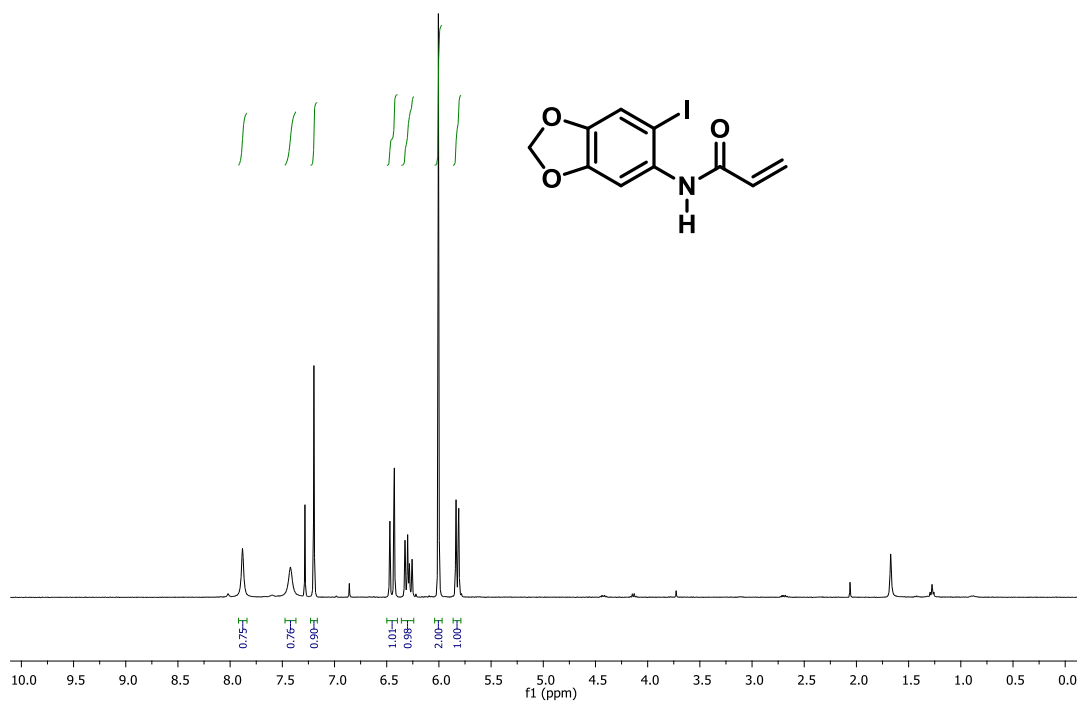


FIGURE 63: ¹H NMR spectrum of 48i precursor, 400 MHz, CDCl₃.

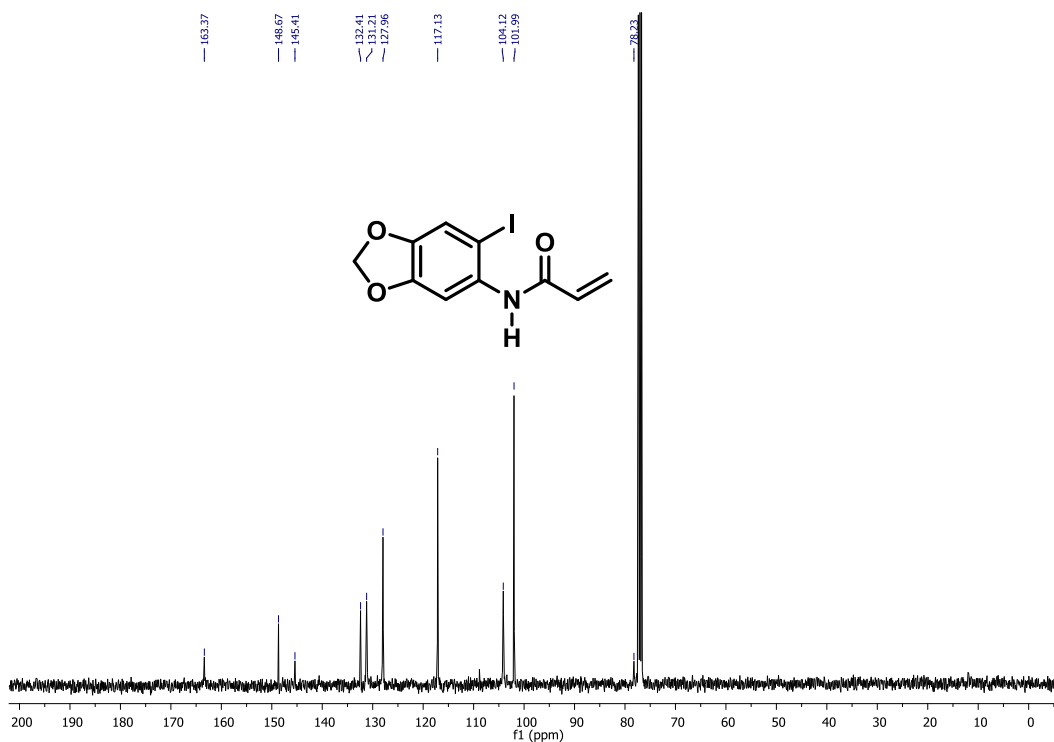


FIGURE 64: ¹³C NMR spectrum of 48i precursor, 100 MHz, CDCl₃.

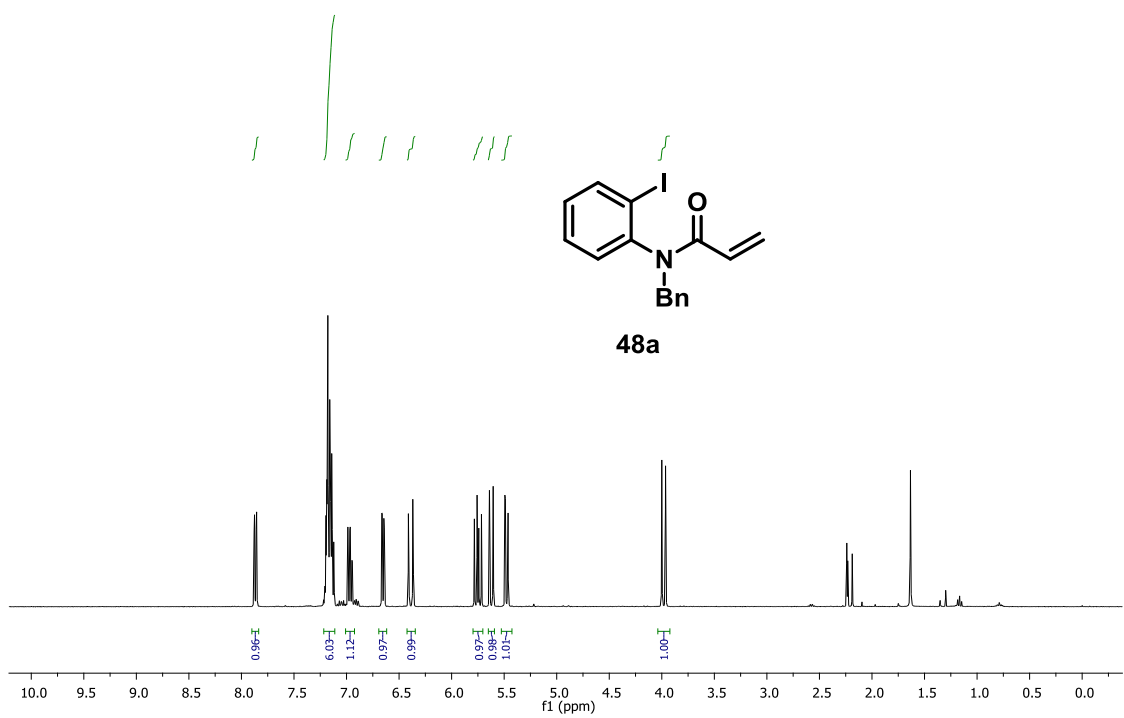


FIGURE 65: ¹H NMR spectrum of 48a, 400 MHz, CDCl₃.

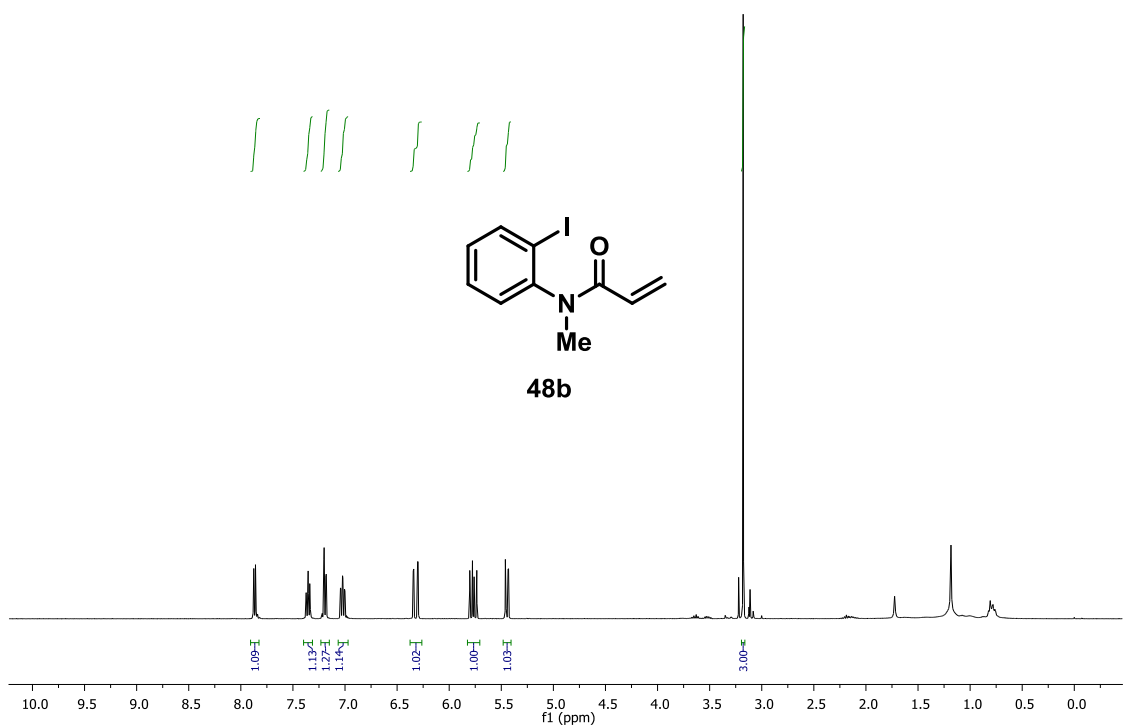


FIGURE 66: ¹H NMR spectrum of 48b, 400 MHz, CDCl₃.

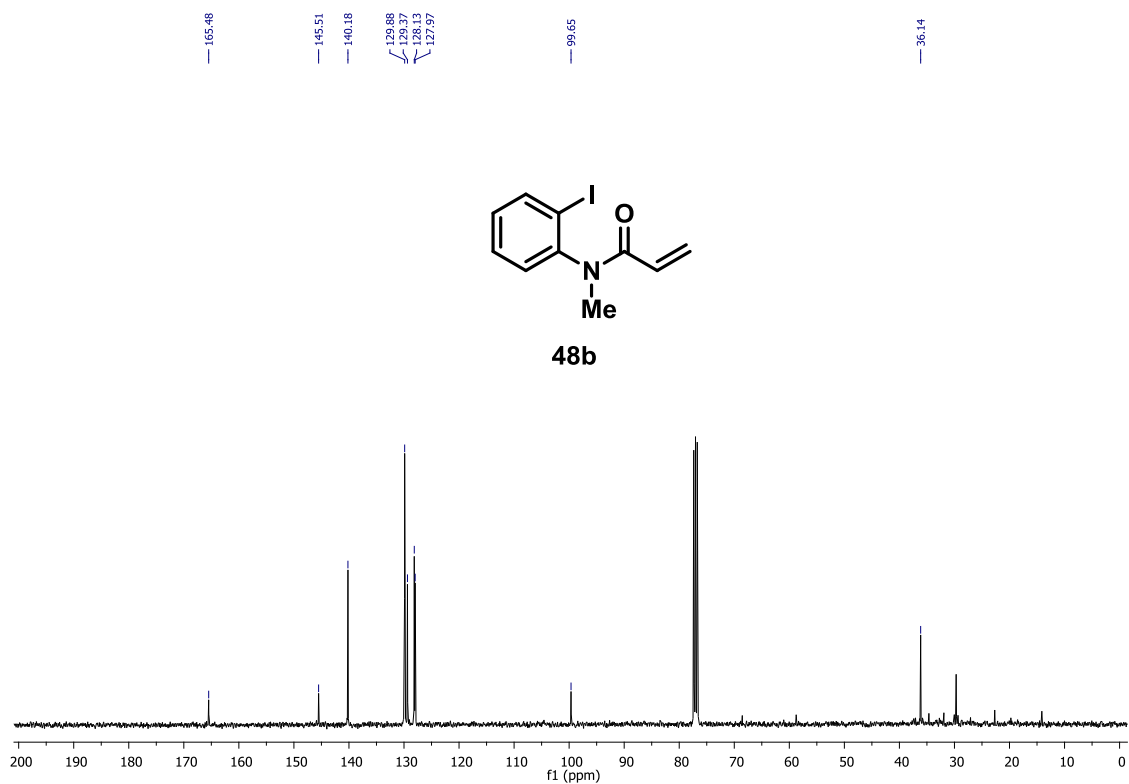


FIGURE 67: ¹³C NMR spectrum of 48b, 100 MHz, CDCl₃.

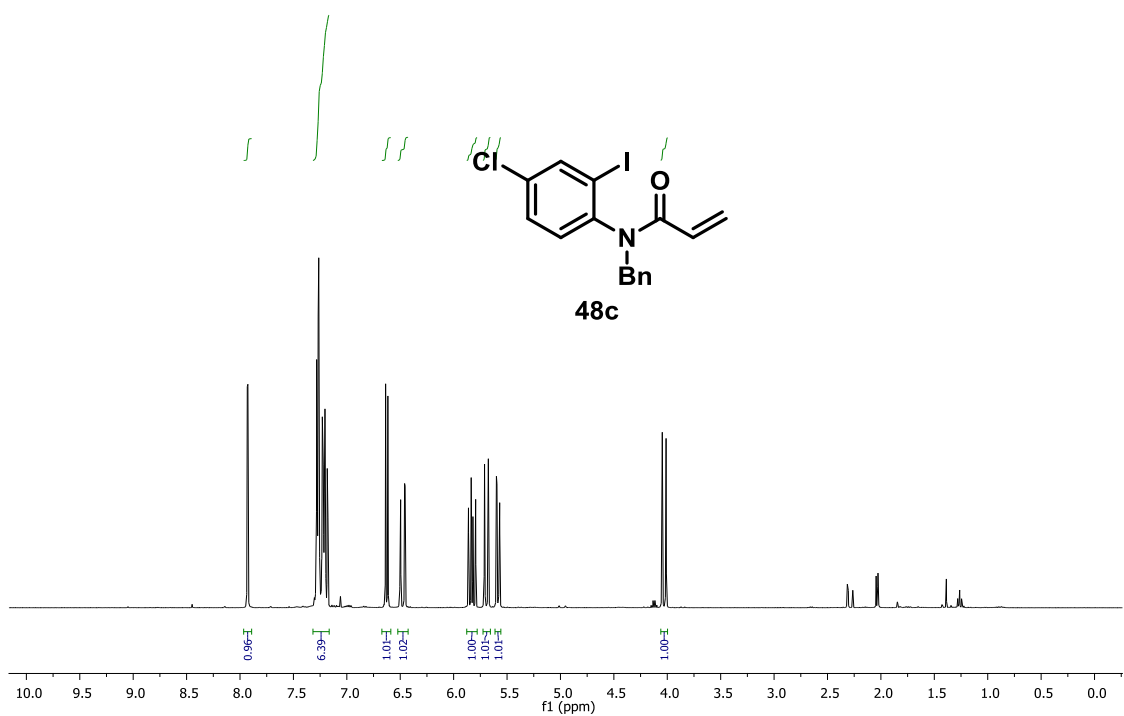


FIGURE 68: ¹H NMR spectrum of 48c, 400 MHz, CDCl₃.

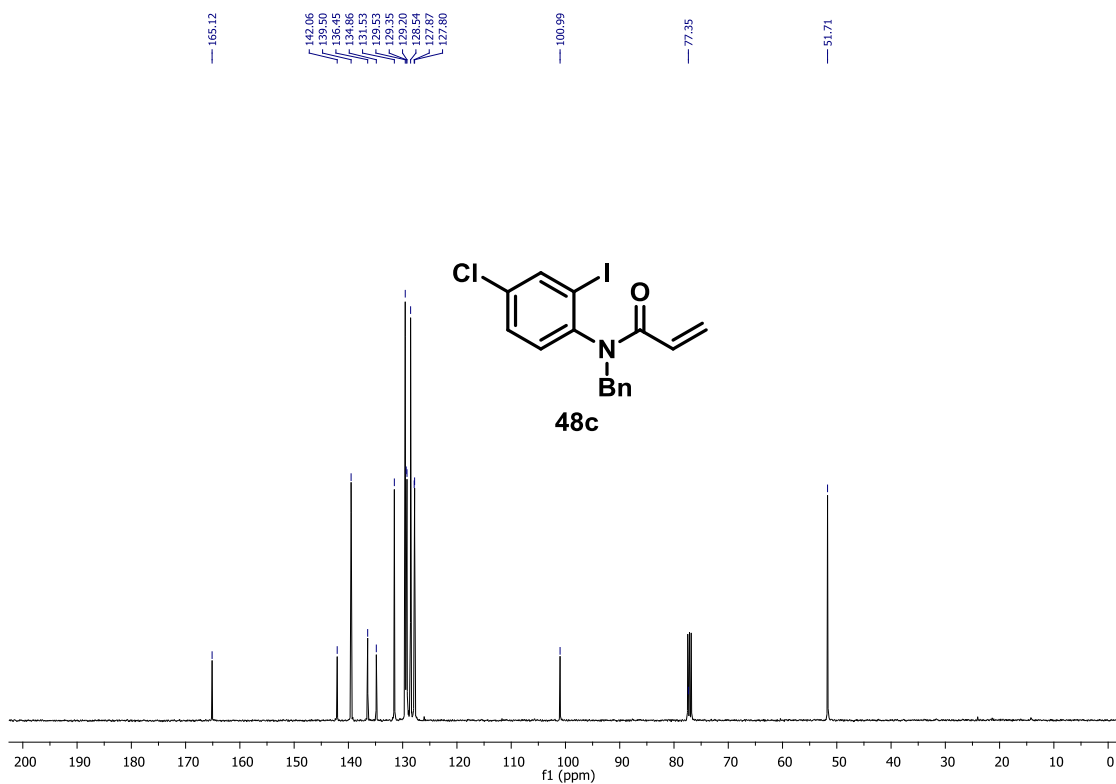


FIGURE 69: ¹³C NMR spectrum of 48c, 100 MHz, CDCl₃.

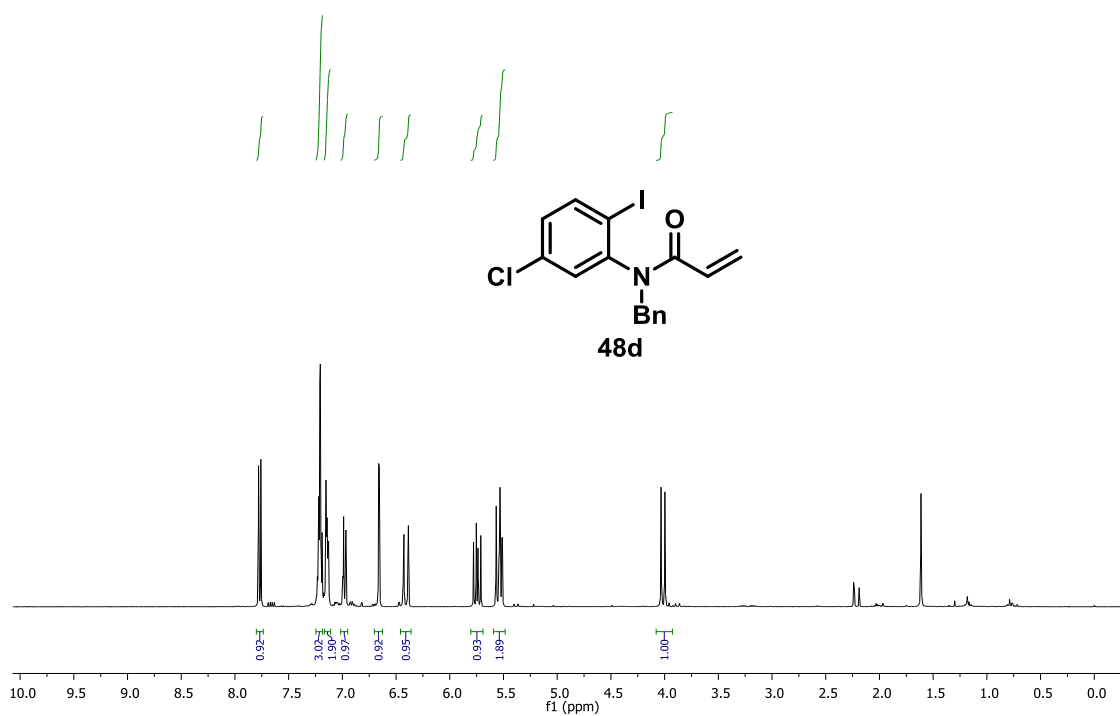


FIGURE 70: ¹H NMR spectrum of 48d, 400 MHz, CDCl₃.

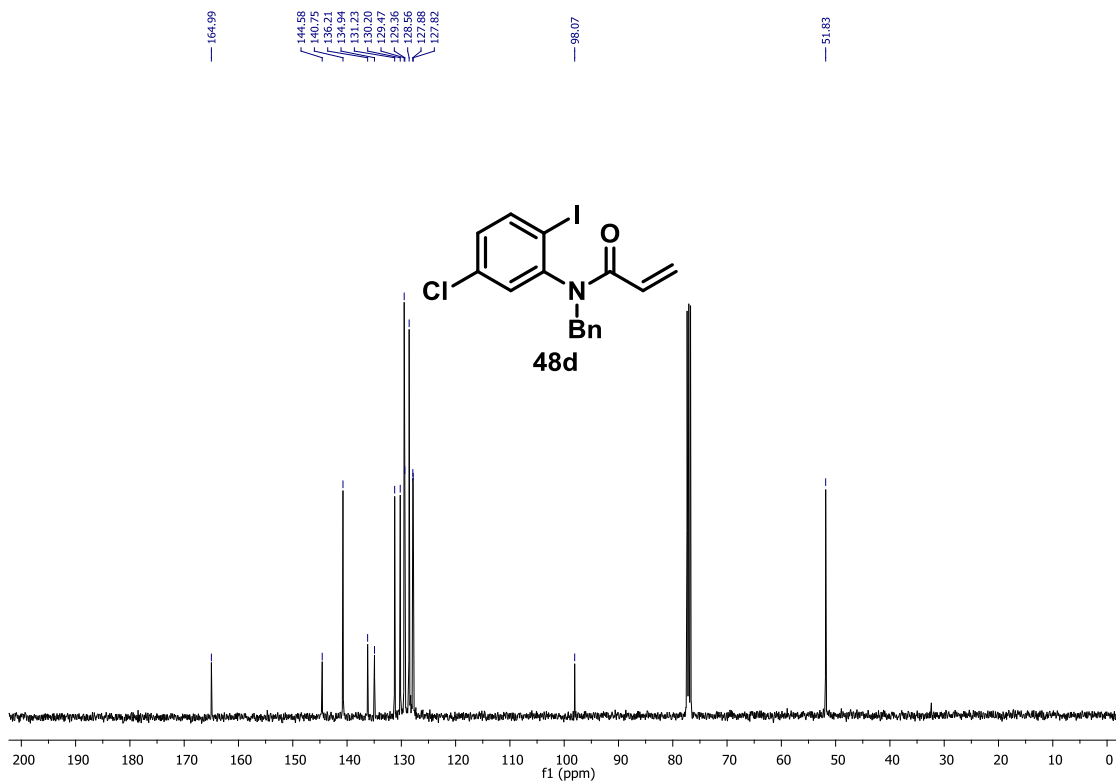


FIGURE 71: ¹³C NMR spectrum of 48d, 100 MHz, CDCl₃.

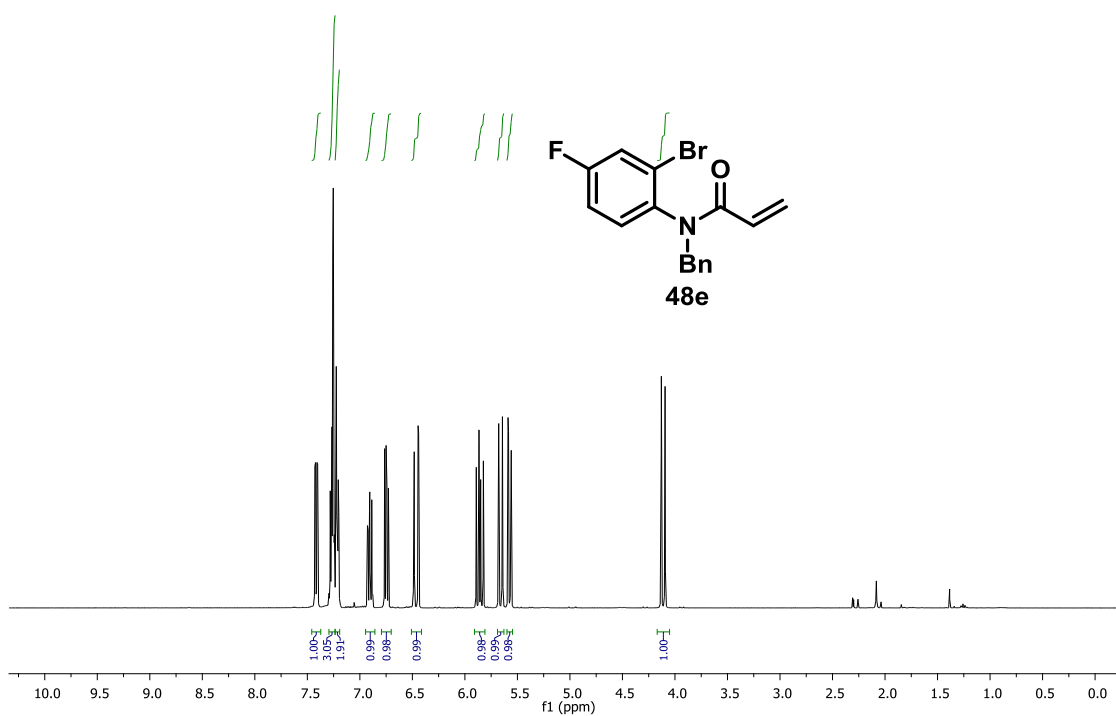


FIGURE 72: ¹H NMR spectrum of 48e, 400 MHz, CDCl₃.

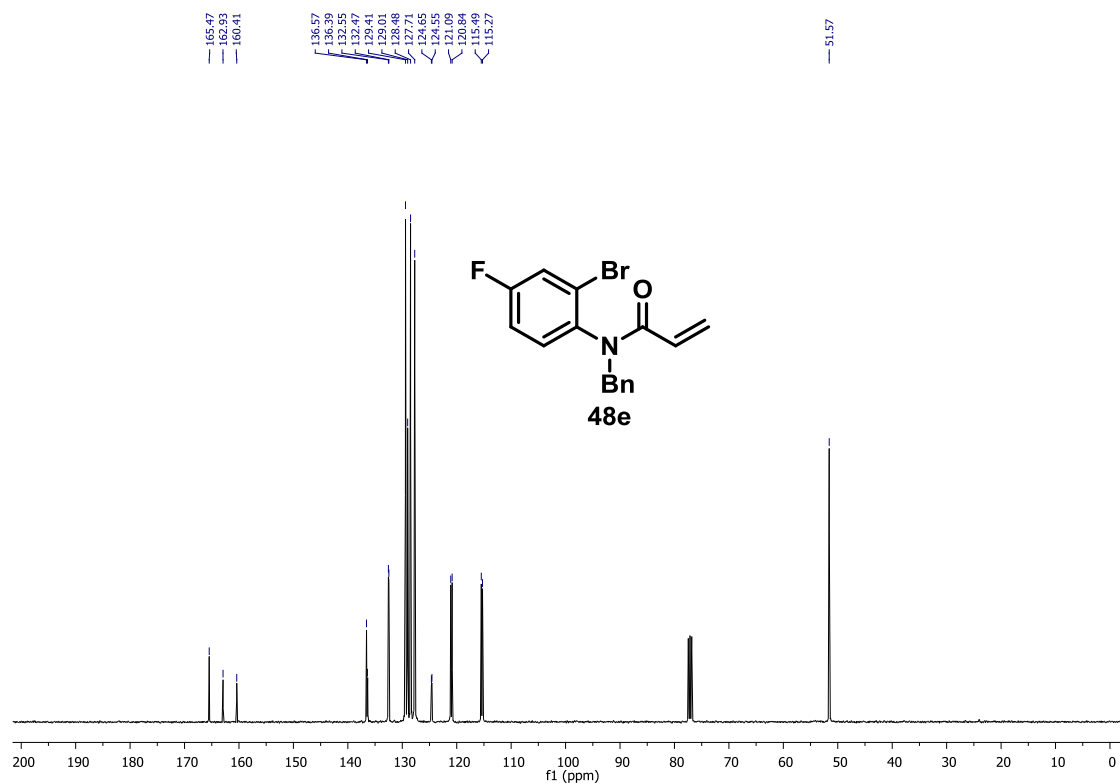


FIGURE 73: ¹³C NMR spectrum of 48e, 100 MHz, CDCl₃.

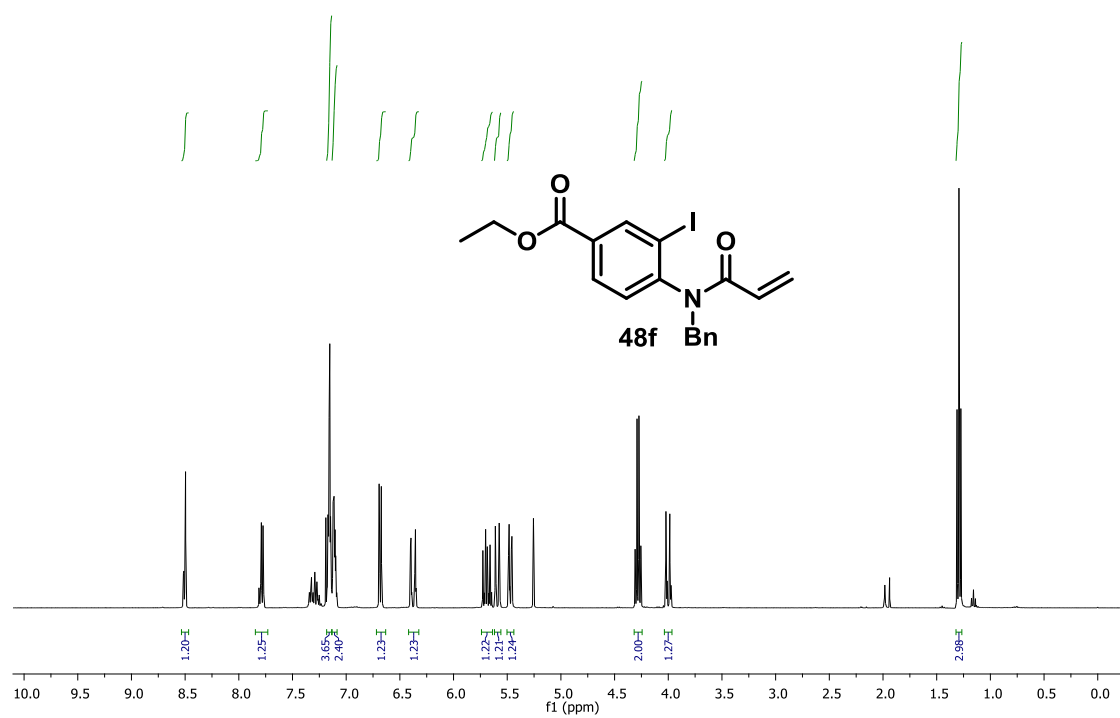


FIGURE 74: ¹H NMR spectrum of 48f, 400 MHz, CDCl₃.

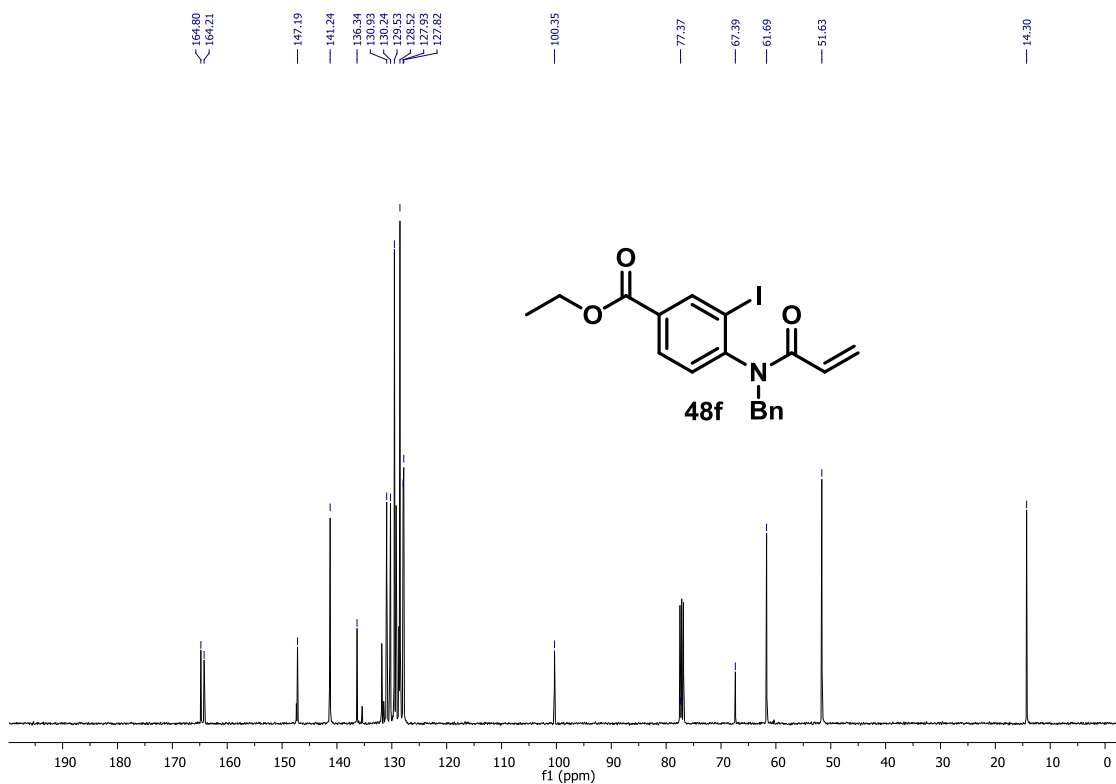


FIGURE 75: ¹³C NMR spectrum of 48f, 100 MHz, CDCl₃.

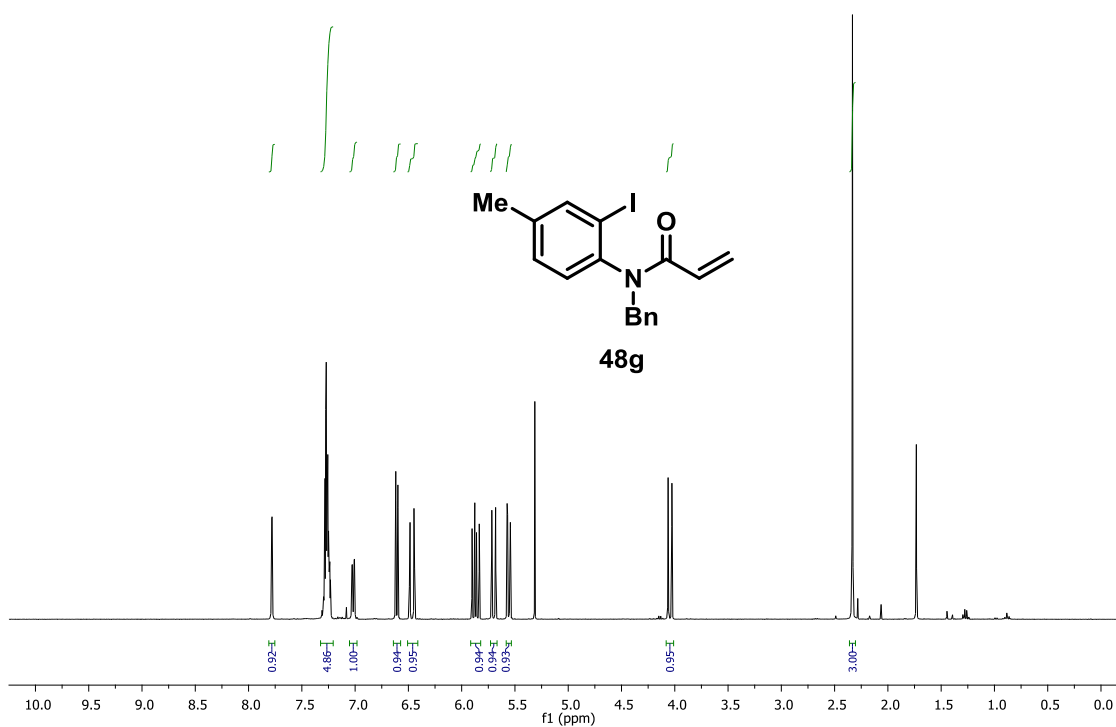


FIGURE 76: ¹H NMR spectrum of 48g, 400 MHz, CDCl₃.

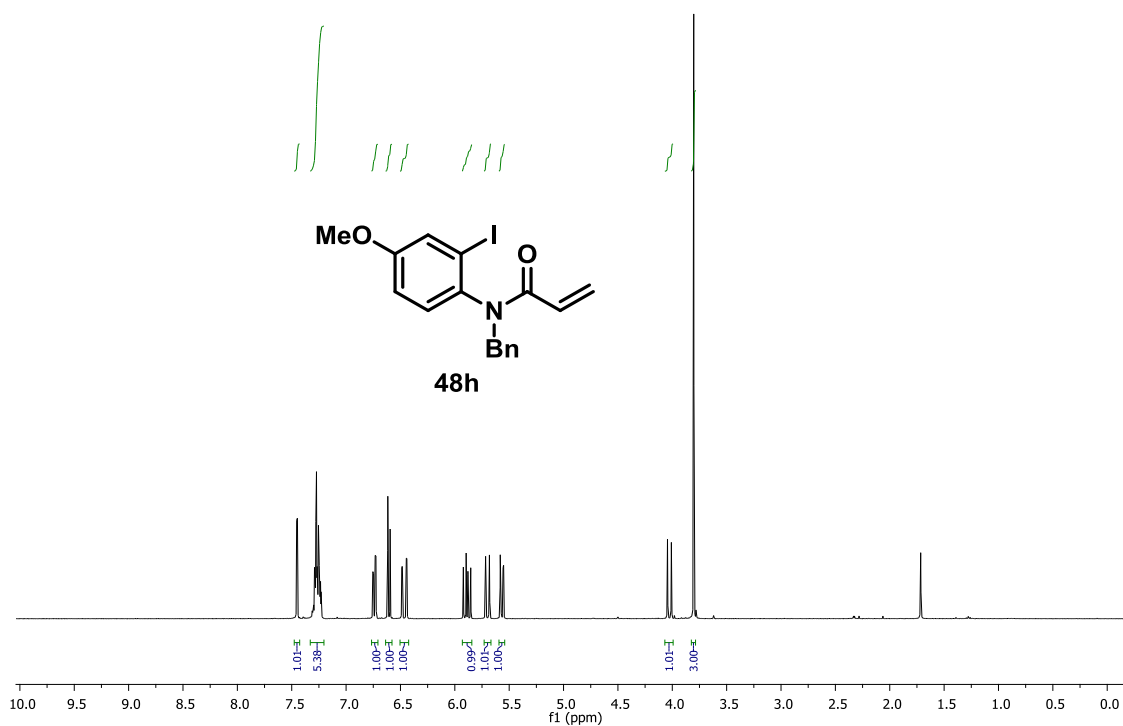


FIGURE 77: ^1H NMR spectrum of 48h, 400 MHz, CDCl_3 .

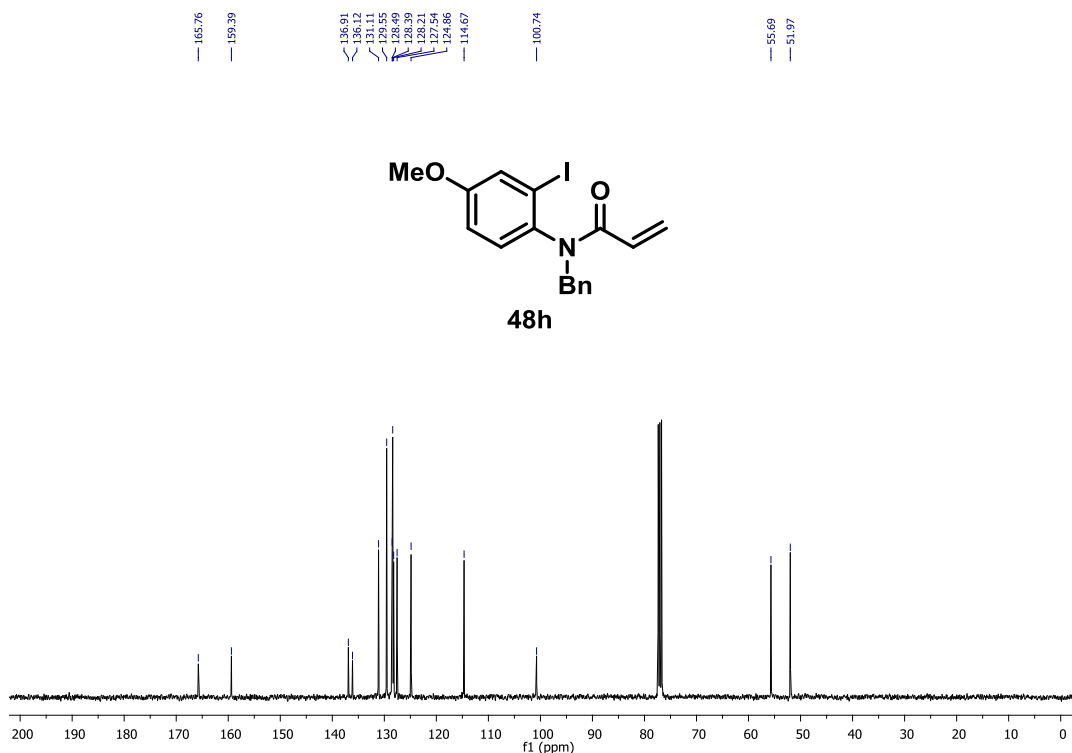


FIGURE 78: ^{13}C NMR spectrum of 48h, 100 MHz, CDCl_3

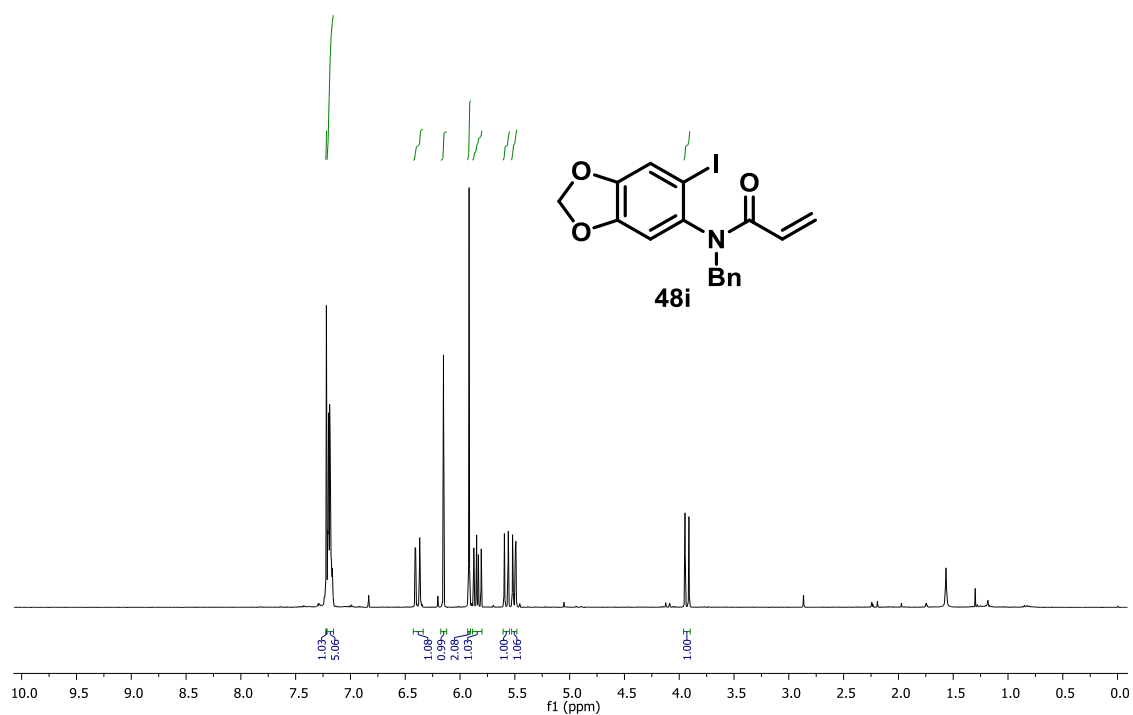


FIGURE 79: ^1H NMR spectrum of 48i, 400 MHz, CDCl_3

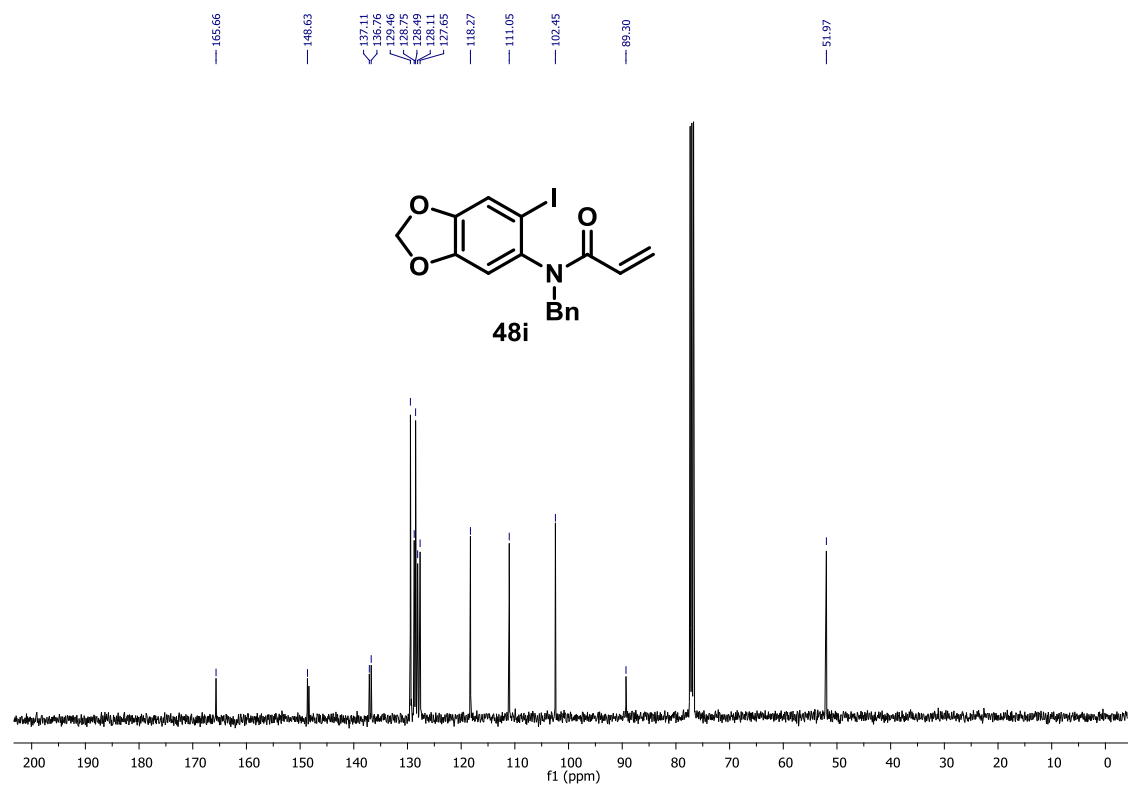


FIGURE 80: ^{13}C NMR spectrum of 48i, 100 MHz, CDCl_3

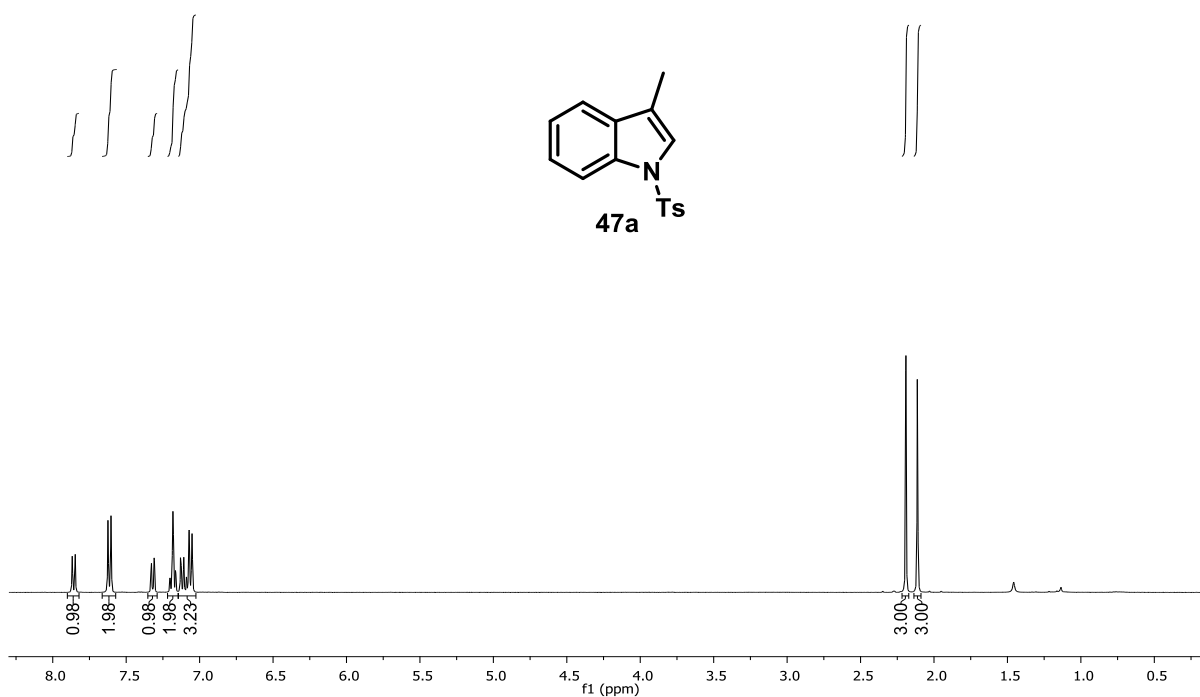


FIGURE 81: ¹H NMR spectrum of 47a, 400 MHz, CDCl₃.

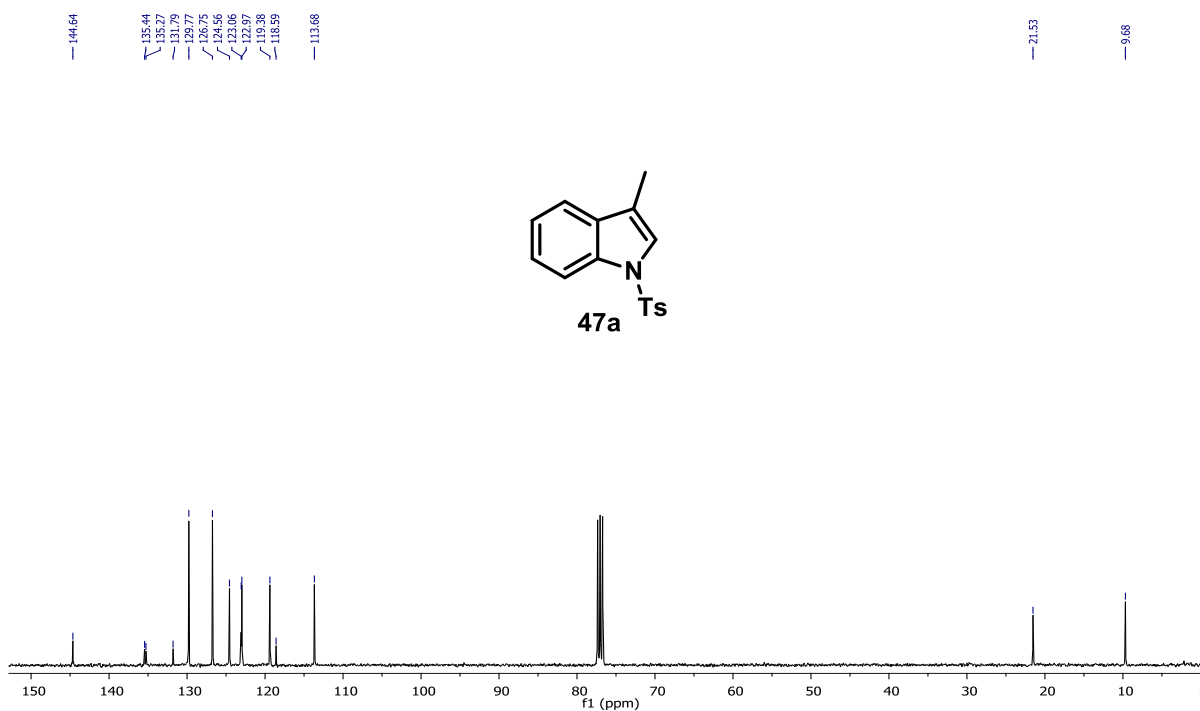


FIGURE 82: ¹³C NMR spectrum of 47a, 100 MHz, CDCl₃.

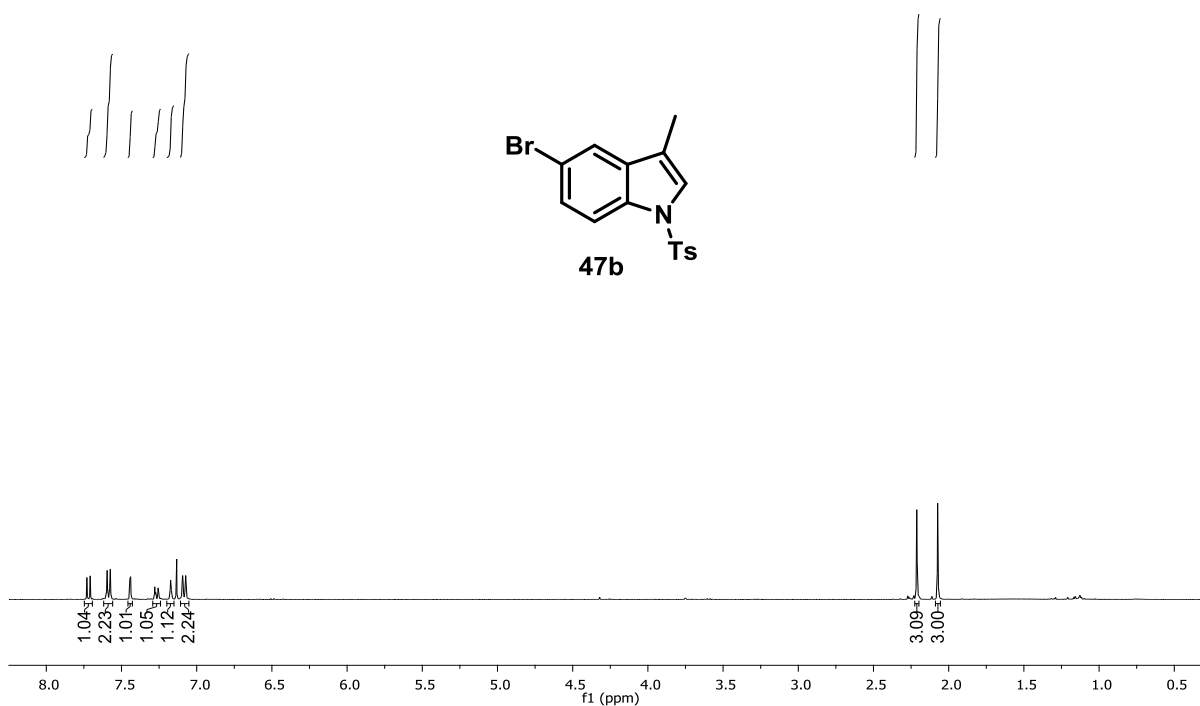


FIGURE 83: ¹H NMR spectrum of 47b, 400 MHz, CDCl₃.

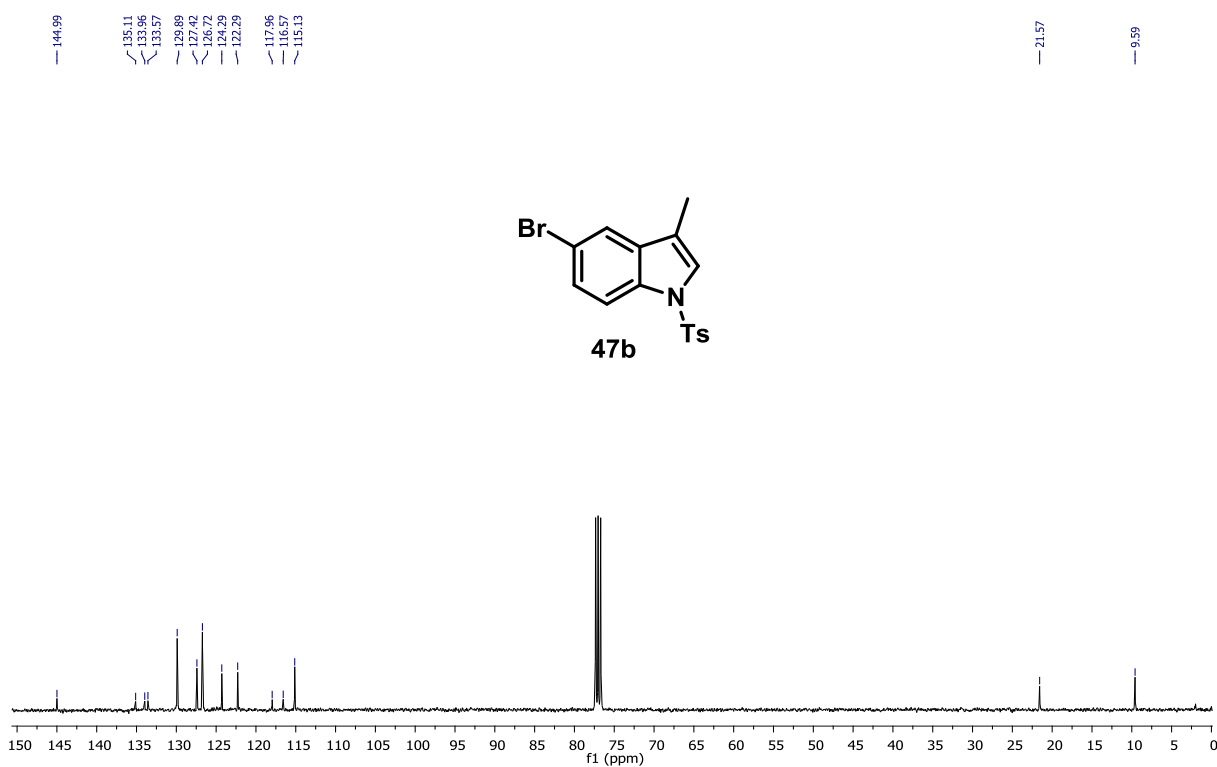


FIGURE 84: ¹³C NMR spectrum of 47b, 100 MHz, CDCl₃.

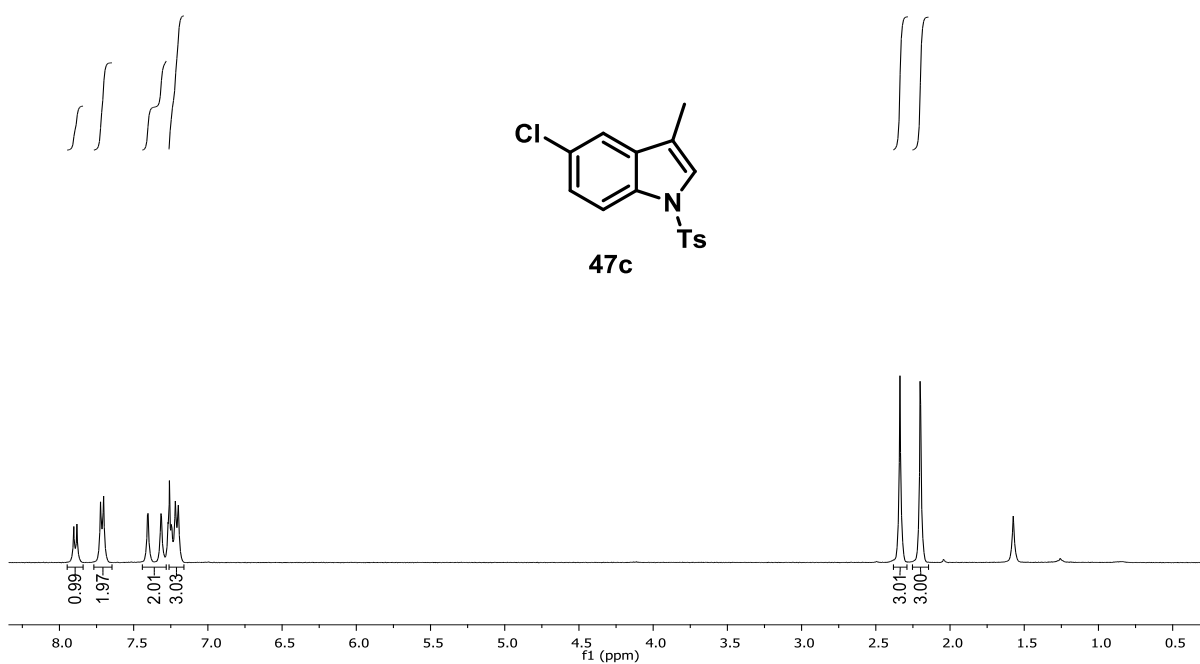


FIGURE 85: ¹H NMR spectrum of 47c, 400 MHz, CDCl₃.

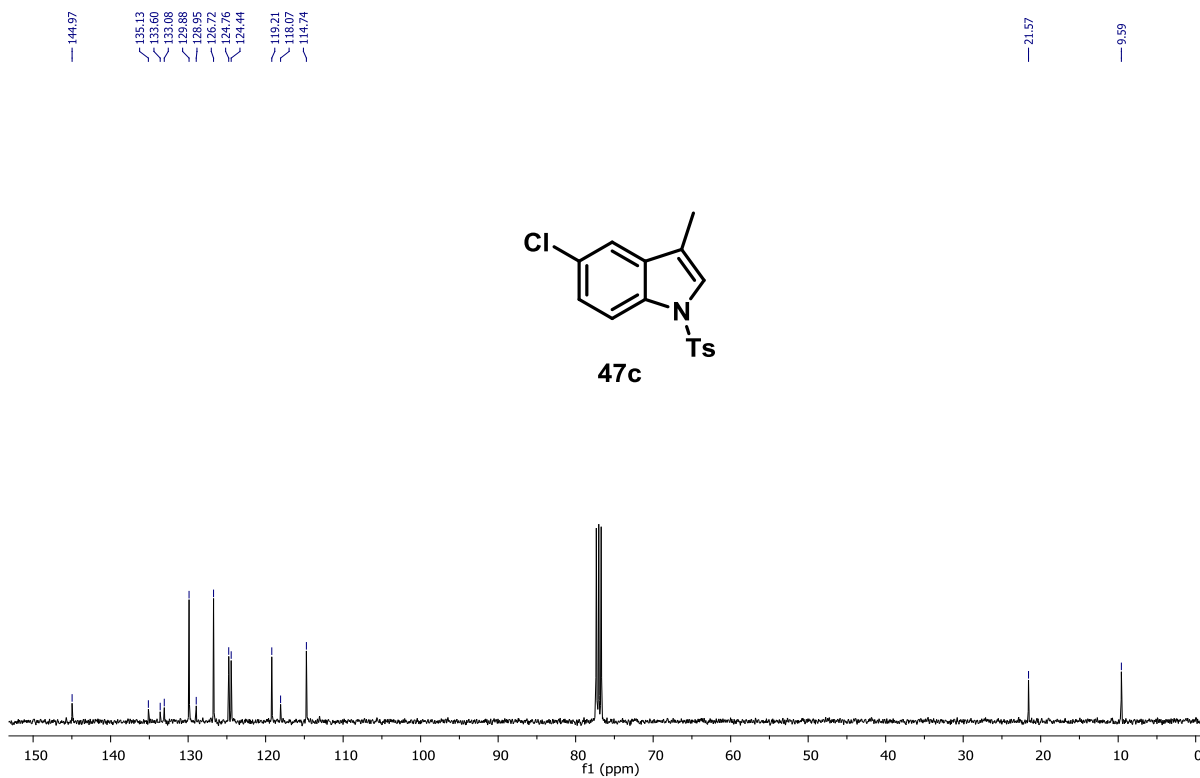


FIGURE 86: ¹³C NMR spectrum of 47c, 100 MHz, CDCl₃.

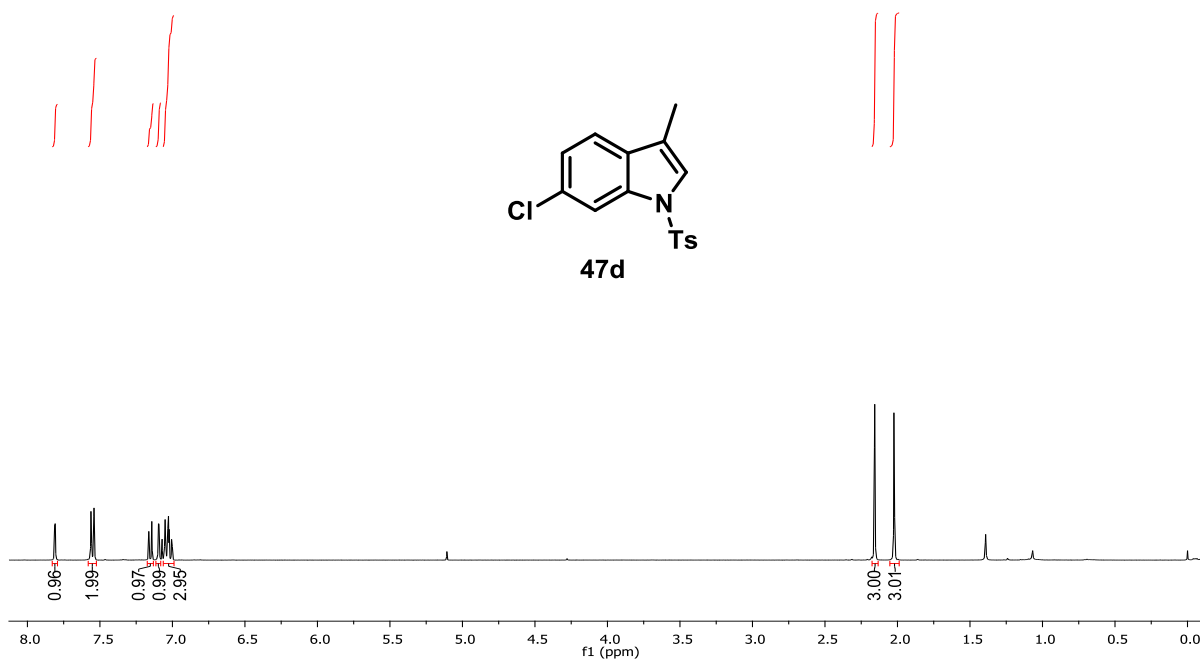


FIGURE 87: ¹H NMR spectrum of 47d, 400 MHz, CDCl₃.

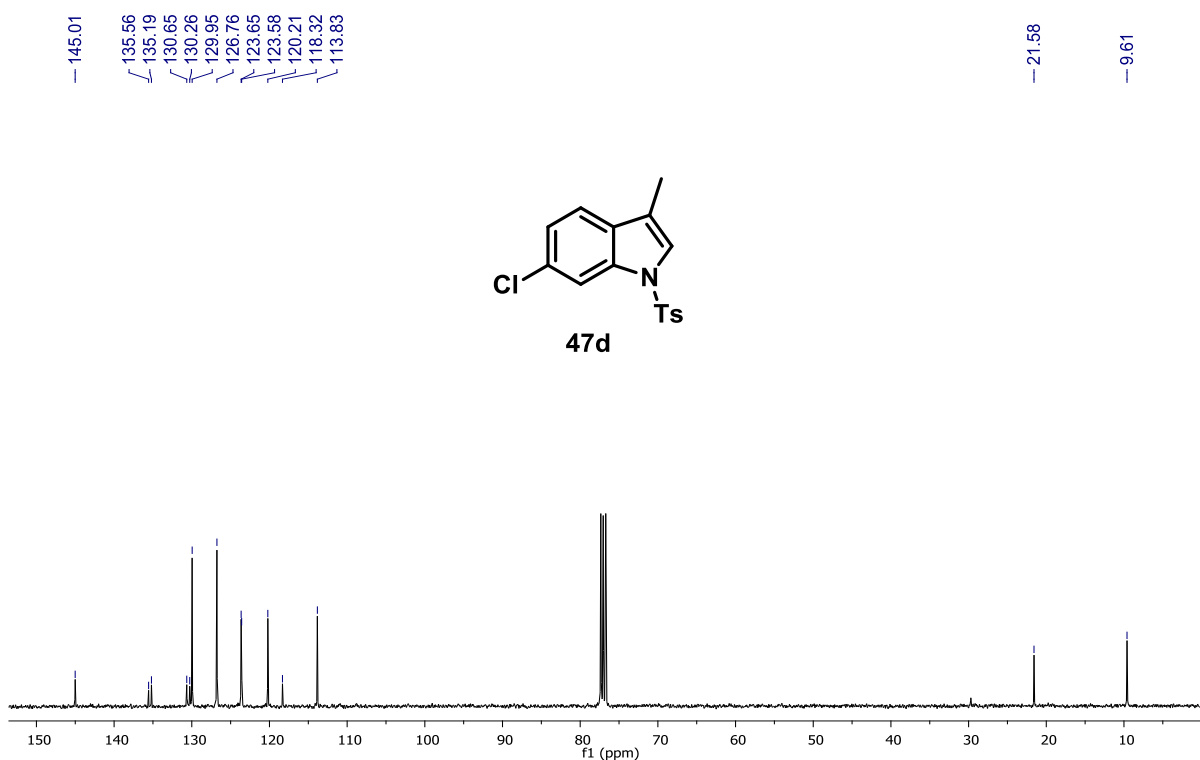


FIGURE 88: ¹³C NMR spectrum of 47d, 100 MHz, CDCl₃.

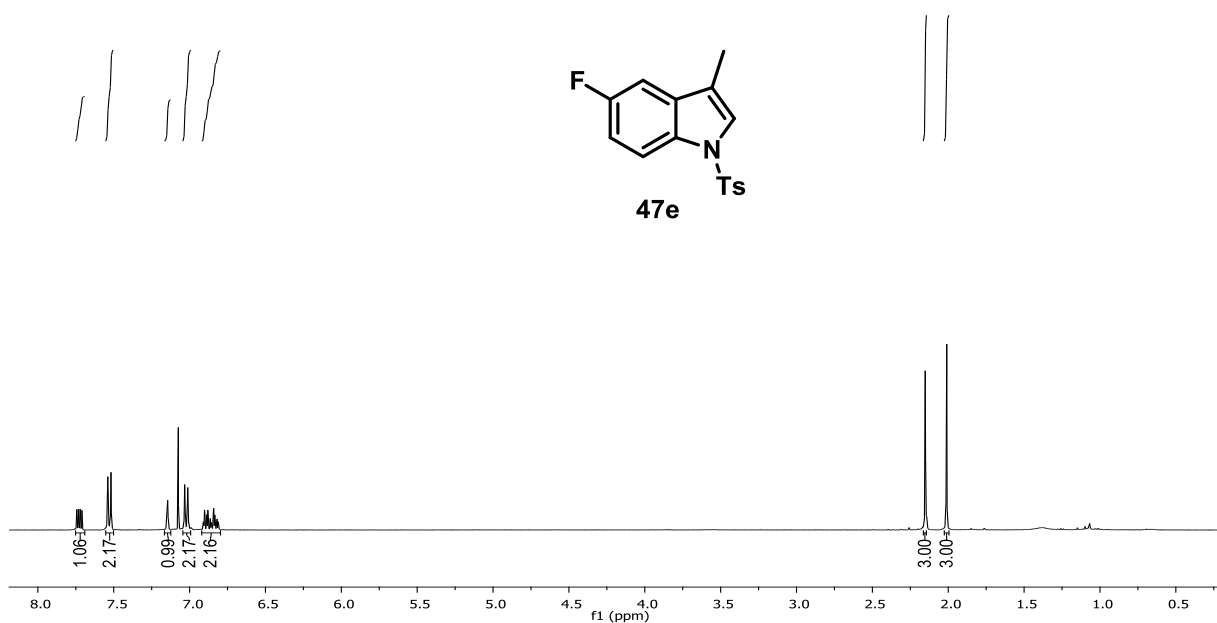


FIGURE 89: ¹H NMR spectrum of 47e, 400 MHz, CDCl₃.

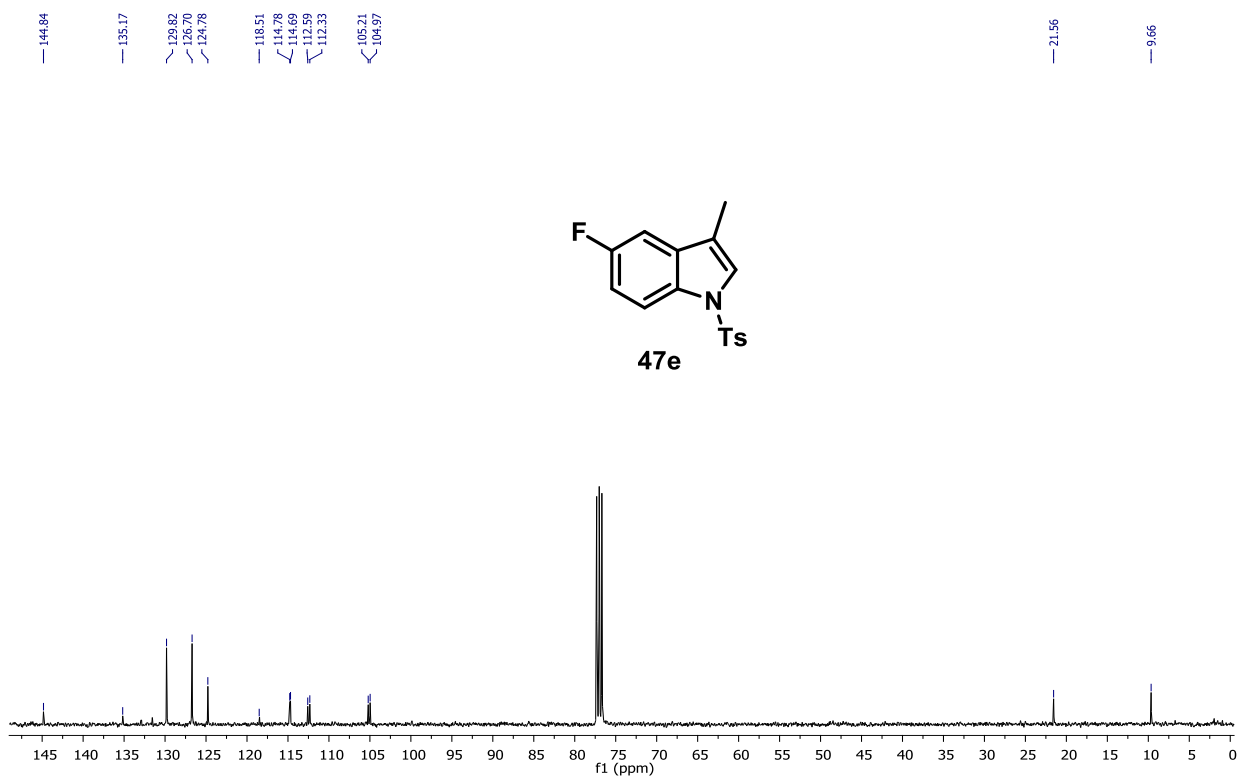


FIGURE 90: ¹³C NMR spectrum of 47e, 100 MHz, CDCl₃.

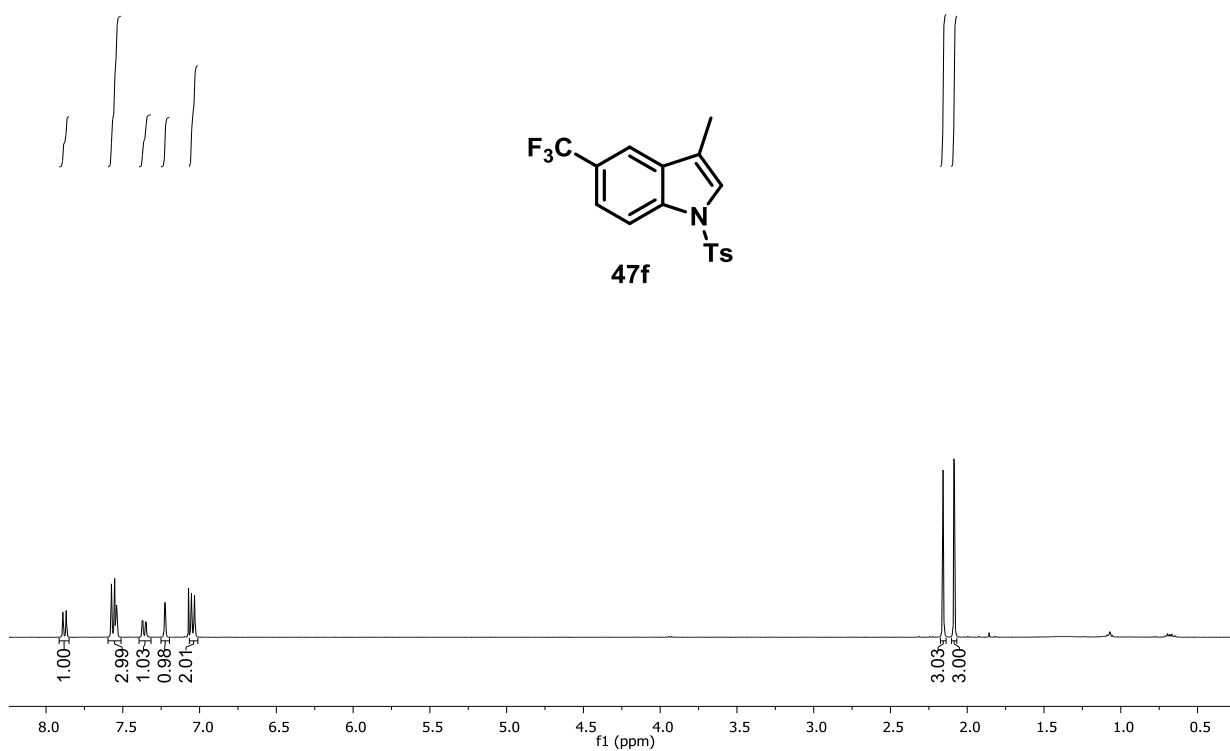


FIGURE 91: ¹H NMR spectrum of 47f, 400 MHz, CDCl₃.

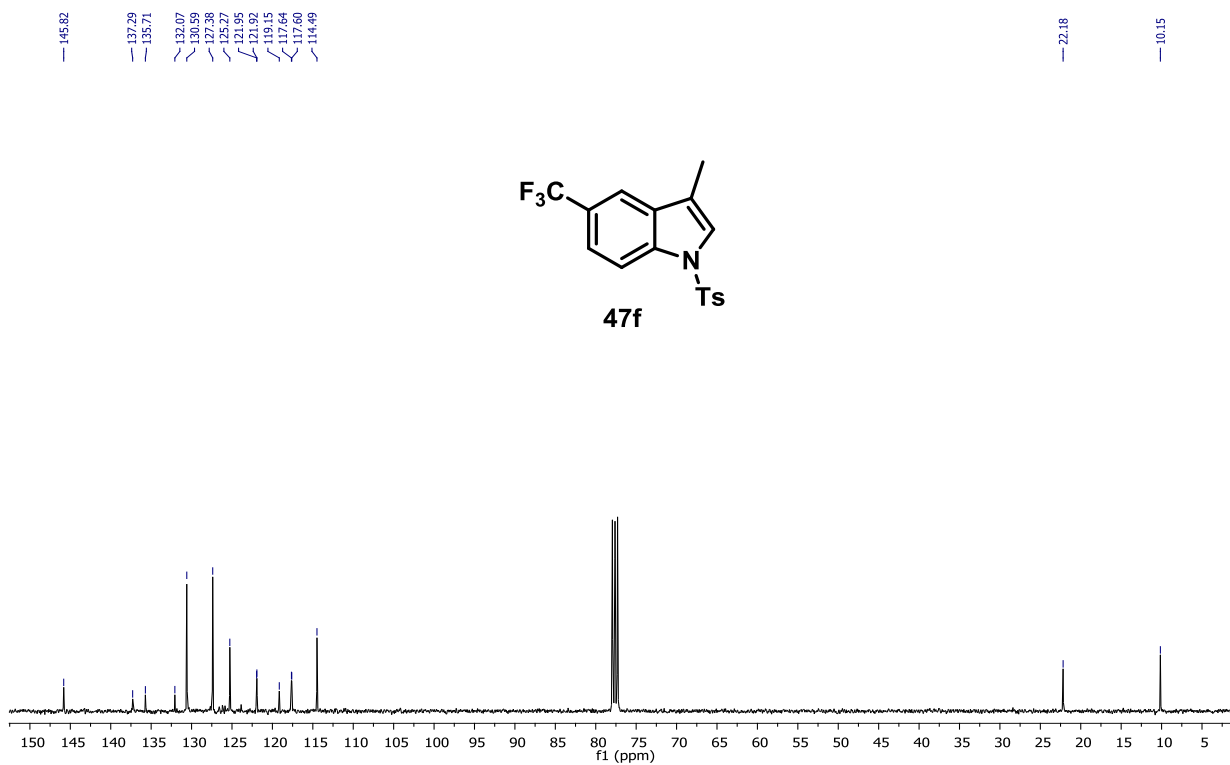


FIGURE 92: ¹³C NMR spectrum of 47f, 100 MHz, CDCl₃.

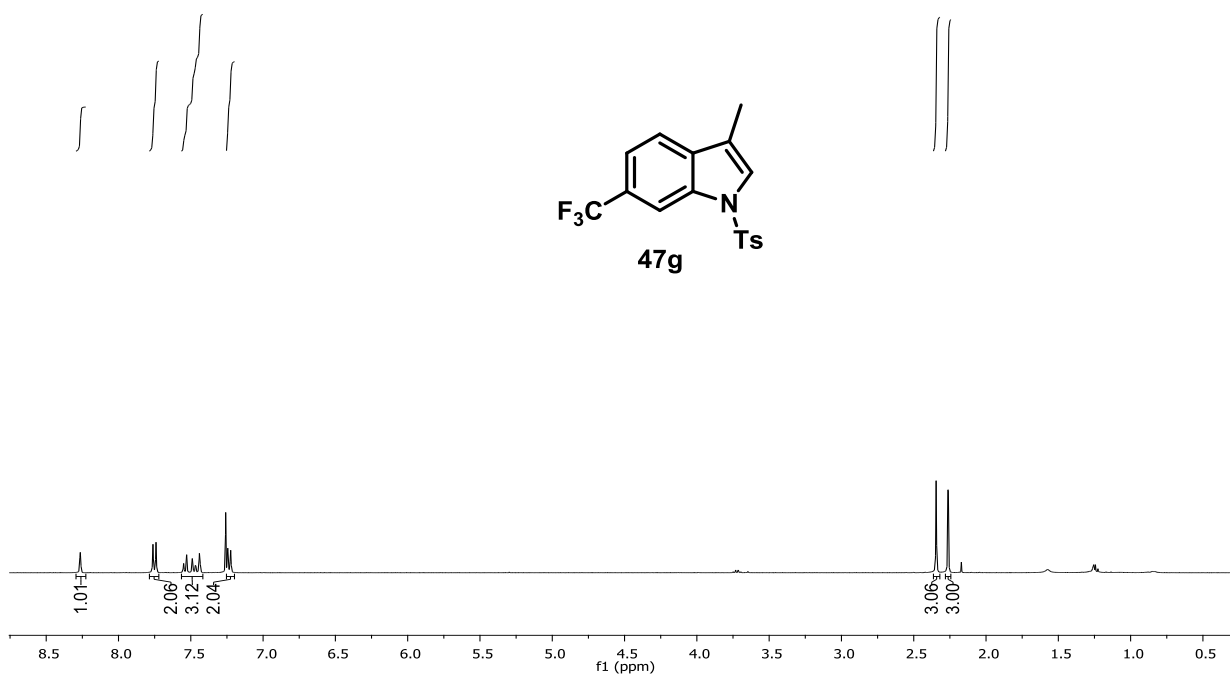


FIGURE 93: ¹H NMR spectrum of 47g, 400 MHz, CDCl₃.

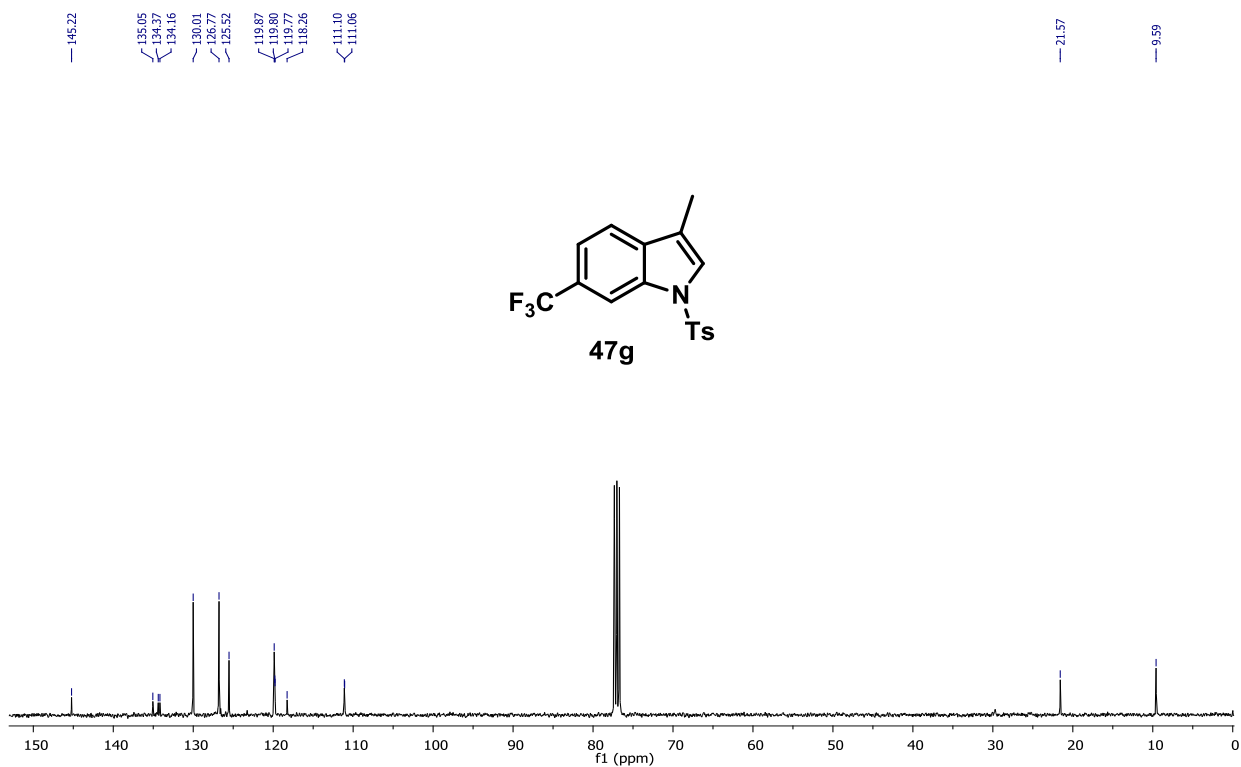


FIGURE 94: ¹³C NMR spectrum of 47g 100 MHz, CDCl₃.

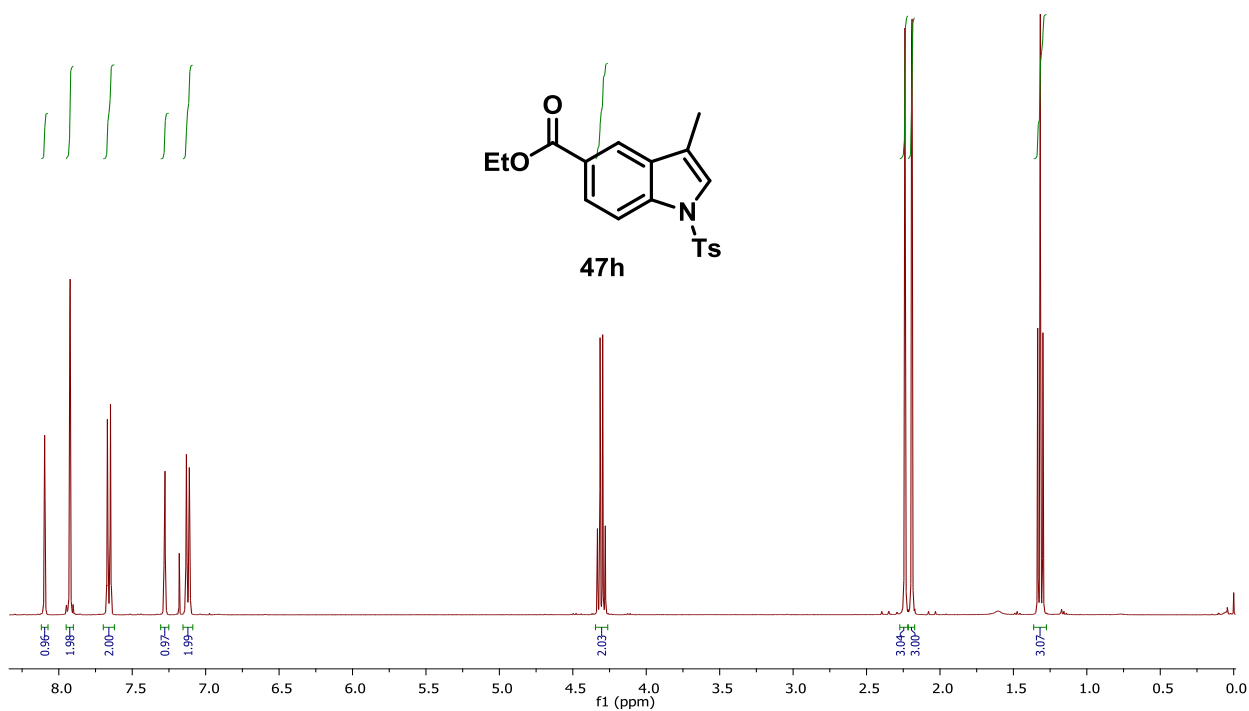


FIGURE 95: ¹H NMR spectrum of 47h, 400 MHz, CDCl₃.

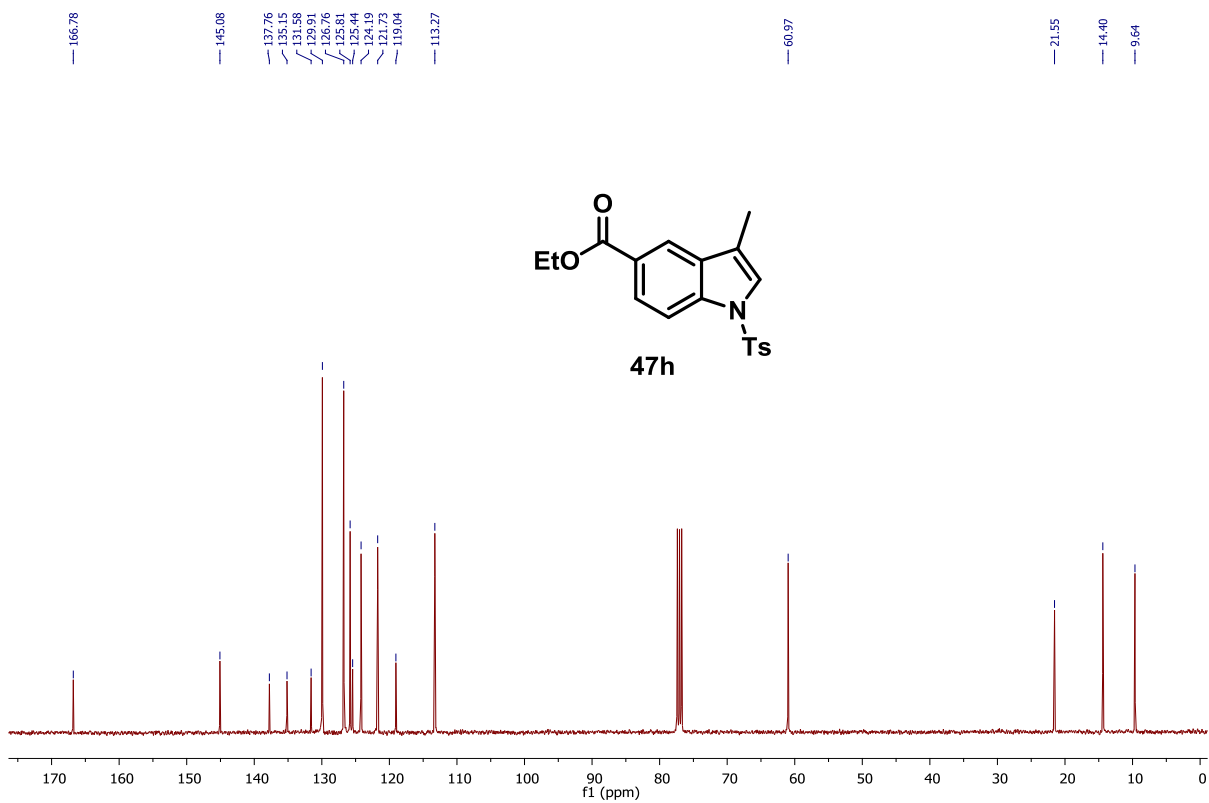


FIGURE 96: ¹³C NMR spectrum of 47h, 100 MHz, CDCl₃.

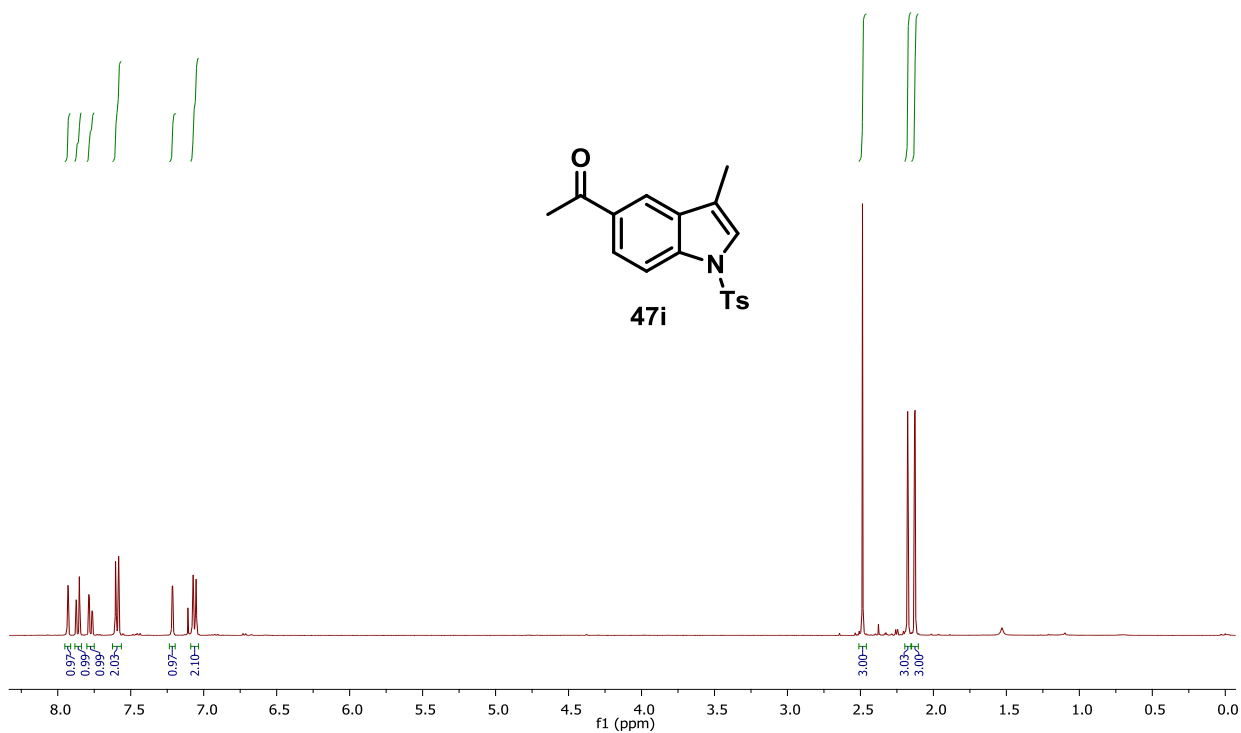


FIGURE 97: ¹H NMR spectrum of 47i, 400 MHz, CDCl₃.

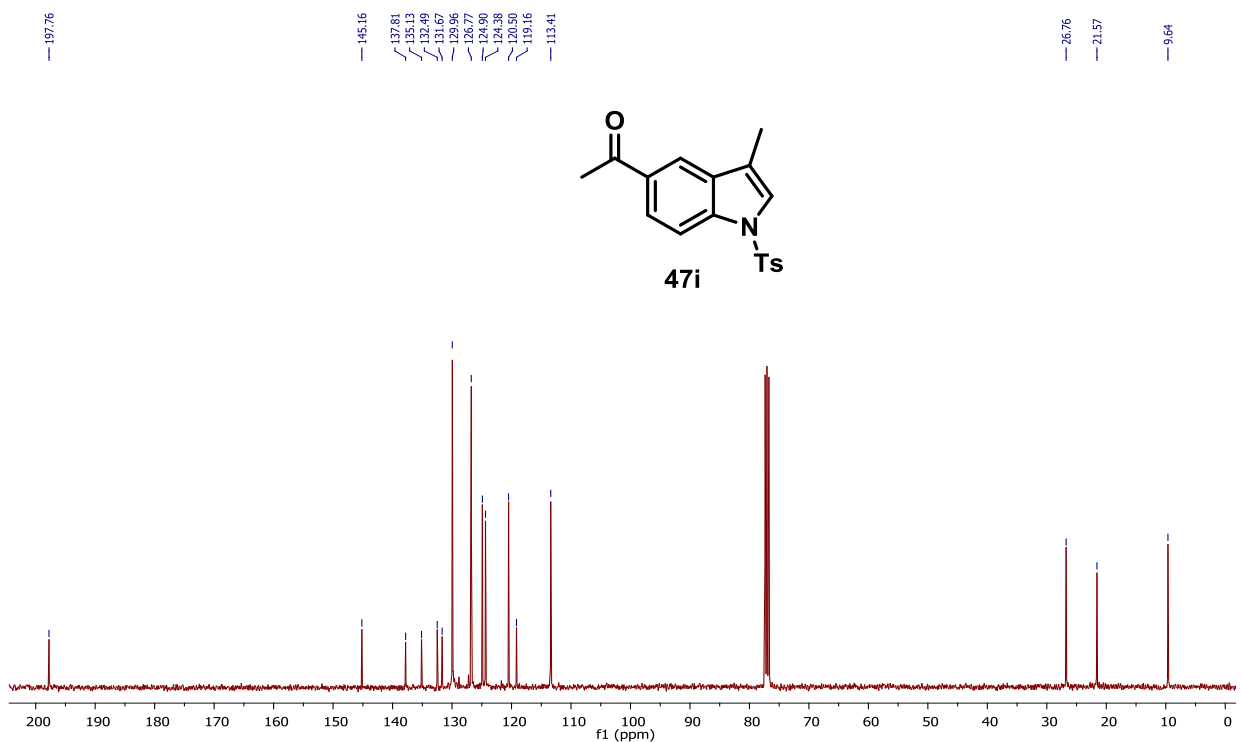


FIGURE 98: ¹³C NMR spectrum of 47i, 100 MHz, CDCl₃.

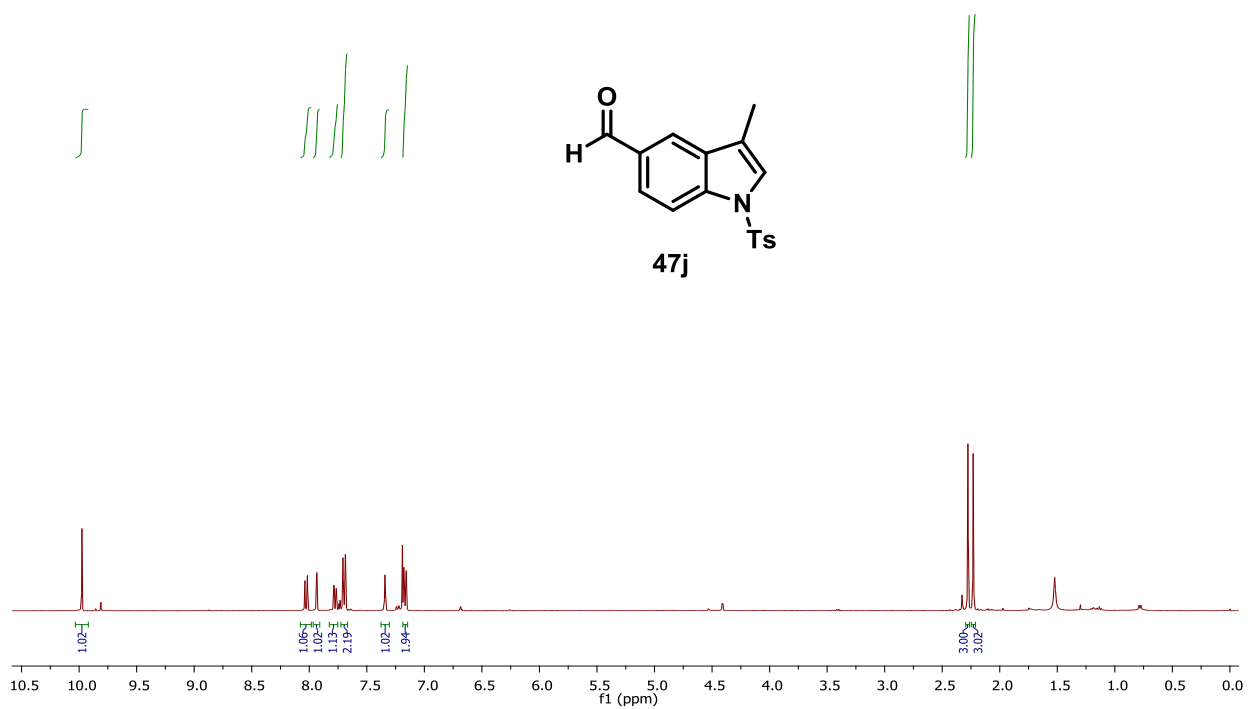


FIGURE 99: ¹H NMR spectrum of 47j, 400 MHz, CDCl₃.

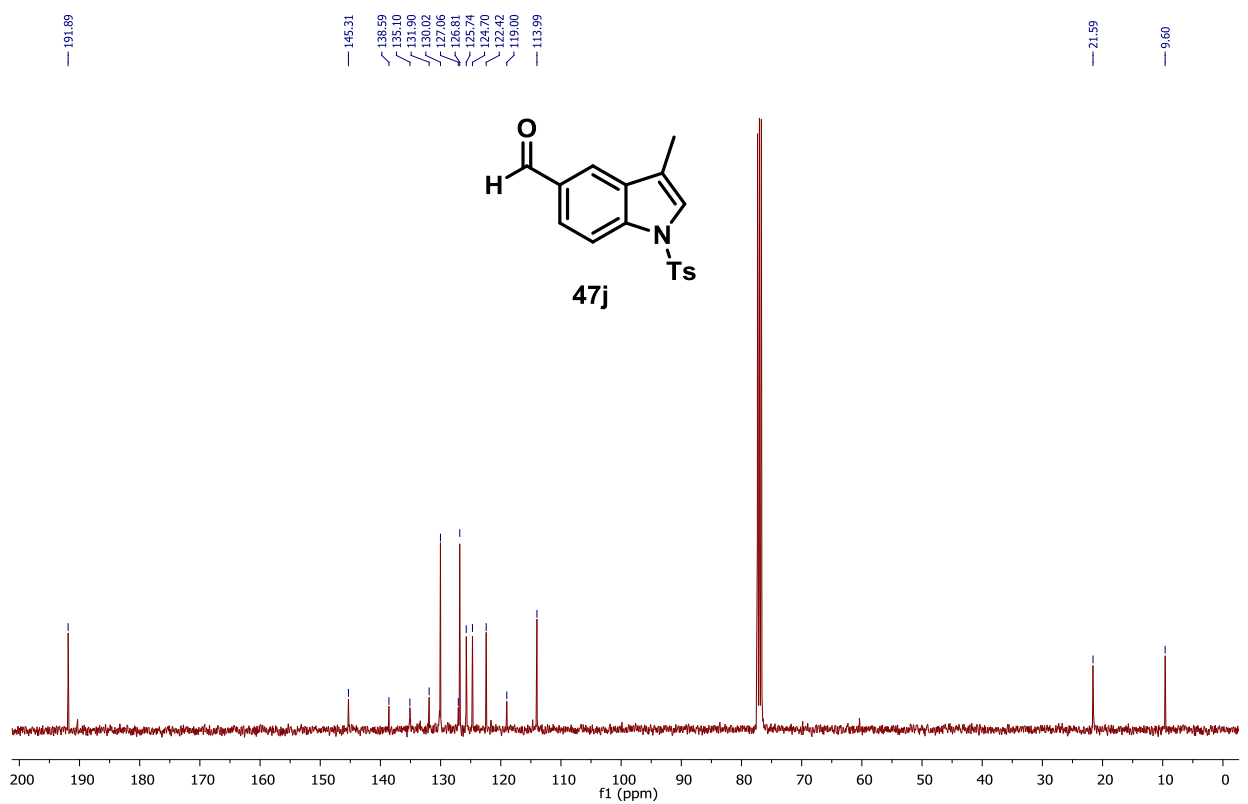


FIGURE 100: ¹³C NMR spectrum of 47j, 100 MHz, CDCl₃.

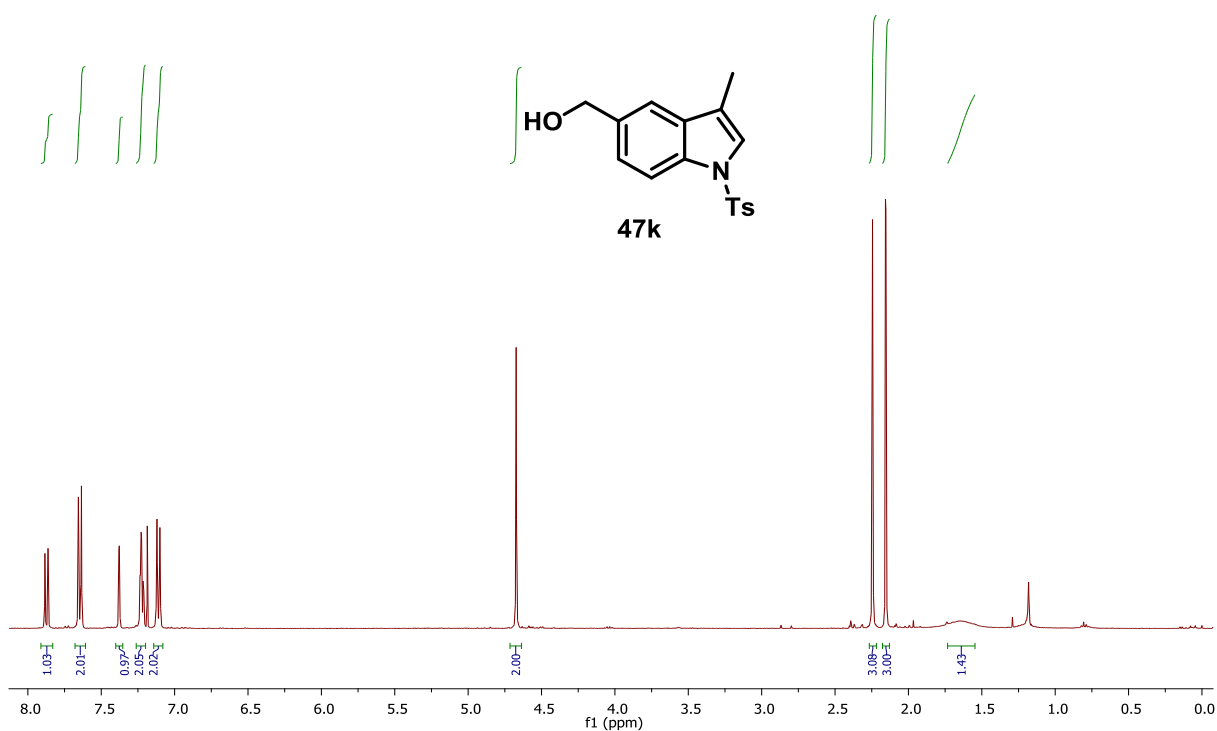


FIGURE 101: ^1H NMR spectrum of 47k, 400 MHz, CDCl_3 .

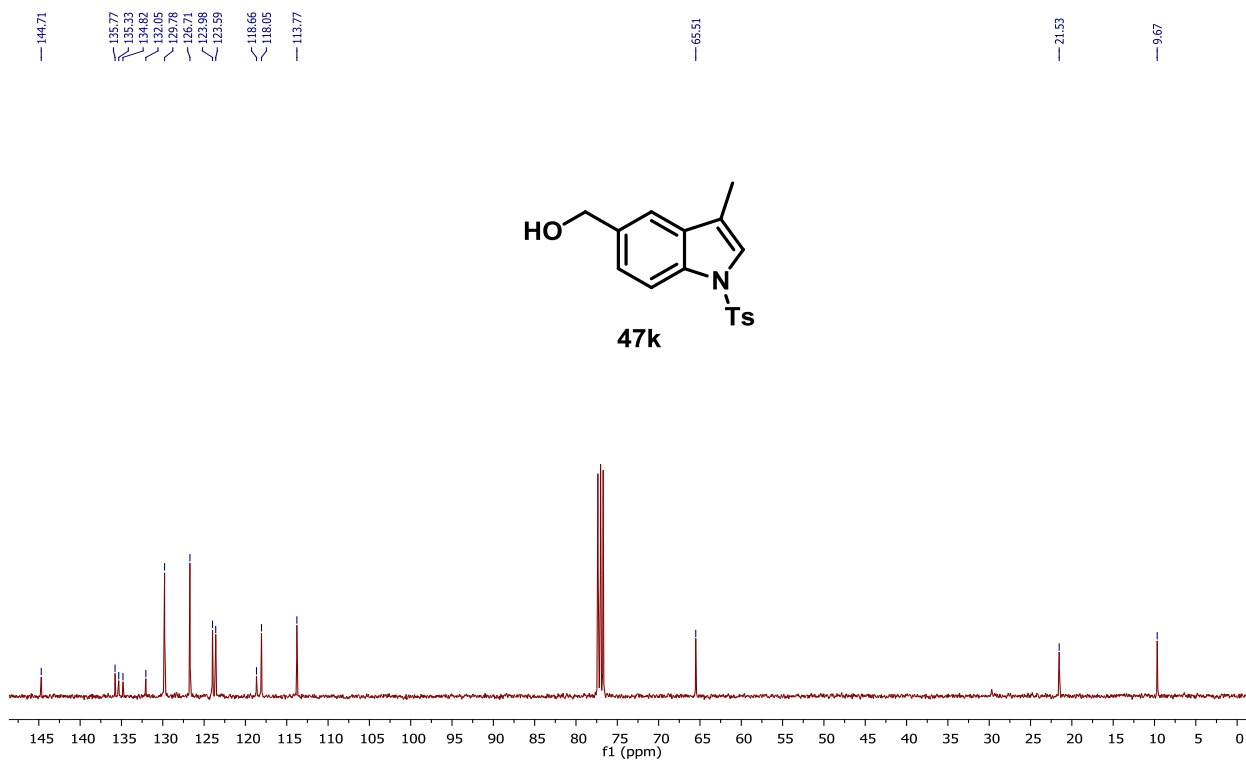


FIGURE 102: ^{13}C NMR spectrum of 47k, 100 MHz, CDCl_3 .

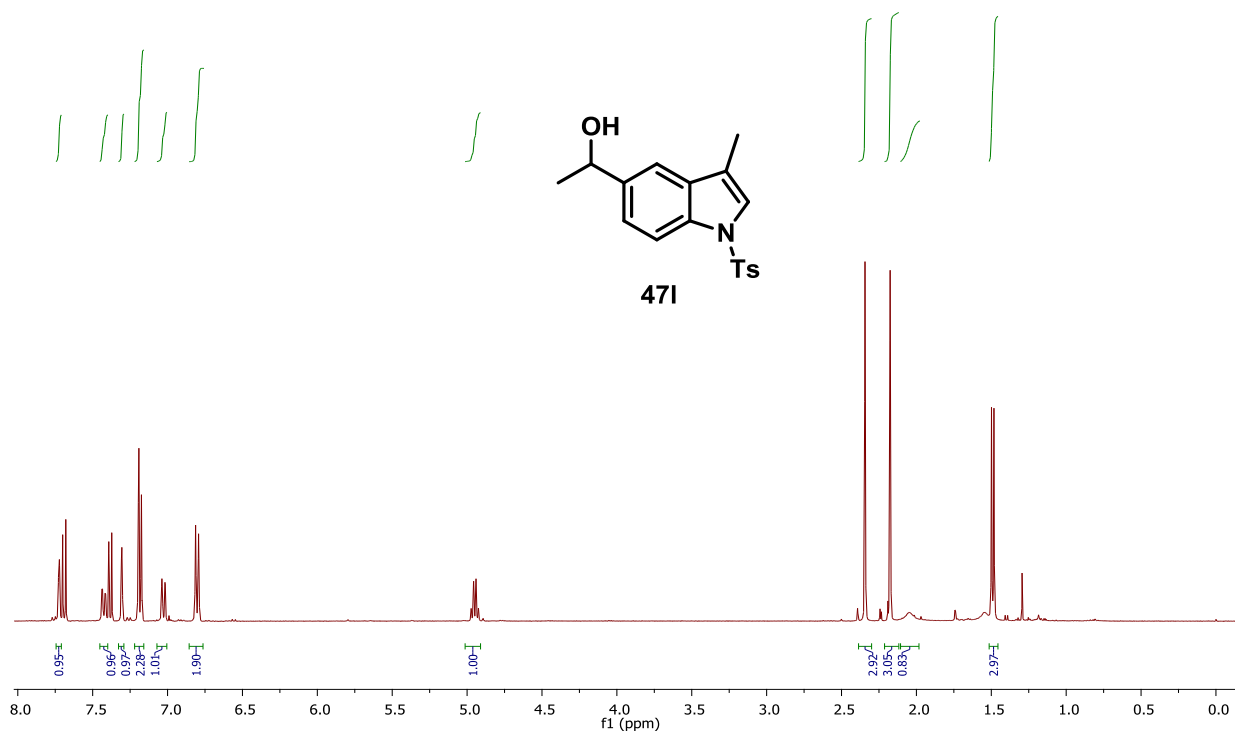


FIGURE 103: ^1H NMR spectrum of 47I, 400 MHz, CDCl_3 .

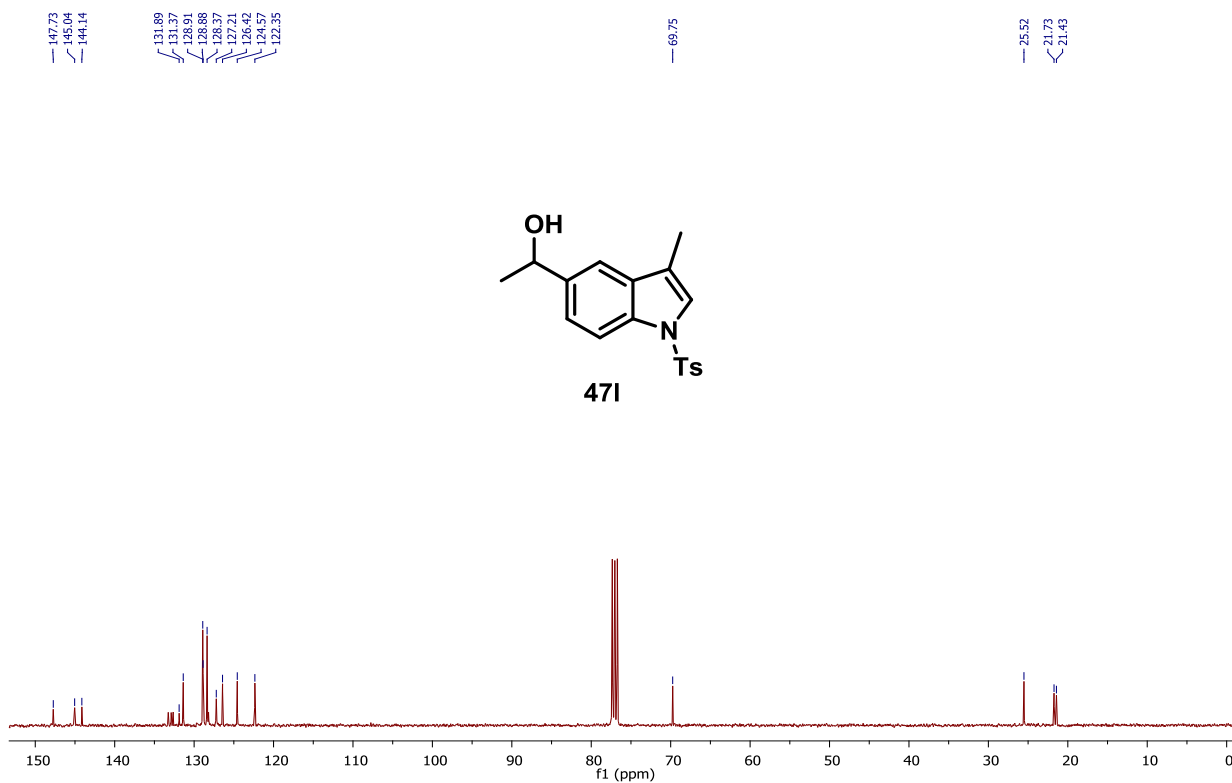


FIGURE 104: ^{13}C NMR spectrum of 47I, 100 MHz, CDCl_3 .

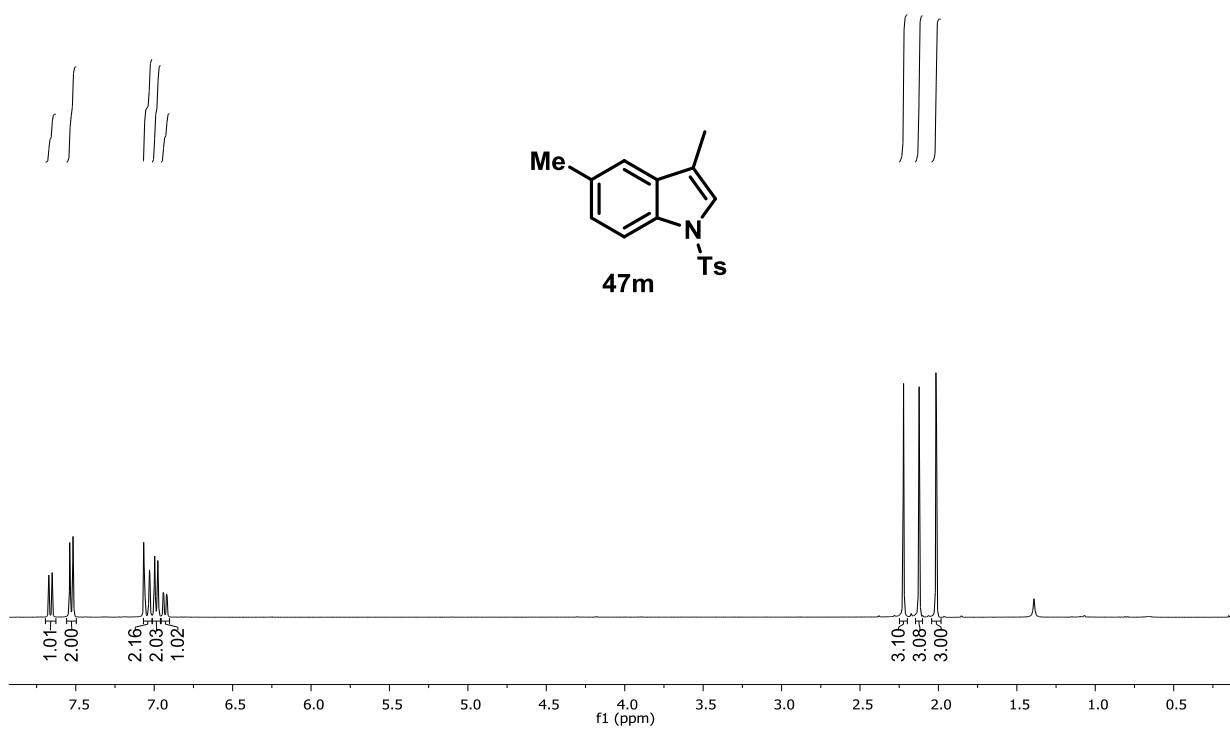


FIGURE 105: ¹H NMR spectrum of 47m, 400 MHz, CDCl₃.

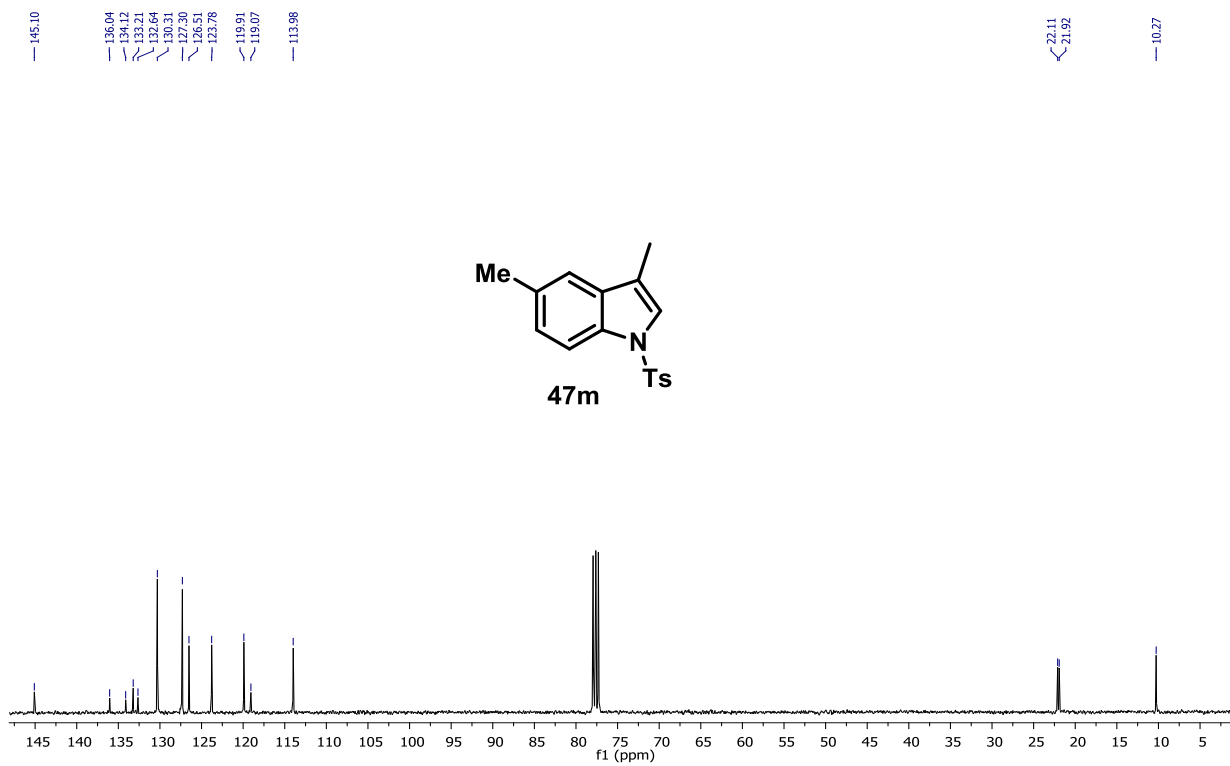


FIGURE 106: ¹³C NMR spectrum of 47m, 100 MHz, CDCl₃.

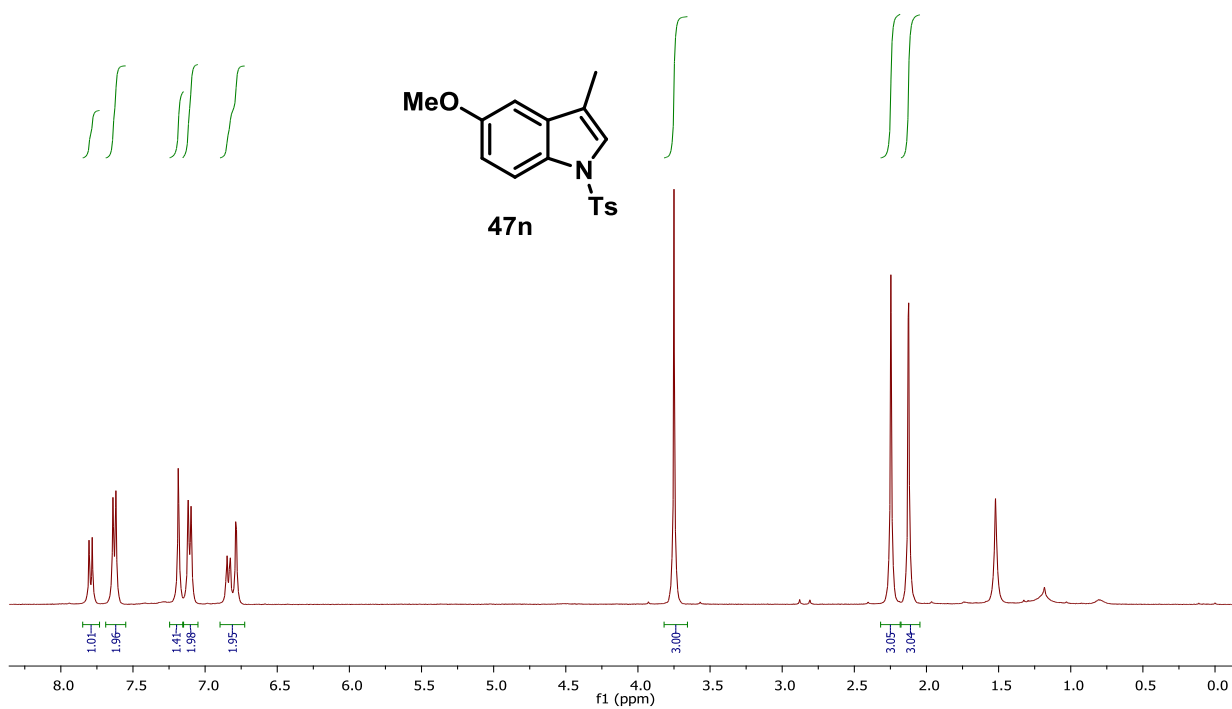


FIGURE 107: ¹H NMR spectrum of 47n, 400 MHz, CDCl₃.

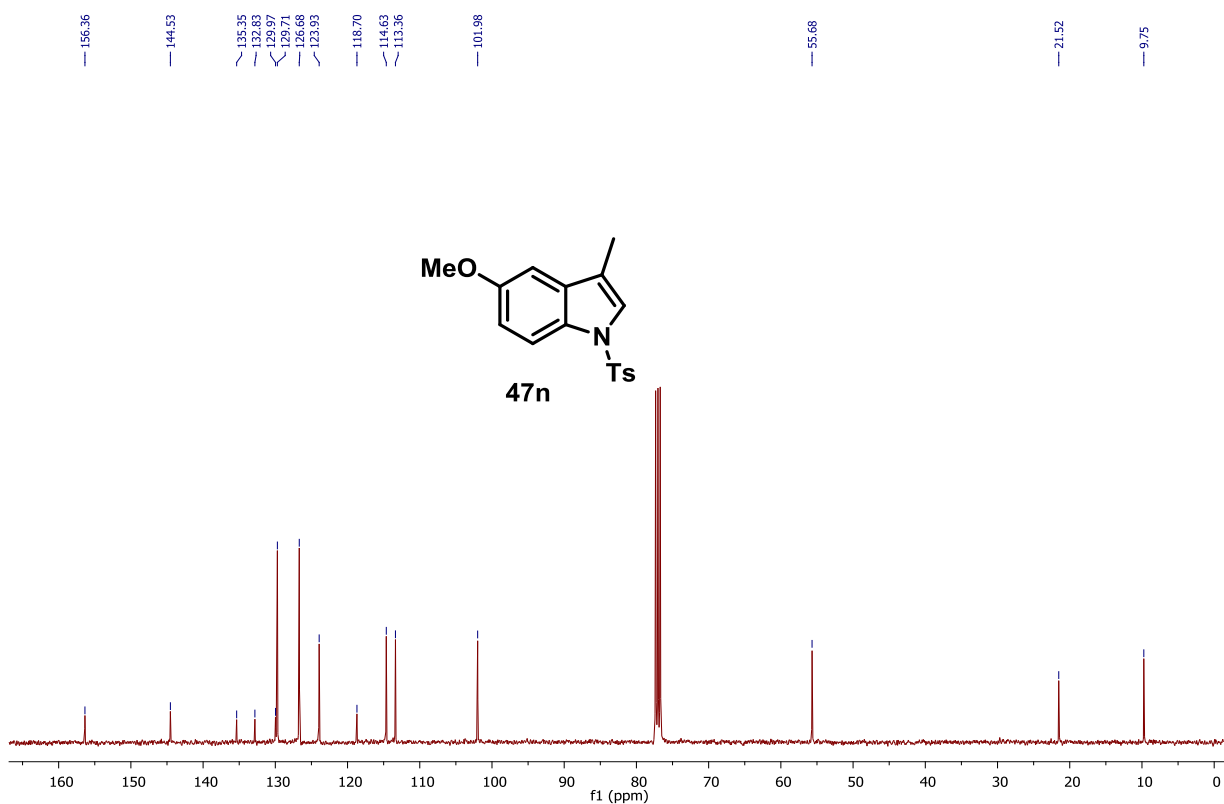


FIGURE 108: ¹³C NMR spectrum of 47n, 100 MHz, CDCl₃.

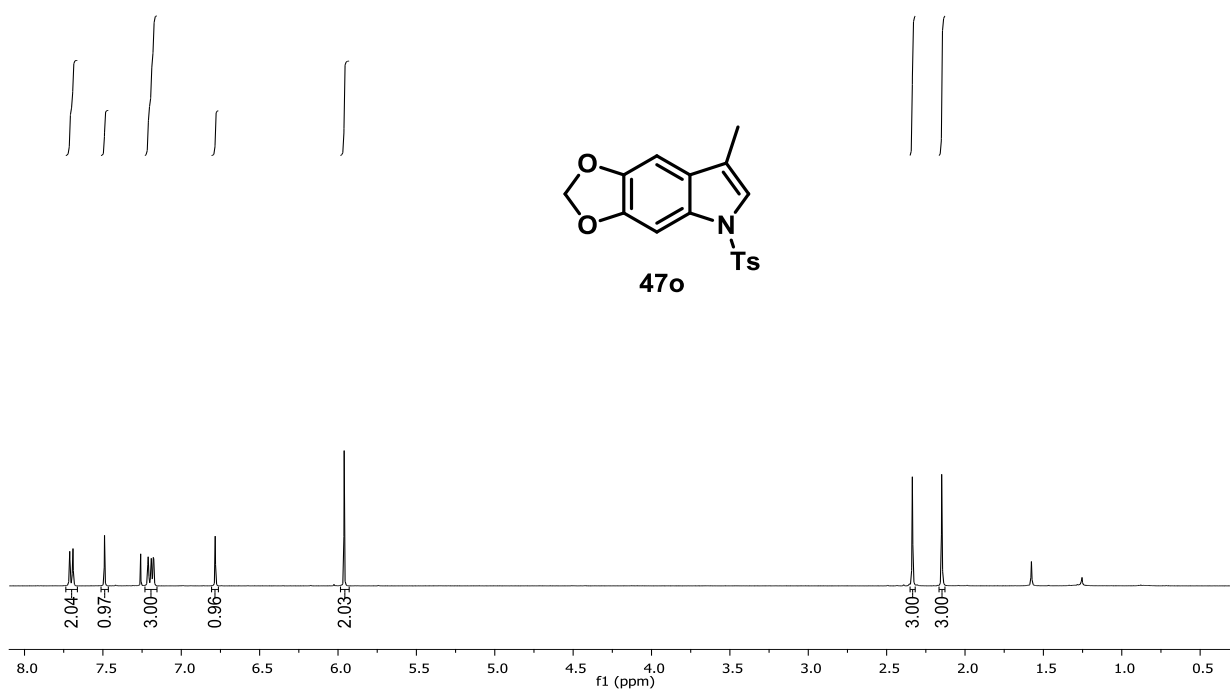


FIGURE 109: ¹H NMR spectrum of 47o, 400 MHz, CDCl₃.

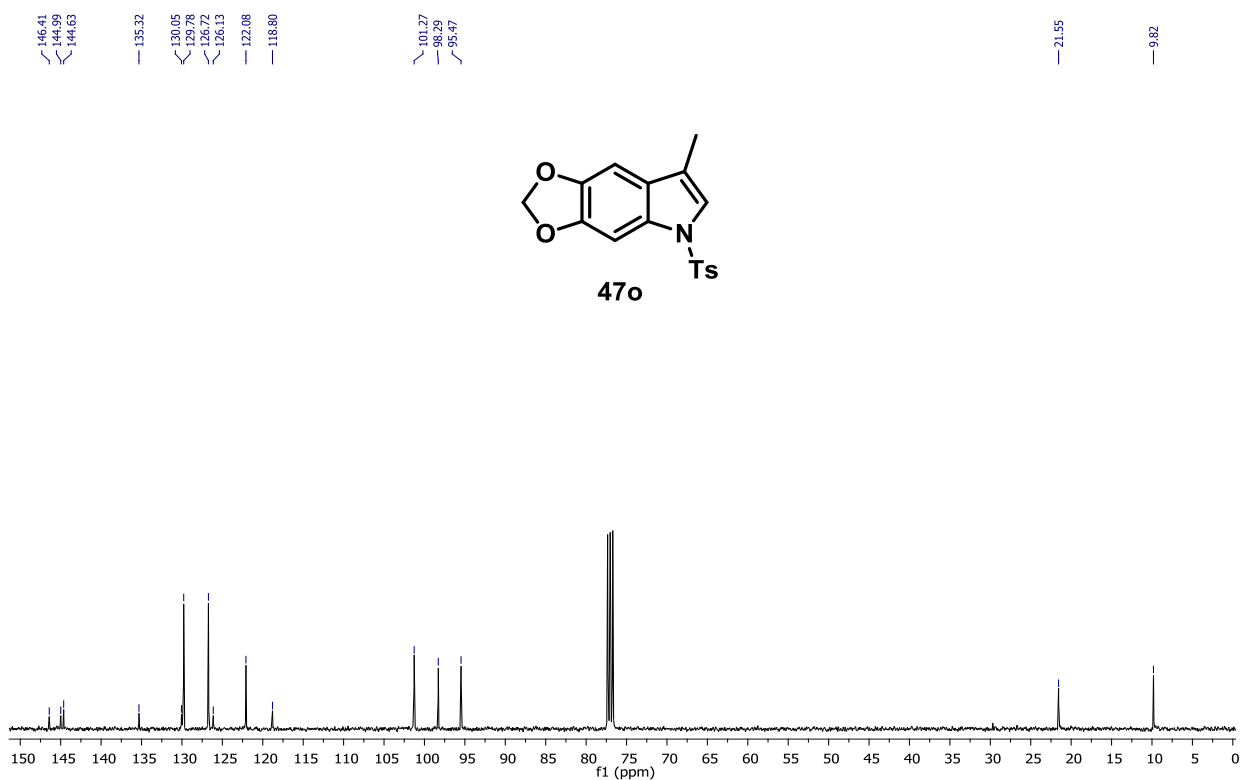


FIGURE 110: ¹³C NMR spectrum of 47o, 100 MHz, CDCl₃.

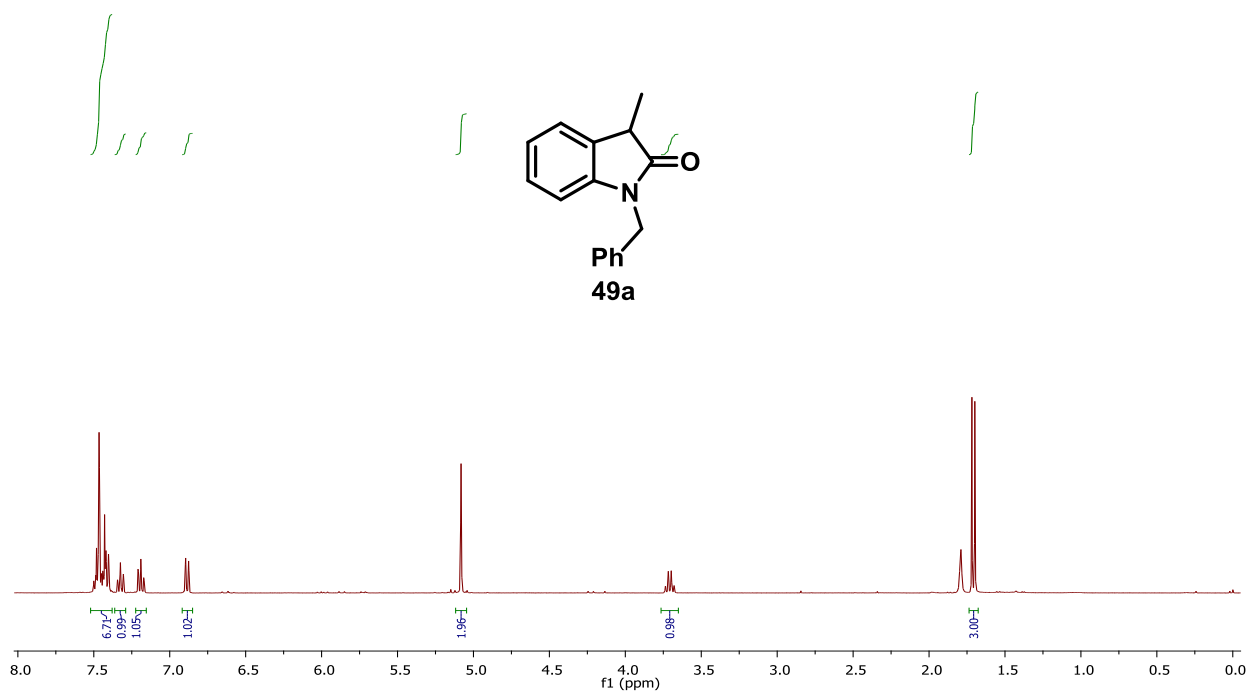


FIGURE 111: ¹H NMR spectrum of 49a, 400 MHz, CDCl₃.

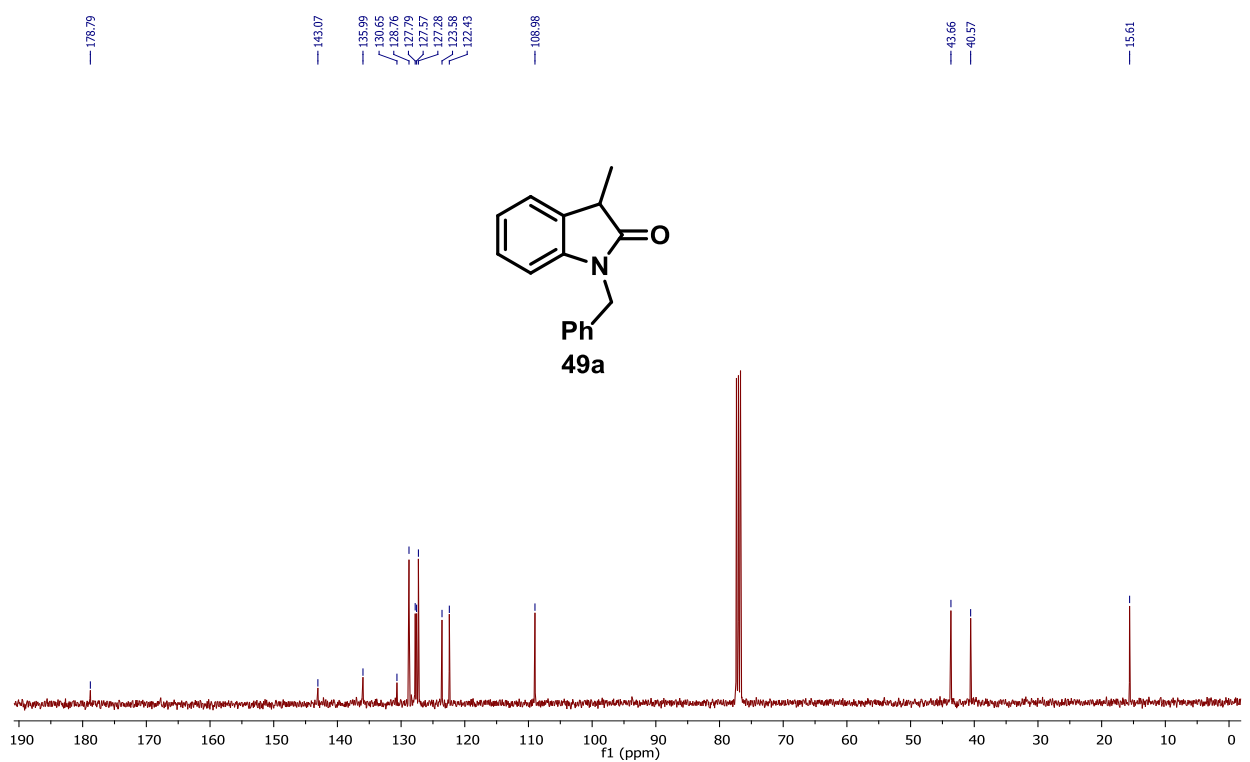


FIGURE 112: ¹³C NMR spectrum of 49a, 100 MHz, CDCl₃.

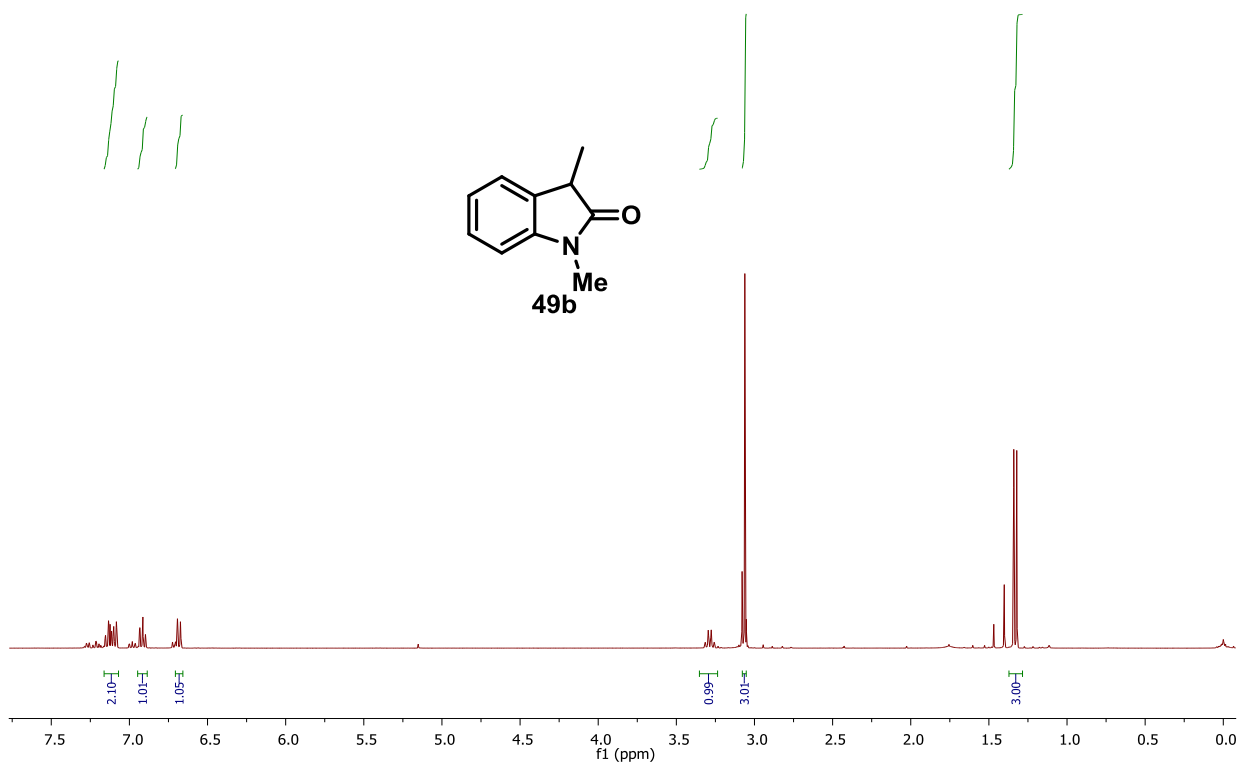


FIGURE 113: ^1H NMR spectrum of 49b, 400 MHz, CDCl_3 .

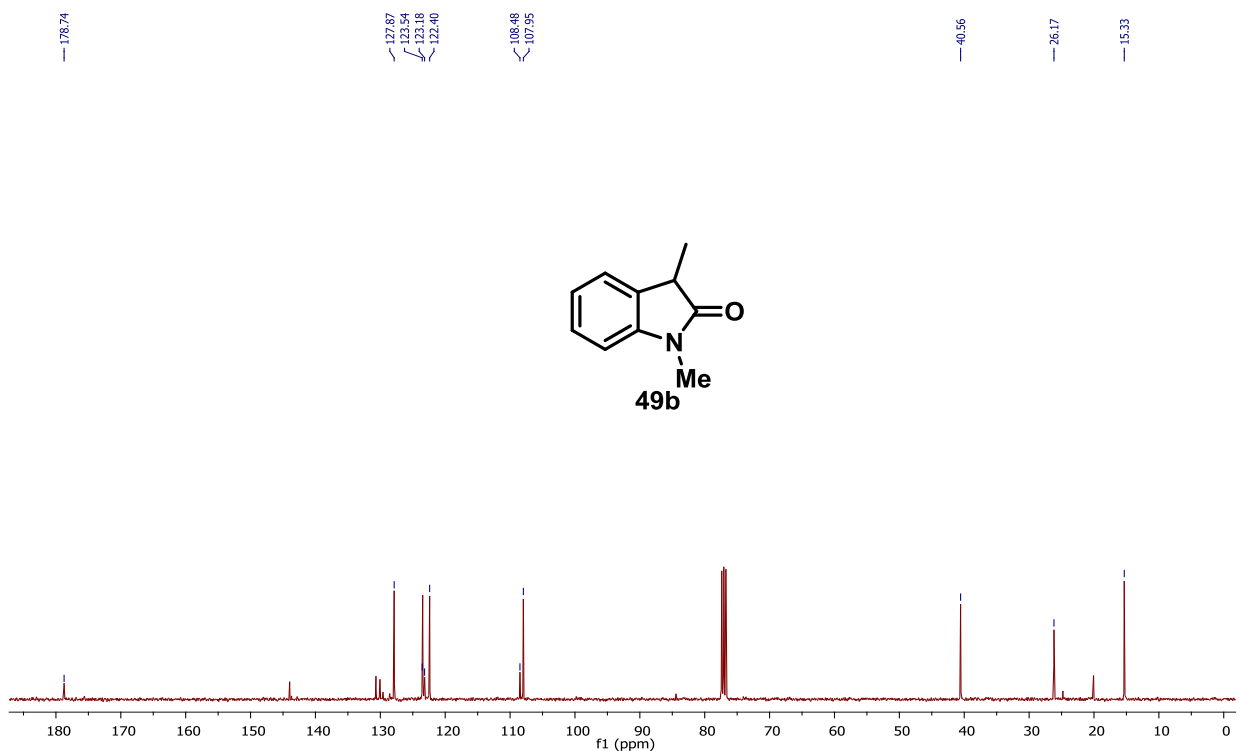


FIGURE 114: ^{13}C NMR spectrum of 49b, 100 MHz, CDCl_3 .

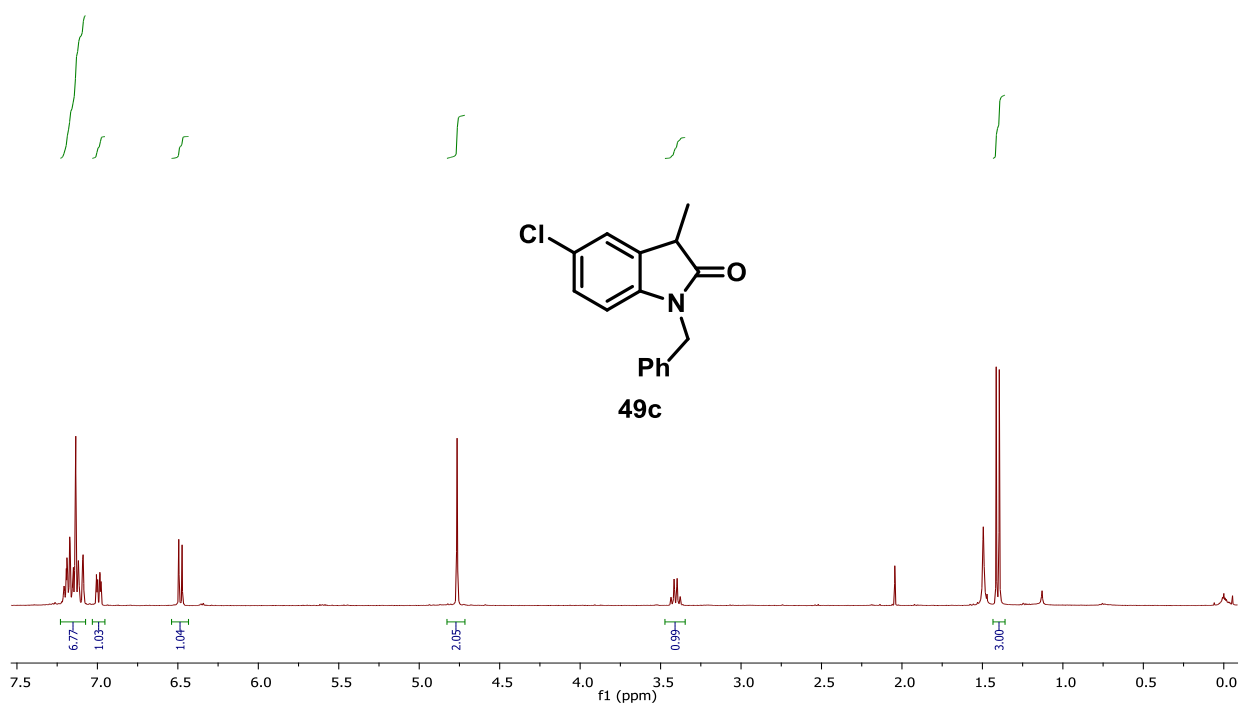


FIGURE 115: ^1H NMR spectrum of 49c, 400 MHz, CDCl_3 .

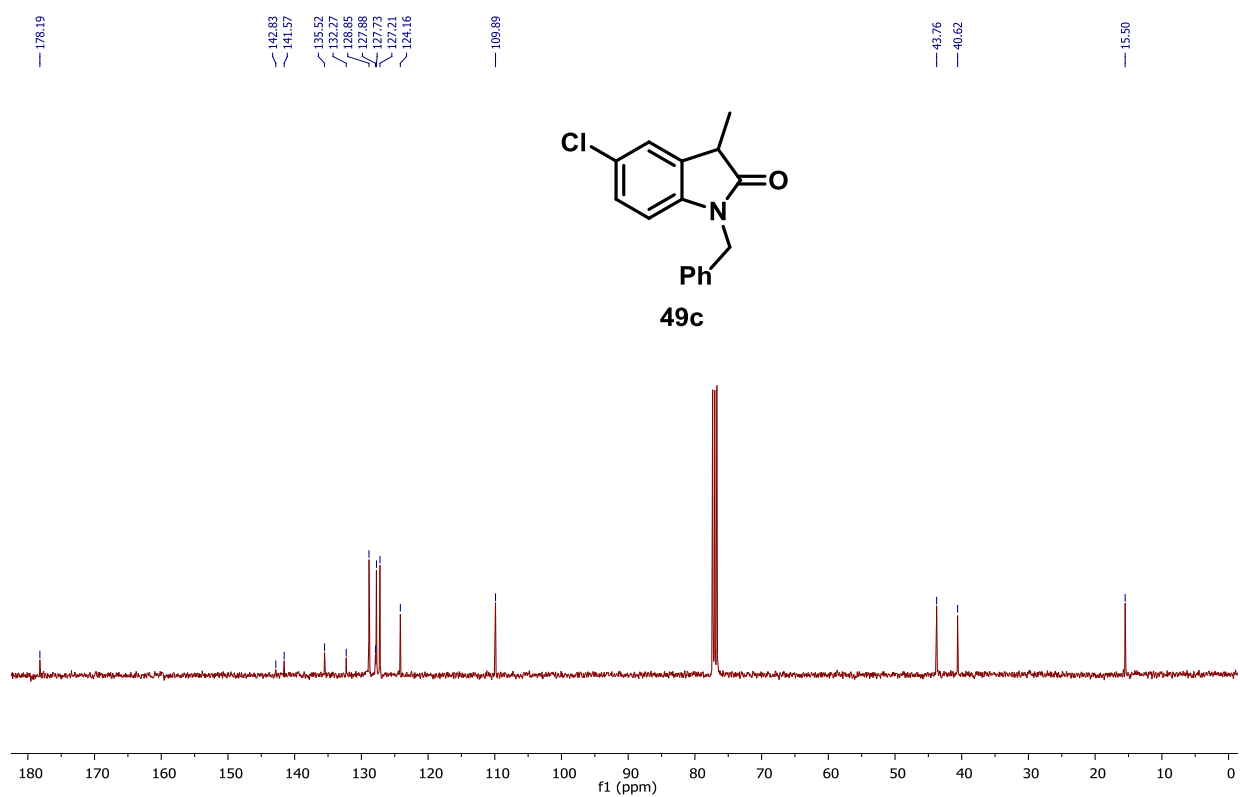


FIGURE 116: ^{13}C NMR spectrum of 49c, 100 MHz, CDCl_3 .

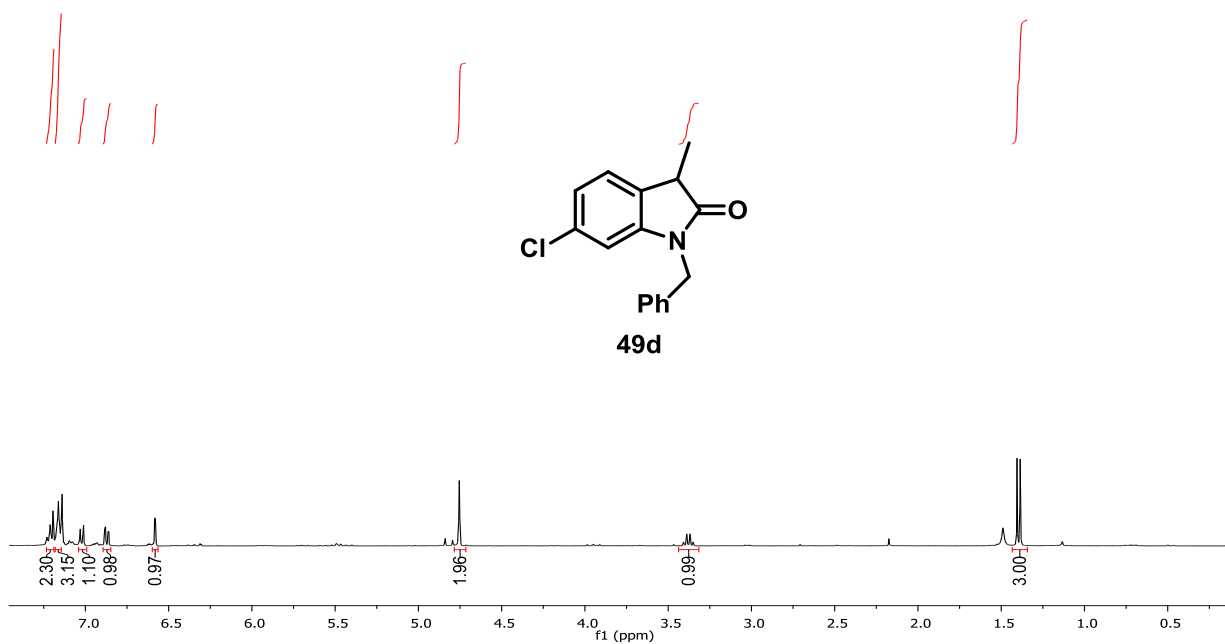


FIGURE 117: ¹H NMR spectrum of 49d, 400 MHz, CDCl₃.

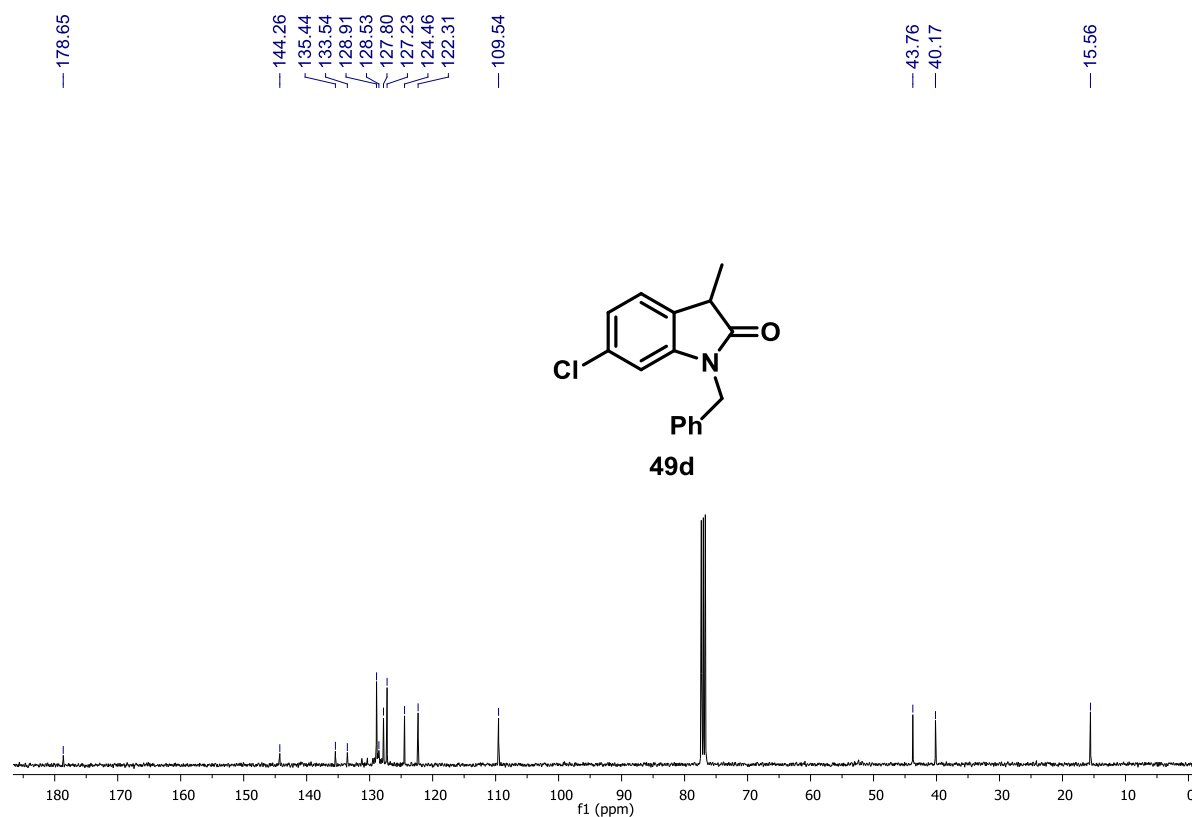


FIGURE 118: ¹³C NMR spectrum of 49d, 100 MHz, CDCl₃.

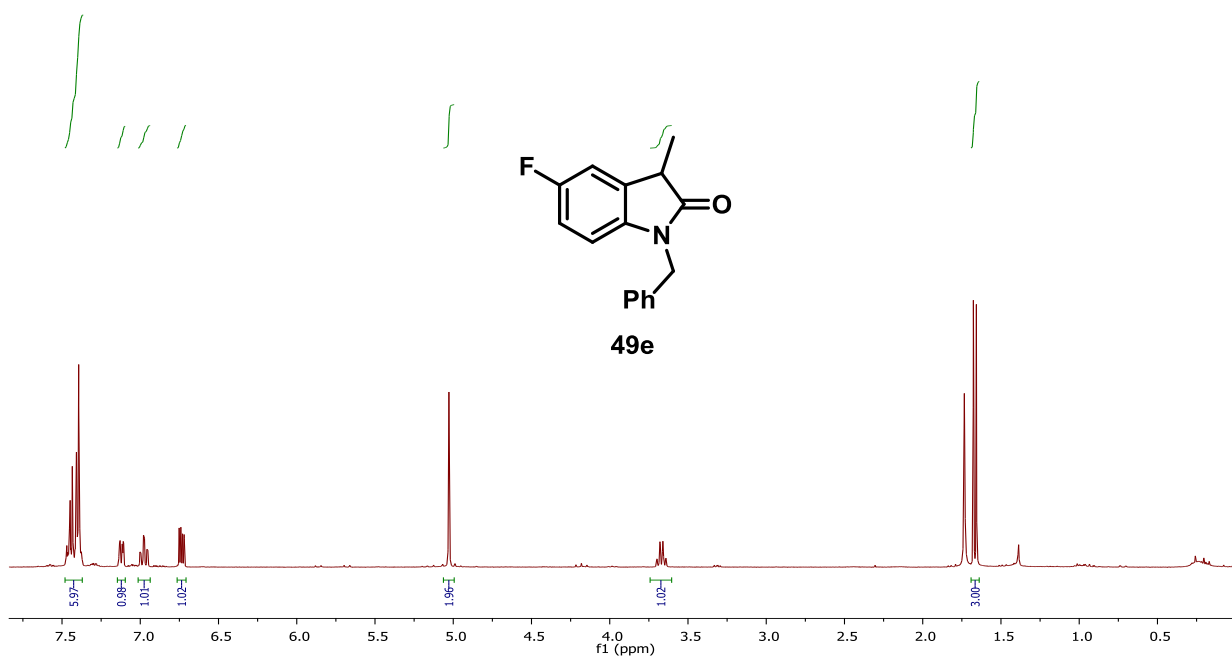


FIGURE 119: ¹H NMR spectrum of 49e, 400 MHz, CDCl₃.

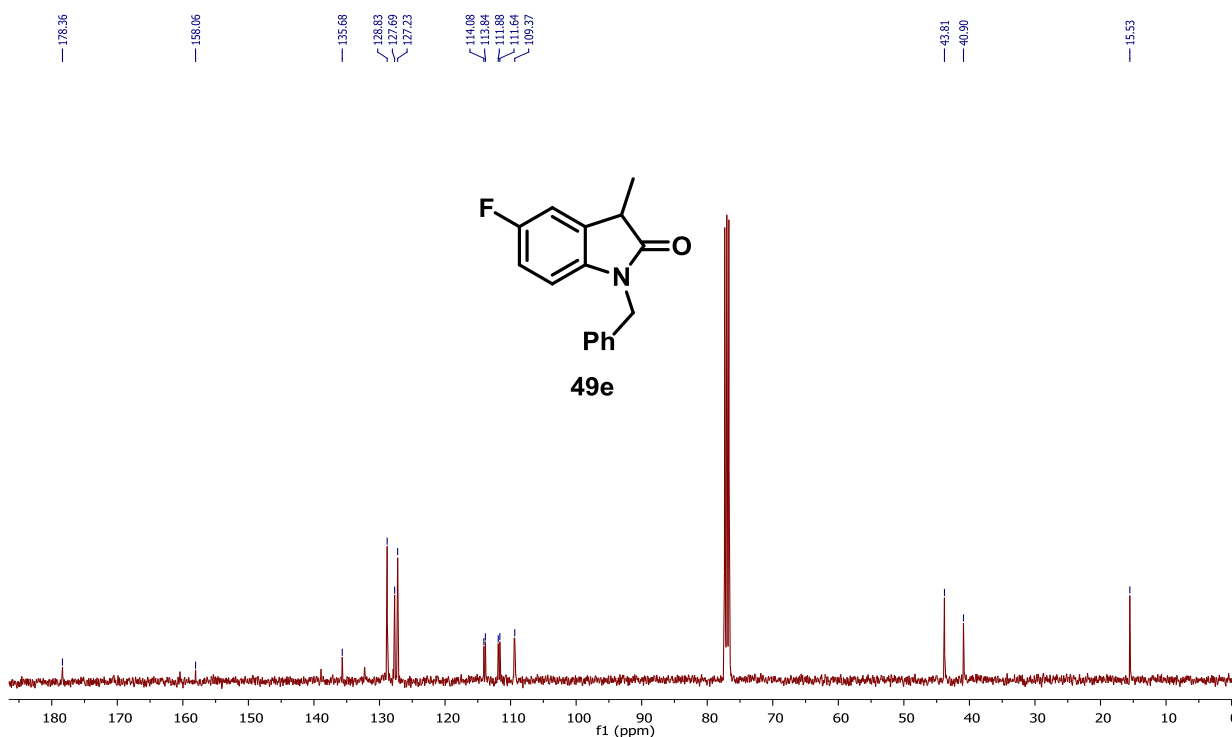


FIGURE 120: ¹³C NMR spectrum of 49e, 100 MHz, CDCl₃.

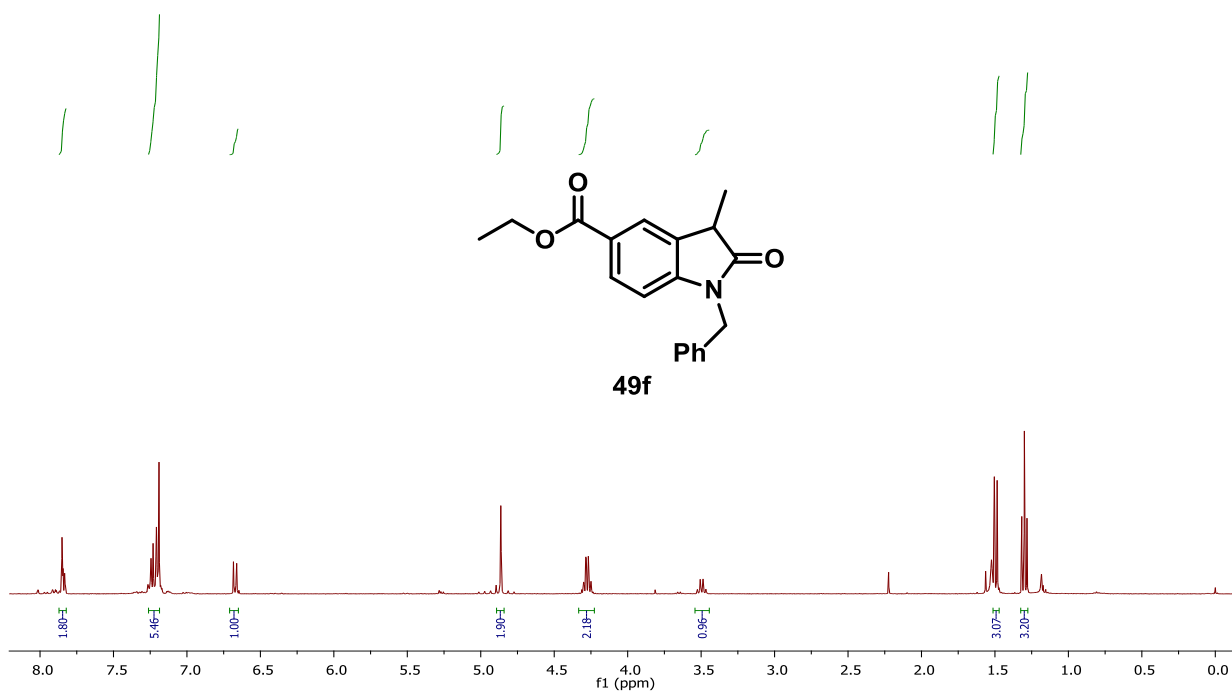


FIGURE 121: ¹H NMR spectrum of 49f, 400 MHz, CDCl₃.

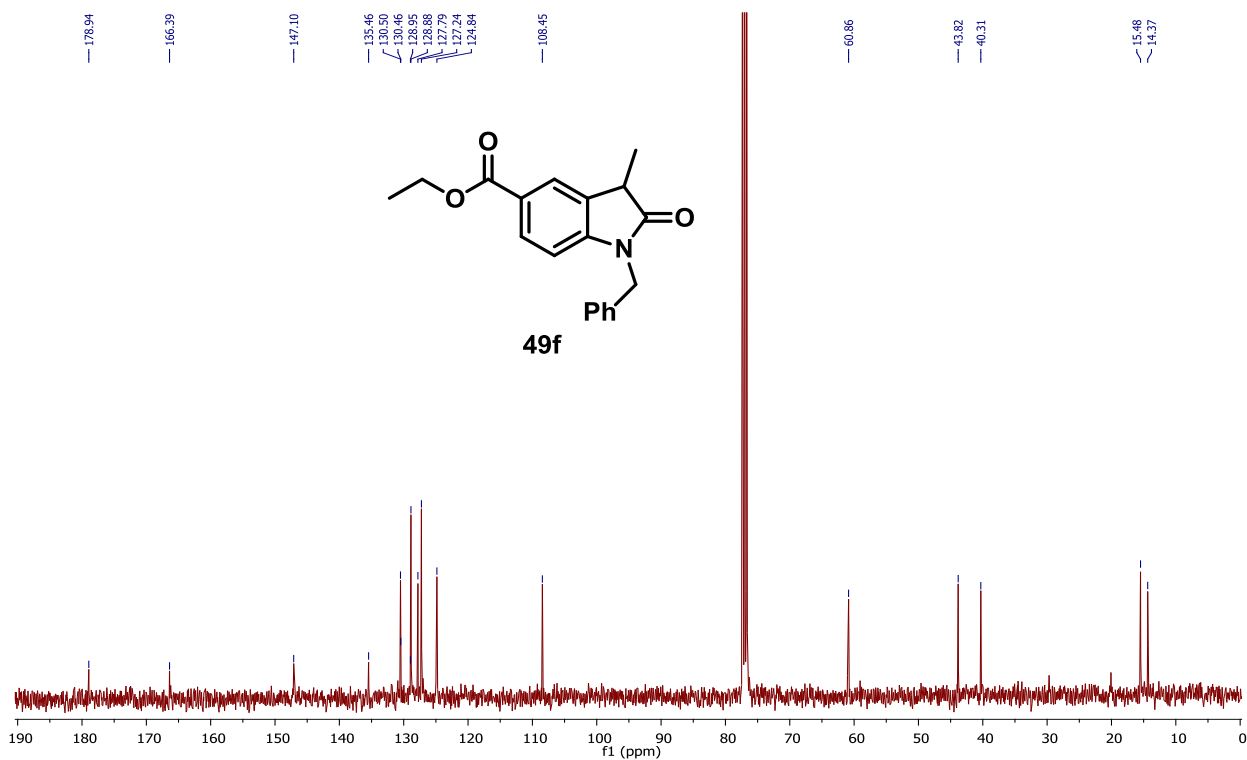


FIGURE 122: ¹³C NMR spectrum of 49f, 100 MHz, CDCl₃.

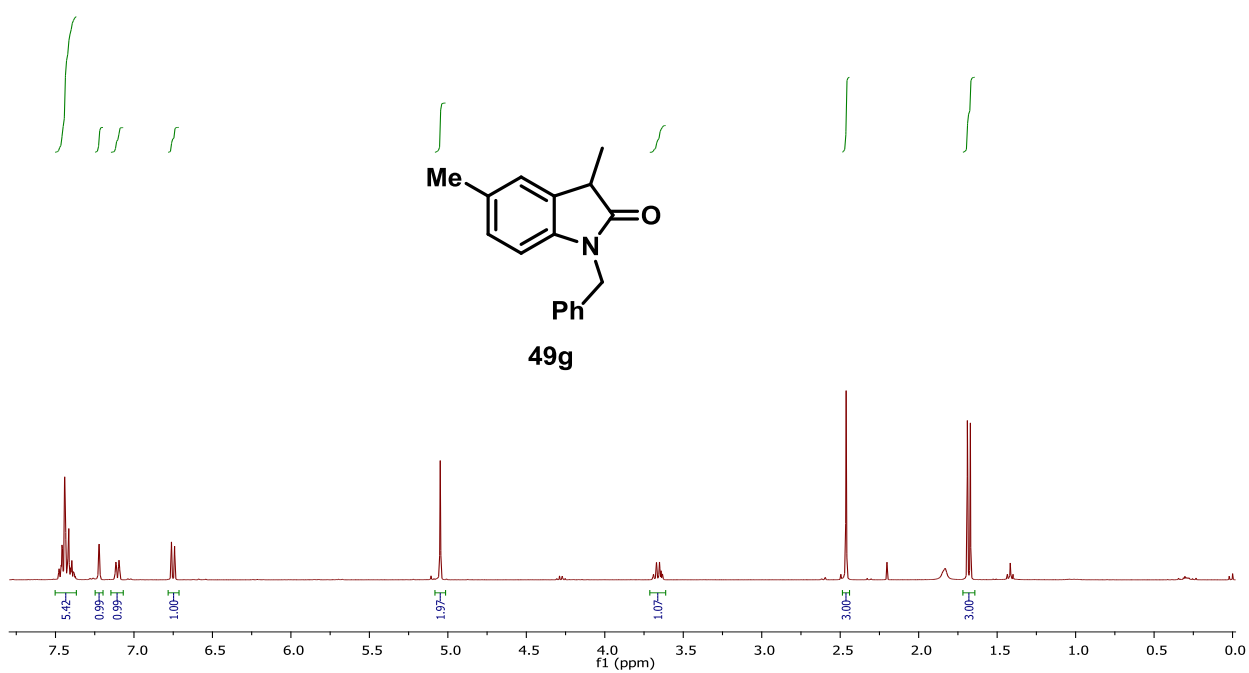


FIGURE 123: ¹H NMR spectrum 49g, 400 MHz, CDCl₃.

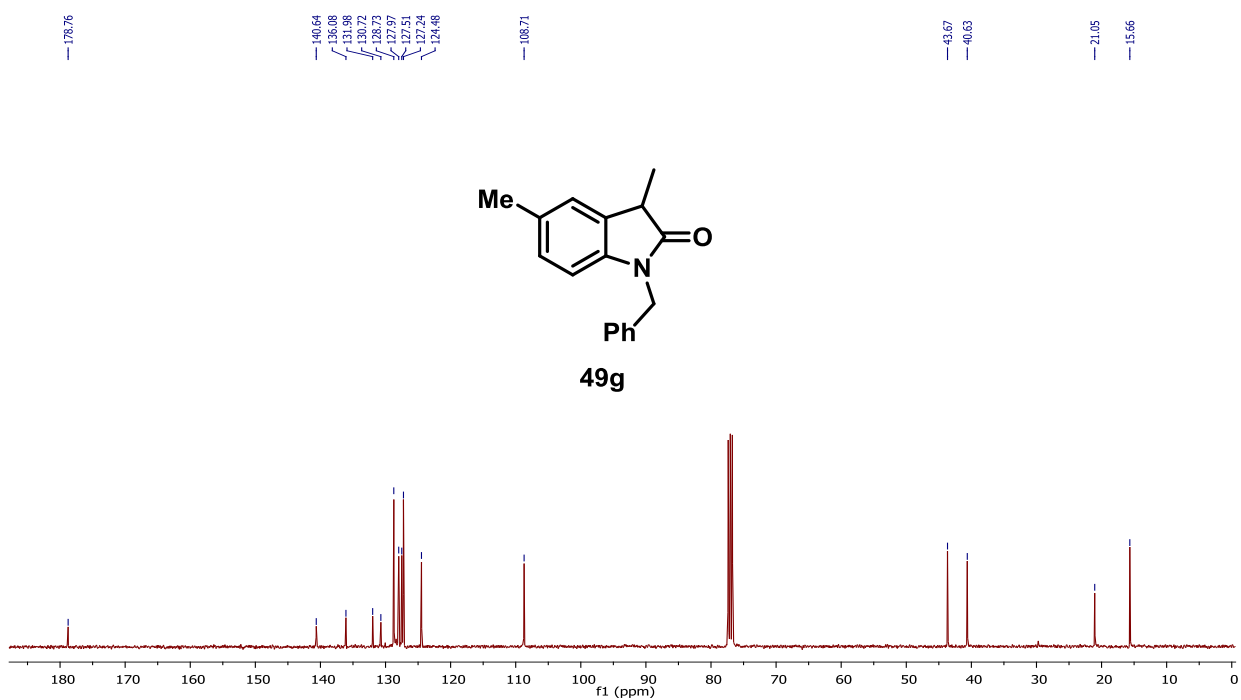


FIGURE 124: ¹³C NMR spectrum of 49g, 100 MHz, CDCl₃.

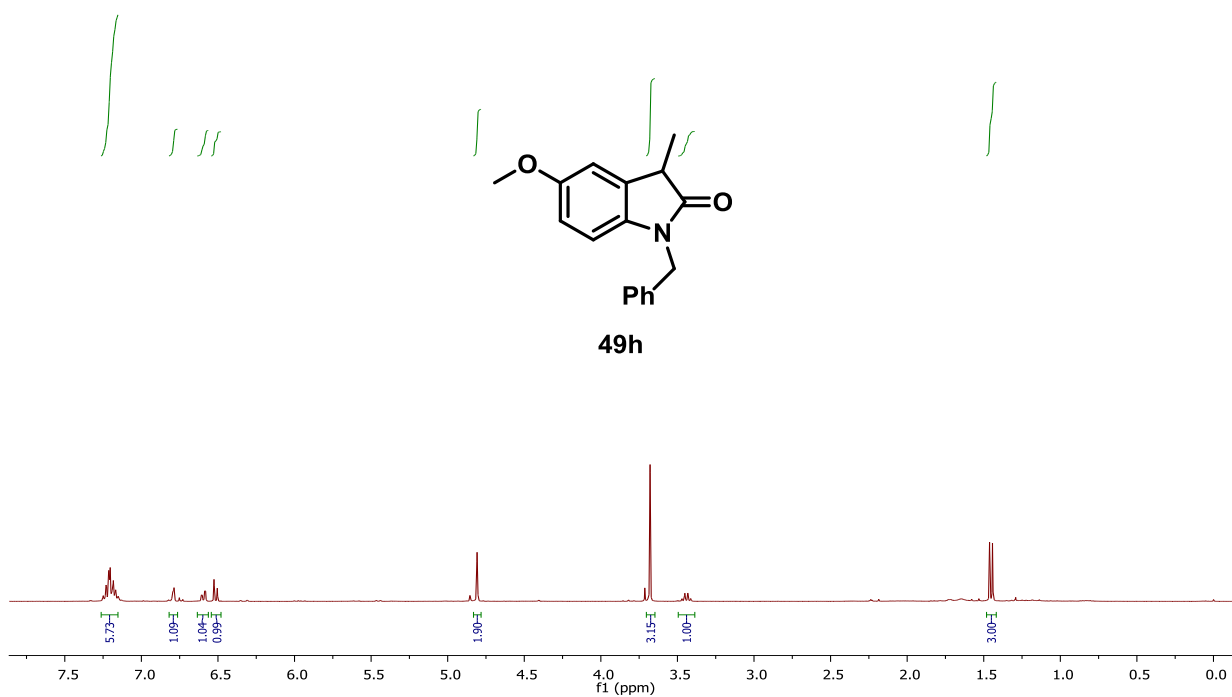


FIGURE 125: ¹H NMR spectrum of 49h, 400 MHz, CDCl₃.

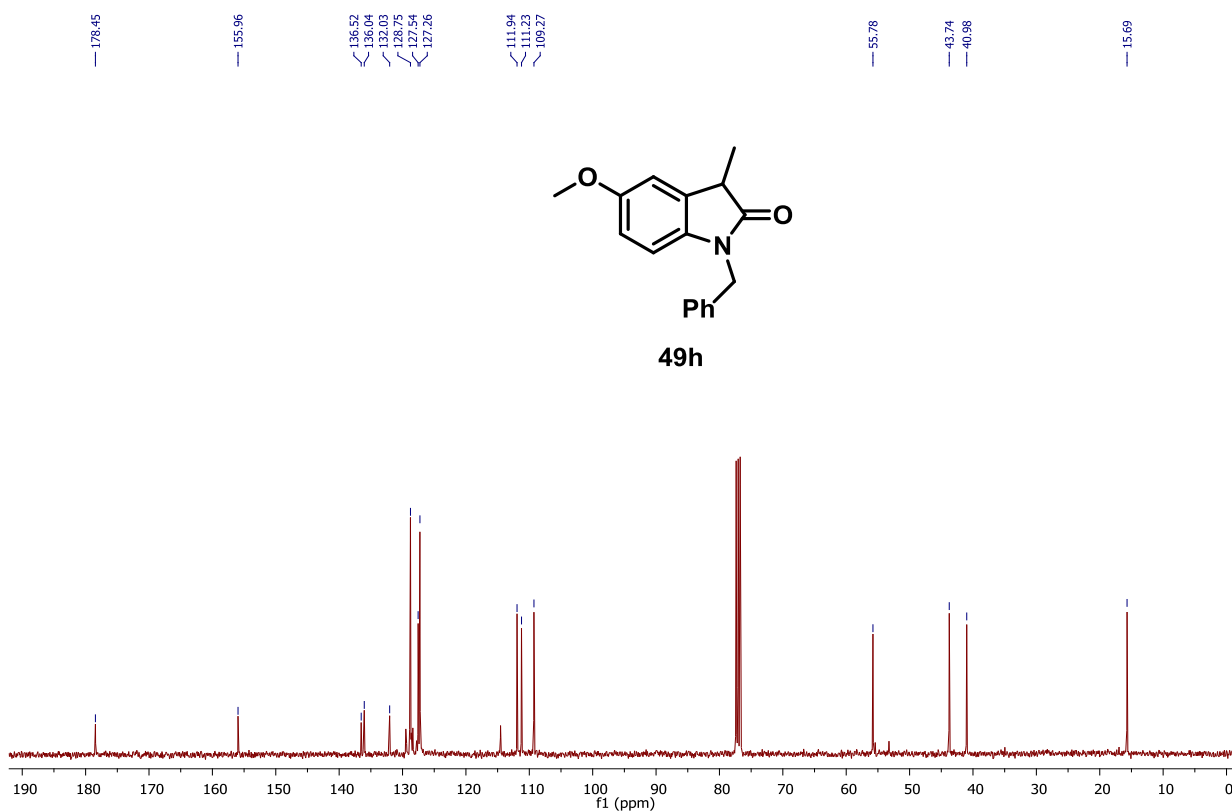


FIGURE 126: ¹³C NMR spectrum of 49h, 100 MHz, CDCl₃.

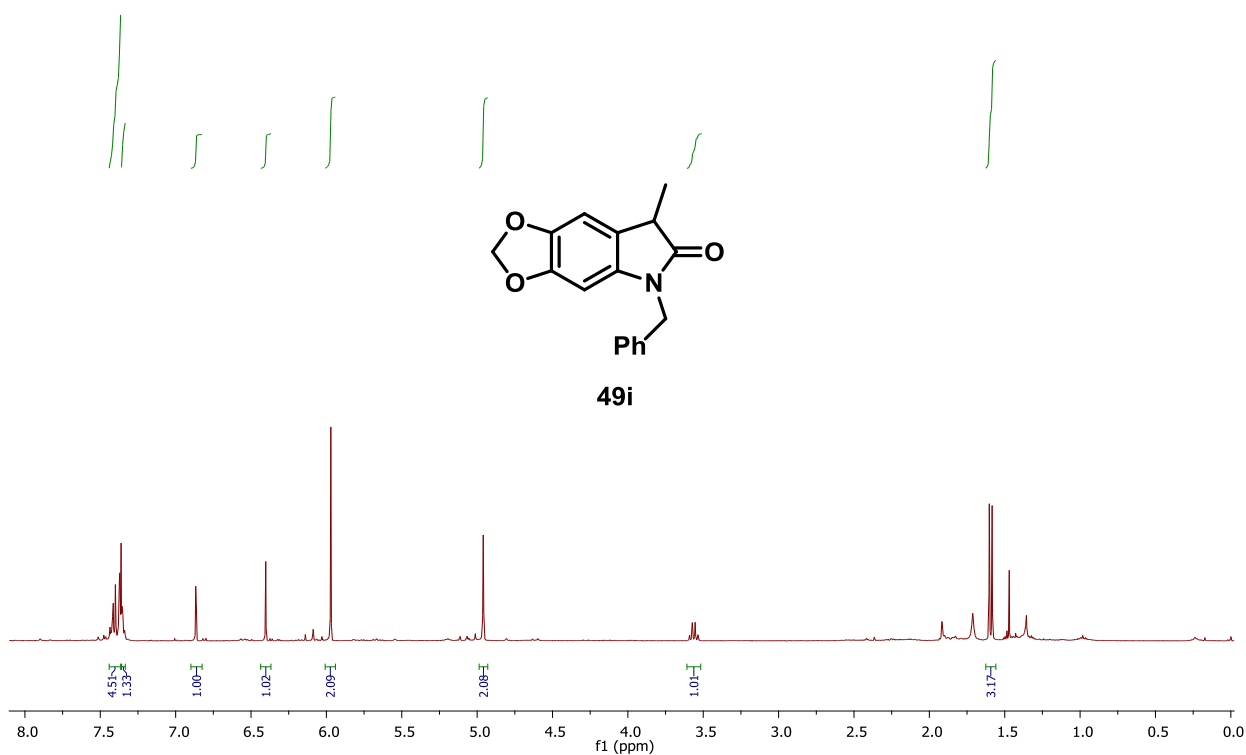


FIGURE 127: ¹H NMR spectrum of 49i, 400 MHz, CDCl₃.

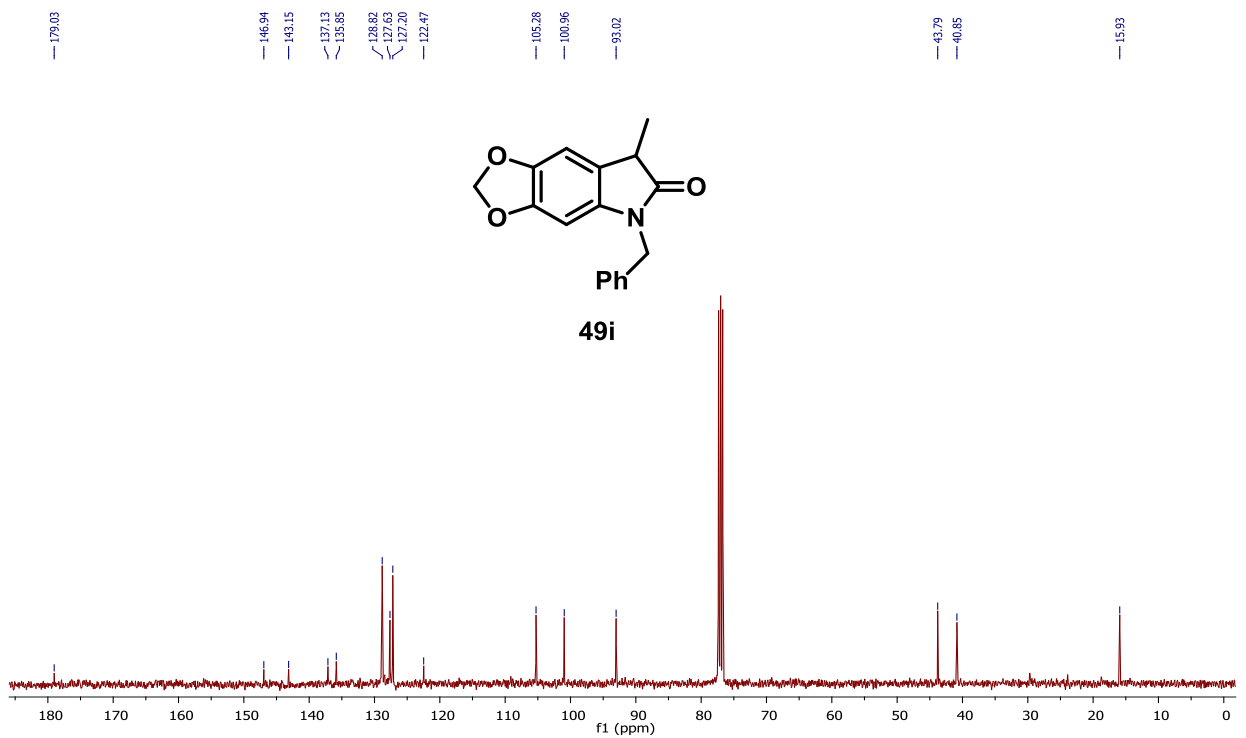


FIGURE 128: ¹³C NMR spectrum of 49i, 100 MHz, CDCl₃.